PORTUGALIAE PHYSICA

VOLUME 15
FASCÍCULO 1-2
1984

SOCIEDADE PORTUGUESA DE FÍSICA

PORTUGALIAE PHYSICA

Fundada em 1943 por A. Cyrillo Soares, M. Telles Antunes, A. Marques da Silva e M. Valadares

Publicação subsidiada pelo INSTITUTO NACIONAL DE INVESTIGAÇÃO CIENTÍFICA

ISSN 0048 - 4903

PORTUGALIAE PHYSICA

VOLUME 15
FASCÍCULO 1 - 2
1984

117

LES TRANSITIONS DE CONNECTIVITÉ (*)

P. G. DE GENNES
Collège de France, 75231 Paris Cedex 05

(Received 19 September 1983)

Beaucoup de structures physiques peuvent être décrites comme formées d'"*îles*" aléatoires. Dans certaines conditions parmi ces îles émerge un "continent" macroscopique. Cette idée a été perçue en premier par Hammersley [1]. L'attention s'est concentrée d'abord sur le cas de réseaux périodiques sur lesquels une fraction p des sites (ou des liens) est active, le reste (1-p) étant inactive, les différents sites (ou liens) étant non corrélés. L'apparition d'un "continent" a été baptisée transition de percolation [1].

On connait maintenant assez bien la statistique *géométrique* des îles, ou amas de percolation [2] et la relation entre percolation et transitions de phases [3]. Par contre, les propriétés de *transport* sur des amas de percolation commencent seulement à se clarifier [4]. Nous ne savons pas encore si les singularités du transport (près du seuil de percolation) sont directement déductibles des données sur la géométrie [5].

Malgré ces lacunes, nous disposons actuellement de données numériques assez détaillées sur les transitions de percolation. Elles ont trouvé des applications variées en physique des solides. Par exemple, on peut réaliser des systèmes magnétiques dilués, où une fraction p de sites est occupée par des atomes A portant des spins, la fraction 1-p portant des atomes B diamagnétiques. Le cas le plus simple correspond par exemple à des couplages ferromagnétiques (Fig. 1) entre atomes A premiers voisins. Alors, à basse température, tous les atomes A d'une même île ont leurs moments parallèles. Mais deux îles distinctes ont des moments

(*) Abridged version of an invited talk at the First Iberian Symposium on Condensed Matter Physics (Lisboa, 19-22 September 1983).

incorrélés. Lorsqu'on a seulement des îles ($p < p_c$) la moitié de celles-ci ont un moment vers le haut, l'autre moitié vers le bas, et au total il n'y a pas d'aimantation macroscopique. Par contre, pour $p > p_c$, il apparaît *un* continent. Les moments des îles se compensent encore mais celui du continent n'est pas compensé: le ferromagnétisme apparaît à $p = p_c$. Cette confluence (à $p = p_c$ et $T = 0$) de deux transitions, l'une géométrique (percolation) l'autre physique (ferromagnétisme) a suscité un assez vaste effort théorique et expérimental [6].

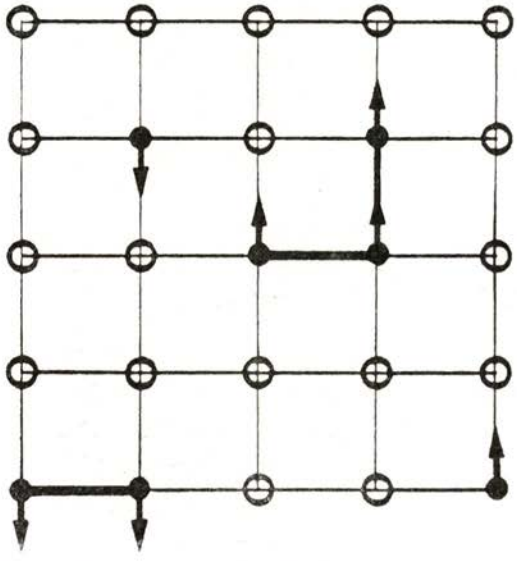

Fig. 1 — Atomes A (points noirs) répartis au hasard parmi des atomes B (points blancs) dans un alliage substitutionnel. Les atomes A forment des "îles" (connectées par des lignes noires). Tous les moments magnétiques des atomes A (marqués par des flèches) sont parallèles à l'intérieur d'une même île.

Dans la présente discussion, on insistera plutôt sur des *généralisations* de la percolation. Il faut noter d'abord que le remplacement du réseau de base périodique par un réseau statistique (ou, plus concrètement, d'un cristal par un verre) ne modifie pas profondément la statistique des îles. Par contre, certaines restrictions physiques sont importantes: nous nous limiterons toujours à des systèmes: *a*) qui sont *mascroscopiquement homogènes; b*) pour lesquels les liaisons qui définissent la connectivité sont à *portée finie*. Ces hypothèses sont souvent

adéquates en physique de la matière condensée. Par contre, dans les sciences humaines, ces conditions sont souvent violées. Par exemple, si nous pensons à l'échange d'informations entre individus, il se fait en partie de bouche à oreille (liaisons à portée finie) mais il se fait aussi par télécommunications (liaisons non locales).

Même avec ces restrictions, on trouve en physique de nombreuses transitions îles-continents qui ressemblent peut-être qualitativement à la percolation, quoique la statistique détaillée des îles puisse être différente. Nous les appelons *transitions de connectivité*. Dans le langage des transitions de phase, ces transitions peuvent éventuellement introduire de nouvelles classes d'universalité (montrer des exposants critiques différents de ceux de la percolation). En voici quelques exemples.

1 — LIQUIDES EN MILIEU POREUX

a) Si l'on injecte du mercure dans un verre poreux (Fig. 2) on constate que lorsque la pression d'injection dépasse un certain

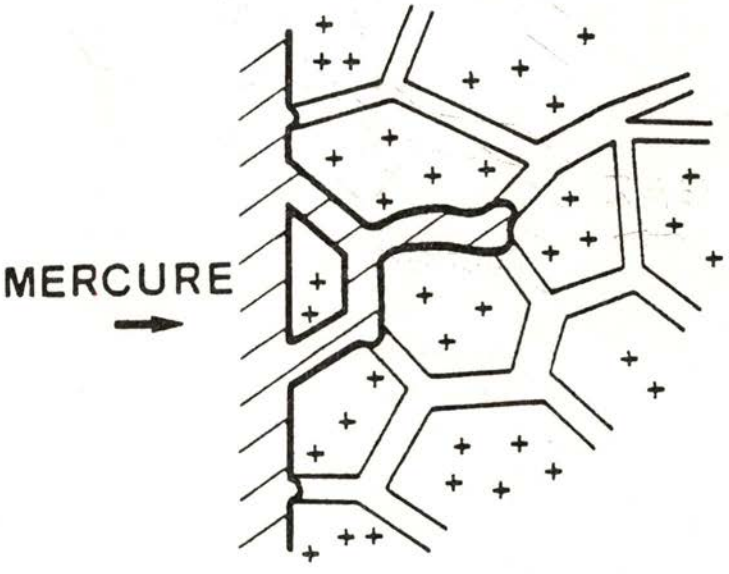

Fig. 2 — Injection de mercure (parties hachurées) dans un verre poreux. Les pores larges sont pénétrés facilement, les pores étroits ne sont pénétrés que lorsque la pression d'injection est forte.

seuil, le mercure pénètre dans la masse du spécimen: il s'est fait un "continent" de mercure, et le matériau injecté devient conducteur du courant électrique. Dans ce cas relativement simple, il y a forte présomption que l'on ait exactement un comportement de percolation.

b) Passons à un cas plus complexe, mais important: celui d'un système gaz + pétrole dans une roche. Le gaz sous pression peut expulser le pétrole, et joue un rôle un peu analogue au mercure de l'exemple (*a*). Mais il y a une différence: dans le cas (*a*), le mercure remplissait des pores vides. Ici, le gaz chasse un liquide (le pétrole). Ceci peut conduire à une situation nouvelle (Fig. 3). Si une "île" de pétrole est entièrement entourée par du gaz, elle ne pourra pas être évacuée (alors qu'une île vide pouvait toujours être envahie par le mercure). On attend encore une transition de connectivité (audelà de laquelle le gaz forme

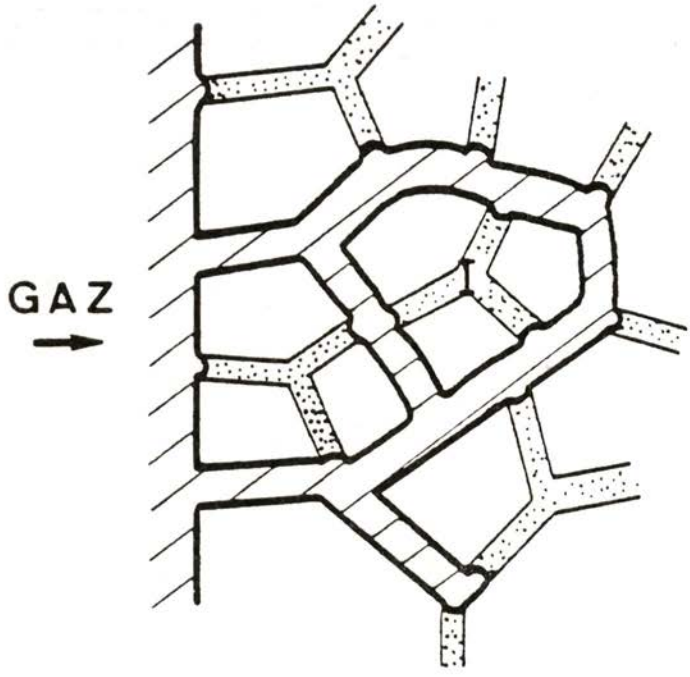

Fig. 3 — Déplacement du pétrole (régions pointillées) par du gaz (régions hachurées) dans une roche poreuse. Noter la région I (île de pétrole entourée de gaz) qui ne peut plus être éliminée.

un "continent"), mais dans certains cas (1), elle diffère de la percolation.

c) Un exemple encore plus complexe nous est fourni par une roche poreuse imprégnée de pétrole, où l'on essaye de déplacer le pétrole en injectant de l'eau. Alors que (*b*) correspond au mode normal de l'exploitation pétrolière, le cas (*c*) est celui de la *récupération assistée*, qui prend une importance croissante de nos jours. Par rapport aux discussions précédentes, il y a (au moins) deux complications nouvelles:

(i) — souvent, l'eau tend à mouiller complètement la surface de la roche: dans un pore, une région huile peut être entourée par un film d'eau; la distinction entre pores remplis d'huile et pores remplis d'eau ne tient plus. Ce cas est très mal compris actuellement;

(ii) — même lorsque la complication (i) n'apparaît pas (c'est-à-dire quand l'angle de contact eau/huile à la surface du solide reste fini), la géométrie est plus riche avec deux fluides: quand on augmente la fraction d'eau injectée f, on traverse *deux* transitions de connectivité. Au-delà d'une certaine fraction f_1 (environ 20 %), on réalise un "continent d'eau", et l'eau peut alors se déplacer à grande échelle. Au-delà d'une deuxième fraction f_2 (environ 80 %), on voit disparaître le "continent de pétrole": tout le pétrole est sous forme d'îles, et est beaucoup plus difficile à déplacer.

2 — LA FORMATION DES GELS

La Fig. 4 décrit qualitativement un gel — un réseau lâche de macromolécules en solution, connectées par des ponts. On peut former les ponts soit par réaction chimique, soit par des procédés physiques (microcristaux, hélices à plusieurs brins, etc.). Partons d'une situation où les ponts sont très rares: alors on a des chaînes déconnectées flottant dans un solvent, et le milieu est un liquide, ou "*sol*". Mais si nous augmentons le nombre de ponts, nous atteignons un seuil de connectivité: un "continent" apparaît — c'est-à-dire un filet macromoléculaire lâche, mais présent dans tout le récipient: le milieu est maintenant un solide fragile: un "*gel*".

---

(1) En particulier à deux dimensions.

(Les gelées de coing en sont un bon exemple: elles sont formées par pontage de longues chaînes de sucres, les pectines). La transition sol $\longleftrightarrow$ gel est connue depuis très longtemps, mais il y a moins de dix ans que sa relation avec les transitions de connectivité est appréciée. Les expériences sont ici surtout

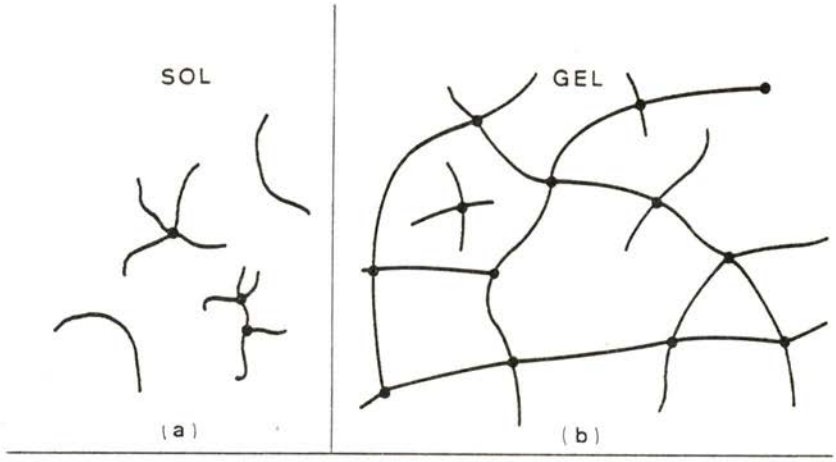

Fig. 4 — L'état sol et l'état gel. (a) Dans le sol, les chaînes macromoléculaires sont légèrement pontées (les ponts sont représentés par des points noirs) mais elles forment des îles finies. (b) Dans le gel, à plus fort taux de pontage, il apparaît un "continent" ponté.

mécaniques (rigidité du gel ou viscosité du sol). Elles montrent qu'il n'existe pas *un* type de transition sol-gel, mais *plusieurs* (selon la cinétique de pontage, la longueur des chaînes initiales, etc.).

3 — LES ÉCOULEMENTS DES SUSPENSIONS

Dans beaucoup de processus industriels, il est important de *fluidiser* une poudre solide, en la mettant en suspension soit dans un gaz, soit dans un liquide comme de l'eau. Le plus souvent, les grains de la poudre sont relativement gros (observables au

microscope optique) et leurs mouvements sont alors entièrement guidés par l'écoulement global du fluide. A l'heure actuelle, nous ne comprenons pas encore ces écoulements de suspensions, au moins dans le cas (essentiel) où la fraction du volume ϕ occupée par les grains est forte (supérieure à 15 %). Pour les suspensions dans l'eau en écoulement de cisaillement simple, il existe probablement une transition de connectivité remarquable: pour ϕ inferieur à une certaine valeur critique ϕ_c, la suspension est fluide, mais pour ϕ supérieur à ϕ_c, elle se comporterait plutôt comme une roche poreuse. Mais les mécanismes sous-jacents ne sont pas clairement établis à ce jour [7].

En conclusion, il est clair que l'idée des transitions de connectivité a fourni un schéma directeur, et unificateur, pour des phénomènes apparemments très différents — pris un peu partout dans les sciences physiques et chimiques, et dans leurs applications industrielles. Il est probable que cette idée diffusera aussi vers les sciences humaines. Mais, comme nous l'avons déjà dit, les réseaux concernés sont ici très différents, et il serait dangereux de vouloir plaquer trop rapidement les schémas de la percolation sur des problèmes trop complexes.

REFERENCES

[1] S. BROADBENT, J. HAMMERSLEY, *Proc. Cambridge Phil. Soc.* **53**, 629 (1957).
P. G. DE GENNES, P. LAFORE, J. P. MILLOT, *J. Physique* (Paris) **20**, 64 (1959).

[2] S. KIRKPATRICK, *Rev. Mod. Phys.* **45**, 574 (1973).
D. STAUFFER, *Phys. Rev. Lett.* **35**, 74 (1975).
Pour une introduction élémentaire, voir
P. G. DE GENNES, *La Recherche* **72**, 919 (1976).
E. GUYON, *Pour la Science* **60**, 14 (1982).

[3] P. KASTELEJN, C. FORTUIN, *Physica* **57**, 536 (1972).

[4] Y. GEFEN, A. AHARONY, S. ALEXANDER, *Phys. Rev. Lett.* **50**, 77 (1983).

[5] R. RAMMAL, G. TOULOUSE, *J. Physique (Lettres)* **44L**, 13 (1983).

[6] D. STAUFFER, *Physics Reports* **54**, 1 (1979).
J. ESSAM, *Reports Prog. Phys.* **43**, 833 (1980).

[7] P. G. DE GENNES, *J. Physique* (Paris) **40**, 783 (1979).
P. G. DE GENNES, *Physico-Chemical Hydrodynamics* **2**, 31 (1981).

FRUSTRATED SPIN SYSTEMS

AYŞE ERZAN

Laboratório de Física, Faculdade de Ciências
Universidade do Porto, 4000 Porto, Portugal

(Received 10 October 1983)

ABSTRACT — This paper aims to review mostly rigorous results on frustrated Ising systems and present a unified approach to the statistical mechanics of frustrated systems. The formalism is presented in a general enough manner to include q-state Potts models wherever this extension was possible.

I — INTRODUCTION

The present review was motivated by two lectures I gave at the Laboratorio de Fisica, Faculdade de Ciências, in Porto. It is intended as a tutorial introduction to the subject, with a pedestrian's approach to the connection with gauge theories. The interested reader is encouraged to go to other existing reviews in the field, notably that by Toulouse (1980), and to the seminal article of Fradkin et al. (1978).

Although in this review I will confine myself to spin models, the usefulness of the concept of frustration is certainly not limited to spin models. The ideas of frustrations and frustration lines have been extended by various authors to continuum models (see for example Dzyaloshinskii and Volovik 1980, and the review article by Halperin 1981 as well as the more recent work of Rivier).

I have, moreover, both for the sake of brevity and unity of presentation, not included models with continuous symmetries, although a few references have found their way in. (This is a big

shortcoming, as some of the most interesting results, analogies and open questions are to be found precisely in these systems). Above all, I do not pretend to make an exhaustive review of the subject, but hope to have included the highlights of the progress in the field, enough to indicate problems and loose ends. At the same time I hope I have been able to introduce the reader to some useful techniques in dealing with frustrated systems.

The paper is organized as follows. In Section II, I will give an intuitive definition of frustration and then proceed to review the results on ground state properties, the existence or nonexistence of phase transitions and their universality class, and the behaviour of the correlation functions, in periodically frustrated and, where available, on randomly frustrated Ising models. (The fully frustrated (ff) models are a special case of the former). This is not meant to be a review of the vast literature existing on spin glasses (SG), and only a few papers dealing with randomly frustrated systems are touched upon, the selection having been made on the basis of emphasis, namely, on the direct interrelation between the behaviour of the system and that of the distribution of frustrations.

In Section III, I introduce the concept of gauge variables and gauge transformations. The invariance of the partition function under these transformations is derived. The continuity between annealed and quenched averages is demonstrated.

In Section IV, the duality transformation and disorder variables are introduced. The interrelations under duality transformations, between disorder-disorder correlation functions in two dimensions (2d) (gauge invariant correlation functions in three dimensions (3d)) and the defects in the ordered spin system are displayed. The relevance of these correlation functions to the probability distributions of configurations of frustrations (and thus quenched averages) is shown. Finally, phase transitions in the frustration system as a function of the concentration of antiferromagnetic (AFM) of ferromagnetic (FM) bonds are considered.

Where possible, the material in Sections III and IV has been presented with enough generality to cover systems with Z_N type symmetries, and some consequences of the generalization to Potts systems of analogous results on the Ising model are indicated.

II — FRUSTRATED SYSTEMS

Consider a system of spin s_i located on the sites, i, of a lattice, with interactions J_{ij} on the bonds. The Hamiltonian is given by

$$H = - \sum_{(ij)} J_{ij} f(s_i, s_j) = \sum_{(ij)} E_{ij} \tag{2.1}$$

where the sum is over all pairs i, j. The most intuitive definition of frustration is to say that the system is *frustrated,* if not all E_{ij} may take their minimum values simultaneously, for any configuration of the spins s_i. Observe that this is a property of the set of interactions J_{ij} on the bonds and the functions $f(s_i, s_j)$; however it does not depend on a particular set of values of the functions $f(s_i, s_j)$ or s_i. From now on we will refer to the situation were E_{ij} takes its minimum value as 'the bond (i, j) being *satisfied*'. (Otherwise, we shall say it is *broken.* Using 'frustrated' in this context gives rise to a lot of confusion).

Let us illustrate. The simplest such spin model is the Ising model, where

$$s_i = \pm 1 ; \quad f(s_i, s_j) = s_i s_j \tag{2.2}$$

It is obvious that on a one dimensional chain with only nearest neighbor interactions (no overlapping bonds) and open ends, it is always possible for the s_i to take on a set of values which will satisfy any given set of J_{ij}. However, as soon as we have a closed loop of bonds, e.g. a triangle with the set J_{ij} of bonds on the edges as shown in Fig. 1a, b the problem is no longer trivial. In fact both of these systems are *frustrated.* It can easily be checked that any such loop with an odd number of bonds equal to $-J$, and the rest equal to J, is frustrated. Moreover, any lattice in d dimensions, incorporating such loops will also be frustrated.

Toulouse (1977) has defined the *frustration function* for the Ising model to be given by

$$\phi_p = \text{sgn} \left(\prod_p J_{ij} \right) \tag{2.3}$$

where the product is over all the bonds on a loop p. This function is positive if the loop is not frustrated, and negative if it is. If this

loop is the smallest loop that can be constructed on the given lattice, it will be called a plaquette. If the function ϕ_p associated with some plaquette is negative, that plaquette will be said to be frustrated, or is a 'frustration'.

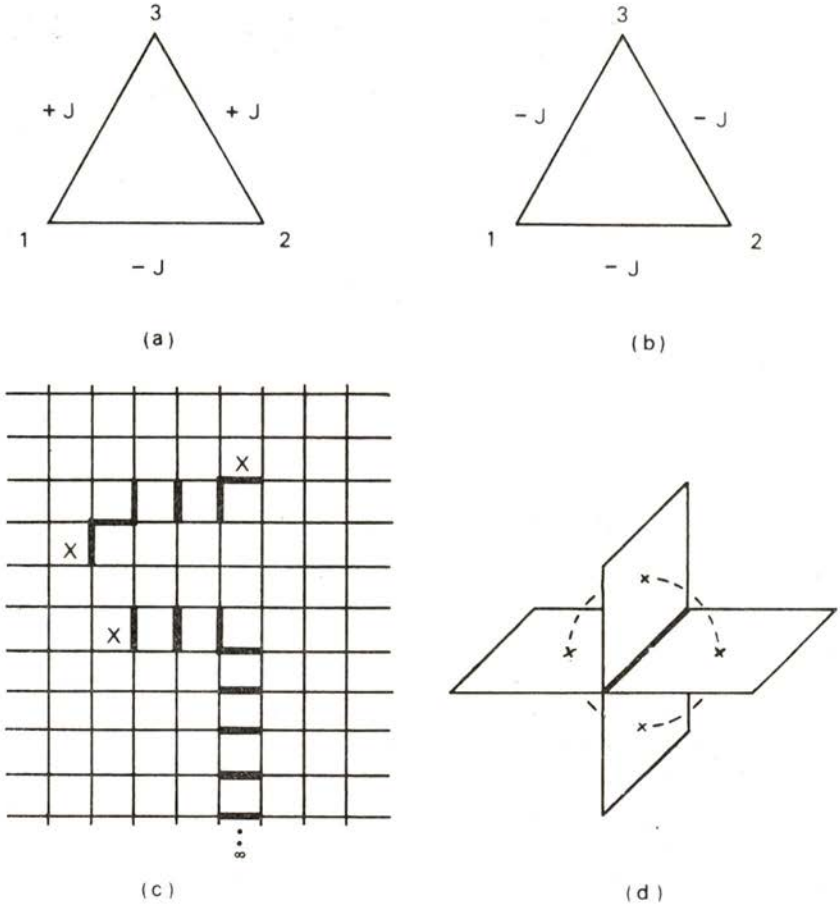

Fig. 1 — (a), (b) Simple frustrated plaquettes, (c) possible configurations of frustrations in two dimensions, (d) smallest possible 'tube' of frustrations in three dimensions. Dark lines are AFM. Frustrations are marked with an 'x'.

The distribution of frustrations on a lattice in d dimensions obeys certain topological constraints. As can be seen from Fig. 1c,

in two dimensions, any finite number of AFM bonds give rise only to pairs of frustrations. A single frustration can only be created with an infinite 'ladder' of AFM bonds going out to the edge of the lattice. In three dimensions, only a closed 'tube' of frustrated plaquettes may exist, the smallest possible such 'tube', surrounding a single AFM bond is shown in Fig. 1d (Fradkin et al. 1978). One can see that in the ordered phase spins would tend to align parallel, except along the faults, or defects, created by the AFM bonds, with the frustrations in two dimensions acting as the sources and sinks of the defect line. In three dimensions, an arbitrary loop of frustrated plaquettes is created by flipping all the spins incident on some surface bounded by this loop.

The concept of frustration has been generalized to other types of spin systems. The frustrated x - y model has been treated by Villain (1977b), Fradkin et al. (1978), José (1979), and more recently by Dzyaloshinskii and Obukov (1982). The latter have also treated a frustrated Heisenberg model. The extension to continuous spins has been provided by Herz (1978). In this review, I will, as already stated, stay for the most part with the Ising model. In section III, and IV, a more general treatment will also include the Potts model.

The usefulness of this quantity can be illustrated as follows: There are many conceivable ways in which bond randomness may be introduced into a Hamiltonian like Eq. (2.1), allowing for J_{ij} to take on both positive and negative values. (For simplicity, let us for the moment assume that the magnitude of the coupling constant stays the same). However it turns out that the models obtained via some of these schemes may be transformed, by a suitable redefinition of the spins, into uniform ferromagnetic models, and thus contain a 'hidden order parameter', namely the magnetization of the related ferromagnetic model. The partition functions and the free energies of the original and transformed models are of course the same, and so are the singularities encountered at the transition temperature, if there is one. The classical example of this phenomenon is the 'Mattis model' (Mattis 1976), where

$$J_{ij} = J\ \sigma_i\ \sigma_j \quad , \quad \sigma_i = \pm 1$$

and σ_i, σ_j are independent random variables. For Ising spin s_i one may define

$$\tau_i = s_i \, \sigma_i$$

so that the partition function

$$Z = \sum_{\{s_i\}} \exp [\beta \, J \sum_{(ij)} \sigma_i \, \sigma_j \, s_i \, s_j]$$

reduces identically to that of the ferromagnetic Ising model:

$$Z = \sum_{\{\tau_i\}} \exp [\beta \, J \sum_{(ij)} \tau_i \, \tau_j]$$

where β is the inverse temperature in units of the Boltzmann constant, as usual. Note that although $< s_i > = 0$ for all temperatures, for an even distribution of the σ_i, $< \tau_i > > 0$ for $T < T_c$, where T_c is the critical temperature of the ferromagnetic model. (See Section III for a more general discussion of this type of transformation). Upon inspecting the original model we see that it is completely unfrustrated! For any closed loop on the lattice,

$$\prod_c \sigma_i \, \sigma_j \equiv 1$$

where the product is over all pairs i, j lying on the loop c. An inspection of the ground state of the system will show that there is in fact a unique way (with the overall degeneracy of 2) of choosing the spins s_i such that all the bonds $J_{ij} = J \, \sigma_i \, \sigma_j$ are satisfied. This ground state is precisely the ferromagnetic ground state in the variables τ_i. In section III we will see that a system with frustrations cannot be transformed into an unfrustrated system by such a redefinition of the spins. We conclude that frustration is a *necessary* and *irreducible* feature of spin glass models.

Random and Periodically Frustrated Systems

An Ising spin glass model where the exchange interactions are distributed independently of each other with some probability P(J), where P(J) includes negative couplings, will give rise

to a lattice with a random distribution of frustrations. (In fact, on a square lattice with an even distribution of $+,-$ bonds, exactly half the plaquettes will be frustrated on the average). One may, on the other hand, construct periodic arrays of frustated plaquettes, or systems where each plaquette is frustrated, namely, *fully frustrated* systems. (See Fig. 2 for the fully frustrated

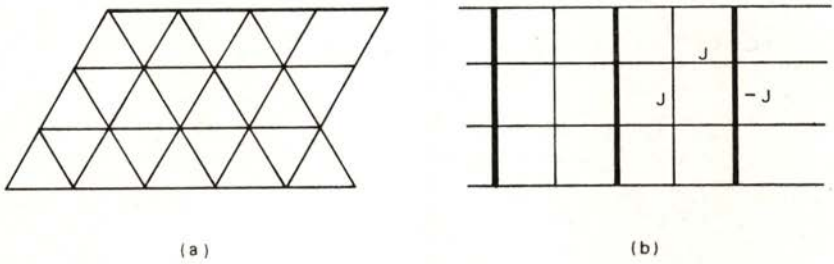

Fig. 2 — (a) Segment of the triangular lattice. Fully frustrated with all AFM interactions, this lattice corresponds to the fcc lattice in three dimensions, and generalizations thereof in higher dimensionality. (Alexander and Pincus 1980). (b) The Odd Model (FFSI) in two dimensions. This model can also be generalized to the fully frustrated hypercubic lattice in d dimensions. (Derrida et al. 1979, Villain 1977 a).

lattices to which we will most frequently refer). Since the periodic systems are easier to treat, and in fact in two dimensions can be solved exactly (Ising, Potts) a lot of effort has gone into determining their properties. (See Fig. 3 and the references given there). Moreover, by considering periodic strips in 2-d, within each of which the distribution of frustrated layers might be random, and then letting the width of these strips go to infinity, certain results may be obtained on systems with translational invariance in one direction and complete randomness on the other. (Hoever et al. 1981, Kardar and Berker 1982). I shall try to review these results here from the point of view of ground state properties, the existence or nonexistence of a phase transition, the nature of the low temperature or zero temperature phase and the behaviour of the correlation functions.

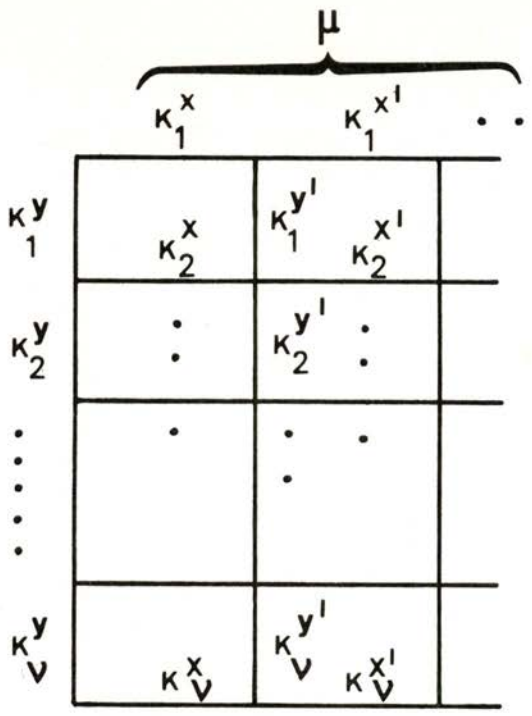

Fig. 3 — Periodically frustrated lattices. For $\mu = 1$, n = number of AFM rows and m = number of FM rows in ν.

(a) $\mu = 1$. Hoever and Zittartz (1981), Wolff et al. (1981).

(b) $\mu = 1$. Kardar and Berker (1982).

(c) $\mu = 1$, $|K_i^y| =$ constant. Hoever et al. (1981), where the same frustration distribution with the minimum number of AFM bonds is also considered. Hoever et al. (1981), Bryskin et al. (1980) with $n = 1$, $m = 3$.

(d) $\mu = 1$, $\nu = 1, 2, 3$, $n/m = 1, 1/2, 1/3$. Longa and Olés (1980).

(e) $\mu = 1$, $\nu = 2$, $|K^y| = |K^x|$ (DUD), $\mu = 2$, $\nu = 2$, $J = K_1^y = K_2^y$, $K_2^y = K_1^{y'} = J'$ (ZZD). André et al. (1979).

(f) $\mu = 2$, $\nu = 2$, $K_1^x = K_2^{x'} = J_2$, $K_1^{x'} = K_2^x = J_4$, $K_1^y = K_2^{y'} = J_3$, $K_2^y = K_1^{y'} = J_1$. Gabay (1980).

(g) $\mu = 2$, $\nu = 2$, $K_1^{y'} = -K_1^y = J_2$, $K_2^{y'} = -K_2^y = J_4$, $K_2^x = K_1^x = J_3$, $K_2^{x'} = K_1^{x'} = J_1$. Garel and Maillard (1983).

(h) $\mu = 1$, $\nu = 2$, $K^x = |K^y|$, $K_2^y = -K_1^y$. The Odd model. Villain (1977a), André et al. (1979), Bryskin et al. (1980), Forgacs (1980).

(i) $\mu = 2$, $\nu = 2$ $|K_i^y| = |K_i^x| = J$, $K_1^x = -J$, $K_1^{x'} = J$, $K_2^x = K_2^{x'} = J$, $K_1^y = -J$, $K_1^{y'} = J$, $K_2^y = K_2^{y'} = J$. The chessboard lattice, Bryskin et al. (1980).

(j) f and i above could also be considered under periodic models with a diagonal symmetry direction, as in André et al. (1979).

Ground State Entropy

One consequence of frustration is the increase in the ground state degeneracy of the system. To illustrate: in Fig. 1, had all the bonds been equal to $+J$, the system would have had a unique ground state (all spins aligned), with the sole degeneracy associated with the overall ($\pm$) symmetry of the Hamiltonian. However, the frustrated system has an additional degeneracy associated with the breaking of a particular bond, e.g., a bond on any edge of the triange may be broken, to yield the same ground state energy, $-J$. On a full lattice the effect is even more strikingly illustrated (Fig. 4).

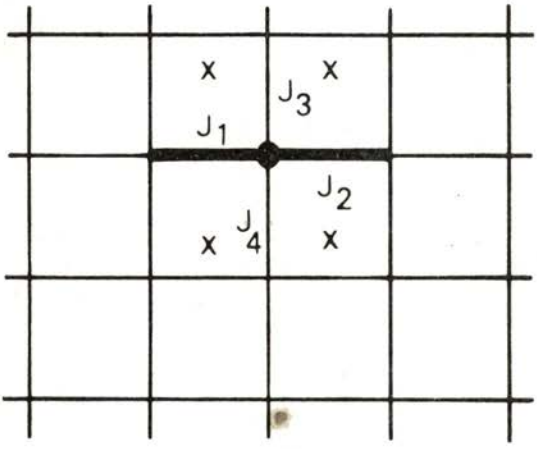

Fig. 4 — The light bonds are FM, dark bonds AFM. The plaquettes marked with an 'x' are frustrated. The central spin indicated by a dark dot is effectively decoupled from the rest of the system, contributing a degeneracy of 2 to the ground state. In other words, the ground state is degenerate with respect to the breaking of the bonds J_1 and J_2 or J_3 and J_4.

In an array, random or ordered, of frustrated plaquettes, there may be macroscopically many such spins, giving rise to a finite ground state entropy *per spin* (Binder 1980). Moreover,

there may be not only such single spins, but many-spin clusters under whose reversal the ground state entropy is invariant, giving rise to the cluster picture of spin glasses (Binder 1980, Miyashita and Suzuki 1981, Smith 1975, Soukoulis and Levin 1977), where one considers a system of uncoupled or loosely interacting clusters of spins who interact strongly within themselves. There is an interplay between dimensionality and ground state entropy that is remarkable; viz., not even all fully frustrated systems have finite ground state entropy (GSE) per spin. Both the triangular Ising AFM (Wannier 1950, Alexander and Pincus 1980) and the odd model of Villain (Villain 1977) have finite GSE, and no transition at finite temperatures. However their three dimensional counterparts, namely the Ising AFM on the fcc lattice and the FFSI in 3-d, have, respectively, ground state degeneracies of the order of $2^{N^{1/3}}$ (Danielian 1961) and $2^{N^{2/3}}$ (Chui et al. 1982) and thus zero GSE per spin. These models are thought to have, respectively, first order (Phani et al., 1979) and second order (Chui et al. 1982) transitions to an ordered low temperature phase ([1]).

Although it is tempting to already try and draw conclusions with respect to the low temperature behaviour (existence or nonexistence of a phase transition, nature of the low temperature phase, etc.) from the existence or nonexistence of a finite rest entropy, it has been demonstrated (Hoever et al. 1981a) that this relationship is rather subtle. In particular, the existence of a finite rest entropy may or may not be accompanied by the absence or presence of a phase transition to an ordered phase at a finite temperature (see also Wolff, Hoever and Zittartz 1981).

Hoever et al. (1981a) have made the following conjecture: 'If all of the ground states (in the ensemble of ground states for the system) can be obtained one from the other by a succession of purely local transformations on the spins ($s \rightarrow -s$), then the global symmetry of the Hamiltonian (all $s \rightarrow -s$, uniformly) cannot be broken, i.e., there cannot be a phase transition to a phase with broken symmetry'. However, as they already point out,

---

([1]) It has been claimed by Villain et al. (1980) that the AFM fcc Ising Model has a re-entrant paramagnetic phase at $T = 0$. The results of Phani et al. (1979) are from Monte Carlo simulations. See also Binder (1980b).

the converse is not true, i.e., in the case where one needs to make some 'global' transformation to go from one gound state to another (in the sense that you have to flip over certain sets of 'rigid spins' (André et al. 1979) simultaneously) no decisive statement can be made. What makes the field so challenging is that most systems of interest happen to fall into this category! (see Fig. 5

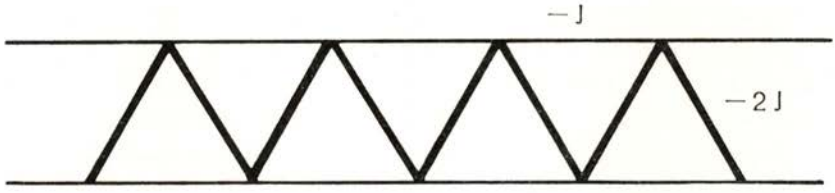

Fig. 5 — As may be easily checked, even the extremely simple system of a triangular strip as shown in the figure, with Ising spins and AFM bonds, has sets of ground states which may be obtained one from the other by purely local transformations, as well as those that differ by 'global' transformations. This system has no phase transition even at zero temperature (de Nunes 1983).

and caption). Monte Carlo simulations of Ising systems on square or simple cubic lattices with a random distribution of $\pm$ bonds have revealed precisely this kind of picture, with large (typically proportional to N) energy barriers between degenerate ground states or low-lying states (Malaspinas, Kirkpatrick 1977).

André et al. (1979) moreover hypothesize that if a phase transition exists in a frustrated system, it would be due to the internal field of the 'rigid spins' aligning the rest of the spins; thus, in a periodic frustrated system the ordered phase would necessarily reflect the periodicity of the 'rigid spins'. This implies that if there exists a transition to an ordered phase in a periodic frustrated system, it cannot be to a spin glass phase. Although the last part of this statement is supported by studies on layered frustrated models (see next paragraphs) the argument is not convincing. A similar assumption is employed by Chui et al. (1982) in constructing a Landau type argument for determining the nature of the phase transition encountered in the FFSI model in 3-d. However, if exact renormalization group (RG) transformations

on fully frustrated hierarchical lattices are any guide at all, we know that the ordering in the low temperature phase may be incommensurate with the underlying lattice, as evidenced by the chaotic RG trajectories. (Mc Kay et al. 1982, Svrakić et al. 1982, Derrida et al. 1983, Erzan 1983).

Derrida et al. (1978) have conjectured that for those frustrated models that have a transition temperature $T_c \neq 0$, there is a *negative* entropy associated with the formation of defects (negative interface entropy). The vanishing of the defect energy at $T = 0$ does not signal the absence of a phase transition, but the vanishing of the negative interface entropy does. They have checked their conjecture in the case of the anisotropic odd model (where the AFM couplings $-J'$ are taken so that $J' > J$, the FM couplings) and the anisotropic triangular AFM, where the AFM couplings in one direction are taken to be stronger than in the other two. In the latter case, $T_c = 0$ although the GSE per spin is zero, and the interface energy in the direction perpendicular to the anisotropy direction is finite; but the interface entropy is zero. In the anisotropic odd model they recover the results that $T_c \to 0$ as $J' \to J$; and they also show that the interface energy tends to zero in this limit as well.

An Exact Criticality Condition

Hoever et al. (1981) have treated random layered frustrated Ising models with translational invariance of both the horizontal and the vertical bonds in one direction, using transfer matrix methods. They have found that if the layering has a period of length ν, with n_+ and n_- being the total number of ferro- and antiferromagnetic couplings in the vertical direction within each period (the horizontal bonds were chosen to be ferromagnetic) (1), the transition temperature depends only on the absolute value of the mean coupling, or, $|n_+ - n_-|/\nu$ and is otherwise independent of the particular distribution of bonds

(1) We will show in Section III that the free energy depends only on the distribution of the plaquette frustration functions ϕ_p (Eq. 2.3). Thus there is no loss of generality in this coiche; ϕ_p is invariant under all $K^x \to -K^x$.

within each period. Their results have been extended by Kardar and Berker (1982) and Wolff et al. (1981) to anisotropic random layered systems involving a distribution of magnitudes as well as signs of the coupling constants. The exact criticality condition is given by

$$\sum_{i=1}^{\nu} \tilde{K}_i^x = \left| \sum_{i=1}^{\nu} K_i^y \right|$$

where $\tilde{K}_i^x$ is the dual (see section IV) of K_i^x and i is the row index. When the average vertical coupling within a strip is equal to zero, the transition temperature is depressed to zero.

For all other values of the average vertical coupling the transition is either to an antiferromagnetic or ferromagnetic phase depending upon the ratio of the horizontal and vertical couplings. The important thing to note is that the transition is of the ordinary Ising type, the specific heat has a logarithmic singularity, except in the case where ν is allowed to go to infinity, in which case one obtains an infinitely weak singularity (Hoever and Zittartz 1981, Mc Coy 1977). For the model with $K_i^x = K$; $K_i^y = K$, $i = 1 \ldots m$, and $K_i^y = -K$, $i = m+1, \ldots \nu$, $\nu = n + m$, Hoever and Zittartz (1981) find that if $n = m$, $T_c = 0$, the specific heat has a rounded maximum with respect to the temperature at some $T \neq 0$; and as $m \to \infty$ this maximum goes over to the logarithmic singularity of the Ising model. Their conjecture, that the rounded maximum signals 'local' ordering within the unfrustrated strips, effectively decoupled from each other by the frustrated layers, in the same spirit as the 'cluster' picture mentioned above, is remarkably born out by the behaviour of the specific heat reported from finite size scaling calculations made on strips of width m (Droz and Malaspinas 1982, Nightingale and Blöte 1980). On the other hand, for $n \neq m$, but $n/m \sim 1$, the amplitude of the logarithmic singularity is extremely small, and only a rounded maximum above T_c is really visible — caution to experimentalists! — quite indistinguishable from the smooth specific heat curves obtaining for $m = n$, or in the limit $\nu \to \infty$ (see also Longa and Olés 1980).

Besides coupling constant anisotropy, the introduction of an external field has been a fruitful approach to studying the effects

of 'fine tuning' (Toulouse 1980) frustration (Villain 1978, Penson et al. 1979). A third venue is provided by RG studies of hierarchical models (McKay et al. 1982, Svrakić et al. 1982, Erzan 1983) where the lattice structure, e.g. the coordination number, can be varied at will. However, there does not yet seem to be a universally applicable, quantitative measure of *competition*, comparable in elegance to the frustration function itself.

Ground State Energy

A way of tackling the problem of determining the ground state energy per spin in frustrated systems has been to define an average internal field (Derrida et al. 1979) equal to the difference between the number of satisfied and broken bonds incident on a spin, the average being taken over the ensemble of ground states. An amazing universality is displayed by this quantity, which is proportional to z, the coordination number of the lattice, for $d < 4$, and $z^{1/2}$ for $d \geq 4$ (Derrida et al. 1979, Alexander and Pincus 1980) for the fully frustrated lattices given in Fig. 2. Another universal feature of these lattices is the existence of a borderline dimensionality above which it is not possible to construct ground states such that only one bond is broken per each plaquette, i.e., the 'overblocking effect'. For the generalized fcc and FFSI lattices this borderline dimensionality is found to be four (Derrida et al. 1979).

The connection between ground state properties and the singularities of the free energy at $T > 0$ remains a subtle matter. Wolff et al. (1981) have shown for a random layered model, containing the odd model as a special case, that the critical surface as a function of the coupling constant anisotropy fails to reflect the discontinuities in the rest entropy, or the singularities (discontinuities in the slope) of the ground state energy surface. More recently, Garel and Maillard (1983) have demonstrated a remarkable fact: the partition function of a four parameter fully frustrated model (1) (see Fig. 3g) is equivalent to the partition function of an anisotropic ferromagnetic model. The $T = 0$ point of

(1) This does not violate gauge invariance. The reduction in the number of parameters is what allows the mapping to be possible.

the fully frustrated model maps to the critical temperature of the ferromagnetic model. In particular, for the odd model, the rest entropy is linked to the critical free energy of the ferromagnetic model. I am unable to comment on the implications of this fact at this moment.

Correlation Functions

Concerning the two point spin-spin correlation function of periodic or random layered, frustrated Ising systems, the following picture emerges: The triangular Ising AFM (Stephenson 1970a) and the FFSI in 2-d (the odd model) (Southern et al. 1980, Forgacs 1980, Wolff and Zittartz 1982) and the ZZD model (see Fig. 3f) (Gabay 1980), where the coupling constants are uniform in magnitude and all the plaquettes are frustrated by a periodic arrangement of $\pm$ bonds, and where $T_c = 0$, have the common feature that at $T = 0$ the correlations decay with a power law,

$$\Gamma(r) \sim r^{-\eta}$$

(quasi-LRO, Halperin 1981). The value of η is universally equal to 1/2. This behaviour is also found for the layered model with $K^y > 0$, $K^y > |K_i^x|$ and $K_i^x = -K_{i+1}^x$ (i is the row index). Note that here, too, $T_c = 0$ (Wolff and Zittartz 1982). These authors have also found that for $T > T_c$,

$$\Gamma(r) \sim \exp(-r/\xi)$$

with $\xi^{-1} \sim \exp(-2K^x)$. However, if $|K^x| > K^y$, although T_c is still zero, there is perfect FM or AFM order within the rows, depending on the sign of K_i^x, and, at $T = 0$, $\Gamma(r)$ within the rows tends to a constant as $r \to \infty$ (Wolff and Zittartz 1982).

In all the cases that a nonzero transition temperature is allowed (and where the periodicity of the random layers stays finite) one has the usual Ising behaviour, i.e.,

$$\begin{aligned}
&\Gamma(r) \sim r^{-\eta} \exp(-\xi/r) && T > T_c \quad ; \quad \xi \sim (T - T_c)^{-1} \\
&\Gamma(r) \sim r^{-\eta} \qquad \eta = 1/4 && T = T_c \\
&\Gamma(r) \underset{r \to \infty}{\to} \text{const} && T < T_c
\end{aligned}$$

This is the case for the anisotropic triangular AFM (Stephenson 1970b) and those layered models where $\Sigma_i K_i^x \neq 0$ (Wolff and Zittartz 1982). The anisotropic triangular AFM has the further peculiarity that for some T_D, $T_c < T < T_D$, short range order of the above type obtains; however for $T > T_D$ the exponential decay of the correlation functions is modulated in the direction of the anisotropy axes by an oscillatory factor, with a temperature dependent wavelength (Stephenson 1970b).

Another class of fully frustrated systems is afforded by the checkerboard lattice (Bryskin et al. 1980, André et al. 1979) and the ff hexagonal and Kagomé lattices (Sütö 1981). For these *'superfrustrated'* lattices (Sütö 1981) there is no quasi-LRO even at $T = 0$: the correlation length stays finite even at this temperature. Unfortunately, so far one cannot give a rule by which one may *a priori* decide if a lattice is superfrustrated or not. Bryskin et al. (1980) have given explicit expressions for the free energy, from which the zeroes of the partition function in the complex temperature plane may be calculated, for a partially frustrated lattice with a nonzero transition temperature, the odd model, and the checkerboard lattice. Work is in progress at this point for a full characterization of these systems via the distribution of the zeroes of their partition functions.

The effect of frustrations on the correlation functions of systems with a quenched random distribution of frustrations has been studied by various authors. Fradkin et al. (1978) have made a high temperature study of pair correlations and shown that the correlation functions decrease in the presence of frustrations (1). Miyashita (1983) has considered the behaviour of correlations on frustrated lattices in 2-d, in the whole temperature range, depending on the relative positions of frustrated plaquettes with respect to the correlated spins. The results are extremely intriguing in that they reveal a non-monotonic suppression of correlations for certain configurations. This non-monotonicity of near-neighbour spin correlations had shown up in Migdal-Kadanoff type RG calculations on ff hierarchical lattices (Derrida et al. 1983, Erzan 1983) and was the origin of the novel RG behaviour (stable and unstable periodic RG trajectories) found in those models.

---

(1) See Section IV for further details.

Dilute Frustrated Systems

Another approach to the spin glass problem has been to investigate the effect of dilution on fully frustrated systems, or, alternatively, the effect of low concentrations of frustration on the properties of unfrustrated systems.

De Seze (1977) has given a phenomenological argument for the existence of a spin glass phase with a concentration dependent critical temperature in bipartite fully frustrated lattices ($T_c > 0$ for $x < 1$). Ono (1980) finds an ordered phase in a bond diluted AFM triangular 'cactus tree' in an intermediate concentration range. André et al. (1979) give an argument that for the diluted odd model the critical temperature remains at $T = 0$, and that the correlations will have the same power law decay as in the pure lattice.

Grest and Gabl (1979) have performed Monte Carlo computations on the triangular and fcc AFM lattices, and have found spin glass-like 'freezing' behaviour for concentrations above the percolation threshold. In the fcc lattice the transition to the AFM phase is first changed from first to second order, and then for $.8 < x < .4$ a phase appears with no LRO but strong hysteresis effects (The Edwards-Anderson order parameter has been calculated and shows slow decay). The prevailing wisdom in spin glass literature rules out a stable SG phase in 2-d, but not in 3-d (see, for example, Sherrington 1983).

De Nunes (1983) has performed a real space RG calculation on an AFM ff hierarchical lattice with bond dilution. At lower effective dimensionalities (or coordination number, z), the $T = 0$ critical point is destroyed by dilution, whereas for higher z one has a transition to an antiferromagnetically ordered phase. For these higher effective dimensionalities, at fixed concentration x, the recursion relations exhibit stable periods (rather than fixed points) in the low temperature region. The transition line terminates at some x bigger than the percolation threshold, at a critical point of infinite order.

The introduction of AFM bonds into an FM square lattice has been found (Vannimenus and Toulouse 1977) to destroy the FM transition at a concentration c of AFM bonds equal to .09. De Almeida et al. (1981) report a value of $c = .166$

obtained via an effective field approach. It is believed that the frustrated plaquettes percolate at this concentration (or an infinite string of frustrated plaquettes first appears). Miyashita and Suzuki (1981) have found a cluster (of rigid spins effectively decoupled from the rest by frustrated bonds) boundary percolation threshold at $c = .15$. For a triangular lattice the frustrated plaquette percolation threshold $c_f^* = .10 - .15$ (Sadiq et al. 1981). It is interesting to note that the concentration of frustrated plaquettes, c_f, shows a saturation effect, and stays nearly constant at about 1/2, while c is varied above c_f^*, up to the percolation threshold for the FM bonds (1/2 for the square lattice; the situation is of course symmetric around this concentration). The ground state energy per spin is therefore rather insensitive to the variation of c above c_f^* (Kirkpatrick 1977).

Schuster (1979), by implementing methods to be outlined in section III, has shown that there is a further transition in the frustration network as a function of c. Namely, an infinite ladder of AFM bonds first appears at $c = .29$, leading to the possibility of isolated frustrations. His results have been corroborated by Kolan and Palmer (1980) using Monte Carlo methods. It still remains to be ascertained whether this transition in the frustration network is accompanied by a corresponding 'transition' in the behaviour of the spin system at $T > 0$. For a topological phase transition in a frustrated x - y model, see Dzyaloshinskii and Obukov (1982).

III — GAUGE VARIABLES, GAUGE INVARIANCE AND THE FRUSTRATION FUNCTION

In the preceding section we have tried to give an overview of the phenomenology of frustrated systems. The methods employed to derive the results reported up to here were generalizations of methods applicable to conventional (unfrustrated) spin systems; in particular, transfer matrix methods, high temperature expansions (this last, however, making use of the gauge invariance and duality transformation concepts to be presented henceforth (Fradkin et al. 1978)), renormalization group analysis, and of course, Monte Carlo simulations. In this section we will introduce *gauge variables* as an extension of systems with spin degrees of freedom (Kadanoff 1976, Fradkin et al. 1978) and

the natural language in which to discuss 'bond randomness'. This allows us to extract the thermodynamically relevant features of an ensemble of frustrated systems, as well as allowing us to treat annealed and quenched bond randomness as part of one continuous picture.

Gauge Variables and Symmetries

We shall define *gauge variables* to be those variables that depend on two nearest neighbour site (vertex) indices on the lattice. As opposed to the *spin* variables which are located at the vertices of the lattice and depend on only one site index, the gauge variables can be thought of as variables living on the edges connecting the nearest neighbor sites. They are, then, a type of random variable custom made for representing a system of random interactions between nearest neighbor sites on a lattice. (Actually, the generalization to long range interactions as, for example, in the case of the infinite range spin glass, has also been made, Nishimori and Stephen 1983) Clearly, we can label the gauge variables ψ, either ψ_{ij} where i and j are site indices, or $\psi_{i,\mu}$ where i indicates a site and μ a particular lattice direction.

Let us recall that the Hamiltonian in (2.1)

$$H = - \sum_{(ij)} J_{ij} \, f(s_i, s_j)$$

is usually invariant under a set of symmetry operations

$$\{ s_i \} \rightarrow \{ s_i' \} \, . \tag{3.1}$$

The simplest example is the Ising model, where $s_i = \pm 1$, $f(s_i, s_j) = s_i s_j$, and the only nontrivial such symmetry operation consists of

$$\{ s_i \} \rightarrow \{ - s_i \} \, . \tag{3.2}$$

This is a *global* symmetry: the operation is applied to all the spins s_i in the system at once. We can easily construct other examples. The q-state Potts model has

$$f(s_i, s_j) = \delta_{s_i s_j} \tag{3.3}$$

where $\delta_{s_i s_j}$ is the Kroenecker delta and spins s_i can take on q different values. The relevant set of symmetry operations is obviously the group of permutations of q objects. We could, in fact, write the Potts spins (including the Ising model as the special case with $q = 2$) as q-dimensional vectors,

$$\mathbf{s}^{\dagger}(\mathbf{r}) = (s_1(\mathbf{r}), s_2(\mathbf{r}) \ldots s_q(\mathbf{r})) \tag{3.4}$$

with $s_k(\mathbf{r}) = 0, 1$ and $\sum_k s_k(\mathbf{r}) = 1$. We can then express the permutation transformations as

$$s'_k(\mathbf{r}) = \sum_l M^{\alpha}_{kl} s_l(\mathbf{r}) \tag{3.5}$$

where the matrix M is a realization of the group of permutations of q objects, and α labels a particular element of this group. Following Kadanoff (1976), one can generalize this formulation to any set of spins $s(\mathbf{r})$ with some number (not necessarily discrete) of internal states, and the group of transformations between these states. Let us choose M to be a unitary representation. Then the simplest scalar that can be formed from these spins $\mathbf{s}(\mathbf{r})$, under the group of transformations M, is, in matrix notation,

$$f(\mathbf{s}(\mathbf{r}), \mathbf{s}(\mathbf{r}')) = \mathbf{s}^{\dagger}(\mathbf{r}) (M^{\alpha})^{-1} M^{\alpha} \mathbf{s}(\mathbf{r}') \tag{3.6}$$

where $\mathbf{r}$, $\mathbf{r}'$ label lattice sites. Note that the particular element of the group, α, employed, is taken to be independent of $\mathbf{r}$, and the resulting Hamiltonian is invariant under this *global* transformation (3.5).

Now let us consider a more general form of interactions between generalized spins residing at the lattice sites $\mathbf{r}$, $\mathbf{r}'$, which may depend not only on the lattice sites $\mathbf{r}$, $\mathbf{r}'$, but also on the internal states of the spins at those sites, and must have the matrix form $\psi_{kl}(\mathbf{r}, \mathbf{r}')$ where k, l label the internal states of the spins at $\mathbf{r}$, $\mathbf{r}'$. In matrix notation,

$$H = -J \sum_{(\mathbf{r}, \mathbf{r}')} \mathbf{s}^{\dagger}(\mathbf{r}) \psi(\mathbf{r}, \mathbf{r}') \mathbf{s}(\mathbf{r}') \tag{3.7}$$

The simplest example is again the Ising model, where

$$\mathbf{s}(\mathbf{r}) = \begin{pmatrix} 1 \\ 0 \end{pmatrix} \text{ or } \begin{pmatrix} 0 \\ 1 \end{pmatrix}$$

and (3.8)

$$\psi(\mathbf{r}, \mathbf{r}') = \begin{pmatrix} 1 & 0 \\ 0 & 1 \end{pmatrix} \text{ or } \begin{pmatrix} 0 & 1 \\ 1 & 0 \end{pmatrix}$$

the first giving rise to FM, the second to AFM interactions. If the spins in (3.7) are Potts spins as defined in eq. (3.4), and the $\psi(\mathbf{r}, \mathbf{r}')$ then elements of the group of permutations of q objects (traceless except for the identity element), the Hamiltonian (3.7) represents a random vector Potts model (1). (Nishimori and Stephen 1983. These authors use a one dimensional representation of the symmetry group).

These (matrix) variables $\psi(\mathbf{r}, \mathbf{r}')$ which can be thought of as residing on the bonds connecting the lattice sites $\mathbf{r}$, $\mathbf{r}'$, we shall call gauge variables. They, in turn, transform under *gauge transformations*, which one can write

$$\psi'_{mn}(\mathbf{r}, \mathbf{r}') = \sum_{kl} M^{\alpha(\mathbf{r})}_{mk} \psi_{kl}(\mathbf{r}, \mathbf{r}') (M^{\alpha(\mathbf{r}')}_{ln})^{-1} \qquad (3.9)$$

Note that here one has the extra freedom of allowing the particular element α of the symmetry group to depend on $\mathbf{r}$, $\mathbf{r}'$. One may

---

(1) In Nishimori and Stephen's (1983) notation, the Hamiltonian is given by

$$H = -J \sum_{(ij)} \delta(\sigma_i - \sigma_j + r_{ij}) = -\sum_{(ij)} \sum_{p} J^p_{ij} \exp(2\pi i(\sigma_i - \sigma_j) p/q)$$

where $J_{ij} = \exp(2\pi i r_{ij}/q)$, $r_{ij} = 0, 1, \ldots q-1$ may have any desired distribution. Clearly, $r_{ij} = 0$ reduces to the FM Potts model. $r_{ij} \neq 0$ constrains spins on adjacent sites i, j to be in states differing by r_{ij}. The AFM Potts model is equivalent to taking

$$H = \sum_{(ij)} \sum_{r \neq 0} \sum_{p} J^p_{ij} \exp(2\pi i(\sigma_i - \sigma_j) p/q)$$

(This model also correctly reduces to the Ising model for $q = 2$). The cyclic matrices ψ in the matrix representation above are given explicitly by $\psi_{kl}(ij) = \delta_{k, l+r_{ij}}$, $l + r_{ij} = l + r_{ij} - q$; $r_{ij} = 0, \ldots q-1$; $k, l = 1, \ldots q$.

construct scalars from these gauge variables, that will be invariant under the *(local)* gauge transformation (3.9). The simplest such scalar is the *trace* of products of $\psi(\mathbf{r}, \mathbf{r}')$, such that $\mathbf{r}_1, \mathbf{r}_2, \ldots$ form a closed loop, and where we have again taken M to be unitary (Kadanoff 1976); see Fig. 6.

$$\hat{f}_\Gamma(\psi) = \mathrm{Tr}\ \psi(\mathbf{r}_1, \mathbf{r}_2)\ \psi(\mathbf{r}_2, \mathbf{r}_3) \ldots \psi(\mathbf{r}_n, \mathbf{r}_1)$$
$$= \mathrm{Tr}\ M^{\alpha(\mathbf{r}_1)}\ \psi(\mathbf{r}_1, \mathbf{r}_2)\ (M^{\alpha(\mathbf{r}_2)})^{-1} M^{\alpha(\mathbf{r}_2)} \ldots \psi(\mathbf{r}_n, \mathbf{r}_1)\ (M^{\alpha(\mathbf{r}_1)})^{-1} \tag{3.10}$$

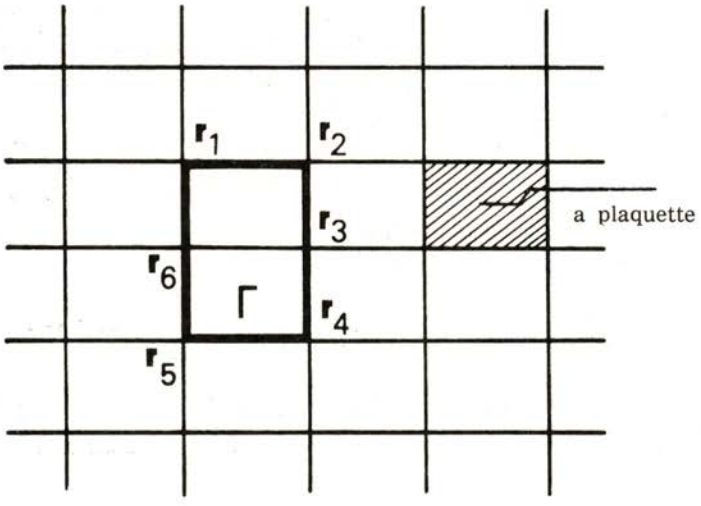

Fig. 6 — Γ labels the path formed by the bonds $(\mathbf{r}_1, \mathbf{r}_2)$, $(\mathbf{r}_3, \mathbf{r}_3) \ldots (\mathbf{r}_6, \mathbf{r}_1)$. See Eq. (3.10).

The smallest such loop Γ that may be formed on any given lattice is what is called a plaquette. Therefore, the simplest gauge-invariant objects we can construct out of the gauge variables, live on plaquettes (as opposed to the functions (3.6) formed from spin variables, which are invariant under global transformations, and live on bonds).

In the case of the Potts model ([1]) (with $q > 1$) let us define

$$\phi_p \equiv (\mathrm{Tr} \prod_p \psi - 1) / (q - 1) \tag{3.11}$$

where $\prod_p \psi$ denotes the (matrix) product of the ψ variables around the plaquette p. The function ϕ_p may be taken as the frustration function for the (vector) Potts model (1) with

$$\phi_p = \begin{cases} -1/(q-1) & \text{plaquette frustrated} \\ 1 & \text{" unfrustrated.} \end{cases}$$

Obviously, ϕ_p is invariant under the transformation (3.9). For $q = 2$, ϕ_p reduces to the plaquette frustration function as defined by Toulouse (1977) using a one dimensional representation of the symmetry group Z_2 of the Ising model (2).

Symmetries of the Partition Function

After Kadanoff (1976) we shall call those representations of the symmetry groups of the spin and gauge variables *simple*, where one may write

$$\operatorname{Tr}_s f(\mathbf{s}) = \sum_\alpha f(M^\alpha \mathbf{s})$$

and (3.12)

$$\operatorname{Tr}_\psi \hat{f}(\psi) = \sum_\alpha \hat{f}(M^\alpha \psi)$$

where f, $\hat{f}$ are some function of the variables. Thus, if we have chosen simple representations for our spin and gauge variables,

---

(1) Clearly this choice is not unique.

(2) In taking such a one dimensional representation of the symmetry group Z_N, the form of Eq. (3.9) should be kept in mind, since it implies a constraint on the transformations that may be performed on a string of gauge variables forming a loop. E.g., in Fig. 1a, b, 'flipping' all the bonds simultaneously (multiplying each bond by -1) is not an allowed gauge transformation, as will be immediately seen if one takes care to write

$$J'_{ij} = M(i)\, J_{ij}\, M(j)^{-1}$$

where $i, j = 1, 2, 3$ are the vertices of the triangle, $M(i) = \pm 1$, $M(i)^{-1} = M(i)$. However, Fig. 1 a and b *are* related by a gauge transformation, where $M(1) = M(2) = -1$, $M(3) = 1$. Notice that the frustration function for this loop is again invariant under this transformation.

we may write the partition function of a quenched random bond system as

$$Z = \sum_{\{\alpha(r)\}} \exp\left[K \sum_{(r,\, r')} \mathbf{s}(\mathbf{r})^{\dagger} \left(M^{\alpha(r)}\right)^{-1} \psi(\mathbf{r}, \mathbf{r}') \, M^{\alpha(r')} \, \mathbf{s}(\mathbf{r}')\right] \tag{3.13}$$

where $K = \beta J$.

Now notice that Z is invariant under the set of gauge transformations (eq. 3.9)

$$\psi(\mathbf{r}, \mathbf{r}') \rightarrow M^{\alpha(r)} \, \psi(\mathbf{r}, \mathbf{r}') \, \left(M^{\alpha(r')}\right)^{-1}.$$

Thus we have our first result that the partition functions of two spin systems on lattices whose bond configurations may be obtained one from the other by a set of transformations (3.9) for some $\{\alpha(\mathbf{r})\}$, are equal (Fradkin et al. 1978).

A further symmetry of the partition function and, furthermore, of the (field free) *Hamiltonian*, is given by the following local transformation that affects not only the gauge variables impinging upon a particular site $\mathbf{r}$, but also the spin variable at that site

$$\begin{aligned} \psi(\mathbf{r}, \mathbf{r}') &\rightarrow M^{\alpha(r)} \, \psi(\mathbf{r}, \mathbf{r}') \, I \\ \mathbf{s}(\mathbf{r}) &\rightarrow \mathbf{s}(\mathbf{r}) \, \left[M^{\alpha(r)}\right]^{-1} \end{aligned} \tag{3.13a}$$

where I is the identity matrix. (In the more familiar language of the Ising model, this would, for example, correspond to reversing the sign of all the bonds impinging on $\mathbf{r}$, and redefining the spin at $\mathbf{r}$ such that $s \rightarrow -s$). This *mixed* transformation is not needed for the development in this section, but in Section IV, when dealing with correlation functions, we will see that the correlation functions $< s(\mathbf{r}) \, s(\mathbf{r}') >$ are not invariant under a mixed gauge transformation performed at the site $\mathbf{r}$ or $\mathbf{r}'$, and therefore we have to consider slightly more generalized objects.

It follows immediately from this invariance, that the partition function of a quenched random bond system must depend only on those sets of quantities (constructed from gauge variables) that are scalars under such transformations, and the partition function may be labeled by this set of quantities. We have already constructed such a quantity in Eqs. (3.10, 3.11) and for q-state Potts models we have shown that it is the direct generalization

of the frustration function of Toulouse for the Ising case. Thus, for a quenched random system we way write

$$Z = Z \{ \phi_p \} \tag{3.14}$$

where p runs over all the plaquettes of the lattice. This is a rather remarkable fact. In particular, it leads, e.g. on the square lattice, to the simplification, that one may treat, instead of a system with a completely random distribution (magnitudes being held fixed), one where, say, the horizontal bonds are taken to be all of the same sign, and the vertical bonds are chosen randomly, since any distribution of ϕ_p may be realized in this way (Hoever et al. 1981a).

Another immediate consequence of Eq. (3.13) is that Z can be written

$$Z = \sum_{\{\alpha(r)\}} \exp \left[K \sum_{(r,r')} \mathbf{s}_0^{\dagger} (M^{\alpha(r)})^{-1} \psi (\mathbf{r}, \mathbf{r}') \; M^{\alpha(r')} \; \mathbf{s}_0 \right] \tag{3.15}$$

where $\mathbf{s}_0$ is an arbitrarily chosen state of the variables $\mathbf{s}(\mathbf{r})$, which leads to (via Eq. 3.12)

$$Z \{ \phi_p \} = \Omega_M \sum_{\{\psi\}}{}' \exp \left[K \sum_{(r,r')} \mathbf{s}_0^{\dagger} \psi (\mathbf{r}, \mathbf{r}') \; \mathbf{s}_0 \right] \tag{3.16}$$

where Ω_M is the 'volume' of the group of transformations M at each site (e.g. for the Z_2 symmetric Ising model, this is just 2^N), and where the prime on the sum indicates that the sum over the ψ is restricted to those configurations of ψ that give the same distribution of plaquette functions ϕ_p. Without this constraint, we clearly have the partition function of the *annealed* system. We may express this constraint by means of delta functions, viz.,

$$\begin{aligned} Z \{ \phi_p \} = \Omega_M \sum_{\{\psi\}} \Big\{ & \prod_p \delta \left[\phi_p - (\mathrm{Tr} \prod_p \psi - 1) / (q - 1) \right] \\ & \cdot \exp \left[K \sum_{(r,r')} \psi_{00} (\mathbf{r}, \mathbf{r}') \right] \Big\} \end{aligned} \tag{3.17}$$

where $\psi_{00} = \mathbf{s}_0^{\dagger} \psi \; \mathbf{s}_0$. If we can construct some $\tilde{f}_p$ such that

$$\begin{aligned} \tilde{f}_p > 0 \quad & \phi_p = (\mathrm{Tr} \prod_p \psi - 1) / (q - 1) \\ \tilde{f}_p < 0 \quad & \phi_p \neq (\mathrm{Tr} \prod_p \psi - 1) / (q - 1) \end{aligned} \tag{3.18}$$

the ψ being the integration variables and ϕ_p now a fixed set of numbers for the plaquettes p, then we could write (Fradkin et al. 1978)

$$Z\{\phi_p\} = \Omega_M \lim_{K_p \to \infty} \sum_{\{\psi\}} \exp\left[K \sum_{r,r'} \psi_{00}(r, r') + K_p \sum_p \tilde{f}_p \right] \quad (3.19)$$

For the Potts model, with definition (3.11), we may take

$$\tilde{f} = \phi_p \left(\mathrm{Tr} \prod_p \psi - 1 \right) / (q-1) \quad (3.20)$$

Notice that this has the interesting (and foreseeable) consequence that as $q \to \infty$, those configurations which are frustrated contribute to Z with a vanishing weight compared to those that are not, i.e., in this limit, with $K_p \to \infty$, the model becomes completely unfrustrated.

Some comments as to the consequences of Eq (3.19) are in order. For instance, Toulouse and Vannimenus (1980) have proposed a 'restricted annealing scheme' where, instead of inserting the delta-functions in Eq. (3.17), one takes

$$Z = \Omega_M \sum_{\{\psi\}} \exp\left[K \sum_{r,r'} \psi_{00} + K_p \sum_p \phi_p \right] \quad (3.21)$$

with the constraint that

$$\partial \ln Z / \partial K_p = \left\langle \sum_p \phi_p \right\rangle = 0 \quad (3.22)$$

($K_p = 0$ is, of course, the annealed model). In the Ising case, which they treat, this corresponds to a constrained – annealed system with an equal number of frustrated and unfrustrated plaquettes. Since this is also expected to be true of the quenched model with an equal number of $\pm$ bonds, on the average, this provides a first order approximation to the properties of the quenched system. With our definition of the frustration function for the Potts model, this same approximation holds true, for a distribution of couplings (in the one dimensional representation) given by

$$\begin{aligned} J_{ij} &= J && \text{with probability} && p \\ J_{ij} &= J \exp(2\pi i r / q) && \text{"} && \text{"} && (1\text{-}p) / (q\text{-}1) \\ & && (r = 1, 2, \ldots, q\text{-}1) && && (3.23) \end{aligned}$$

The solution of Eq. (3.22) in the space of K, K_p (a solution exists only for $K_p < 0$) defines a subset, then, of models with spin and gauge coupling terms, which approximate the quenched random frustrated spin models in some sense. Note that the limit $K_p \to \infty$ gives the pure Potts partition function. The limit $K_p \to -\infty$ gives the *fully* frustrated system. The line (3.22) interpolates between the annealed and the fully frustrated cases (Toulouse and Vannimenus 1980, Toulouse 1980). It would be interesting to work out how this line actually behaves for different models in d dimensions. Toulouse and Vannimenus (1980) ask the question whether it intersects any phase transition lines in the K, $-K_p$ space. This would be an approximation to a SG transition. One would also like to know if there is another transition on the $K_p \to -\infty$ line and whether the $< \Sigma_p \phi_p > = 0$ line comes close to this in some way, as, say, the dimensionality is raised. Do the two transitions (if there are two) merge? This would be a step in the direction of the conjecture of Alexander and Pincus (1980) that the SG transition might become 'like' a transition in ff systems at high enough dimensionality.

Quenched Averages

Clearly, now, the task of taking 'quenched averages', or averaging the observables over all possible realizations of the (bond) randomness is simplified to a great extent, since one does not have to take into account each such possible realization but only those that differ from each other in a gauge invariant way, namely, those that give rise to distinct distributions of the generalized frustration function ϕ_p. These configurations will then have to be weighted by the probability of occurence of $\{ \phi_p \}$ namely by $P\{ \phi_p \}$, given a certain distribution $P\{ \psi \}$. Let us write this (Fradkin et al. 1978, Schuster 1979)

$$< Q > = \sum_{\{\phi_p\}} P\{ \phi_p \}\, Q\{ \phi_p \} \tag{3.24}$$

where Q is any gauge independent quantity, and $<>$ indicates a quenched average. Now one has to determine $P\{ \phi_p \}$. Let us

assume that each bond (gauge) variable is distributed independently with a probability $p_{r\ r'}(\psi)$. Then,

$$P\{\phi_p\} = \sum_{\{\psi\}}' P\{\psi\} / \sum_{\{\psi\}} P\{\psi\}$$

$$= \sum_{\{\psi\}}' \prod_{(r,r')} p_{r,r'}(\psi) / \sum_{\{\psi\}} \prod_{(r,r')} p_{r,r'}(\psi)$$

$$= \sum_{\{\psi\}}' \exp\left[\sum_{(r,r')} \ln p_{r,r'}(\psi)\right] / \sum_{\{\psi\}} \exp\left[\sum_{(r,r')} \ln p_{r,r'}(\psi)\right]$$

where the prime indicates that the sum includes only those configurations of ψ that give rise to $\{\phi_p\}$. Let us again consider

$$f_0 \equiv s_0\ \psi(r, r')\ s_0$$

Notice that if we have a distribution for the ψ such that $p_{r,r'}(\psi)$ is independent of r, r', and for example,

$$p(\psi) = \tilde{p}(f_0) = \begin{cases} x & f_0 = 1 \\ x-1 & f_0 = 0 \end{cases} \tag{3.25}$$

we may write,

$$\tilde{p}(f_0) = \rho^{1/2} \exp[K_f (f_0 - 1/2)] \tag{3.26}$$

where,

$$\rho = x(1-x)\ ,\quad K_f = \ln[x/(1-x)] \tag{3.27}$$

with the result that

$$P\{\phi_p\} = \sum_{\{\psi\}}' \exp\left[K_f \sum_{r,r'} f_0(r,r')\right] / \sum_{\{\psi\}} \exp\left[K_f \sum_{r,r'} f_0(r,r')\right] \tag{3.28}$$

Factors of $\rho \exp(-K_f)$ have cancelled from the numerator and denominator: One immediately sees that $P\{\phi_p\}$ is nothing but the ratio of the partition functions of the original spin system in the fixed gauge with all the $s(r) = s_0$ (see Eq. 3.16), i.e.,

$$P\{\phi_p\} = Z\{\phi_p\}_{K_f} / \sum_{\{\phi_p\}} Z\{\phi_p\}_{K_f} \tag{3.29}$$

with the effective coupling constant (temperature) given by Eq. (3.27) (Fradkin et al. 1978, Schuster 1979).

Nishimori (1981) has noticed that this form of $P\{\phi_p\}$ together with Eq. (3.24) allows one to rigorously calculate the internal energy, and obtain bounds on the specific heat and correlation functions, on a subspace of the phase diagram given by $K_f = K$. This leads to constraints on the form of the PM - SG - FM phase boundaries. (Nishimori 1981, Nishimori and Stephen 1983).

To calculate $P\{\phi_p\}$ is not a trivial matter. In the next section, we will see that if $\{\phi_p\}$ has n frustrations, this task is equivalent to calculating an n-point correlation function in the system dual to the original system. This is certainly no great simplification! However, there are certain results that are accessible, as we shall see.

IV — DUALITY TRANSFORMATIONS

Duality is essentially a geometrical concept. Since we are dealing with statistical mechanical models on lattices, it is useful to introduce the notion of a *simplex* as an s dimensional element of the lattice in d dimensions. Thus, a point (vertex) has simplex number 0, a bond (edge) has simplex number 1, a plaquette 2, and an elementary volume, simplex number 3, etc. The *dual* to any lattice can be constructed by 'intersecting' each element of simplex number s of the original lattice by a simplex of dimensionality $\tilde{s} = d - s$. (It is easy to convince oneself, that for a hypercubic lattice, where the dual can be obtained simply by displacing the lattice by 1/2 the lattice spacing in the (111...) direction, the above scheme holds. Thus, e.g., in 3d, each vertex ($s = 0$) of the original lattice is surrounded by a cube ($\tilde{s} = 3$), each bond ($s = 1$) is intersected by a plaquette ($\tilde{s} = 2$) and each plaquette ($s = 2$) is in turn intersected by a bond of the dual lattice ($\tilde{s} = 1$) etc.) (Savit 1980).

Statistical mechanical models may be characterized by a simplex number s (Savit 1980, Toulouse 1980). The terms appearing in the Hamiltonian — invariants constructed from objects (spins, gauge variables etc.) living on simplices of dimension s — are

obtained by multiplying together such objects bounding a simplex of dimension $s+1$, on the given lattice. Thus in Eq. (3.6), spin-spin interactions involve a product of spins at the two ends of a bond, and the invariant constructed from gauge variables (Eq. 3.10) involves a product of gauge variables around a plaquette of the given lattice.

Duality transformations are exact transformations that map a theory with simplex number s into one with simplex number $\tilde{s} = d - s$, in such a way that the partition functions of the two theories are simply proportional to each other, with a temperature dependent proportionality factor, and the temperature (coupling constant) of the dual theory is a monotone decreasing function of the first (In those theories that are self-dual – e.g. the Ising and Potts models on square lattices – this provides a unique way of determining the critical temperature).

Duality transformations for the Ising model (Kadanoff and Ceva 1971, Wegner 1971), Ising model with gauge coupling term (Balian et al. 1975), models with Z_N and U (1) symmetry (Savit 1980) and the ordinary Potts model (Wu 1982) have already been extensively treated in the literature. What I propose to do here is to illustrate the basic ideas by deriving the duality transformation for the 2d Ising model with a gauge coupling term (The generalization of this to vector Potts models is given in the Appendix). Then I will discuss the concept of *disorder variables* and show how the partition function of a model with *n frustrations* (Eq. 3.29) is related to an n-point (disorder-disorder) *correlation function* in the dual model. I will then consider *gauge invariant correlation functions* and a few remarks about their asymptotic behaviour and phase transitions will follow.

The Two-Dimensional Ising model

Following Balian et al. (1975) let us consider the partition function in Eq. (3.19) with a finite gauge coupling constant K_p. We may represent the gauge variables by $A_{ij} = \pm 1$ in this case, and write, with the choice all $s_i = 1$, up to numerical factors,

$$Z = \sum_{\{A_{ij}\}} \exp\left[K \sum_{(ij)} A_{ij} + K_p \sum_p \prod_p A_{ij} \right] \tag{4.1}$$

where $\Pi_p A_{ij}$ indicates a product of the gauge variables around the plaquette p, and Σ_p runs over all plaquettes. Note that we have set all the frustration functions $\phi_p = 1$ for the time being, i.e., we are dealing with an unfrustrated system. Writing

$$\begin{aligned} \exp(KA_{ij}) &= \cosh K\ (1 + A_{ij} \tanh K) \\ \exp(K_p \prod_p A_{ij}) &= \cosh K_p\ (1 + \prod_p A_{ij} \tanh K_p) \end{aligned} \tag{4.2}$$

Z becomes

$$\begin{aligned} Z = (\cosh K)^E\ (\cosh K_p)^N \sum_{\{A_{ij}\}} \prod_l (1 + A_{ij} \tanh K) \\ \tilde{\prod_p}\ (1 + \prod_p A_{ij} \tanh K_p) \end{aligned} \tag{4.3}$$

where N and E are the total number of sites and edges on the lattice, $\tilde{\Pi}_p$ denotes a product over all plaquettes and Π_l denotes a product over all links (i, j). We may represent the result of expanding the products as a sum over graphs G on a lattice consisting of all distributions of plaquettes p and edges l on the lattice, $\mathcal{L}$,

$$\begin{aligned} &\prod_l (1 + A_{ij} \tanh K)\ \tilde{\prod_p}\ (1 + \prod_p A_{ij} \tanh K_p) \\ &= \sum_{G \subset \mathcal{L}} \prod_{l \subset G} A_{ij} \tanh K \tilde{\prod_{p \subset \mathcal{L}}} (\Pi_p A_{ij}) \tanh K_p \end{aligned} \tag{4.4}$$

Now it is easy to see that as a result of the trace in Eq. (4.3), only those terms will survive where each plaquette edge is shared between two plaquettes, or coincides with a link l, and is not shared by other plaquettes. This gives

$$Z = (\cosh K)^E\ (\cosh K_p)^N \sum_{G \subset \mathcal{L}} (\tanh K)^L\ (\tanh K_p)^P \tag{4.5}$$

where P is the total number of such plaquettes and L the total length of the boundary of the clusters of plaquettes, i.e., the total number of plaquette edges that belong to only one plaquette. Now we can construct $\mathcal{L}_D$, the dual graph to $\mathcal{L}$, and make a one to one correspondance with spin variables located on $\mathcal{L}_D$ with the

graphical elements of G. Thus we shall stipulate that if a plaquette on $\mathcal{L}$ belongs to G, then a spin residing at the site dual to this plaquette on $\mathcal{L}_D$, has the value $s_{\tilde{i}} = -1$, and if not, $s_{\tilde{i}} = +1$. Thus we have

$$P = \sum_{\tilde{i}} (1 - s_{\tilde{i}}) / 2 \tag{4.6}$$

where $\tilde{i}$ now runs over the sites of $\mathcal{L}_D$. This gives us automatically

$$L = \sum_{(\tilde{i}, \tilde{j})} (1 - s_{\tilde{i}} s_{\tilde{j}}) / 2 \tag{4.7}$$

where the $(\tilde{i}, \tilde{j})$ are the adges of $\mathcal{L}_D$, and each of them intersects an edge of $\mathcal{L}$. Clearly, Eq. (4.7) holds, because the product $s_{\tilde{i}} s_{\tilde{j}}$ is positive for $(\tilde{i}, \tilde{j})$ crossing any link on $\mathcal{L}$ that is shared by two plaquettes on G, and is only negative if this link happens to be on the boundary of a cluster of plaquettes on G. Finally we have

$$Z = (\cosh K)^E (\cosh K_p)^N \Sigma_{s_{\tilde{i}}} \{ \exp [1/2 \ln \tanh K \sum_{\tilde{i}\,\tilde{j}} (1 - s_{\tilde{i}} s_{\tilde{j}})] \cdot \exp [1/2 \ln \tanh K_p \sum_{\tilde{i}} (1 - s_{\tilde{i}})] \}$$

which we may write

$$Z = (\cosh K)^E (\cosh K_p)^N \cdot \sum_{\{s_{\tilde{i}}\}} \exp [K^* \sum_{(\tilde{i}\,\tilde{j})} (s_{\tilde{i}} s_{\tilde{j}} - 1) + h \sum_{\tilde{i}} (s_{\tilde{i}} - 1)] \tag{4.8}$$

where

$$\begin{aligned} K^* &= -1/2 \ln \tanh K \\ h &= -1/2 \ln \tanh K_p \end{aligned} \tag{4.9}$$

are the dual couplings (inverse temperatures). Observe that the term in Eq. (4.1), of simplex number 1 has given rise to another such term, and the gauge coupling ($s = 2$) has given rise to a field term, with $\tilde{s} = d - 2 = 0$. The transformation in 3d proceeds in like manner (Balian et al. 1975) where now the terms of the form $\Sigma_{ij} A_{ij}$ generate plaquette couplings and vice versa.

endpoints. It is easy to convince oneself that it is possible to deform this path arbitrarily, by performing a series of gauge transformations on the dual lattice. However, the correlation functions, unlike the partition function, are *not* invariant under the full mixed transformation, Eq. (3.13a). performed on the gauge variables impinging on $\tilde{i}$ or $\tilde{i} + r$ and the spins at these points.

In the more familiar language of the Ising model, the transformation

$$s_{\tilde{i}} \to (-1)\ s_{\tilde{i}}$$

$$A_{\tilde{i},\,\tilde{i}+\mu} \to (-1)\ A_{\tilde{i},\,\tilde{i}+\mu}$$

gives out a factor of (-1) in front of Eq. (4.18) (Fradkin et al. 1978, Savit 1980).

Gauge Invariant Correlation Functions

Having obtained a recipe (Eq. 3.24) for calculating quenched averages of gauge invariant quantities, let us proceed to construct the gauge invariant correlation functions for the Ising model in two and three dimensions. In two dimensions one has,

$$\langle s_i \prod_{\Gamma_{ij}} A_{kl}\, s_j \rangle \quad \xrightarrow[\text{in a system with n frustrations}]{\text{Duality}} \quad \begin{array}{l}\text{n-point correlation function in a system with two frustrations at the plaquettes dual to i, j.}\end{array} \tag{4.23}$$

where Γ_{ij} is now a *closed loop* going through the points i, j (Fradkin et al. 1978, Savit 1980). In three dimensions, the correlation function

$$\langle \Pi_p\ A\ \Pi_{p'} A \rangle$$

where p, p′ are two different plaquettes is a gauge invariant quantity. But it turns out that the following object leads to more interesting results. For a pure gauge coupling theory, take any *loop* Γ and take the product of the plaquette functions lying on

any surface bounded by this loop. In the Ising case, with $A_{ij}^2 = 1$ clearly only the gauge variables lying on the loop Γ itself survive. The correlation function

$$< \prod_{\Gamma} A > \xrightarrow{\text{Duality}} \frac{\text{Partition function of the 3d Ising spin system with all the bonds intersecting the surface bounded by } \Gamma, \text{ reversed.}}{\text{Partition function of the unfrustrated system.}} \tag{4.24}$$

Fradkin et al. 1978, Savit 1980). Note that the configuration of bonds described in the numerator of the RHS of (4.24) corresponds, for a system originally without frustrations, to the creation of a closed loop of frustrations threaded by Γ. The from of Eq. (4.24) again allows one to calculate the excess free energy due to such a closed tube of frustrations, the simplest configuration of frustrations possible in 3d. In the high and low temperature limits. respectively, of the dual (gauge) model, one has

$$\Delta F \sim \begin{cases} \alpha_1 \, A_\Gamma / K & K > K_c \\ \alpha_2 \, L_\Gamma / K & K < K_c \end{cases} \tag{4.25}$$

where α_1, α_2 are temperature dependent coefficients, A_Γ and L_Γ are the minimal area enclosed by Γ and the perimeter of Γ. K_c is the critical coupling of the 3-d Ising model (Fradkin et al. 1978).

Phase Transitions in the Frustration System

Let us go back to the probability of finding a certain configuration of frustrations in an ensemble of random configurations of bonds. Consider the normalized probability (Schuster 1979)

$$P\{\phi_p\} / P\{\phi \equiv 1\} = Z\{\phi_p\}_{K_f} / Z\{\phi \equiv 1\}_{K_f} \tag{4.26}$$

by Eq. (3.29). Clearly, the RHS is the same as Eq. (4.13), for a 2d Ising system, with K_f being the dual temperature to K^*.

path $\Gamma_{\tilde{i},\tilde{i}+r}$ on the dual lattice gives rise to two frustrations precisely at those plaquettes dual to $\tilde{i}$ and $\tilde{i}+r$. This construction can be generalized to any 2n-point correlation function. Paths connecting these points pairwise will give rise, in the dual lattice, to n pairs of frustrations (Fradkin et al., Savit 1980). Thus we are back to the picture in the previous subsection, Eq. (4.13) and the following paragraph. Note, however, the added twist: the disorder-disorder correlation function of the Ising model in 2d is found to be equal to the partition of the model with frustrations located at the plaquettes dual to the disorder variables, normalized by the partition function of the unfrustrated model. One could equally well say that the disorder variables act as *sources* and *sinks* of *defects* within an ordered system (see Fig. 7). On the

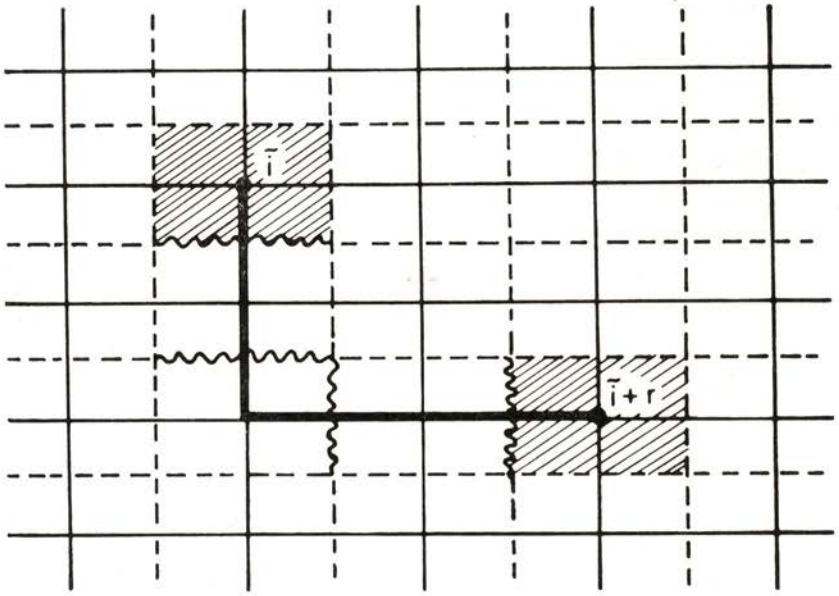

Fig. 7 — A path (heavy line) $\Gamma_{\tilde{i},\tilde{i}+r}$ connects the disorder variables $\sigma_{\tilde{i}}$, $\sigma_{\tilde{i}+r}$ on the original lattice. The dual lattice (dashed lines) has the signs of the links dual to Γ reversed (wiggly lines). The shaded plaquettes on the dual lattice are frustrated.

dual system, the dual path of reversed couplings costs ground state energy proportional to the length of the path Γ (see Fradkin et al. for a detailed discussion).

In the 2d Potts model, a similar (though not quite identical) picture emerges. The relevant two point correlation function is

$$(q-1)^{-1} \cdot < q\,\delta_{\sigma_{\tilde{i}}\,\sigma_{\tilde{i}+r}} - 1 > = Z^{-1} \sum_{\tilde{G} \subset \mathcal{L}} u^{b(\tilde{G})}\, q^{n(\tilde{G})} \tag{4.20}$$

where $u = e^K - 1$, $\tilde{G}$ are all possible graphs in $\mathcal{L}$, consisting of points and edges such that they contain a continuous path connecting the points $\tilde{i}$, $\tilde{i} + r$, $b(\tilde{G})$ and $n(\tilde{G})$ are the number of edges and connected parts of $\tilde{G}$, respectively. Performing the duality transformation on the RHS of (4.20), one obtains

$$(q-1)^{-1} \cdot < q\,\delta_{\sigma_{\tilde{i}}\,\sigma_{\tilde{i}+r}} - 1 > = Z^{-1}\, q^N \sum_{\tilde{D} \subset \mathcal{L}_D} (u^*)^{b(\tilde{D})}\, q^{n(\tilde{D})} \tag{4.21}$$

where $u = e^{K^*} - 1$; $K^*(K)$ being given by Eq. (10) of the Appendix. The graphs $\tilde{D}$ on the dual lattice $\mathcal{L}_D$ now contain all possible graphs which have a seam of missing links between the plaquettes dual to $\tilde{i}$ and $\tilde{i} + r$ (the seam being dual to the path connecting $\tilde{i}$, $i + r$ in $\tilde{G}$).

The extension of the above considerations to the 3d Ising model is also given in Savit (1980). One finds, upon performing a duality transformation on the correlation function $< \sigma_{\tilde{i}}\ \sigma_{\tilde{i}+r} >$ that

$$< \sigma_{\tilde{i}}\ \sigma_{\tilde{i}+r} > \xrightarrow{\text{Duality}} \frac{\text{Partition function of the gauge coupling theory where for all the plaquettes pierced by a path connecting } \tilde{i}, \tilde{i}+r, \; K_p \to -K_p:}{\text{Partition function of the frustration free gauge theory.}} \tag{4.22}$$

with the disorder variables again acting as sources and sinks of a line of defects, this time in the dual gauge system.

The correlation functions (4.18) and (4.22) are clearly independent of the position of the paths Γ apart from their

be in the direction 1. The coupling constants have been normalized by a constant factor $q/(q-1)$.

Replacing an unfrustrated plaquette by a frustrated one now involves the replacement

$$K_p \to -K_p/(q-1)\,.$$

at that plaquette (Eq. 3.11). Taking the limit $K_p \to \infty$, one sees that at the site dual to this plaquette

$$h \to \ln(q-1) - i\pi\,,$$

giving a factor, in the partition function, that is precisely

$$\exp\{[\ln(q-1) - i\pi]\,\delta_{\sigma_{\tilde{i}},1}\} = 1 - q\,\delta_{\sigma_{\tilde{i}},1}\,.$$

At the sites dual to the unfrustrated plaquettes ($K_p > 0$), $\lim_{K_p \to \infty} h(K_p) = 0$. Once more, we have

$$\lim_{K_p \to \infty} Z\{\phi_p\}_{K,K_p} / Z\{\phi_p = 1\}_{K,K_p} \tag{4.15}$$

$$= \lim_{K_p \to \infty} \langle \prod_{\tilde{i}} (q\,\delta_{\sigma_{\tilde{i}},1} - 1) \rangle_{K^*(K)} \exp nK_p(2-q)/(q-1)$$

where the product runs over the sites dual to the frustrated plaquettes and n is the number of frustrations. Note that the RHS of Eq. (4.15) is in the usual form of an n-point correlation fuction for the Potts model, in the absence of a field, at the uniform coupling given by $K^*(K)$.

Disorder Variables

Let us take a step back and consider how the dual variables are related to the original ones. To do this, it is instructive to go back to Eq. (4.1) and rewrite it in terms of spin variables. Let us set the plaquette coupling to zero. Then, from Eqs. (4.1) and (4.8),

$$Z = \sum_{\{s_i\}} \exp[K \sum_{(ij)} s_i\, s_j]$$

$$= 2^{N-1}\,(\cosh K)^E \sum_{\{\sigma_i\}} \exp[K^* \sum_{\tilde{i}\,\tilde{j}} (\sigma_{\tilde{i}}\,\sigma_{\tilde{j}} - 1)] \tag{4.16}$$

where we have denoted the dual spin variables by $\sigma_{\tilde{i}}$. Not that there is no one to one correspondance between the configurations of the s and the σ (Savit 1980). However, the relationship (4.9) maps the high temperature region of one model into the low temperature region of its dual. If there *is* a phase transition to an ordered phase, the critical temperature for this self dual model is uniquely given by

$$K_c = -1/2 \ln \tanh K_c \tag{4.17}$$

Moreover, for $K > K_c$ ($K^* < K_c$) the order parameter $<s> \neq 0$ ($<\sigma> = 0$) and vice versa. Thus in the temperature region that s is disordered, σ is ordered, and vice- versa. With K^* as a function of K (Eq. 4.9) we can call $<\sigma>_{K^*(K)}$ a *disorder parameter.* (Kadanoff and Ceva 1971, Fradkin et al. 1978, Savit 1980). The usefulness of this term will be more apparent when we consider the *disorder-disorder correlation function,* which is nothing but the correlation function of the dual variables at an inverse temperature $K^*(K)$.

$$<\sigma_{\tilde{i}}\,\sigma_{\tilde{i}+r}> = \sum_{\{\sigma_{\tilde{i}}\}} \exp\left[K^* \sum_{\tilde{i}\,\tilde{j}} (\sigma_{\tilde{i}}\,\sigma_{\tilde{j}} - 1)\right] \prod_{\Gamma_{\tilde{i},\tilde{i}+r}} \sigma_{\tilde{k}}\,\sigma_{\tilde{l}} \;/\; Z(K^*) \tag{4.18}$$

where $\Gamma_{\tilde{i}\,\tilde{i}+r}$ is any path connecting the points $\tilde{i}$, $\tilde{i}+r$ and $(\tilde{k}, \tilde{l})$ are links that lie on $\Gamma_{\tilde{i},\tilde{i}+r}$. (This particular cancellation, due to the fact that $(\sigma_{\tilde{i}})^2 = 1$ is of course peculiar to the Ising model.) Now we can again use the identity (4.12): notice that replacing K^* by $K^* - i\pi/2$ in Eq. (4.16) for those links lying on $\Gamma_{\tilde{i},\tilde{i}+r}$, will give precisely the numerator in Eq. (4.18). Now making the duality transformation on the RHS of Eq. (4.18) we find (with the cancellation in the numerator and denominator of spin independent terms)

$$<\sigma_{\tilde{i}}\,\sigma_{\tilde{i}+r}> = \sum_{\{s_i\}} \exp\left[\sum K_{ij}\, s_i\, s_j\right] \;/\; Z(K(K^*)) \tag{4.19}$$

where $K_{ij} = K(K^*)$ on all links except those dual to the path $\Gamma_{\tilde{i},\tilde{i}+r}$ where $K_{ij} = -K(K^*)$ (Kadanoff and Ceva 1971, Savit 1980). The situation is illustrated in Fig. 7. Observe that the insertion of negative couplings on those bonds intersecting the

The above calculation can be generalized, among, to Z_N models (Savit 1980; here they are called vector Potts models) where the Hamiltonian has the form

$$H_p = \sum_{(ij)} \cos\, 2\pi p\, (s_i - s_j + r_{ij}) / N \qquad (4.10)$$

where the s_i are now angle variables, taking on values $2\pi q / N$, $q = 0, \ldots N-1$; and to models with continuous symmetry, e.g., the x-y model (Savit 1980). However, the Z_N models are not self-dual, although the dual model also has Z_N symmetry (Savit 1980). Note, however, that our vector Potts model can be written as a *sum* of such models, in fact

$$H_{\text{vector Potts}} = \sum_{p=0}^{N-1} H_p$$

and it is also self-dual. The derivation of the duality relation proceeds very much like the standard Potts model (Wu 1982). I give a derivation of the duality relation in the gauge representation of the partition function, in the Appendix. Note that duality is a local transformation, so that non-uniform interactions, as in (4.10) can be easily accomodated.

Partition function of system with frustrations

Now let us return to Eq. (4.1). Recall from Eq. (3.19) that we could represent the partition function of a pure spin system with quenched — in frustrations by inserting in the gauge coupling term in Eq. (4.1) a set of numbers ϕ_p, such that $\phi_p > 0$ if the plaquette is unfrustrated and $\phi_p < 0$ if it is frustrated, and then taking the limit $K_p \to \infty$. In the present case, this would amount to nothing more than replacing K_p by $-K_p$ at those plaquettes where there is a frustration before taking the limit $K_p \to \infty$. The effect this has on the *dual* couplings (Eq. 4.9) is that the field at the sites dual to those plaquettes would be replaced by

$$h \to h - i\pi / 2 \qquad (4.11)$$

Inserting this in Eq. (4.8), and using the identity

$$\exp [\, i\pi (1 - s) / 2 \,] = s \qquad (4.12)$$

for $s = \pm 1$ we see that (for finite K_p)

$$Z\{\phi_p\} / Z\{\phi_p \equiv 1\} = \langle \prod_{\tilde{i}'} s_{\tilde{i}} \rangle_{K^*, h} \tag{4.13}$$

where the $\tilde{i}'$ are sites dual to the frustrated plaquettes (Kadanoff and Ceva 1971, Fradkin et al. 1978). (Note that if we had factored out the constant terms from Eq. (4.8) we would have gotten $\exp(-i\pi s/2) = -is$ giving out a factor of $(-i)^n$, n = number of frustrations, in front of the correlation function in Eq. 4.13)). In order to quench the frustrations, we can now take $K_p \to \infty$ ($h \to 0$)! Thus the partition function of an Ising model with n frustrations, normalized by the unfrustrated partition function, is equal to an n-point correlation function of the dual system (Fradkin et al. 1978).

Expression (4.13) also gives an immediate way of writing down the difference in free energies between a system with two frustrations and an unfrustrated system. Obviously

$$\begin{aligned} -\beta \Delta F &= \ln Z\{\phi_p\} - \ln Z\{\phi_p \equiv 1\} \\ &= \ln \langle \prod_{\tilde{i}'} s_{\tilde{i}} \rangle_{K^*, \lim h \to 0} \end{aligned} \tag{4.14}$$

and this gives us a way of defining an *effective interaction* between frustrations (Fradkin et al. 1978, Savit 1980) with the excess free energy due to two frustrations in an unfrustrated background, as a function of r, the seperation of the frustrations, going asymptotically as r (diverging) for $K^* < K_c$, and decaying exponentially with r for $K^* > K_c$.

The generalization to the Potts case is straightforward. One obtains the duality relations (see Appendix)

$$\begin{aligned} K^* &= -\ln [(e^K - 1)/(e^K + q - 1)] \\ h &= -\ln [(e^{Kp} - 1)/(e^{Kp} + q - 1)] \end{aligned}$$

where h is a field acting on the sites $\tilde{i}$ of the dual lattice, via a coupling of the form $h\, \delta_{\sigma_{\tilde{i}}, 1}$. Here the Potts spins are represented via the scalar variables $\sigma_{\tilde{i}}$, which take on values between 1 and q, and the field has been chosen (arbitrarily) to

THE LX RAY SPECTRUM OF ARGON, KRIPTON AND XENON (*)

M. T. RAMOS, J. G. FERREIRA, M. L. CARVALHO and L. SALGUEIRO

Departamento de Física, Faculdade de Ciências, Universidade de Lisboa
Av. Gama Pinto, 2 — 1699 Lisboa, Portugal

(Received 4 November 1983)

ABSTRACT — The LX-Ray spectrum of argon, kripton and xenon is interpreted in terms of the initial distribution of single and multiple vacancies. The relative intensity values of the diagram lines (I_d), hidden satellites (I_h) and visible satellites (I_v) is calculated.

The LX - Ray satellites are due to the following processes in multihole configurations:

1. Satellites originated by LM and LN double holes, created by Coster-Kronig (C. K.) $L_3 \rightarrow L_{1,2}$ and $L_2 \rightarrow L_1$ transitions or due to shake-off (s. o.) M, N following the L_i ($i = 1, 2, 3$) ionization. The satellites due to double ionized states can be divided in several classes: $LN \rightarrow MN$; $LN \rightarrow NN$; $LM \rightarrow MM$; $LM \rightarrow MN$.

The $LN \rightarrow MN$ and $LN \rightarrow NN$ satellites are not separated from the parent lines (hidden satellites).

2. Satellites due to shake-off and Coster-Kronig transitions which produce states L_iMM, L_iMN and L_iNN; the last one leads to hidden satellites.

We can generalize the following conclusions: satellites which arise from LM and LMX states are separated from the parent lines; satellites due to LN or LNN states coincide with parent lines.

(*) This work has been supported by I. N. I. C. (Portugal).

The number of diagram photons from single-hole states in the L_i subshells is given by

$$F_i(L_i) = n_i(L_i) \cdot P^R_{L_i} / (P^R_{L_i} + P^A_{L_i}) \quad (i = 1, 2, 3) \qquad (1)$$

For a $L_i \rightarrow X$ transition the number of diagram photons is

$$F_i(L_i) \cdot P^R_{L_iX} / P^R_{L_i} \quad (i = 1, 2, 3) \qquad (2)$$

We denote by $n_i(L_i)$ the vacancies in the L_i level following the initial ionization and the rearrangement by Coster-Kronig transitions and shake-off processes; $P^R_{L_i}$ and $P^A_{L_i}$ correspond respectively to the radiative and Auger probabilities in atoms single ionized in the L_i level.

The relations (1) and (2) are valid for double and triple ionized states; however the parameters involved are respectively n'_{L_i}, $P'^R_{L_i}$, $P'^A_{L_i}$, $P'^R_{L_iY,XY}$ and n''_{L_i}, $P''^R_{L_i}$, $P''^A_{L_i}$, $P''^R_{L_iYZ,XYZ}$.

In the present work we assume $P = P' = P''$. The intensity ratios of visible satellites to diagram lines I_v / I_d and hidden satellites to diagram lines I_h / I_d are respectively

$$I_v / I_d = [\, n'_i(L_iM) + n''_i(L_iMM) + n''_i(L_iMN) \,] / n_i(L_i)$$

and

$$I_h / I_d = [\, n'_i(L_iN) + n''_i(L_iNN) \,] / n_i(L_i)$$

The triple ionizations are due to shake-off and Coster-Kronig processes or double Coster-Kronig transitions; obviously $L_iXY = 0$.

These ratios for the elements argon, kripton and xenon have been calculated in the present work; the values for L_1, L_2 and L_3 levels are displayed in tables 1, 2 and 3.

TABLE 1 — Ratios of satellite to diagram lines (L_1 level).

Z	I_h (s.o.) / I_d	I_v (s.o.) / I_d
18	0	0.167
36	0.161	0.058
54	0.214	0.007

CHUI, S. T., FORGACS, G. and HATCH, D. M., *Phys. Rev.* **B25**, 6925 (1982).

DANIELIAN, A., *Phys. Rev. Lett.* **6**, 670 (1961).

DERRIDA, B., MAILLARD, J. M., VANNIMENUS, J. and KIRKPATRICK, S., *J. Physique Lett.* **39**, 465 (1978).

DERRIDA, B., POMEAU, Y., TOULOUSE, G. and VANNIMENUS, J., *J. Physique* **40**, 617 (1979).

DERRIDA, B., ECKMANN, J.-P. and ERZAN, A., *J. Phys.* **A16**, 893 (1983).

DROZ, M. and MALASPINAS, A., *J. Phys.* **C16**, L231 (1982).

DZYALOSHINSKII, I. E. and VOLOVIK, G. E., *Ann Phys.* (N. Y.) **125**, 67 (1980).

DZYALOSHINSKII, I. E. and OBUKOV, S. P., *Sov. Phys. JETP* **56**, 456 (1982).

ERZAN, A., *Phys. Lett.* **93A**, 237 (1983)

FRADKIN, E., HUBERMAN, B. A. and SHENKER, S. H., *Phys. Rev.* **B18**, 4789 (1978).

FORGACS, G., *Phys. Rev.* **B22**, 4473 (1980).

GABAY, M., *J. Physique* **41**, 427 (1980).

GAREL, T. and MAILLARD, J. M., *J. Phys.* **A16**, 2257 (1983).

GREST, G. S. and GABL, E. G., *Phys. Rev. Lett.* **16**, 1182 (1979).

HALPERIN, B. I., 'Statistical Mechanics of Topological Defects', in Les Houches Session XXXV. Physics of Defects. Ed. R. Balian, M. Kleman, J. P. Poirier (North Holland 1981).

HERZ, J. A., *Phys. Rev.* **B18**, 4875 (1978).

HOEVER, P., WOLFF, W. F. and ZITTARTZ, J., *Z. Phys.* **B41**, 43 (1981a).

HOEVER, P. and ZITTARTZ, J., *Z. Phys.* **B44**, 129 (1981b).

JAUSLIN, H. R. and SWENDSEN, R. H., *Phys. Rev.* **B24**, 313 (1981).

JOSÉ, J. V., *Phys. Rev.* **B20**, 2167 (1979).

KADANOFF, L. P. and CEVA, H., *Phys. Rev.* **B3**, 3918 (1971).

KADANOFF, L. P., *Ann Phys.* (N. Y.) **100**, 359 (1976).

KARDAR, M. and BERKER, A. N., *Phys. Rev.* **B26**, 219 (1982).

KIRKPATRICK, S., *Phys. Rev.* **B16**, 4630 (1977).

KOLAN, A. J. and PALMER, R. G., *J. Phys.* **C13**, L575 (1980).

LONGA, L. and OLÉS, A. M., *J. Phys.* **A13**, 1031 (1980).

MALASPINAS, A., private communication.

MATTIS, D. C., *Phys. Lett.* **56A**, 421 (1976).

MCCOY, B., in *Phase Transitions and Critical Phenomena*, Domb, C. and Green, M. S., Ed., Vol. 2 (Academic Press, N. Y. 1977).

MCKAY, S., BERKER, A. N., KIRKPATRICK, S., *Phys. Rev. Lett.* **48**, 767 (1982).

MIYASHITA, S. and SUZUKI, M., *J. Phys. Soc. Jap.* **50**, 1840 (1981).

MIYASHITA, S., *Prog. Theor. Phys.* **69**, 714 (1983).

NIGHTINGALE, M. P. and BLÖTE, H. W. J., *Physica* **104A**, 352 (1980).

NISHIMORI, H., *Prog. Theor. Phys.* **66**, 1169 (1981).

NISHIMORI, H. and STEPHEN, M. J., *Phys. Rev.* **B27**, 5644 (1983).

DE NUNES, J. M., Project Report, Faculty of Sciences, University of Porto (1983).

ONO, I., *J. Phys. Soc. Jap.* **48**, 1084 (1980).

PENSON, K. A., JULLIEN, R., PFEUTY, P., *J. Phys.* **C12** (1979).

PHANI, M. K., LEBOWITZ, J. L., KALOS, M. H., TSAI, C. C., *Phys. Rev. Lett.* **42**, 577 (1979).

SADIQ, A., TAHIR-KHELI, R. A., WORTIS, M., BHATTI, N., *Phys. Lett.* **84A**, 439 (1981).

SAVIT, R., *Rev. Mod. Phys.* **52**, 453 (1980).

SCHUSTER, H. G., *Z. Phys.* **B35**, 163 (1979).

DE SEZE, L., *J. Phys.* **C10**, L353 (1977).

SHERRINGTON, D., Imperial College preprint SST/8283/19.

SMITH, D. A., *J. Phys.* **F5**, 2148 (1975).

SOUKOULIS, C. M. and LEVIN, K., *Phys. Rev. Lett.* **39**, 581 (1977).

SOUTHERN, B. W., CHIU, S. T. and FORGACS, G., *J. Phys.* **C13**, L827 (1980).

STEPHENSON, J., *J. Math. Phys.* **11**, 413 (1970a), 420 (1970b); *Can. J. Phys.* **48**, 1724 (1970c).

SÜTÖ, A., *Z. Phys.* **B44**, 121 (1981).

SVRAKIĆ, N. M., KERTÉSZ, J. and SELKE, W., *J. Phys.* **A15**, L427 (1982).

TOULOUSE, G., *Comm. Phys.* **2**, 115 (1977).

TOULOUSE, G., 'Gauge Concepts in Condensed Matter Physics' in *Recent Developements in Gauge Theories*, G. 't Hooft et al. ed, (Plenum Publish Corp. 1980).

TOULOUSE, G., VANNIMENUS, J., *Phys. Rept.* **67**, 47 (1980).

VANNIMENUS, J., TOULOUSE, G., *J. Phys.* **C10**, 537 (1977).

VILLAIN, J., *J. Phys.* **C10**, 1717 (1977a), 4793 (1977b); **C11**, 745 (1978).

VILLAIN, J. BIDEAUX, R., CARTON, J.-P., CONTE, R., *J. Physique* **41**, 1263 (1980).

WANNIER, G. H., *Phys. Rev.* **79**, 357 (1950).

WEGNER, F. J., *J. Math. Phys.* **12**, 2259 (1971).

WOLFF, W. F., HOEVER, P., ZITTARTZ, J., *Z. Phys.* **B42**, 259 (1981).

WOLFF, W. F. and ZITTARTZ, J., *Z. Phys* **B49**, 229 (1982).

WU, F. Y., *Rev. Mod. Phys.* **54**, 235 (1982).

NOTE ADDED IN PROOF: The representation chosen for the frustration function of the q-state vector Potts model in this paper leads to an asymmetry in the plaquette couplings (viz. Eqs. (3.19, 3.20), and therefore to vanishing weights for the frustrated configurations for $q \neq 2$. This may be remedied by choosing a slightly different representation. Details are given in a forthcoming publication.

where the graphs

G consist of bonds and lattice points on the lattice $\mathcal{L}$.

G_p consist of plaquettes on $\mathcal{L}$.

Performing the sums over the spin and gauge variables, yields, after a bit of work,

$$\exp(NK_p/q)\cdot Z\{\phi_p=1\}_{K_p}= \tag{6}$$

$$q^{E+N}\sum_{G,G_p\subset\mathcal{L}}(u/q)^{b(G)}\,(v/q)^{p(G_p)}\,q^{c_1(G,G_p)}$$

where E and N are the number of edges and vertices in $\mathcal{L}$, $b(G)$ is the number of bonds in G, $p(G_p)$ is the total number of plaquettes in G_p, and $c_1(G, G_p)$ is the number closed circuits in G that are completely filled by clusters of plaquettes in G_p.

Now consider the (unfrustrated) random vector Potts model in the presence of a field. The partition function is

$$Z(K^*,h)=\sum_{\{s\}}\exp\Big[K^*\sum_{(\tilde{i}\,\tilde{j})}\mathbf{s}_{\tilde{i}}^{\dagger}\,\psi_{\tilde{i}\,\tilde{j}}\,\mathbf{s}_{\tilde{j}}+h\sum_{\tilde{i}}\mathbf{s}_{\tilde{i}}^{\dagger}\,\mathbf{s}_0\Big] \tag{7}$$

where $\mathbf{s}_0$ has been chosen in the 1 (Potts) direction. (The interaction $h\,\mathbf{s}_{\tilde{i}}^{\dagger}\,\mathbf{s}_0$ may be written $h\,\delta_{\sigma_{\tilde{i}},1}$ in terms of the scalar variables $\sigma_{\tilde{i}}$). The Whitney polynomial representation is

$$Z(K^*,h)=\sum_{\{s\}}\sum_{G,G_k\subset\tilde{\mathcal{L}}}\prod_{(\tilde{i}\,\tilde{j})\,\in\,\tilde{G}}u^*\,\mathbf{s}_{\tilde{i}}^{\dagger}\,\psi_{\tilde{i}\,\tilde{j}}\,\mathbf{s}_{\tilde{j}}\prod_{K\,\in\,G_k}w\,\mathbf{s}_k^{\dagger}\,\mathbf{s}_0 \tag{8}$$

where $u^*=e^{K^*}-1$, $w=e^h-1$, and the graphs

$\tilde{G}$ consist of vertices (points) and bonds on the dual lattice $\tilde{\mathcal{L}}$

G_k consist only of points.

Performing the summation over the spin variables gives,

$$Z(K^*,h)=\sum_{\tilde{G},G_k}(u^*)^{b(\tilde{G})}\,w^{p(G_k)}\,q^{m(\tilde{G},G_k)} \tag{9}$$

where b has the same meaning as before, $p(G_k)$ is the total number of points in G_k, and $m(\tilde{G}, G_k)$ is the number of connected graphs in $\tilde{G}$ that do not contain any points of G_k.

Define, as usual, the dual of the graph G (on $\mathcal{L}$) to be the graph obtained on $\tilde{\mathcal{L}}$ by placing bonds (rotated by 90°) on all links on $\mathcal{L}$ not occupied by bonds in G. Define the dual of G_p to be the graph obtained by placing points on all plaquettes in $\mathcal{L}$ not occupied by plaquettes in G_p. Clearly, the graphs generated are of the type $\tilde{G}$ and G_k. Moreover, observe that

$$b(G) = E - b(\tilde{G})$$
$$p(G_p) = N - p(G_k)$$
$$c_1(G, G_p) = m(\tilde{G}, G_k)$$

if G is taken to be the dual of G and G_k the dual of G_p. Re-expressing Eq. (6) in terms of the sums over G and G_k, we have

$$e^{NK_p/q} Z\{\phi_p = 1\}_{K_p} = u^E v^N Z(K^*, h)$$

provided that

$$(u^*)^{-1} = u/q$$
$$(w)^{-1} = v/q$$

yielding the duality relations

$$\begin{aligned} K^* &= -\ln[(e^K - 1)/(e^K + q - 1)] \\ h &= -\ln[(e^{K_p} - 1)/(e^{K_p} + q - 1)] . \end{aligned} \tag{10}$$

REFERENCES

ALEXANDER, S. and PINCUS, P., *J. Phys.* **A13**, 263 (1980).

DE ALMEIDA, J. R. L., FITTIPALDI, I. P., SÁ BARRETO, F. C., *J. Phys.* **C14**, L403 (1981).

ANDRÉ, G., BIDEAU, R., CARTON, J.-P., CONTE, R. and DE SEZE, L., *J. Physique* **40**, 479 (1979).

BALIAN, R., DROUFFE, J. M. and ITZYKSON, C., *Phys. Rev.* **D11**, 2098 (1975).

BINDER, K., 'Statistical Mechanics of Ising Spin Glasses', *Fundamental Problems in Statistical Mechanics* V, Ed. EGD Cohen (North Holland 1980a).

BINDER, K., *Phys. Rev. Lett.* **45**, 811 (1980b).

BRYSKIN, V. V., GOL'TSEV, A. YU. and KUDINOV, E. E., *J. Phys.* **C13**, 5999 (1980).

Then, for only two frustrations in $\{ \phi_p \}$, this probability behaves with the distance between the frustrations according to the exactly known two-point correlation fuction of the (field free) Ising model in two dimensions (Schuster 1979). Recall that K_f is given as a function of the concentration x of (in this case) FM bonds (Eq. 3.27). Thus, Eqs. (4.26) and (4.13) predict a phase transition in the system of frustrations. With $K_f = -1/2 \ln (2x - 1)$ we have:

i) $1 > x > x_0 = K^*_{f\,crit}$ (~ .7072). The probability to find two frustrations separated by r decays like $\exp(-r/\xi)$ with ξ being the correlation length of the Ising model at temperature K^*_f.

ii) $x = x_0$. ξ diverges, so that one obtains 'pair dissociation' of frustrations.

iii) $x < x_0$. In this case there is a finite probability to find a single frustrated plaquette – thus necessarily an infinite 'ladder' of AFM bonds in the system (see Fig. 1c) (Schuster 1979).

Notice that FM order is already destroyed at $x < x^* = .91$ (Vannimenus and Toulouse 1977) by the possibility of having infinite strings of frustrated plaquettes – at x_0, however, new types of 'domain walls' (defects of infinite length on the spin system) associated with the 'ladders' of AFM bonds appear. Thus the ground state seems to be qualitatively changed as we go through x_0. Although there is no finite temperature phase transition for this system, i.e., it remains paramagnetic down to $T = 0$, the singularities introduced into the quenched average for the free energy, via the probabilities $P\{ \phi_p \}$ persist at all temperatures! This was essentially foreseen by Schuster (1979), and it also has its generalization to the arbitrary - q Potts model.

I would like to thank Prof. J. M. Araújo for encouraging me to undertake the writing of this article. Thanks are also due to Mr. J.M. de Nunes for bringing to my attention some of the references cited in this work, and to all members of the Grupo de Fisica Teorica for their unfailing support and friendship. Finally, I am grateful to Dr. E.J.S. Lage for a critical reading of the manuscript.

APPENDIX

Here I present the duality transformation for the Potts model in the presence of quenched randomness. (A different treatment has been given by Jauslin and Swendsen (1981).)

Consider the partition function

$$Z\{\phi_p\} = \lim_{K'_p \to \infty} \sum_{\{\psi_{ij}\}} \sum_{\{s_i\}} \exp\left(K \sum_{(ij)} \mathbf{s}_i^\dagger \psi_{ij} \mathbf{s}_j\right) \cdot \exp\left[K'_p \sum_p \phi_p \left(\mathrm{Tr} \prod_p \psi - 1\right)/(q-1)\right] \tag{1}$$

A slightly more condensed notation has been used that in Section 3, which should be self explanatory. The bond labels have been dropped from the gauge variables appearing in products around plaquettes, as in $\prod_p \psi$. The frustration function ϕ_p is defined via Eq. (3.11). Extracting a constant factor from the sum, and defining

$$K_p = q\,K'_p/(q-1)\,,$$

we have

$$Z\{\phi_p\} = \lim_{K_p \to \infty} \exp(-NK_p/q) \sum_{\{\psi\}} \sum_{\{s\}} \exp\left(K \sum_{ij} \mathbf{s}_i^\dagger \psi_{ij} \mathbf{s}_j\right) \cdot \exp\left[K_p \sum_p \left(\mathrm{Tr} \prod_p \psi\right)/q\right] \tag{2}$$

Define

$$\begin{aligned} u &= e^K - 1 \\ v &= e^{K_p} - 1\,. \end{aligned} \tag{3}$$

Then

$$\begin{aligned} \exp\left(K\, \mathbf{s}_i^\dagger \psi_{ij} \mathbf{s}_j\right) &= \left(\mathbf{s}_i^\dagger \psi_{ij} \mathbf{s}_j\right) u + 1 \\ \exp\left(K_p\, \mathrm{Tr} \prod_p \psi/q\right) &= \left(\mathrm{Tr} \prod_p \psi\right) v/q + 1\,. \end{aligned} \tag{4}$$

Now setting all $\phi_p = 1$, and going over to the Whitney polynomial representation, we have for finite K_p,

$$Z\{\phi_p = 1\}_{K_p} = \exp(-NK_p/q)\,.$$

$$\cdot \sum_{\{\psi\}} \sum_{\{s\}} \sum_{G, G_p \subset \mathcal{L}} \prod_{(ij) \in G} u\, \mathbf{s}_i^\dagger \psi_{ij} \mathbf{s}_j \prod_{p \in G_p} \left(\mathrm{Tr} \prod_p \psi\right) v/q \tag{5}$$

TABLE 2 — Ratios of satellite to diagram lines (L_2 level).

Z	I_h (C.K.) / I_d	I_h (s.o.) / I_d	I_h (s.o. + C.K.) / I_d	$(I_h)_t$ / I_d	I_v (C.K.) / I_d	I_v (s.o.) / I_d	I_v (s.o. + C.K.) / I_d	$(I_v)_t$ / I_d
18	0	0	0	0	0.240	0.178	0.040	0.458
36	0.029	0.164	0.005	0.198	0.213	0.051	0.054	0.318
54	0.179	0.219	0.045	0.443	0	0.008	0.001	0.009

TABLE 3 — Ratios of satellite to diagram lines (L_3 level).

Z	I_h (C.K.) / I_d	I_h (s.o.) / I_d	I_h (s.o. + C.K.) / I_d	$(I_h)_t$ / I_d	I_v (C.K.) / I_d	I_v (s.o.) / I_d	I_v (s.o. + C.K.) / I_d	$(I_v)_t$ / I_d
18	0	0	0	0	0.240	0.177	0.040	0.457
36	0.062	0.163	0.015	0.240	0.224	0.051	0.050	0.325
54	0.208	0.217	0.042	0.467	0	0.007	0.0014	0.008

The energies of diagram and satellite lines are very close; so the energy corrections can be disregarded. The $n_i(L_i)$, $n_i'(L_i)$ and $n_i''(L_i)$ results have been obtained from ref. [1]; values of shake-off probabilities are from ref. [2] and Coster-Kronig parameters are from ref. [3, 4].

We can conclude that it seems impossible to observe a pure line (true diagram line); the diagram lines so observed are always contaminated by hidden satellites.

Table 1 shows that satellite lines due to L_1 ionization are not negligible as it should be if they were only due to Coster-Kronig transitions.

From tables 2 and 3 we can see that the total values of the ratio $(I_h)_t / I_d$ increase with the atomic number; thus for high values of Z there is a strong contamination of the diagram lines due to hidden satellites.

REFERENCES

[1] M. O. KRAUSE, F. WUILLEUMIER and C. W. NESTOR, JR., *Phys. Rev.* **A6**, 871 (1972).

[2] T. A. CARLSON and C. W. NESTOR, JR., *Phys. Rev.* **A6**, 2887 (1973).

[3] M. O. KRAUSE, *J. Phys. Chem. Data* **8**, 307 (1979).

[4] M. H. CHEN and B. CRASEMAN, *At. Data and Nucl. Data Tables* **19**, 97 (1977).

β^+ / EC DECAY OF ^{181}Au : γ - RAY IDENTIFICATION

F. BRAGANÇA GIL (1), C. BOURGEOIS, P. KILCHER, G. PAROT, M. G. PORQUET (2), B. ROUSSIÈRE, J. SAUVAGE-LETESSIER and the ISOCELE Collaboration

Institut de Physique Nucléaire, 91406 Orsay, France

(Received 30 November 1983)

ABTRACT — The β+/EC decay of ^{181}Au has been studied with mass separated sources from the ISOCELE facility. Main γ-rays which belong to the ^{181}Au $\rightarrow$ ^{181}Pt decay have been identified from X-γ coincidence measurements. A rotational band built on the 1/2− [521] Nilsson state has been developed up to the 7/2− state in ^{181}Pt.

1 — INTRODUCTION

The nuclei of platinum have been studied extensively [1-8] and a shape transition has been found for A = 186. ^{185}Pt corresponds indeed to a prolate-shaped nucleus, whereas ^{187}Pt seems to correspond to an oblate-shaped one. However some phenomena observed in this transitional region are not yet well understood: the existence of highly converted transitions in ^{187}Pt [8], ^{187}Au [9], ^{185}Au [10, 11], $^{193, 195, 197}$Hg [12, 13] for example. So we have extended the study of the platinum nuclei down to the very neutron-deficient isotopes. The present work is the first step of the study of the β^+ / EC decay of ^{181}Au. Gold isotopes were produced by Pt (p,xn) Au reactions, then mass-separated using the ISOCELE II facility at Orsay. X - γ coincidence measure-

---

(1) Centro de Física Nuclear, 1699 Lisboa, Portugal.

(2) Centre de Spectrométrie Nucléaire et de Spectrométrie de Masse, 91406 Orsay, France.

ments allowed us to clearly attribute twenty four γ - rays to the $^{181}Au \rightarrow {}^{181}Pt$ decay.

Such results can also be very useful to identify the ^{181}Au or ^{181}Pt nuclei produced by (HI,xn) reactions.

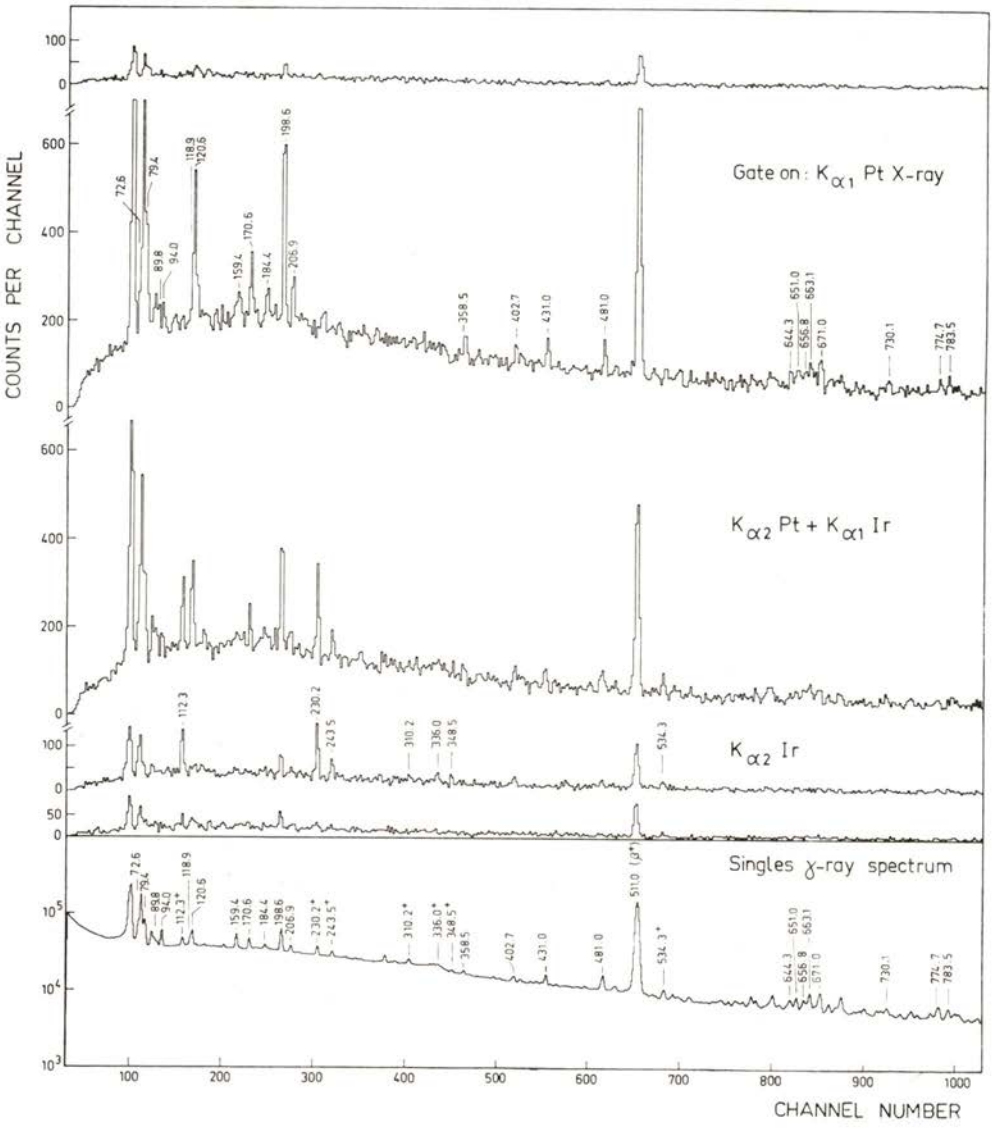

Fig. 1 — Coincidence spectra (2 keV gates from 60 to 70 keV) and singles γ-ray spectrum. + indicates γ-lines which belong to the $^{181}Pt \rightarrow {}^{181}Ir$ decay.

2 — EXPERIMENTAL PROCEDURE

A thick target of molten Pt - β alloy was bombarded by a 200 MeV proton beam from the Orsay synchrocyclotron in order to produce gold nuclei via Pt (p,xn) Au reactions.

The proton beam intensity was 2.5 μA . The target was placed inside the high-temperature ion source [14] of the ISOCELE II isotope separator [15]. The mass-separated gold ions were collected on a mylar / aluminium tape and then carried to the counting station using a fast mechanical tape-transport system.

Singles gamma - rays were measured with a planar Ge (HP) X - ray detector (0.6 keV FWHM resolution at 122 keV) and a 12 % efficiency coaxial Ge (HP) detector (2 keV FWHM resolution at 1.33 MeV). The energy ranges were from 4 keV to 400 keV and from 30 keV to 1500 keV respectively. The X - γ - t coincidence data were simultaneously recorded event by event on magnetic tapes. The experimental data were analysed off-line on the Orsay IBM 138-370 computer. The coincidence events have been treated in order to get prompt coincidence bidimensional matrix. The coincidence spectra shown in Fig. 1 were obtained by setting 2 keV gates on K_α X - rays e.g. from 60 to 70 keV. Collecting and counting times were 5 s per source and the data were accumulated for ten hours.

3 — EXPERIMENTAL RESULTS AND DISCUSSION

Energies and intensities of γ - rays deduced from the γ and X spectra are listed in table 1 together with the coincidence results. Twenty three γ - rays can be clearly ascribed to the $^{181}Au \rightarrow {}^{181}Pt$ decay.

In spite of lack of intensity for the 159.4 keV γ - line observed in coincidence with K_α X - rays of Pt (see Fig. 1), we can attribute this transition to the $^{181}Au \rightarrow {}^{181}Pt$ decay because the 40.5 keV γ - line has been observed in coincidence with the 118.9 keV γ - line and the sum 40.5 + 118.9 corresponds to 159.4 keV. This fact suggests a rather long lifetime for the state which decays by both the 159.4 keV transition and the 40.5 - 118.9 keV cascade.

TABLE 1—Gamma-ray data for the decay of ^{181}Au (collecting and counting times, for ^{181}Au sources, were 5 s): energy error $\leqslant$ 0.3 keV; intensity error ~ 10%.

Energy (keV)	I_γ relative	Main coincidences		Energy (keV)	I_γ relative	Main coincidences	
		K_α X-rays	γ-rays			K_α X-rays	γ-rays
40.5	15	Pt	118.9	402.7	15	Pt	
49.9	23	Pt	120.6	431.0	45	Pt	
			431.0	481.0	74	Pt	
72.6	~ 15	Pt	120.6	491.8	23		
79.4	84	Pt	198.6	534.3	42	Ir	
87.7	10			542.3	24		
89,8	13	Pt		556.4	20		
94.0	56	Pt		591.4	14		
112.3	23	Ir	230.2	611.0	41		
118.9	23	Pt	40.5	615.2	27		
120.6	43	Pt	49.9	629.3	58		
148.6	10			644.3	40	Pt	
159.4	55	(Pt)		651.0	44	Pt	
170.6	38	Pt		656.8	48	(Pt)	
184.4	19	Pt	94.0	663.1	72	Pt	
198.6	100	Pt	79.4	671.0	84	Pt	
206.9	26	Pt		679.0	29		
230.2	36	Ir	112.3	689.7	72		
243.5	24	Ir		710.1	29		
289.4	35			721.0	20		
310.2	23	Ir		730.1	23	Pt	
328.9	4			750.6	29		
332.3	6			756.4	15		
336.0	6	Ir		767.6	26		
348.5	8	Ir		774.7	61	Pt	
358.5	13	Pt		783.5	48	Pt	

The studies of the α decay of the mercury isotopes allowed E. Hagberg et al. [16] to propose level schemes for $^{177, 179, 181}$Pt and to identify the $1/2^-$ [521] state and the $3/2^-$, $5/2^-$ rotational states built on it. Recently we have studied the β^+/EC decay of ^{185}Au [17] and ^{183}Au [18], and identified the $1/2^-$ [521] rotational band built on the isomeric state of ^{185}Pt and on the

ground state of ^{183}Pt. The results obtained in the present work support the previous identification of the 5/2, 3/2, and 1/2 states of the $1/2^-$ [521] band in ^{181}Pt and allow us to propose the additional 7/2 $1/2^-$ [521] state. The systematic of the $1/2^-$ [521]

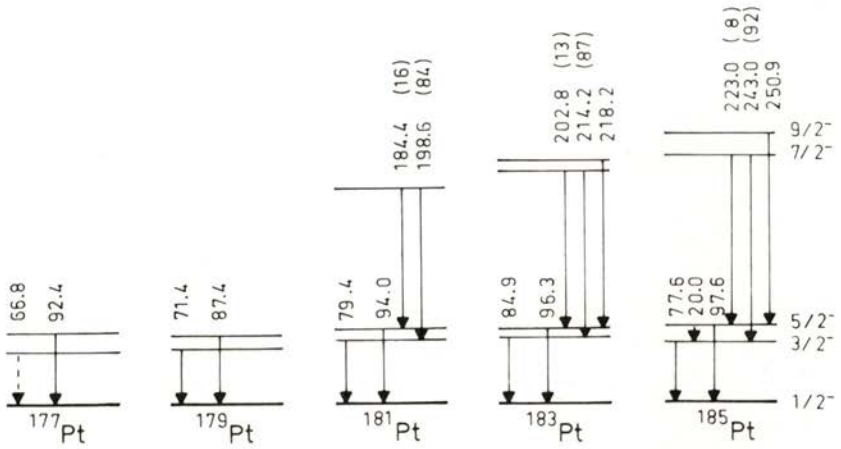

Fig. 2 — The systematic of the rotational band built on the $1/2^-$ [521] state. Data were taken from ref. 16 ($^{177,179,181}Pt$), this work (^{181}Pt), ref. 18 (^{183}Pt), and ref. 17 (^{185}Pt). Dashed line indicates transition not observed experimentally. Numbers in parentheses are γ-line intensities.

rotational band through the platinum isotopes is shown in Fig. 2. The stability observed indicates clearly that all the $^{177-185}Pt$ isotopes correspond to prolate-shaped nuclei contrary to the heavier platinum isotopes.

REFERENCES

[1] M. FINGER et al., *Nucl. Phys.* **A188** (1972), 369.

[2] V. BERG, *Thesis Orsay* (1976).

[3] M. A. DELEPLANQUE et al., *Coll. de la Société Française de Physique*, DIJON (1975); *J. de Phys.* C5 **36** (1975), 97.

[4] C. BOURGEOIS et al., *3rd Int. Conf. on nuclei far from stability*, CARGESE (1976); CERN 76-13, p. 456.

[5] J. KALIFA, G. BERRIER-RONSIN, G. ROTBARD, M. VERGNES, J. VERNOTTE and R. SELTZ, *Phys. Rev.* **C22** (1980), 997.

[6] M. PIIPARINEN, J.-C. CUNNANE, P. J. DALY, C. L. DORS, F. H. BERNTHAL, and T. L. KHOO, *Phys. Rev. Lett.* **34** (1975), 1110.

[7] A. VISVANATHAN, E. F. ZGANJAR, J. L. WOOD, R. W. FINK, L. L. RIEDINGER and F. E. TURNER, *Phys. Rev.* **C19** (1979), 282.
B. E. GNADE, R. W. FINK, J. L. WOOD, *Nucl. Phys,* **A406** (1983), 29.

[8] A. BEN BRAHAM et al., *Nucl. Phys.* **A332** (1979), 397.

[9] E. F. ZGANJAR, J. D. COLE, J. L. WOOD and M. A. GRIMM, *4th Int. Conf. on nuclei far from stability,* HELSINGOR (1981), CERN 81-09 p. 630.

[10] C. BOURGEOIS, M. G. DESTHUILLIERS-PORQUET, P. KILCHER, B. ROUSSIÈRE, J. SAUVAGE-LETESSIER and the ISOCELE Collaboration, *4th Int. Conf. on nuclei far from stability,* HELSINGOR (1981), CERN 81-09 p. 618.

[11] C. BOURGEOIS, P. KILCHER, B. ROUSSIÈRE, J. SAUVAGE-LETESSIER, M. G. PORQUET and the ISOCELE Collaboration, *Nucl. Phys.* **A386** (1982), 308.

[12] G. M. GOWDY, *Ph. D. thesis,* School of Chemistry, Georgia Institute of Techonology (1976).

[13] G. M. GOWDY, J. L. WOOD and R. FINK, *Nucl. Phys.* **A312** (1978), 56.

[14] J. C. PUTAUX et al., *10th EMIS Conf.,* ZINAL (1980); *Nucl. Instr.* **186** (1981), 321.

[15] P. PARIS et al., *10th EMIS Conf.,* ZINAL (1980); *Nucl. Instr.* **186** (1981), 91.

[16] E. HAGBERG, P. G. HANSEN, P. HORNSHOJ, B. JONSON, S. MATTSSON, P. TIDEMAND-PETERSSON, the ISOLDE collaboration, *Nucl. Phys.* **A318** (1979), 29.

[17] B. ROUSSIÈRE, C. BOURGEOIS, P. KILCHER, M. G. PORQUET, J. SAUVAGE-LETESSIER, *Annuaire IPN Orsay* (1983), DRE.

[18] C. BOURGEOIS, P. KILCHER, M. I. MACIAS-MARQUES, M. G. PORQUET, B. ROUSSIÈRE, J. SAUVAGE-LETESSIER, C. SCHÜCK, *Annuaire IPN Orsay* (1982), DRE, E82.

D-STATE AND NUCLEAR STRUCTURE EFFECTS IN (d , α) REACTIONS

F. D. SANTOS and A. M. EIRÓ

Centro de Física Nuclear da Universidade de Lisboa
Av. Gama Pinto, 2 — 1699 Lisboa Codex, Portugal

(Received 14 December 1983)

ABSTRACT —A general discussion is given of the effects of the α-particle D-state in (d , α) and (α , d) reactions. The dependence of the cross section and of the tensor analysing powers T_{2q} on the asymptotic D- to S-state ratio ρ in the α particle and on the spectroscopic amplitudes of two-nucleon cluster transfer is discussed using a plane wave peripheral model. It is shown that the T_{2q} in (d , α) reactions contain specific information on the α-particle D-state and also on the coherence properties of the two-nucleon states populated.

1 — INTRODUCTION

It is well known that the polarization observables of transfer reactions can be used to investigate the internal structure of composite particles. This property has been extensively applied to study the two and three body bound systems via the (d, p) [1, 2], (d , t) and (d , ^{3}He) [3, 4] reactions. Recently it was suggested by Santos et al. [5] that the tensor analysing powers of ($\vec{d}$, α) reactions display the effect of a relative D-state motion of two deuteron clusters in the α particle. This low energy (d , α) data is primarily sensitive to the parameter D_2 [1-6] which is closely related to the asymptotic D to S-state ratio ρ.

The calculations of ref. [5] used a very simplified reaction model based in the plane wave approximation and did not take into account the effect of L mixing in the transition amplitude to unnatural parity states. More recently full finite range DWBA calculations [7] have shown that the tensor analysing powers

of $(\vec{d}, \alpha)$ reactions are specially sensitive to the L mixing in unnatural parity transitions. This effect can be used to study the coherence properties of the states populated and to determine the spectroscopic amplitudes corresponding to each L value. Furthermore it was realized [7, 8] that the interference between L mixing and D-state effects in the presently available $(\vec{d}, \alpha)$ tensor analysing power data makes it difficult to extract D_2 from the data.

The cross section of (α, d) and (d, α) reactions is also sensitive to the α-particle D-state. Nagarajan and Satchler [9] have shown that the D-state effects have a J-dependence which is qualitatively in agreement with the J-dependence observed in the cross section of ^{208}Pb (α, d) reactions [10]. This was previously interpreted as resulting from multistep processes [10]. To compare these two types of J-dependence we need a more complete understanding of the D-state effects in (d, α) reactions and in particular a realistic estimate of D_2.

Here we develop the DWBA theory of (α, d) and (d, α) reactions including both the S and D-state components of the α-particle. In section 2 the decomposition of the transition amplitude for two nucleon transfer reactions is performed. These results are then applied to the particular case of (α, d) and (d, α) reactions in section 3. In section 4 using a perturbative approach to generate the D-state component of the α-particle we calculate D_2 using gaussian wave functions and realistic tensor interactions. Finally in section 5 the special sensitivity of the tensor analysing powers to the L mixing and D-state effects is studied using a peripheral model for the transfer.

2 — TWO NUCLEON TRANSITION AMPLITUDE

We consider a transfer reaction A (a , b) B where $a = b + x$ and x is the transferred cluster. The transition amplitude for the reaction, scattering from momentum $\mathbf{k}_a$ to momentum $\mathbf{k}_b$ is

$$T = < B\, J_B\, M_B\, , b\, s_b\, \sigma_b\, ; \mathbf{k}_b \,|\, T \,|\, A\, J_A\, M_A\, , a\, s_a\, \sigma_a\, ; \mathbf{k}_a > \qquad (1)$$

where J_A, s_a, J_B, s_b are the spins of A, a, B, b. Performing

an expansion into terms with definite angular momentum transfer [11] we can write

$$T = \sum_{sJl} (J_A M_A J M_J | J_B M_B) (l \lambda s \sigma | J M_J) \\ (-1)^{s_b - \sigma_b} (s_a \sigma_a s_b - \sigma_b | s \sigma) B^{l\lambda}_{sJ} \quad (2)$$

where $(J_A M_A J M_J | J_B M_B)$ is the usual Clebsch-Gordan coefficient [12].

The amplitudes $B^{l\lambda}_{sJ}$ contain the reaction dynamics and transform under rotations like the conjugate of the spherical harmonic Y^{λ}_{l}. It is important to notice that the expansion (2) in the angular momentum transfer representation is model independent since it is based only on the transformation properties under rotations of states with definite angular momentum. Therefore it does not assume any approximations regarding, for instance, spin dependent forces in the entrance and exit channels, the internal structure of the nuclei involved in the reaction and the one-step or sequential transfer nature of the reaction mechanism.

We shall now particularize eq. (2) to two-nucleon transfer. In this case $a = b + 2$ and $B = A + 2$. To proceed with the analysis of the transition amplitude we consider a double-parentage decomposition of the state $J_B\ M_B$ [13]

$$| B\ J_B\ M_B > = \sum_{\eta A' J M_J} \mathcal{S}_J (\eta) | \eta\ J\ M_J > | A'\ J_{A'}\ M_{A'} > \\ (J_{A'} M_{A'} J M_J | J_B M_B) \quad (3)$$

where $\mathcal{S}_J(\eta)$ is the spectroscopic amplitude for the η, J configuration of the two nucleons with total angular momentum J relative to the state $J_{A'}\ M_{A'}$. The state $| \eta\ J\ M_J >$ results from coupling two single particle states with angular momenta j_1, j_2 which are abbreviated by the parameter η. By transforming from j - j to L - s coupling we can write

$$| \eta (j_1 j_2)\ J M_J > = \\ \sum_{L M s_x \sigma_x} \mathcal{G}_{L s_x J} (\eta) | l_1 l_2, L M > | s_x \sigma_x > (L M s_x \sigma_x | J M_J) . \quad (4)$$

Here $\mathcal{G}_{L s_x J}(\eta)$ are the usual symmetrized [13] Ls - jj recoupling

coefficients and $|\, s_x\ \sigma_x >$ is a spin-only wave function for the two nucleons with total spin s_x. The dependence on the position coordinates $\mathbf{r}_1$ and $\mathbf{r}_2$ of the two nucleons relative to A (Fig. 1) is contained in $|\, l_1\ l_2\ ,\ \mathrm{LM} >$.

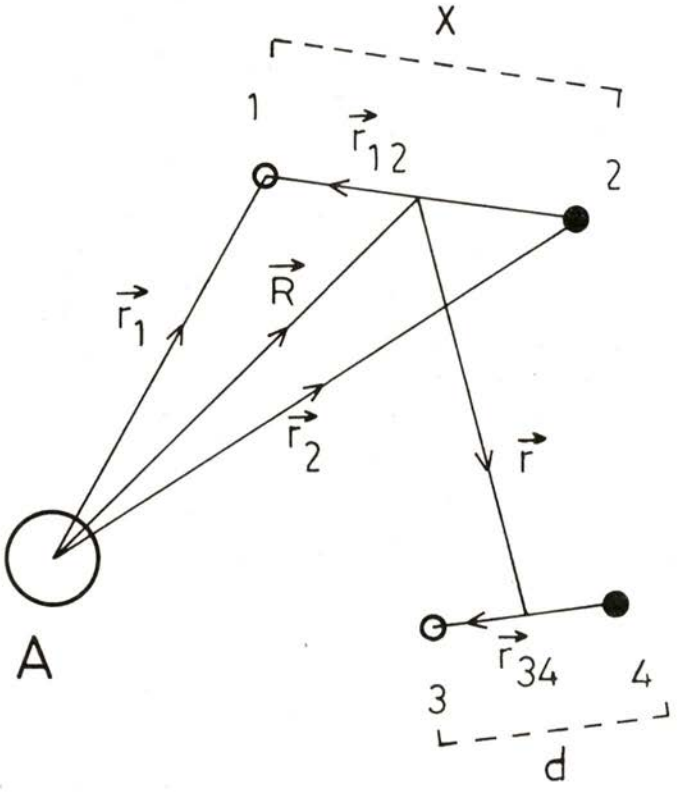

Fig. 1 — Coordinate vectors for a A (α , d) B reaction.

It is now assumed that there is no exchange of nucleons between particles in the entrance and exit channels, no excitation of the target and no reorientation of the target spin through spin-dependent forces. With this assumption the integration over the target internal coordinates selects from eq. (3) the term $A' = A$ in which the target is in its ground state. Putting eqs. (3) and (4) into eq. (1), performing the integration over the internal coordinates

of A and writing the resulting expression in the form of eq. (2) we find that

$$B^{l\lambda}_{sJ} = \sum_{\eta\, s_x L} \mathcal{S}_J(\eta)\; \mathcal{G}_{L\, s_x\, J}(\eta) \sum_{L'} A^{LL'}_{lsJs_x}\, \beta^{l\lambda}_{s_x L'L} . \tag{5}$$

The coefficients $A^{LL'}_{lsJs_x}$ are the same as in ref. [14] and are given by

$$A^{LL'}_{lsJs_x} = \hat{s}_a\, \hat{l}\, (-1)^{J-s-l-L'}\, W(L\, s_x\, l\, s\, ;\, J\, L') \tag{6}$$

while

$$\beta^{l\lambda}_{s_x L'L} = \frac{\hat{L}'^2}{\hat{s}_a\, \hat{s}} \sum_{\sigma_x \sigma_a \sigma_b \sigma\, M\, M'} (-1)^{M'} (L\, M\; L'\text{-}M' \mid l\lambda)\, (-1)^{s_b - \sigma_b} (s_a\, \sigma_a\, s_b\, \text{-}\sigma_b \mid s\sigma)\; (L'\, M'\, s_x\, \sigma_x \mid s\sigma) \tag{7}$$

$$< b\, s_b\, \sigma_b\, ;\, s_x\, \sigma_x\, ;\, l_1\, l_2\, L\, M\, ;\, \mathbf{k}_b \mid T \mid a\, s_a\, \sigma_a\, ;\, \mathbf{k}_a > .$$

Here $(2s+1)^{1/2}$ is abbreviated by $\hat{s}$. We notice that the total orbital angular momentum transfer in the reaction, l, is composed of a part L and a part L′ which in turn results from the decomposition of the spin transfer s into a spin part s_x and an orbital part L′.

In the microscopic approach to two-nucleon transfer reactions the amplitudes $\beta^{l\lambda}_{s_x L'L}$ are calculated from states $|\, l_1\; l_2\; LM >$ constructed from shell model wave functions in the nucleon coordinates $\mathbf{r}_1$ and $\mathbf{r}_2$. However to obtain the projectile form factor it is convenient to transform from the coordinates $\mathbf{r}_1$ and $\mathbf{r}_2$ to $\mathbf{r}_{12} = \mathbf{r}_1 - \mathbf{r}_2$ and $\mathbf{R} = (\mathbf{r}_1 + \mathbf{r}_2)/2$. These vectors are represented schematically in Fig. 1. Using a basis of normalized wave functions ϕ_{nl} we can perform the expansion

$$< \mathbf{r}_1\, \mathbf{r}_2 \mid l_1\, l_2\, L\, M > = \sum_{n l_x N \Lambda} c_{n l_x N \Lambda}(\eta) \left[\phi_{n l_x}(\mathbf{r}_{12}) \otimes \phi_{N\Lambda}(\mathbf{R}) \right]^M_L \tag{8}$$

where n and N are quantum numbers that specify the number of nodes of the wave functions ϕ. In the particular case of harmonic oscillator wave functions the $c_{n l_x N \Lambda}$ are the well known Moshinsky coefficients [15].

We now assume that the reaction is a one-step process and take V_{bx} for the transfer interaction. It is then straightforward to conclude that the T amplitude in eq. (7) depends on the internal structure of the projectile through the matrix element $< b s_b \sigma_b ; n j_x m_x | V_{bx} | a s_a \sigma_a >$. Here $\mathbf{j}_x = \mathbf{l}_x + \mathbf{s}_x$ is the total angular momentum of the transferred two-nucleon cluster.

To proceed with the analysis of the transition matrix elements we use the DWBA theory. No spin dependent interactions either in the entrance or the exit channel are considered in order to simplify the discussion. With this assumption the DWBA amplitude in eq. (7) is [14]

$$
\begin{aligned}
&< b\, s_b \sigma_b ; s_x \sigma_x ; l_1 l_2 L M ; \mathbf{k}_b | T | a\, s_a \sigma_a ; \mathbf{k}_a > = \\
&\sum_{\substack{n N \Lambda \xi \\ l_x \lambda_x j_x m_x}} c_{n l_x N \Lambda}(\eta)\, (l_x \lambda_x \Lambda \xi | L M)\, (l_x \lambda_x s_x \sigma_x | j_x m_x) \\
&\qquad \int d^3R \int d^3r\, \chi_b^{(-)*}(\mathbf{k}_b, \mathbf{r}_b)\, \phi_{N\Lambda}(R)\, Y_\Lambda^{\xi *}(\hat{\mathbf{R}}) \\
&\qquad < b\, s_b \sigma_b ; x\, (n l_x s_x)\, j_x m_x | V_{bx} | a\, s_a \sigma_a > \chi_a^{(+)}(\mathbf{k}_a, \mathbf{r}_a) .
\end{aligned}
\tag{9}
$$

Here χ_a and χ_b are distorted waves and $\mathbf{r}$ is the displacement vector between the centers of mass of the two-nucleon clusters x and b.

3 — (α , d) AND (d , α) REACTIONS

Our present interest is to consider the particular case of (α , d) reactions. The range of n, l_x, s_x values to be considered in eqs. (5), (7) and (9) depends on the assumptions that are made regarding the wave functions of the α-particle and residual nucleus. Conservation of isospin implies that the transferred two-nucleon cluster has $T = 0$. Thus it must be either an even parity state with $s_x = 1$ or an odd parity state with $s_x = 0$. The contribution from the latter type of state is believed to be small since it can only arise from the overlap with odd parity components in the variable $\mathbf{r}_{12}$ in the α particle.

It is therefore usually assumed that the transferred two-nucleon cluster has even parity and only the $l_x = 0$ state is taken into

account in DWBA calculations. Furthermore it is frequently supposed that the two nucleons are in a relative S state with no nodes (n = 0). However we note that the $l_x = 2$ states have a non-vanishing overlap with parts of the α particle wave function and in particular with its D-state component.

With $l_x = 0$ we conclude that $j_x = 1$ and the V_{dx} matrix element of eq (9) can be expanded as [7]

$$< d\ 1\ \sigma_d ;\ x\,(n\,0\,1)\ 1\ \sigma_x \,|\, V_{dx} \,|\, \alpha > = \\ 1/2 \sum_{L'=0,2} (-1)^{\sigma_d} (L'\, M'\, 1\, \sigma_x \,|\, 1\, -\sigma_d)\, v_{nL'}(r)\, Y_{L'}^{M'}(\hat{\mathbf{r}}) . \tag{10}$$

The vector $\mathbf{r}$ represented in Fig. 1 is the separation between the centers of mass of the clusters; $\mathbf{r} = (\mathbf{r}_{32} + \mathbf{r}_{41}) / 2$ with $\mathbf{r}_{ij} = \mathbf{r}_i - \mathbf{r}_j$. As before we denote by 1,2 the transferred nucleons and by 1,3 and 2,4 the identical particles in the α particle. Conservation of parity implies that L′ can only be 0 and 2. The L′ = 0 and L′ = 2 terms on the right hand side of eq. (10) correspond to two different spin configurations in the α particle in which the spins of the two spin one clusters are antiparallel and parallel, respectively. When substituting eqs. (9) and (10) into eq. (7) and performing the summations over magnetic quantum numbers it is found that the orbital angular momentum L′ in eq. (10) is in fact the same as L′ in eq. (7). This gives

$$\beta^{l\lambda}_{1L'L} = \sum_{nN} c_{n0NL}(\eta)\ \tilde{B}^{l\lambda}_{nNLL'} , \tag{11}$$

with

$$\tilde{B}^{l\lambda}_{nNLL'} = \sqrt{3}/2 \sum_{MM'} (-1)^{1+M'}\ (L\, M\, L' - M' \,|\, l\, \lambda) \\ \int d^3R \int d^3r\ \chi_d^{(-)^*}(\mathbf{k}_d, \mathbf{r}_d)\ \phi_{NL}(R)\ Y_L^{M^*}(\hat{\mathbf{R}}) \\ v_{nL'}(r)\, Y_{L'}^{M'}(\hat{\mathbf{r}})\, \chi_\alpha^{(+)}(\mathbf{k}_\alpha, \mathbf{r}_\alpha) . \tag{12}$$

Using eqs. (5) and (11) we can write

$$B^{l\lambda}_{1J} = \sum_{nNL} G_{nNLJ} \sum_{L'} A^{LL'}_{l1J1}\, \tilde{B}^{l\lambda}_{nNLL'} . \tag{13}$$

Here the information on the nuclear structure of the A + 2 nucleus is as much as possible concentrated in the amplitude

$$G_{nNLJ} = \sum_{\eta} \mathcal{S}_J(\eta)\ \mathcal{G}_{L1J}(\eta)\ c_{n0NL}(\eta)\ . \tag{14}$$

On the other hand the information on the α particle is contained in the sum over L′.

The differential cross section for the A (α , d) B reaction is an incoherent sum over l and J

$$\begin{aligned} d\sigma / d\Omega \ &\propto \sum_{Jl\lambda} (2J_B + 1) / (2l + 1) \, |B^{l\lambda}_{1J}|^2 \\ &= \sum_{Jl\lambda} (2J_B + 1) / (2l + 1) \, \Big| \sum_{nNL} G_{nNLJ} \sum_{L'} A^{LL'}_{l1J1} \, \tilde{B}^{l\lambda}_{nNLL'} \Big|^2 . \end{aligned} \tag{15}$$

With the inclusion of the α-particle D-state the total orbital angular momentum transfer l may not be equal to L. Furthermore we notice that the L′ = 2 contribution introduces a J dependence into the cross section through the $A^{LL'}_{l1J1}$ coefficients.

Here we are particularly interested in the analysing powers of the inverse reaction B ($\vec{d}$, α) A. From invariance under time reversal the analysing powers T_{kq} of the B ($\vec{d}$, α) A reaction are related with the polarization tensors t_{kq} of the A (α , $\vec{d}$) B reaction by [11]

$$T_{kq} = (-1)^k \, t_{kq} \tag{16}$$

when using the same coordinate system on both sides of eq. (16). The polarization tensors t_{kq} are given by

$$t_{kq} = \text{Trace}\,(T^{\dagger} \tau_{kq}(1)\, T) \,/\, \text{Trace}\,(T^{\dagger} T) \tag{17}$$

where T is the transition amplitude for the (α , d) reaction and $\tau_{kq}(1)$ are the usual spin one operators [16]. Using eqs. (2), (16) and (17) we obtain

$$\begin{aligned} T_{kq} = -\sqrt{3}\, \Big(\sum_{l\lambda} (2l + 1)^{-1} |B^{l\lambda}_{1J}|^2 \Big)^{-1} \\ \sum_{Jl\lambda l'\lambda'} (-1)^{k+J+\lambda} \, W(1\,l\,1\,l'; Jk)\, (l\,-\lambda\ l'\,\lambda' \,|\, kq)\, B^{l\lambda}_{1J}\, B^{l'\lambda'*}_{1J} . \end{aligned} \tag{18}$$

Unlike the cross section the T_{kq} involve a coherent sum over $B^{l\lambda}_{1J}$ amplitudes with different l.

4 — THE ASYMPTOTIC D- to S-STATE RATIO IN THE α PARTICLE

A full finite range DWBA calculation for $B(\vec{d},\alpha)A$ reactions requires the knowledge of the radial wave functions $v_{nL'}(r)$, defined in eq. (10). We consider only the V_{dx} matrix element for $n = 0$ because the dominant component of the expansion (8) in the internal variable r_{12} of the transferred cluster is an S state with no nodes [17]. In the following it is therefore assumed that $n = 0$ and all dependence on n is dropped. However we note that at least in the $L' = 0$ part of the transition amplitude the contributions from S state cluster states with $n \neq 0$ are not negligible for some cases [18].

The overlap between the α particle wave function and the two spin-one clusters has an expansion analogous to eq. (10) [5, 7]

$$< \phi_d^{\sigma_d}(3,4)\,\phi_x^{\sigma_x}(1,2) \mid \phi_\alpha > = \tag{19}$$

$$1/2 \sum_{L'=0,2} (-1)^{\sigma_d} (L'\,M'\,1\sigma_x \mid 1\,-\sigma_d)\; u_{L'}(r)\; Y_{L'}^{M'}(\hat{r})\,.$$

This function satisfies the equation

$$-(B_\alpha - B_d - B_x + T_r) < \phi_d^{\sigma_d}(3,4)\,\phi_x^{\sigma_x}(1,2) \mid \phi_\alpha > \tag{20}$$

$$= < \phi_d^{\sigma_d}(3,4)\,\phi_x^{\sigma_x}(1,2) \mid V_{dx} \mid \phi_\alpha >$$

where on the right hand side the matrix element is the same as in eq. (10). B_α, B_d, B_x are binding energies and T_r is the kinetic energy in r. Combining eqs. (10), (19) and (20) we conclude that the radial wave functions $u_{L'}$ and $v_{L'}$ are related by

$$v_{L'}(r)\; Y_{L'}^{M'}(\hat{r}) = -(\hbar^2/2M)\,(\alpha^2 - \nabla^2)\; u_{L'}(r)\; Y_{L'}^{M'}(\hat{r})\,, \tag{21}$$

where $\alpha = [\,2M\,(B_\alpha - B_d - B_x)\,/\,\hbar^2\,]^{1/2}$ is the wave number of the relative motion between clusters in the α particle. Eq. (21) shows that asymptotically, for large r,

$$u_{L'}(r) \xrightarrow[r \to \infty]{} \mathcal{N}_{L'}\; i^{L'}\; h_{L'}(i\,\alpha\,r)\,, \tag{22}$$

neglecting the Coulomb interaction between clusters. The asymptotic D- to S-state ratio in the α particle is [5]

$$\rho = \mathcal{N}_2 / \mathcal{N}_0 \ . \tag{23}$$

In low energy (d , α) reactions the DWBA calculations are not very sensitive to the precise and presently unknown short range behaviour of the functions $u_{L'}(r)$ [7, 8]. The calculated tensor analyzing powers depend to a good approximation upon u_0 and u_2 only through the parameter D_2 defined by [1]

$$D_2 = \int_0^\infty u_2(r)\, r^4\, dr \,/\, 15 \int_0^\infty u_0(r)\, r^2\, dr \tag{24}$$

An alternative expression

$$D_2 = (2M / \hbar^2\alpha^2) \int_0^\infty v_2(r)\, r^4\, dr \,/ \int_0^\infty u_0(r)\, r^2\, dr \tag{25}$$

is obtained using eq. (21) to relate the coefficients of the k^2 term in a power series expansion of u_2 and v_2 in momentum space. The substitution of the asymptotic forms (22) into eq. (24) gives the well known relation [1, 19]

$$D_2 \simeq \rho \,/\, \alpha^2 \ . \tag{26}$$

However the reliability of this approximate relation is expected to be much smaller in (d , α) reactions than in (d , p) reactions because of the large α particle binding energy.

A non-vanishing D_2 can only be obtained through the nucleon-nucleon tensor interaction in the four body bound system. To obtain an estimate of D_2 we assume, in analogy with what is presently known about the three body bound system [3], that u_0 and u_2 are primarily determined, respectively, by the overlaps $< \phi_d(3,4)\ \phi_x(1,2) \mid \phi_{\alpha S} >$ and $< \phi_d(3,4)\ \phi_x(1,2) \mid \phi_{\alpha D} >$ with the S and D state components of the α particle wave function

$$\phi_\alpha = \phi_{\alpha S} + \phi_{\alpha D} \ . \tag{27}$$

It is important to emphasize that this is an approximation. For instance it is easily verified that the S state component $\phi_{\alpha S}$ gives

contributions to u_2 through the D-states in the spin one clusters. These contributions are probably small because they arise from low probability components in $\phi_{\alpha S}$ that result from coupling states with non-zero orbital angular momenta in the coordinates $\mathbf{r}_{12}$, $\mathbf{r}_{34}$, $\mathbf{r}$ to a total $L' = 0$.

A model to generate $\phi_{\alpha D}$ is required in order to calculate D_2 . Using a perturbative treatment [5] we can write, to first order in the tensor interaction,

$$(T + \sum_{i<j} V_c(i,j) + B_\alpha) \mid \phi_{\alpha D} > \simeq - \sum_{i<j} V_T(i,j) \mid \phi_{\alpha S} > . \qquad (28)$$

Here $V_c(i,j)$ and

$$V_T(i,j) = V_T(r_{ij})\, S_{12}(i,j) \qquad (29)$$

are the central and tensor parts of the nucleon-nucleon interaction. The overlap of eq. (28) with the spin one clusters satisfies the equation

$$\begin{aligned}(B_\alpha - B_d - B_x + T_r) < \phi_d^{\sigma_d}(3,4)\, \phi_x^{\sigma_x}(1,2) \mid \phi_{\alpha D} > \simeq \\ - < \phi_d^{\sigma_d}(3,4)\, \phi_x^{\sigma_x}(1,2) \mid \sum_{i<j} V_T(i,j) \mid \phi_{\alpha S} >\end{aligned} \qquad (30)$$

if the central interactions between clusters are neglected. This approximation is based on the fact that the effect of V_c is reduced by the centrifugal barrier associated with the D-state in $\mathbf{r}$.

On the right hand side of eq. (30) there are no contributions from $V_T(1,3)$ and $V_T(2,4)$ since the nucleon pairs 1,3 and 2,4 are in singlet states. Furthermore the tensor interactions $V_T(1,2)$ and $V_T(3,4)$ do not generate a relative D-state motion of the cluster if we consider only the dominant component of $\phi_{\alpha S}$ exclusively with S states in $\mathbf{r}_{12}$, $\mathbf{r}_{34}$, $\mathbf{r}$. Thus combining eqs. (10), (21) and (30) yields

$$\begin{aligned}< \phi_d^{\sigma_d}(3,4)\, \phi_x^{\sigma_x}(1,2) \mid V_T(2,3) + V_T(1,4) \mid \phi_{\alpha S} > = \\ 1/2\,(-1)^{\sigma_d}(2\,M'\,1\,\sigma_x \mid 1\,-\sigma_d)\, v_2(r)\, Y_2^{M'}(\hat{\mathbf{r}}) .\end{aligned} \qquad (31)$$

Using eqs. (19), (25) and (31) it is now straightforward to calculate the parameter D_2. This calculation is considerably simplified by the use of gaussian wave functions to represent the bound states

$$\phi_{\alpha S} = E(\lambda) \exp[-\lambda(r_{12}^2 + r_{34}^2 + 2r^2)/4] \chi_0(1,3) \chi_0(2,4), \quad (32)$$

$$\phi_d^{\sigma_d}(3,4) \phi_x^{\sigma_x}(1,2) = F^2(\nu) \exp[-\nu(r_{34}^2 + r_{12}^2)/2] \chi_1^{\sigma_d}(3,4) \chi_1^{\sigma_x}(1,2). \quad (33)$$

In eq. (33) we made the usual assumption of describing x by a deuteron wave function. $E(\lambda) = 2^{-3/2}(\lambda/\pi)^{9/4}$ and $F(\nu) = (\nu/\pi)^{3/4}$ are normalization constants and $\chi_0(i,j)$ and $\chi_1^{\sigma}(i,j)$ are singlet and triplet spin wave functions. The parameters λ and ν are related to the α - particle and deuteron rms radius by

$$\langle r^2 \rangle^{1/2}_{\alpha \text{ particle}} = 3/(2\sqrt{2\lambda}), \quad (34)$$

$$\langle r^2 \rangle^{1/2}_{\text{deuteron}} = 1/2\sqrt{3/2\nu}. \quad (35)$$

With the wave functions (32) and (33), the radial function u_0 is a gaussian function

$$u_0(r) = 4\sqrt{2}\,\delta^{-3}(\pi^{-1}\lambda^9\nu^6)^{1/4} e^{-\lambda r^2/2} \quad (36)$$

where $\delta = \nu + \lambda/2$. To calculate $v_2(r)$ from eq. (31) it is convenient to write

$$\chi_0(1,3)\chi_0(2,4) = -1/2[\chi_0(1,4)\chi_0(3,2) + \sum_m (-1)^{1+m} \chi_1^m(1,4)\chi_1^{-m}(3,2)] \quad (37)$$

since we are interested in the tensor force in the nucleon pairs 1,4 and 2,3. Using the relation

$$S_{12}(\hat{r})\chi_1^{\sigma} = 4\sqrt{2\pi} \sum_{\sigma' M} (1\,\sigma'\,2\,M \mid 1\,\sigma)\, Y_2^M(\hat{r})\, \chi_1^{\sigma'} \quad (38)$$

and eqs. (32) and (33) we obtain

$$v_2(r) = 2^7 (\lambda^3/\pi)^{3/4} (\nu/\delta)^{3/2} \exp[-(\nu+\lambda) r^2] \int_0^\infty j_2(2i\delta r x) \exp(-\delta x^2) V_T(x) x^2 dx \ . \quad (39)$$

Finally doing the integrations over r in eq. (25) gives

$$D_2 = (8/15)(B_\alpha - 2B_d)^{-1} (\lambda^3/\pi)^{1/2} [\delta/(\nu+\lambda)]^{7/2} \int_0^\infty V_T(x) \exp[-\lambda\delta x^2/2(\nu+\lambda)] x^4 dx \ . \quad (40)$$

Using the one-pion-exchange tensor potentital (OPEP)

$$V_T(r) = -C_T h_2(i\mu r) \quad (41)$$

with $C_T = 10.463$ MeV and $\mu = 0.7$ fm^{-1} [20] we obtain $D_2 = -0.153$ fm^2 for deuteron and α particle rms radius of 1.96 fm and 1.42 fm [21], respectively. The introduction of a cutoff factor [22], $1 - \exp(-Ar^2)$ where $A = 0.735$ fm^{-2}, in the OPEP tensor potential increases D_2 to -0.117 fm^2. This change of 23 % indicates that the parameter D_2 depends on the behaviour of the tensor interaction at distances smaller than 2 fm. The sensitivity of D_2 to the tensor interaction at short distances is much stronger in (d , α) than in (d , p), (d , t) or (d , ^{3}He) reactions. The values of D_2 become slightly larger when either the rms radius of the deuteron or the rms radius of the α particle are increased. For instance $D_2 = -0.124$ fm^2 for deuteron and α particle rms radii of 2.10 fm and 1.70 fm, respectively.

Although the model used to calculate D_2 is probably realistic the bound state wave functions are not adequate. In fact D_2 is very sensitive to the asymptotic region of large r . Thus we can expect that the calculated values of D_2 are overestimated because they were obtained with gaussian functions. The same problem of overestimated values of D_2 was also found in calculations of D_2 for ^{3}H when using wave functions with incorrect asymptotic

behaviour [23]. Calculations based on the very simplified model for ρ developed in ref. [5] give $-0.35 < D_2 < -0.15$ fm² [24]. This model has the unrealistic feature that the tensor interaction between clusters depends only on the coordinate **r** but, on the other hand, the calculations were performed with wave functions $u_0(r)$ with correct asymptotic behaviour.

5 — PERIPHERAL MODEL OF (d , α) AND (α , d) REACTIONS

To study the dependence of the cross section and of the analysing powers on the amplitudes G_{NLJ} and also on the asymptotic D- to S-state ratio ρ we use the peripheral model developed in refs. [5, 25]. The bound state wave functions of the transferred two nucleon cluster in the α particle and in the nucleus B are represented by their asymptotic forms for large r

$$u_{L'}(r) \simeq \mathcal{N}_{L'}\, i^{L'}\, h_{L'}(i\alpha r)\,, \tag{42}$$

$$\phi_{NL}(r) \simeq \mathcal{N}_{NL}\, i^{L}\, h_{L}(i\beta r)\,. \tag{43}$$

Here β is the wave number corresponding to the binding energy of the cluster x in B and $\mathcal{N}_{NL}$ are asymptotic normalization constants. For small recoil effects the $\tilde{B}^{l\lambda}_{NLL'}$ amplitudes can be approximated by

$$\tilde{B}^{l\lambda}_{NLL'} \simeq \sqrt{3}/2 \sum_{MM'} (-1)^{1+M'} (L\,M\,L'\,-M' \mid l\,\lambda) \int d^3R \int d^3r\, \chi_d^{(-)*}(\mathbf{k}_d, (m_A/m_B)\,\mathbf{R})\, \phi_{NL}(|\mathbf{R} - a\,\mathbf{r}|) \tag{44}$$

$$Y_L^{M*}(\mathbf{R} - \hat{a}\,\mathbf{r})\, v_{L'}(r)\, Y_{L'}^{M'}(\hat{\mathbf{r}})\, \chi_\alpha^{(+)}(\mathbf{k}_\alpha, \mathbf{R})\,.$$

The value of the parameter a depends on the particular assumptions made in the derivation of eq. (44). For instance if we choose **R** as the average of the arguments of the two distorted waves [26] then $a = 3/4$. In the usual form of the non-recoil approximation [27] for heavy ion transfer reactions $a = 1$.

With the bound state wave functions (42) and (43) the **r** integration in eq. (44) can be performed analytically. In fact the formula A. 46 of ref. [14] gives

$$\int d^3r\, i^L h_L(i\beta\,|\,\mathbf{R}-\mathbf{r}\,|)\, Y_L^{M\,*}(\hat{\mathbf{R}-\mathbf{r}})\,(\nabla^2-\alpha^2)\, i^{L'} h_{L'}(i\alpha r)\, Y_{L'}^{M'}(\hat{\mathbf{r}})$$
$$= \sqrt{4\pi}\,\hat{L}'\,(L'0\,l\,0\,|\,L0)\,(-1)^{L'+M'}\,(L\,M\,L'-M'\,|\,l\,\lambda) \qquad (45)$$
$$(\beta^{L'}/\alpha^{L'+1})\, i^l h_l(i\beta R)\, Y_l^{\lambda\,*}(\hat{\mathbf{R}})\,.$$

Therefore using eqs. (42), (43) and (45) we obtain

$$\sum_{MM'}(-1)^{1+M'}\,(L\,M\,L'-M'\,|\,l\,\lambda)\cdot$$
$$\int d^3r\,\phi_{NL}(|\mathbf{R}-a\,\mathbf{r}\,|)\, Y_L^{M*}(\hat{\mathbf{R}-a\,\mathbf{r}})\, v_{L'}(r)\, Y_{L'}^{M'}(\hat{\mathbf{r}}) = \qquad (46)$$
$$-\frac{\hbar^2}{2\,M\alpha}\,\mathcal{N}_{NL}\,\mathcal{N}_{L'}\,\sqrt{4\pi}\,\hat{L}'\,(L'0\,l\,0\,|\,L0)\left(\frac{a\,\beta}{\alpha}\right)^{L'} i^l h_l(i\beta R)\, Y_l^{\lambda\,*}(\hat{\mathbf{R}})$$

The neglect of the recoil induced by the transfer implies that only normal parity values of l are allowed

$$l + L + L' = \text{even}\,. \qquad (47)$$

The substitution of eq. (46) into eq. (44) and the use of plane waves to represent the scattering states gives

$$\tilde{B}^{l\lambda}_{NLL'} = I_l(Q)\, Y_l^{\lambda\,*}(\hat{Q})\,\hat{L}'\,(L'0\,l\,0\,|\,L0)\,(a\,\beta/\alpha)^{L'}\,\mathcal{N}_{NL}\,\mathcal{N}_{L'}\,. \qquad (48)$$

Here

$$\mathbf{Q} = \mathbf{k}_\alpha - (m_A/m_B)\,\mathbf{k}_d\,, \qquad (49)$$

is the momentum transfer in the reaction and

$$I_l(Q) = 2\sqrt{3}\,\pi\,(\hbar^2/M\alpha)\,(-1)^{l+1}\int h_l(i\beta R)\, j_l(Q\,R)\, R^2 dR\,. \qquad (50)$$

Finally the combination of eqs. (13) and (48) yield

$$B_{1J}^{l\lambda} = U_{lJ} Y_l^{\lambda\,*} (\hat{Q}) \ , \tag{51}$$

with

$$U_{lJ} = I_l (Q) \sum_{LL'} S_{LJ} \hat{L}' (L' 0 \, l 0 \, | \, L0) A_{l1J1}^{LL'} \mathcal{R}_{L'} (a \beta / \alpha)^{L'} \ . \tag{52}$$

The information on the A + 2 nucleus is now entirely contained in the spectroscopic amplitude

$$S_{LJ} = \sum_{N} G_{NLJ} \mathcal{R}_{NL} = \sum_{N\eta} \mathcal{S}_J (\eta) \mathcal{G}_{L1J} (\eta) c_{0NL} (\eta) \mathcal{R}_{NL} \ . \tag{53}$$

Using eqs. (15) and (51) it is easily concluded that the cross section is an incoherent sum of the square of the amplitudes U_{lJ} over l and J

$$d\sigma / d\Omega \ \propto \ (2J_B + 1) / 4\pi \sum_{lJ} U_{lJ}^2 \ . \tag{54}$$

It is also straightforward to obtain an expression for the analysing powers T_{kq} as a function of U_{lJ}. Since the dependence on the magnetic quantum number in $B_{1J}^{l\lambda}$ is now given by the spherical harmonic Y_l^{λ} the summation over λ and λ' in eq. (18) gives rise to a Clebsch-Gordan coefficient ($l\,0\,l'0 \,|\, k0$) and implies that the T_{kq} are proportional to $Y_k^{q} (\hat{Q})$. Furthermore there is a restriction in the values of k. In a given transition the allowed values of L have all the same parity and L′ is even. Therefore the selection rule (47) implies that all values of the total orbital angular momentum transfer l have the same parity. In conclusion the analyzing powers with k odd vanish in the peripheral model. This is a general property of plane wave approximations [28]. For k = 2 eqs. (18) and (51) yield

$$T_{2q} = - (8 \pi / 5)^{1/2} A \, Y_2^{q} (\hat{Q}) \ , \tag{55}$$

with

$$A = (3/2)^{1/2} (\sum_{lJ} U_{lJ}^2)^{-1} \sum_{ll'J} \hat{l} \, \hat{l}' (l\,0\,l'0 \,|\, 20) \, W (l\,1\,l'1 \, ; J2) \, U_{lJ} \, U_{l'J} \ . \tag{56}$$

Eq. (55) shows that in the peripheral model the angular dependence of the tensor analyzing powers is essentially determined by the spherical harmonics $Y_2^q(\hat{Q})$. In the Madison convention coordinate system [16] where the z axis is along $\mathbf{k}_d$ and the y axis is along $\mathbf{k}_d \times \mathbf{k}_p$

$$T_{20} = -(1/\sqrt{2})\, A\, (3\cos^2\gamma - 1)\,, \tag{57a}$$

$$T_{21} = \sqrt{3}\, A \sin\gamma \cos\gamma\,, \tag{57b}$$

$$T_{22} = -(\sqrt{3}/2)\, A \sin^2\gamma\,. \tag{57c}$$

The angle

$$\gamma = \text{arc tg}\left\{ \sin\theta \left[\cos\theta - (m_A / m_B)(k_d / k_\alpha) \right]^{-1} \right\} \tag{58}$$

is the angle between $\mathbf{Q}$ and $\mathbf{k}_d$ and θ is the scattering angle. The relations (57) acquire a particularly simple form when the tensor analyzing powers are expressed in a cartesian representation

$$A_{xx} = -(1/\sqrt{2})(T_{20} - \sqrt{6}\, T_{22}) = (A/2)(3\cos 2\gamma - 1)\,, \tag{59a}$$

$$A_{yy} = -(1/\sqrt{2})(T_{20} + \sqrt{6}\, T_{22}) = A\,, \tag{59b}$$

$$A_{zz} = -(A_{xx} + A_{yy}) = -(A/2)(3\cos 2\gamma + 1)\,. \tag{59c}$$

The most significant aspect of eq. (59) is that A_{yy} is, to a good approximation, independent of θ. This property of A_{yy} is common to other reactions [25] and has a simple physical interpretation. The difference between the unpolarized cross section and a cross section for a spin orientation perpendicular to the reaction plane is insensitive to the scattering angle because the correlation between spin and deformation implies that the wave function of relative motion between clusters has spherical symmetry in the reaction plane. This spherical symmetry is broken for other spin orientations and as a result the tensor analyzing powers become dependent on θ. For instance the analyzing power A_{xx} has a minimum of -2A at $\theta = \text{arc cos}\,(m_A k_d / m_B k_\alpha)$ and is equal to A at $\theta = 0^\circ$ and 180°.

5.1 — *Natural parity transitions*

In natural parity transitions L = J . From eqs. (6) and (52) and with the help of tables of angular momentum coupling coefficients [12] we obtain

$$U_{lJ} = \delta_{lJ} (\mathcal{N}_0 / \sqrt{3}) \, I_J \, S_{JJ} [1 + (\rho / \sqrt{2}) (a \beta / \alpha)^2] . \tag{60}$$

The differential cross section in a transition with a given J is

$$(d\sigma / d\Omega)_J \propto (\mathcal{N}_0^2 / 12\pi) \{ I_J \, S_{JJ} [1 + (\rho / \sqrt{2}) (a \beta / \alpha)^2] \}^2 . \tag{61}$$

The fact that ρ is negative implies that the D-state of the α particle decreases the cross section of (d , α) and (α , d) natural parity transitions. This effect is particularly noticeable in transitions with large β .

For the tensor analyzing powers the substitution of eq. (60) into eq. (56) gives $A = -1/2$ and therefore

$$A_{yy} = -1/2 . \tag{62}$$

This simple result is interesting to understand. A_{yy} is equal to the polarization component [16]

$$p_{yy} = < 3 s_y^2 - 2 > \tag{63}$$

of the outgoing deuteron beam in a (α , $\vec{d}$) reaction. In a peripheral reaction the vector **L** is perpendicular to the reaction plane and therefore either parallel or antiparallel to the y axis. For L = J and because $\mathbf{J} = \mathbf{L} + \mathbf{s}_x$, the spin $\mathbf{s}_x$ is either parallel or antiparallel to the z axis. This is also true for the outgoing deuteron because of the spin correlation between the spin one clusters in the α particle. Thus in natural parity transitions the (α , d) reaction acts as a spin filter supressing the $m_z = 0$ states. In a polarization state where $m_z = \pm 1$, $< s_y^2 > = 1/2$ and therefore from eq. (63) $p_{yy} = A_{yy} = -1/2$.

5.2 — *Unnatural parity transitions*

In unnatural parity transitions for a fixed J the orbital angular momentum of the transferred cluster can be $L = J - 1$ and $L = J + 1$. Again from eqs. (6) and (52) we obtain [12] for $L = J - 1$

$$U_{J-1,J} = (\mathcal{N}_0/\sqrt{3})\, I_{J-1}\,[\, S_{J-1,J} + (\rho/\sqrt{2})\,(2J+1)^{-1}\,(a\beta/\alpha)^2 \\ (3\,[\,J(J+1)\,]^{1/2}\, S_{J+1,J} - (J-1)\, S_{J-1,J})\,] \qquad (64)$$

and for $L = J + 1$

$$U_{J+1,J} = (\mathcal{N}_0/\sqrt{3})\, I_{J+1}\,[\, S_{J+1,J} + (\rho/\sqrt{2})\,(2J+1)^{-1}\,(a\beta/\alpha)^2 \\ (3\,[\,J(J+1)\,]^{1/2}\, S_{J-1,J} - (J+2)\, S_{J+1,J})\,]\,. \qquad (65)$$

Given J , the differential cross section is

$$(d\sigma/d\Omega)_J \propto (1/4\pi)\,(U^2_{J-1,J} + U^2_{J+1,J})\,. \qquad (66)$$

Notice that for $\rho = 0$

$$(d\sigma/d\Omega)_J \propto (\mathcal{N}_0^2/12\pi)\,(I^2_{J-1}\, S^2_{J-1,J} + I^2_{J+1}\, S^2_{J+1,J}) \qquad (67)$$

is insentitive to the sign of the spectroscopic amplitures $S_{L,J}$.

Eqs. (64-66) show that, because ρ is negative, the D-state of the α particle has generally the effect of increasing the cross section of unnatural parity transitions. This is the case, for instance, of a pure $L = J - 1$ transition and also of a pure $L = J + 1$ transition. The opposite effect of the D-state in natural and unnatural parity transitions introduces in the cross section a J-dependence which qualitatively is in agreement with that observed in the ^{208}Pb (α , d) ^{210}Bi reaction feeding members of the $\{ h_{9/2}, g_{9/2} \}$ multiplet [10].

We now consider the tensor analysing powers in unnatural parity transitions. Eqs. (56) and (59b) give

$$A_{yy} = A = \frac{(J+2)\,x^2 - 6\,[\,J(J+1)\,]^{1/2}\,x + J - 1}{2\,(2J+1)\,(1+x^2)} \qquad (68)$$

with

$$x = U_{J+1,J} / U_{J-1,J} \ . \tag{69}$$

Thus A_{yy} varies from a minimum value of $-1/2$ for $x = [J/(J+1)]^{1/2}$ to a maximum value of 1 for $x = -[(J+1)/J]^{1/2}$.

In the absence of D-state effects $\rho = 0$ and

$$x = K_J \ S_{J+1,J} / S_{J-1,J} \tag{70}$$

where $K_J = I_{J+1} / I_{J-1}$ is a positive quantity due to the form of the integrals (50). Eqs. (55) and (68) show that the T_{2q} have a strong dependence on the spectroscopic amplitudes S_{LJ}. Unlike the cross section they depend on the relative sign of $S_{J-1,J}$ and $S_{J+1,J}$. Fig. 2 shows the values of

$$(A_{yy})_J = (J-1) / [2(2J+1)] \tag{71}$$

for a pure $L = J-1$ transition ($x = 0$) and

$$(A_{yy})_J = (J+2) / [2(2J+1)] \tag{72}$$

for a pure $L = J+1$ transition ($x = \infty$). Since $K_J > 0$, $x > 0$ when $S_{J+1,J}$ and $S_{J-1,J}$ have the same sign and $x < 0$ when $S_{J+1,J}$ and $S_{J-1,J}$ have opposite signs. The quantity x is a double valued function of A_{yy}. $x < 0$ for $(A_{yy})_J > (J+2) / [2(2J+1)]$, $x > 0$ for $(A_{yy})_J < (J-1) / [2(2J+1)]$ and x is either positive or negative for $(J-1)/[2(2J+1)] < (A_{yy})_J < (J+2)/[2(2J+1)]$ as shown in Fig. 2.

In the presence of D-state effects $\rho \neq 0$ and for a pure $L = J-1$ transition

$$x = \frac{K_J}{3\rho b} \ \frac{3J+1-\rho b(J+2)}{[J(J+1)]^{1/2}} \tag{73}$$

where $b = (a\beta\alpha)^2 / \sqrt{2}$. In a pure $L = J+1$ transition

$$x = 3\rho b \ K_J \ \frac{[J(J+1)]^{1/2}}{2J+1-\rho b(J-1)} \ . \tag{74}$$

In both cases $x < 0$. Therefore the effect of the D-state is to increase A_{yy} relative to the values given by eqs. (71) and (72). The substitution of eqs. (73) and (74) into eq. (68) shows that the α particle D-state effect is relatively larger in $L = J - 1$ than in $L = J + 1$ transitions. This result is important to select transitions where the extraction of ρ from T_{2q} experimental data is favoured.

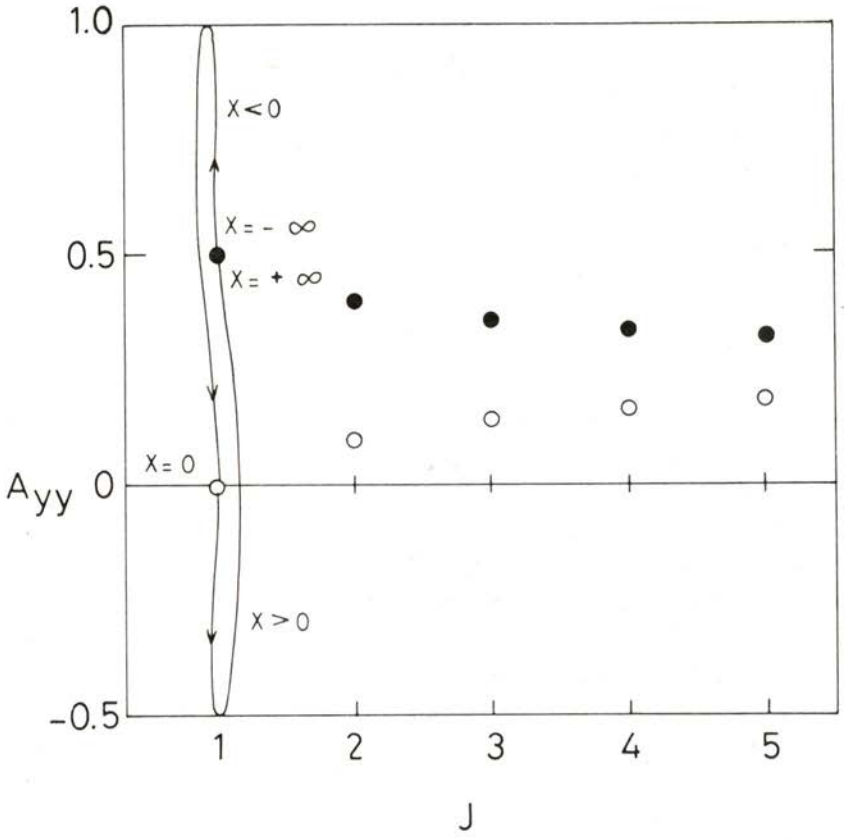

Fig. 2 — The tensor analyzing power A_{yy} of (**d** , α) reactions to unnatural parity states as a function of the total angular momentum transfer J. The open and full points correspond to pure $L = J - 1$ and pure $L = J + 1$ transitions, respectively. For each J , A_{yy} is given by eq. (68) and varies with x from - 1/2 to 1. For $J = 1$ we have represented in a loop the values taken by A_{yy} as function of x .

In an unnatural parity transition with only one pair of values for J , L the measurement of the T_{2q} yields a unique value for x that can be used to estimate ρ. Knowing ρ it becomes possible to determine the amplitudes $S_{J+1,J}$ and $S_{J-1,J}$ in transitions with L mixing. These amplitudes can then be compared with those obtained from shell model calculations.

6 — CONCLUSIONS

A general discussion of the angular momentum structure of the transition amplitude in (α , d) and (d , α) reactions is presented. Particular emphasis is given to the analysis of contributions from the D-state components of the α particle wave function. The parameter D_2 is estimated using a perturbative treatment to first order in the tensor interaction and gaussian wave functions to represent the deuteron and α - particle bound state wave functions. These calculations show that D_2 in (d , α) reactions is sensitive to the form of the nucleon-nucleon tensor interaction at distances smaller than 2 fm. Further calculations of D_2 using more realistic wave functions with correct asymptotic behaviour are required.

The dependence of the cross section and of the tensor analysing powers on the asymptotic D- to S-state ratio ρ and on the spectroscopic amplitudes S_{LJ} is discussed using a plane wave peripheral model. The tensor analyzing power A_{yy} is particularly interesting because it is independent of angle and its value is a simple function of ρ and S_{LJ}. The present analysis indicates that the determination of ρ from T_{2q} data is specially favoured in unnatural parity transitions involving only the orbital angular momentum $L = J - 1$. These occur in (d , α) reactions on closed shell target nuclei leading to outstretched nuclear configurations with $J = L + 1$.

With the peripheral model it is possible to identify the main features of nuclear structure and D-state effects in the cross section and T_{2q}. However the model cannot be applied to the description of iT_{11} and furthermore it cannot be used in a quantitative analysis of the data. For instance the experimental A_{yy} angular distributions oscillate around a certain mean value [5] that varies from transition to transition. This mean value can be

interpreted with the peripheral model but to reproduce the oscillatory behaviour it is necessary to perform a DWBA calculation including a spin-orbit interaction in the deuteron channel [7, 8]. An analysis of recent T_{2q} data in (d α) reactions with full finite range DWBA calculations is in progress and shall be presented elsewhere.

We are thankful to W.J. Thompson for illuminating discussions. One of us (FDS) would like to thank the hospitality of the Department of Physics and Astronomy of the University of North Carolina where part of this work was performed.

REFERENCES

[1] R. C. JOHNSON and F. D. SANTOS, *Particles and Nuclei*, **2**, 285 (1971).

[2] R. P. GODDARD, L. D. KNUTSON and J. A. TOSTEVIN, *Phys. Lett.* **118B**, 241 (1982).

[3] L. D. KNUTSON, B. P. HICHWA, A. BARROSO, A. M. EIRÓ, F. D. SANTOS and R. C. JOHNSON, *Phys. Rev. Lett.* **35**, 1570 (1975).

[4] S. ROMAN, A. K. BASAK, J. B. A. ENGLAND, J. M. NELSON, N. E. SANDERSON, F. D. SANTOS and A. M. EIRÓ, *Nucl. Phys.* **A289**, 269 (1977); J. A. BIESZK and L. D. KNUTSON, *Nucl. Phys.* **A349**, 445 (1980).

[5] F. D. SANTOS, S. A. TONSFELDT, T. B. CLEGG, E. J. LUDWIG, Y. TAGISHI and J. F. WILKERSON, *Phys. Rev.* **C25**, 3243 (1982).

[6] J. L. FRIAR, B. F. GIBSON, D. R. LEHMAN and G. L. PAYNE, *Phys. Rev.* **C25**, 1616 (1982).

[7] F. D. SANTOS, *Prog. Theor. Phys.* **40**, 1679 (1983).

[8] J. A. TOSTEVIN, *Phys. Rev.* **C28**, 961 (1983).

[9] M. A. NAGARAJAN and G. R. SATCHLER, *Phys. Rev. Lett.* **49**, 1899 (1982).

[10] W. W. DAEHNICK, M. J. SPISAK and J. R. COMFORT, *Phys. Rev.* **C23**, 1906 (1981).

[11] G. R. SATCHLER, *Nucl. Phys.* **55**, 1 (1964).

[12] M. E. ROSE, *Elementary theory of angular momentum*, John Wiley, 1963.

[13] R. D. LAWSON, *Theory of the nuclear shell model*, Oxford University Press, 1980.

[14] F. D. SANTOS, *Nucl. Phys.* **A212**, 341 (1973).

[15] T. A. BRODY and M. MOSHINSKY, *Tables of transformation brackets* (Monografias del Instituto di Fisica, México, 1960).

[16] *Proceedings of the 3rd International Symposium on Polarization Phenomena in Nuclear Reactions*, edited by H. H. BARSCHALL and W. HAEBERLI (University of Wisconsin Press, Madison, 1971), p. 25.

[17] N. K. GLENDENNING, *Phys. Rev.* **137**, B102 (1965).

[18] R. J. DE MEIJER, L. M. PUT, J. J. AKKERMAN, J. C. VERMEULEN and C. R. BINGHAM, *Nucl. Phys.* **A386**, 200 (1982).

[19] L. D. KNUTSON, in *Proceedings of the 4th International Symposium on Polarization Phenomena in Nuclear Reactions*, edited by W. GRUEBLER and V. KÖNIG (Birkhauser-Verlag, Basel, 1976), p. 205.

[20] R. V. REID, *Ann. of Physics* **50**, 411 (1968).

[21] R. W. BERARD, F. R. BUSKIRK, E. B. DALLY, J. N. DYER, X. K. MARUYAMA, R. L. TOPPING and T. J. TRAVERSO, *Phys. Lett.* **47B**, 355 (1973); T. KATAYAMA, Y. AKAISHI and H. TANAKA, *Prog. Theor. Phys.* **67**, 236 (1982).

[22] D. O. RISKA and G. E. BROWN, *Phys. Lett.* **32B**, 662 (1970).

[23] F. D. SANTOS, A. M. EIRÓ and A. BARROSO, *Phys. Rev.* **19C**, 238 (1979); L. D. KNUTSON and S. N. YANG, *Phys. Rev.* **20C**, 1631 (1979).

[24] A. M. EIRÓ and F. D. SANTOS, *Proceedings of the International Conference on Nuclear Physics*, Florence 1983.

[25] F. D. SANTOS and A. M. GONÇALVES, *Phys. Rev.* **C24**, 156 (1981).

[26] L. D. KNUTSON, *Ann. Phys.* **106**, 1 (1977).

[27] P. J. A. BUTTLE and L. J. B. GOLDFARB, *Nucl. Phys.* **78**, 409 (1966).

[28] F. D. SANTOS, *Nucl. Phys.* **A236**, 90 (1974).

NUCLEAR HYDRODYNAMICS (*)

J. P. DA PROVIDÊNCIA

Departamento de Física, Universidade de Coimbra,
3000 Coimbra, Portugal

(Received 9 January 1984; final form in 11 April 1984)

ABSTRACT — Based on the local equilibrium assumption and taking as wave function a Slater determinant, the equations of motion and boundary conditions for the first sound are obtained from a variational derivation based on the quantum mechanical lagrangian. Assuming density dependent δ forces, it is shown that in the classical limit the equilibrium density is $\rho_0(r) = \rho_0(0)\Theta(R-r)$, where $\rho_0(0)$ is the nuclear matter equilibrium density.

1 — INTRODUCTION

Giant resonances in atomic nuclei are highly excited states in which an appreciable fraction of the nucleons of a nucleus move in a coherent manner.

On the microscopic level the random phase approximation provides a very detailed description of collective vibrations. It requires, however, a considerable numerical effort, which might obscure the simple physical relations pertinent to strongly collective excitations. Fluid dynamical methods in application to giant multipole resonances [2-11] aim at understanding salient features of these collective modes, without entering into the complexity of detailed numerical descriptions.

In order to reach a deeper understanding of the physical processes associated with the behaviour of atomic nuclei, it is desirable to separate detailed aspects of nuclear properties, which often appear due to shell effects, from gross properties depending

(*) Presented at "3.ª Conferência Nacional de Física", Coimbra, Portugal (June 16 - June 18, 1982).

smoothly on the mass number A. This suggests, therefore, an explanation on the basis of fluid dynamical approximations, which may be formulated in terms of such quantities as matter and current densities, denoted respectively by ρ and $\mathbf{j}$, pressure tensor P_{ij}, etc.

In this note, we will restrict the discussion to hydrodynamics [1-3], which is the simplest example of such an approximation. In the hydrodynamical case, the main assumption is the use of the Thomas-Fermi approximation or, equivalently, that the sphericity of the Fermi surface in momentum space is preserved during the nuclear motion.

Our purpose is to derive the macroscopic equations of motion, which characterize first sound, starting from a microscopic basis. As wave function we consider the following Slater determinant

$$| \phi > = \exp (i \hat{Q} \hbar^{-1}) | \phi_f > \quad , \tag{1}$$

where $| \phi_f >$ is, among the Slater determinants leading to the density ρ_f the one which minimizes the expectation value of the energy. Therefore the distribution function, associated to $| \phi_f >$, may be written as follows

$$f_f = \Theta (p_f^2 (\mathbf{r}) - p^2) \quad , \tag{2}$$

assuming the value 1 when $p_f^2 (\mathbf{r}) > p^2$ and zero otherwise. In this way the Pauli principle is obviously taken into account.

In order to have an appropriate description of the time evolution of the system, we must allow the distribution function to acquire time odd components, which is done with the help of the time even generator $\hat{Q}$. In this note $\hat{Q}$ is just a local field

$$\hat{Q} = \sum_{i=1}^{A} \chi (\mathbf{r}_i , t) \quad . \tag{3}$$

Since we are interested in the classical limit of nuclear dynamics, we restrict our discussion to the leading orders of appropriate Wigner-Kirkwood expansions. To avoid cumbersome notations, we find it most often convenient to denote by the same symbol an operator and its Wigner transform. The density matrix $\hat{\rho}$ is the only exception. In this case, we denote the distribution by $f (\mathbf{r} , \mathbf{p} , t)$, in order to avoid confusion with the density $\rho (\mathbf{r} , t)$.

2 — THE STATIC PROBLEM

The equilibrium distribution function f_0 is obtained by minimizing the energy density functional $W[f]$

$$W[f] = \int d\Gamma_1 f(1)\, p_1^2/(2m) + (1/2!) \iint d\Gamma_1\, d\Gamma_2 f(1) f(2) v_{12} + (1/3!) \iiint d\Gamma_1\, d\Gamma_2\, d\Gamma_3 f(1) f(2) f(3) v_{123} + \ldots \tag{4}$$

and by taking into account the subsidiary condition

$$A = \int d\Gamma\, f \quad , \tag{5}$$

where the quantities v_{12}, v_{123}, ..., stand, respectively, for the two-body, three-body, ... interactions. A is the particle number and $d\Gamma$ is given by the following expression

$$d\Gamma = g\, d^3r\, d^3p\, (2\pi\hbar)^{-3} \, . \tag{6}$$

The distribution function describing a system instantaneously at rest is given by (2). Since the only quantity on which f_f depends is $p_f^2(\mathbf{r})$, it is clear that $W[f_f]$ may be written as a functional of the density ρ_f associated to f_f,

$$\rho_f = g \int d^3p\, (2\pi\hbar)^{-3} f_f \quad , \tag{7}$$

$$W[f_f] = E[\rho_f] = \int_D d^3r\, F(\rho_f) \quad , \tag{8}$$

where the domain D is the region where $p_f^2(\mathbf{r})$ is positive.

A simplified hamiltonian with two-body and three-body δ forces is considered,

$$v_{12} = t_0\, \delta(\mathbf{r}_1 - \mathbf{r}_2) \quad , \tag{9}$$

$$v_{123} = t_3\, \delta(\mathbf{r}_1 - \mathbf{r}_2)\, \delta(\mathbf{r}_2 - \mathbf{r}_3) \quad . \tag{10}$$

For such an hamiltonian $F(\rho_f)$ is

$$F(\rho_f) = (3/10m)\,\rho_f\, p_f^2 + a_2\,\rho_f^2 + a_3\,\rho_f^3 \qquad (11)$$

We choose the following Skyrme parameters: $a_2 = -408.4$ MeV fm^3 and $a_3 = 1079.4$ MeV fm^6. This choice is made in order to enable comparision with the results obtained in ref. [3] for a calculation of first sound in finite droplets of nuclear matter with smooth surface and therefore related to an energy functional which includes, besides the volume terms appearing in (11), also other terms involving derivatives of the density.

We now proceed to a general variation of the energy functional E taking into account as a subsidiary condition that the particle number A remains constant

$$\delta(E - \lambda_0 A) = \int_D d^3r\ \delta\rho\ (dF/d\rho - \lambda_0) + \int_\Sigma d\Sigma\ (\delta \mathbf{R}\cdot\mathbf{n})\ (F(\rho) - \lambda_0\rho)\,. \qquad (12)$$

$\delta\mathbf{R}$ denotes the displacement of the boundary Σ of the domain D and $\mathbf{n}$ is the outwards normal. The equilibrium density ρ_0 is the solution of the following set of equations

$$(dF/d\rho)_{\rho=\rho_0} = \lambda_0 \quad , \qquad (13)$$

$$(F(\rho_0) - \lambda_0\rho_0)_{r=R} = 0 \quad , \qquad (14)$$

where R is the radius of the spherical nucleus.

Equation (13) implies that ρ_0 is independent of $\mathbf{r}$. Combining (13) and (14) it follows that the value of ρ_0 is obtained by minimizing the total energy $A\,F(\rho)/\rho$,

$$(d[\rho^{-1}F(\rho)]/d\rho)_{\rho=\rho_0} = 0\,. \qquad (15)$$

This means that ρ_0 is the equilibrium density of nuclear matter. From now on we will be considering the equilibrium density

$$\rho_0(\mathbf{r}) = \rho_0(0)\ \Theta(R - r) \quad , \qquad (16)$$

where the radius R is fixed by $\rho_0(0)$ and A.

3 — TIME EVOLUTION

The distribution function corresponding to the Slater determinant (1) is

$$f = f_f + \{ f_f , \chi \} + (1/2) \{ \chi , \{ \chi , f_f \} \} + \ldots \qquad (17)$$

Assuming that the field χ is small, we have that the density and the current are

$$\rho = g \int d^3p \ (2\pi\hbar)^{-3} \ f \simeq \rho_f \quad , \qquad (18)$$

$$j = g \int d^3p \ (2\pi\hbar)^{-3} \ f \ \mathbf{p}/m \simeq (\rho_f/m) \ \nabla\chi . \qquad (19)$$

From the quantum mechanical lagrangian

$$L = i\hbar < \phi | \dot{\phi} > - < \phi | H | \phi > \quad , \qquad (20)$$

we obtain in the classical limit the following lagrangian for the fields χ and ρ_f

$$L = \int_D d^3r \ \{ -\dot{\chi} \rho_f - (\rho_f/2m) \ (\nabla\chi)^2 - F(\rho_f) \} \quad , \qquad (21)$$

where

$$< \phi_f | H | \phi_f > = \int d^3r \ F(\rho_f) \quad . \qquad (22)$$

When we minimize the action integral, we take into account the conservation of the particle number by introducing an appropriate Lagrange multiplier λ,

$$\begin{aligned} \delta \int dt \, (L + \lambda A) = & \int dt \{ \int_D d^3r \ \delta\chi \, [\dot{\rho}_f + (1/m) \ \nabla \cdot (\rho_f \nabla\chi)] \\ & + \int_D d^3r \ \delta\rho_f [-\dot{\chi} - (1/2m) \ (\nabla\chi)^2 - dF/d\rho_f + \lambda] \\ & + \int_\Sigma d\Sigma \ \delta\chi \ \rho_f \ \hat{\mathbf{n}} \cdot (\dot{\mathbf{R}} - (1/m) \nabla\chi) \\ & + \int_\Sigma d\Sigma \ (\delta\mathbf{R} \cdot \hat{\mathbf{n}}) \ [-\dot{\chi} \rho_f - (\rho_f/2m) \ (\nabla\chi)^2 - F(\rho_f) + \lambda \rho_f] \, . \end{aligned} \qquad (23)$$

By considering arbitrary variations of the fields χ and ρ_f, the following equations of motion are obtained

$$\dot{\rho}_f + (1/m)\,\nabla\cdot(\rho_f \nabla\chi) = 0 \quad , \tag{24}$$

$$\dot{\chi} + (1/2m)\,(\nabla\chi)^2 + dF/d\rho_f - \lambda = 0 \quad . \tag{25}$$

Equation (24) is obviously the continuity equation and equation (25) leads to the 'Euler type' equation

$$\partial_t\, \mathbf{j} = -(\rho_f/m)\,\nabla\,(dF/d\rho_f) \quad . \tag{26}$$

The two following boundary conditions are obtained

$$\dot{\chi}\,\rho_f + (\rho_f/2m)\,(\nabla\chi)^2 + F(\rho_f) - \lambda\,\rho_f\,|_{r=R} = 0\,, \tag{27}$$

$$\rho_f\,(\dot{\mathbf{R}} - (1/m)\,\nabla\chi)\cdot\hat{\mathbf{n}}\,|_{r=R} = 0\,. \tag{28}$$

The equations (25) and (27) imply the boundary condition (15) at the surface. This means that at the surface ρ_f is equal to ρ_0 and therefore we recover the well known first sound [1-3] boundary condition

$$\rho_f^{(1)}\,|_{r=R} = 0 \quad , \tag{29}$$

where $\rho_f^{(1)} = \rho_f - \rho_0$.

From equations (24) and (25) we obtain the first sound equation for ρ_f

$$\ddot{\rho}_f = (1/m)\,\nabla\cdot(\rho_f \nabla(dF/d\rho_f)) \quad . \tag{30}$$

If we linearize this equation we obtain in the interior of the nucleus

$$-\omega^2\,\rho_f^{(1)} = c_f^2\,\Delta\,\rho_f^{(1)} \quad , \tag{31}$$

with the first sound velocity

$$c_f = (p_F/m)\,\sqrt{(1+F_0)/3} \quad , \tag{32}$$

and where the Landau parameter F_0 is

$$F_0 = (3m/p_F^2)\,\sum_\sigma a_\sigma\,\sigma(\sigma-1)\,\rho_0^{\sigma-1}. \tag{33}$$

The solutions $\rho_f^{(1)}$ have the following analytical form inside the nucleus

$$\rho_f^{(1)} \propto j_l(kr)\ Y_{lm} \quad , \tag{34}$$

where j_l is a spherical Bessel function and $k = \omega/c_f$.

The energies of the first compressive mode according to the present formalism are shown, for different values of l, in the following table, for a nucleus with $A = 208$ and compared with the corresponding energies obtained by solving eq. (30) for a nucleus with a smooth surface [3] based on a more sophisticated formalism, allowing for quantum corrections through the inclusion of the so called surface terms.

TABLE — First sound eigenfrequencies (in MeV) for the first compressional mode for a nucleus with $A = 208$. The energies in the first line are taken from ref. [3], those in the second line are obtained according to the square well model density.

$l=0$	$l=1$	$l=2$	$l=3$
18.4	25.3	30.9	35.5
18.5	26.4	33.9	41.1

4 — CONCLUSION

In this note we have derived the first sound equations of motion and respective boundary conditions, starting from a microscopic point of view, where determinants are taken as trial wave functions and local equilibrium is assumed.

Actually the local equilibrium assumption is not realistic for atomic nuclei at very low temperatures, because then the mean free path λ of the nucleons in nuclei is of the order of the typical wavelength R (nuclear radius) and therefore the basic physical condition for first sound modes (namely $\lambda \ll R$) is generally not met. It is well known that nuclear giant resonances may be obtained in a fluid dynamical picture by means of the generalized scaling approach [3-10]. However in order to obtain a description

of low lying modes in a fluid dynamical approach, one has to go beyond the generalized scaling approach. One possible way of obtaining low lying modes is to allow for the interplay between first sound and the generalized scaling approach [2, 11].

APPENDIX

In eq. (23) we had to perform a partial integration with respect to time leading to a surface term and to a volume term. In order to understand how the surface contribution appears, we consider the integral $\int_{t_1}^{t_2} dt \int_D d^3r\ G(\mathbf{r}, t)$ such that

$$\delta \int_D d^3r\, G(\mathbf{r}, t_1) = \delta \int_D d^3r\, G(\mathbf{r}, t_2) = 0 \tag{A.1}$$

Then, we have

$$\int_{t_1}^{t_2} dt \frac{d}{dt} \int_D d^3r\, G(\mathbf{r}, t) = \int_{t_1}^{t_2} \left\{ \int_D d^3r\, \partial_t G + \int_\Sigma d\Sigma\, (\dot{\mathbf{R}} \cdot \hat{\mathbf{n}})\, G(\mathbf{r}, t) \right\} = 0 \tag{A.2}$$

and, in particular, if $G = \delta\chi\, \rho$, we will have

$$\int_{t_1}^{t_2} dt \left\{ \int_D d^3r\, (\delta\dot{\chi}\, \rho + \delta\chi\, \dot{\rho}) + \int_\Sigma d\Sigma\, (\dot{\mathbf{R}} \cdot \hat{\mathbf{n}})\, \delta\chi\, \rho \right\} = 0 \tag{A.3}$$

so that

$$\int_{t_1}^{t_2} dt \left\{ \int_D d^3r\, \delta\dot{\chi}\, \rho \right\} = \int_{t_1}^{t_2} dt \left\{ - \int_D d^3r\, \delta\chi\, \dot{\rho} + \int_\Sigma d\Sigma\, (\dot{\mathbf{R}} \cdot \hat{\mathbf{n}})\, \delta\chi\, \rho \right\} \tag{A.4}$$

REFERENCES

[1] A. BOHR and B. MOTTELSON, *Nuclear Structure* (Benjamin, N. Y., 1975) vol. 2, ch. 6A.

[2] J. P. DA PROVIDÊNCIA, Ph. D. Thesis, Siegen 1983.

[3] G. ECKART, G. HOLZWARTH and J. P. DA PROVIDÊNCIA, *Nucl. Phys.* **A364** (1981) 1.

[4] G. F. BERTSCH, *Ann. of Phys.* **86** (1974) 138, *Nucl. Phys.* **A249** (1973) 253.

[5] S. STRINGARI, *Nucl. Phys.* **A279** (1977) 454, **A325** (1979) 199; *Ann of Phys.* **151** (1983) 35.

[6] G. ECKART and G. HOLZWARTH, *Nucl. Phys.* **A325** (1979) 1.

[7] J. P. DA PROVIDÊNCIA and G. HOLZWARTH, *Nucl. Phys.* **A398** (1983) 59, Proceedings of the "Topical Meeting on Nuclear Fluid Dynamics", Trieste, 11-15 October 1982, p. 123.

[8] M. DI TORO and D. M. BRINK, *Nucl. Phys.* **A372** (1981) 151.

[9] F. E. SERR, G. F. BERTSCH, J. BORYSOWICZ, *Phys. Lett.* **92B** (1980) 241.

[10] K. ANDŌ and S. NISHIZAKI, *Prog. Theor. Phys.* **68** (1982) 1196.

[11] J. P. DA PROVIDÊNCIA, Proceedings of the "Workshop on Semiclassical Methods in Nuclear Physics" Grenoble, 5-8 March 1984 (to be published in the "Journal de Physique-Colloques").

EFFECTS OF THE MAGNETIC FIELD SHAPE IN THE CHARACTERISTICS OF A DOUBLE FOCUSING ELECTRON SPIN POLARIMETER

P. AMORIM [1] e J. P. RIBEIRO [2]

Complexo II do I.N.I.C. — Av. Prof. Gama Pinto, 2 — 1699 Lisboa Codex, Portugal

(Received 12 January 1984; revised version 13 March 1984; final form in 17 April 1984)

ABSTRACT — In this paper we discuss the influence of a magnetic field of the form $B_z = B_0 (R/r)^{1+\alpha}$ on the characteristics of a double focusing $\pi/2$ sector field polarimeter. The influence of α in the radial and axial focusing distances is studied for the energy range 100-1000 keV. We conclude that for $\alpha \neq 0$ the anastigmatism of the polarimeter can be very important for measurements at several hundred keV whereas it is negligible for electrons of a few keV. The effect introduces a systematic error which must be carefully estimated in each experimental situation.

1 — INTRODUCTION

The experimental results of longitudinal polarization of electrons emitted in beta decay have been obtained using different methods [1]. One of them, the Mott scattering method, is an exclusively transverse polarization sensitive method [2] and, therefore, it is necessary to put the electron in a system which converts longitudinal into transverse polarization for any electron energy. This system is usually known as "polarimeter" and can be achieved with a crossed electric and magnetic field configuration which, in the neighbourhood of an equilibrium orbit of radius of curvature R, has the approximate form [3]

$$E_r = E_0 (R/r)^2 , \; E_\theta = E_z = 0 \; ; \; B_r = B_\theta = 0 \; , \; B_z = B_0 (R/r) \qquad (1.1)$$

---

(1) Centro de Física dos Fenómenos de Ionização Interna da Universidade de Lisboa.

(2) Centro de Física Nuclear da Universidade de Lisboa.

Such an instrument (Fig. 1) has i) independent selection of both electron energy and spin orientation at a fixed momentum direction; ii) focusing in both radial and axial directions, if the configuration field satisfies exactly the eqs. (1.1). The electric

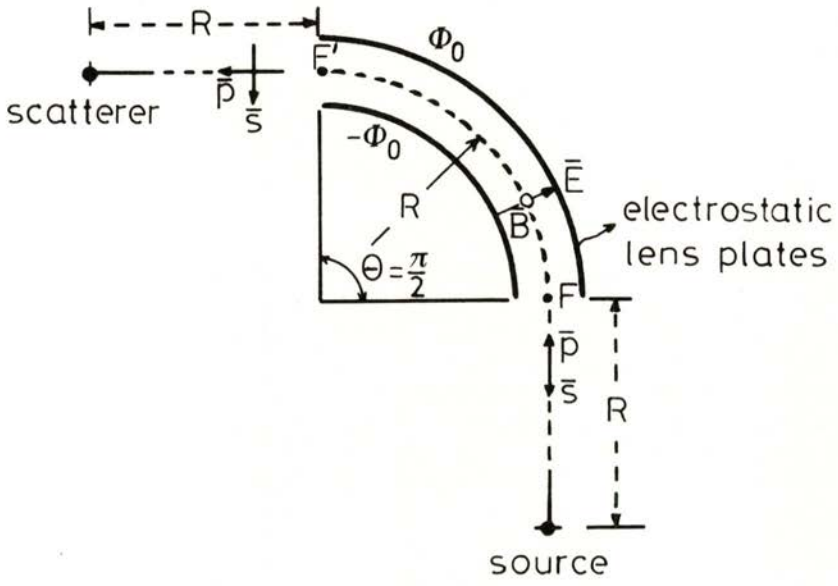

Fig. 1 — Electron trajectories in a $\pi/2$ sector configuration of crossed electric (**E**) and magnetic (**B**) fields.

field can be easily obtained with aid of two concentric spheres of radius R_1 and R_2 ($R_2 > R_1$) at the potentials $-\phi_0$ and ϕ_0 respectively. The magnetic field can be produced by a sector ring magnet with a radially increasing gap between the pole pieces (Fig. 2). The expression $B_z = B_0 (R/r)$ is valid only if the magnetic pole pieces are normal to the spheres defined by the electric lenses [3], [4]. Usually the magnetic field is of the form $B_z = B_0 (R/r)^{1+\alpha}$.

In the following sections these topics are analysed in detail with special emphasis on the influence of α on the characteristics of the polarimeter. It is a numerical analysis and in the calculations

we assume that the angular width of the sector field is $\Theta = \pi/2$, the real parts of object and image spaces are located in field free regions and the distance d_1 from the object to the entrance boundary of the sector field is equal to R (Fig. 1).

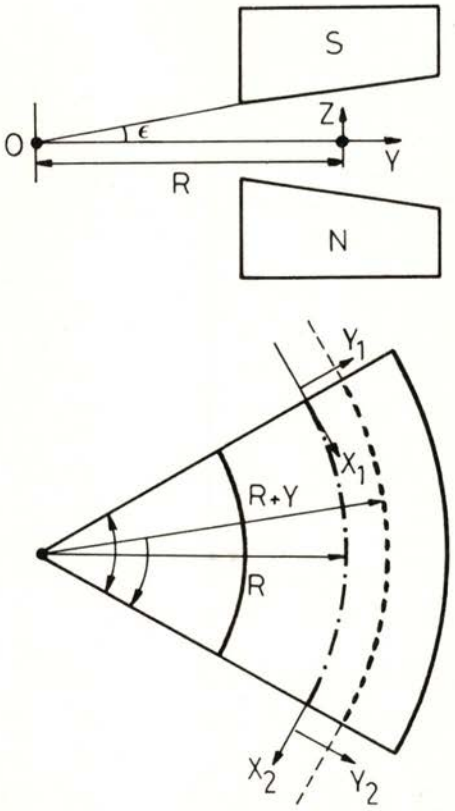

Fig. 2 — Schematic view of the pole pieces of the magnet.

2 — PARTICLES IN PRESENCE OF ELECTROMAGNETIC FIELDS

Consider the motion of an electron of velocity $v = \beta c$ (charge – e and mass $m = m_0 (1 - \beta^2)^{-1/2}$) under the influence of a radial electric field E_0 in the plane of its orbit and an axial magnetic field B_0 normal to that plane. Assuming cylindrical

symmetry the equilibrium trajectory in the laboratory frame is a circle of radius R given by [3]

$$1/R = 1/\rho_e + 1/\rho_m \ , \qquad (2.1)$$

where

$$1/\rho_e = e\,E_0\,W/(c^2\,p^2) \quad , \quad 1/\rho_m = e\,B_0/p \ . \qquad (2.2)$$

In these equations $mc^2 = \gamma\, m_0\, c^2 = W$ is the total relativistic energy and $mv = mc\,\beta = p$ is the momentum.

On the other hand, if the angular width of the sector field is equal to Θ the angle between the spin of the electron and its momentum changes by [3]

$$\Delta\sigma = -R\,\Theta/(\rho_e\,\gamma) = -(R/\rho_e)\ (1-\beta^2)^{1/2}\ \Theta \ . \qquad (2.3)$$

Eqs. (2.1) and (2.3) allow the conversion of longitudinal into transverse polarization for all values of the energy.

This transverse polarization P of the electrons is determined by recording the left-right asymmetry A in Mott scattering from spinless nuclei [4]. This asymmetry is $A = S\ P$ where the Sherman function S is known [5]. This function depends on the electron energy and the scattering angle.

The focusing properties of the sector field can be derived by studying the electron motion slightly displaced from the equilibrium orbit of radius R. The coordinates of the electron are s, representing the displacement along the equilibrium orbit, and y and z representing the displacements parallel to the curvature radius and perpendicular to the plane of the equilibrium orbit, respectively. For small displacements the equation of motion are [6]

$$d^2\,y/ds^2 = -K_y^2(s)\,y \ , \ d^2\,z/ds^2 = -K_z^2(s)\,z \qquad (2.4)$$

where the coefficients $K_y^2(s)$ and $K_z^2(s)$ are

$$K_y^2(s) = R^{-2}\,[1 + (R/\rho_e)^2\,(1-\beta^2)] - K_z^2(s)$$

$$K_z^2(s) = -R^{-2}\{(R/\rho_e)\,[1 + (\partial\,E_r/\partial\,r)_{r=R}\ (E_0/R)^{-1}] \qquad (2.5)$$

$$+ (R/\rho_m)\ (\partial\,B_z/\partial\,r)_{r=R}\ (B_0/R)^{-1}\} \ .$$

To determine the position of the electron source and its image we apply the usual techniques of electron optics. Assuming that the real parts of object and image spaces are located in field free regions and that within the polarimeter the trajectories are determined by the solutions of eqs. (2.4), the condition for stigmatic imaging is found to be [3]

$$1/d_1 + 1/d_2 = [\, K - (K\, d_1\, d_2)^{-1} \,] \tan K R \Theta \qquad (2.6)$$

where d_1 is the distance from the object (electron source) to the entrance boundary of the sector field and d_2 the distance from the exit boundary to the image. The condition that the object and image distance (focusing distances) should be equal is also obtained directly from eq. (2.6), i.e.,

$$K d_1 = K d_2 = \begin{matrix} + \cot \\ - \tan \end{matrix} (K R \Theta/2) \qquad (2.7)$$

The positive and negative signs refer to negative and positive lateral magnifications respectively. When object and image lie in their respective real plane, i.e. real images are obtained, the positive sign is taken in eq. (2.7) expressing the fact that the image is inverted. Thus, if the electric field and magnetic field are given by eq. (1.1) and $\Theta = \pi/2$ the previous equations show that $d_1 = d_2 = R$.

3 — RESULTS

For $\alpha \neq 0$ eqs. (2.5) become

$$\begin{aligned} K_y^2(s) &= R^{-2} \left[(R/\rho_e)^2 (1-\beta^2) - \alpha (1 - R/\rho_e) \right] \\ K_z^2(s) &= R^{-2} \left[1 + \alpha (1 - R/\rho_e) \right] \end{aligned} \qquad (3.1)$$

and the condition for astigmatic focusing is evidently $K_y = K_z$, i.e.

$$(1-\beta^2)(R/\rho_e)^2 + 2\alpha (R/\rho_e) - (1 + 2\alpha) = 0 \,. \qquad (3.2)$$

From these equations we see that for $\alpha \neq 0$ it is not possible to have simultaneously the conversion of electron longitudinal polar-

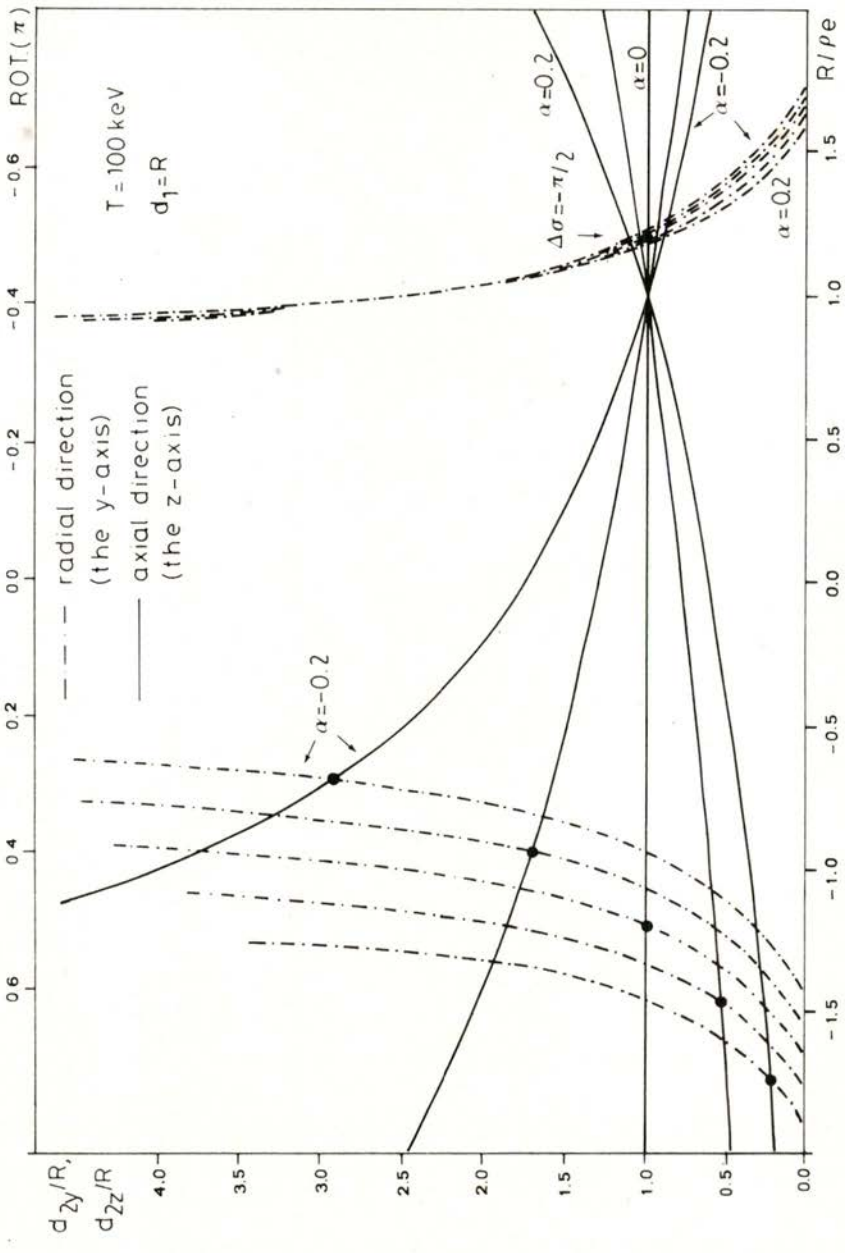

Fig. 3 — Radial and axial focusing ratios d_y/R and d_z/R at 100 keV plotted as a function of R/ρ_e for a range of values of the magnetic field index α. The top scale gives the $\Delta\sigma$ values.

ization into transverse polarization and astigmatic focusing. The condition $d_1 = d_2 = R$ is no longer valid and the distances d_2 (d_{2y} , d_{2z}) can be obtained from eq. (2.6). Writing

$$K d_2 = -[2 \tan(KR\Theta/2) + Kd_1 (1 - \tan^2(KR\Theta/2))] \cdot [1 - \tan^2(KR\Theta/2) - 2K d_1 \tan(KR\Theta/2)]^{-1} \quad (3.3)$$

the radial and the axial focusing ratios d_{2y}/R and d_{2z}/R can be determined as a function of R/ρ_e for a range of values of the magnetic field index α. Assuming that $\Theta = \pi/2$ and $d_1 = R$, these ratios were computed for different electron energies. This is shown in Figs. 3, 4 and 5. These Figs. are quite general and so they can be used to predict the anastigmatism of any polarimeter where $\Theta = \pi/2$ and $d_1 = R$. The top scale of these Figs. gives the $\Delta\sigma$ values which were calculated from eq. (2.3).

In all Figs. we see that for a given α the intersection of the two curves is an astigmatic focusing point ($d_{2y} = d_{2z}$). To each astigmatic point corresponds a value of R/ρ_e. If the electron energy is small we see in Fig. 3 that the value of (R/ρ_e) = 1.2 corresponding to the astigmatic point is roughly equal to the value needed to rotate the spin by $-\pi/2$. However for higher energies (Figs. 4 and 5) this situation is no longer true.

To further illustrate this point, let us consider an electron of 1000 KeV and $\alpha = -0.1$ (Fig. 5). To achieve a spin rotation of $-\pi/2$ we need (R/ρ_e) = 2.97 whereas double focusing occurs for (R/ρ_e) = 3.65. In other words setting (R/ρ_e) = 2.97 we obtain (d_{2y}/R) = 1.67 and (d_{2z}/R) = 0.61 which means that the image of the source rather than being a point is spread over a 1.06 R region. Obviously, the scatterer must be positioned within this region. Clearly, a situation like that implies two things. For a scatterer big enough to maximize the number of scattered electrons the spread in the electron incoming angles will imply a large error in the estimation of the Sherman function. On the other hand, if the scatterer is small in order to avoid the previous problem then there will be a drastic reduction of the number of scattered electrons. This condition implies a large statistical error

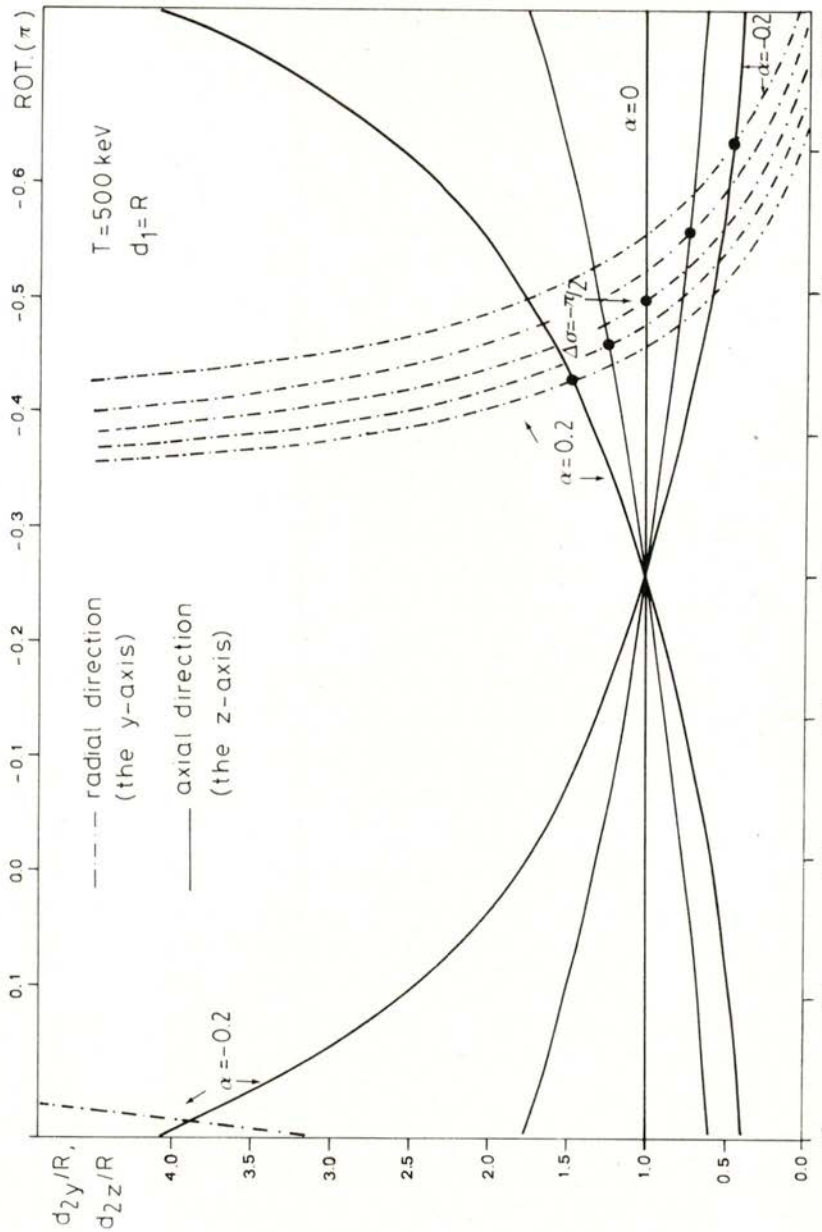

Fig. 4 — Radial and axial focusing ratios d_y/R and d_z/R at 500 keV plotted as a function of R/ρ_e for a range of values of the magnetic field index α. The top scale gives the $\Delta\sigma$ values.

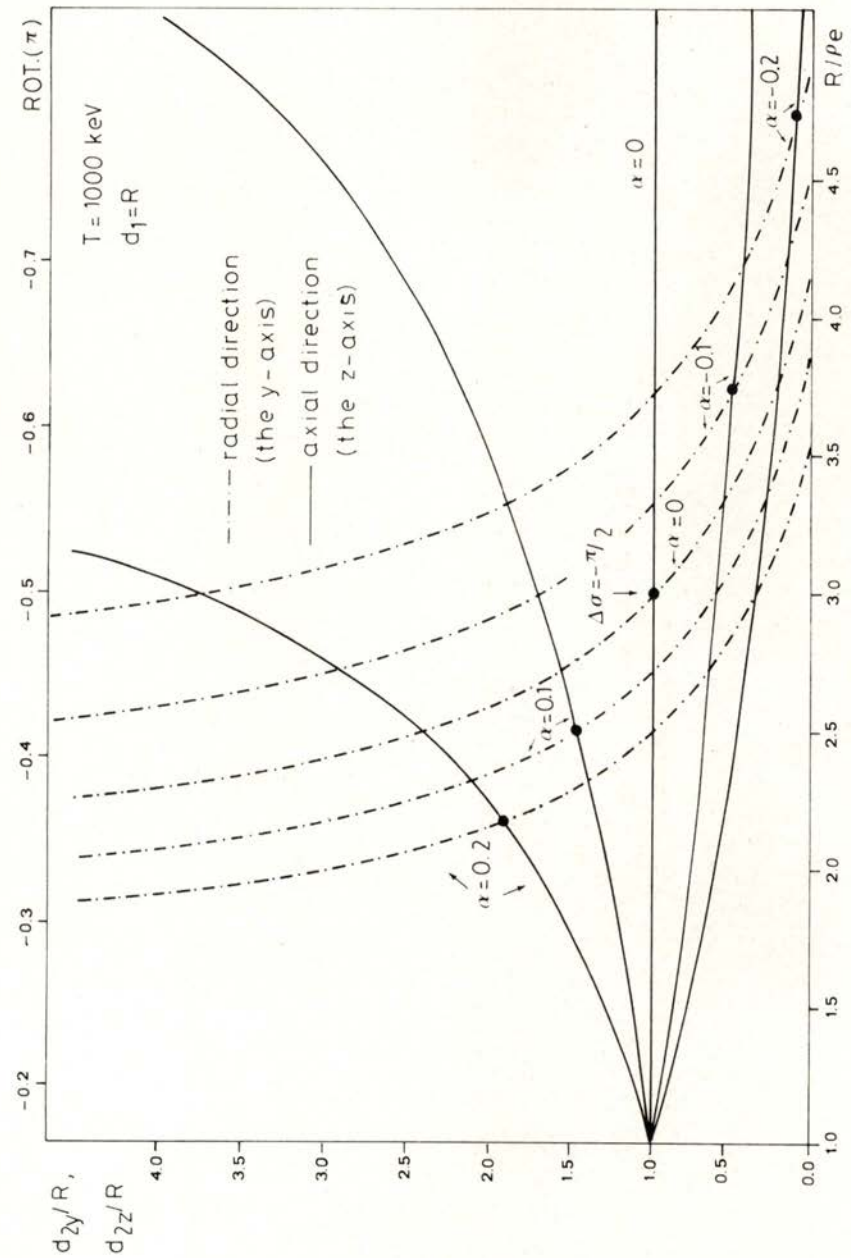

Fig. 5 — Radial and axial focusing ratios d_y/R and d_z/R at 1000 keV plotted as a function of R/ρ_e for a range of values of the magnetic field index α. The top scale gives the $\Delta\sigma$ values.

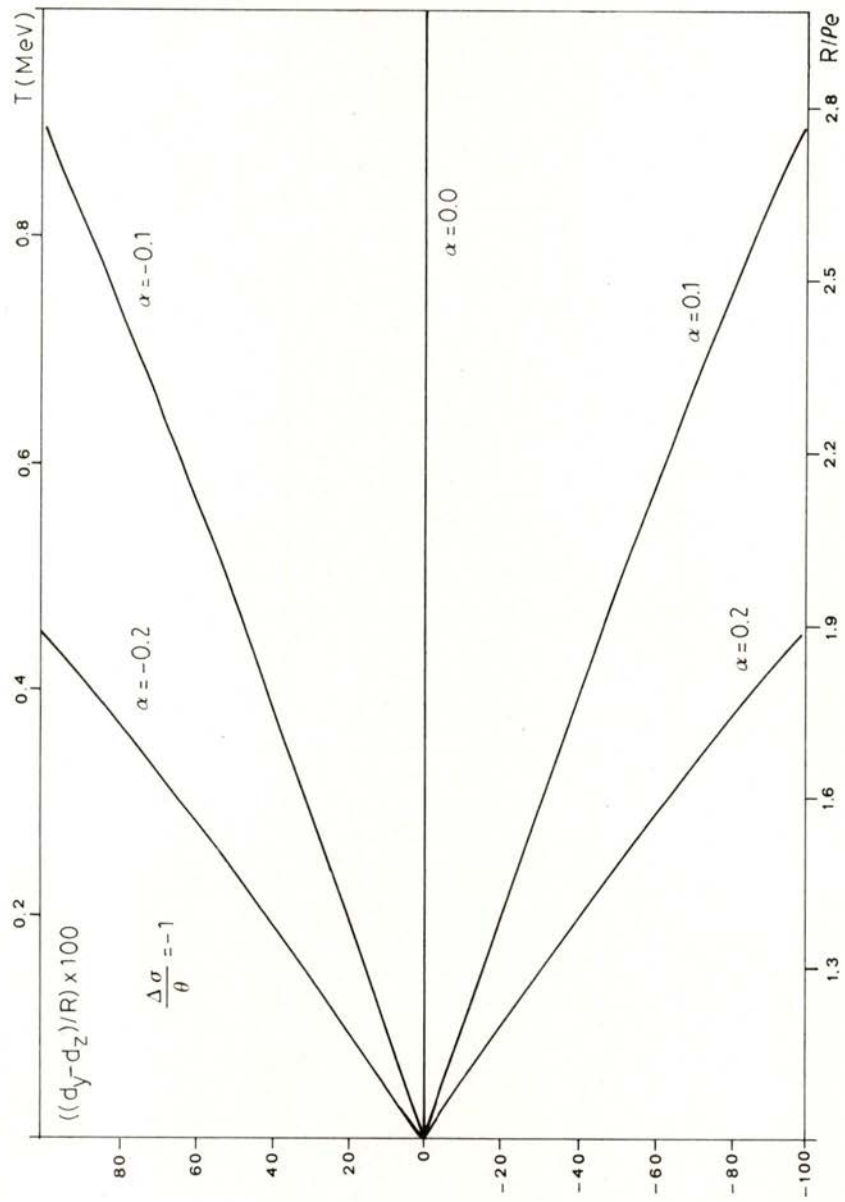

Fig. 6 — The anastigmatism of the lenses at $\Delta\sigma/\Theta = -1$ plotted as a function of the energy and of the index α. The R/ρ_e values are taken from eq. (2.3).

in the measurements. Fig. 6 shows for an electron spin rotation of $-\pi/2$ the anastigmatism of the polarimeter. We see that for a given $\alpha \neq 0$ the anastigmatism is energy dependent.

4 — CONCLUSIONS

We would like to emphasize that our conclusions come from numerical calculations and they can be summarized as follows:

1 — To transform electron longitudinal polarization into transverse polarization by an astigmatic ($d_y = d_z$) polarimeter we must have $\alpha = 0$.

2 — The anastigmatism of the polarimeter depends on the magnetic field index α, and for $\alpha \neq 0$ the focusing caracteristics of the apparatus do not remain constant when we change the electron energy.

3 — For small α and low values of electron energies it is not critical to know accurately the shape and homogeneity of the magnetic field.

4 — For higher energies and $\alpha \neq 0$ the distortions of the image introduce errors in the measurements and they are energy dependent.

REFERENCES

[1] SCHOPPER, H. F., *Weak Interactions and Nuclear Beta Decay* (North-Holland Publ. Co., 1966).

[2] MOTT, N. F. and MASSEY, H. S. W., *Theory of Atomic Collisions* (Clarendon Press, 1965), 3rd edition. Chapter 9.

[3] FARAGO, P. S., *Nucl. Inst. and Meth.* **15**, 222 (1962).

[4] RIBEIRO, J. P. and BYRNE, J., *Nucl. Inst. and Meth.* **154**, 279 (1978).

[5] SHERMAN, N., *Phys. Rev.* **103**, 1601 (1956).

[6] FARAGO, P. S., *Free Electron Physics* (Penguin Books, 1970).

APPROXIMATE SOLUTION FOR THE CONCENTRATIONS OF IMPERFECTIONS IN A PURE METAL OXIDE MO_y WITH SCHÖTTKY DISORDER

C. A. C. SEQUEIRA

Laboratório de Electroquímica, Instituto Superior Técnico,
Avenida Rovisco Pais, 1000 Lisboa, Portugal

(Received 9 June 1983; revised version 12 January 1984)

ABSTRACT — A description of the defect structure of a pure metal oxide MO_y with Schöttky disorder in equilibrium with a surrounding oxygen gas phase is presented. Appropriate defect reactions are formulated and equilibrium concentrations of the different defects as a function of the ambient oxygen partial pressure are calculated using the Brouwer's method of approximation.

1 — INTRODUCTION

Many inorganic compounds above absolute zero are known to deviate from the ideal crystalline state and such deviations which may be attributed to lattice defects can occur in different ways and to varying degree. According to the Wagner-Schöttky statistical thermodynamic model (Wagner and Schöttky 1930), the structure and the chemistry of nonstoichiometric compounds can be interpreted in terms of lattice defects and this has led to the concept that all crystalline compounds are inherently nonstoichiometric to a greater or less degree. In a nonstoichiometric compound, generally only one type of point defect predominates and electrical neutrality in such a compound is maintained through the formation of an electronic or valence defect to every point defect.

A very common situation occurs predominantly in high temperature systems consisting of ionic oxides with a Schöttky

defect structure in equilibrium with the atmosphere defined by the oxygen pressure $P(O_2)$. The defects encountered in a MO_y compound in such cases and their concentrations as a function of the oxygen partial pressure of the gas phase in equilibrium with the oxide determine a number of properties of (or processes in) the oxide such as mass transport, solid state reactions, gas-metal reactions, etc.; and if these defect-controlled properties or processes are to be interpreted, it is important that the defect concentrations are known. The derivation of expressions for the relevant defect concentrations as $f[P(O_2)]$ is to be the subject of this paper. The general character of the arguments and the way of presentation follows very much the lines of many available papers (Kröger 1974).

As a basis for those derivations, the remainder of this introduction briefly discusses the notation for description of point and electronic defects, and the effective charges of the defects.

In order to describe the point defects which are formed in pure crystals and to express their formation in terms of equations, different systems have been put forth by Schöttky (1959), Rees (1954), Kröger and Vink (1956, 1964), and others. The symbols and system used by Kröger and Vink will be employed in this paper, as this is being increasingly adopted in the literature.

The native point defects in an oxide MO_y include M and O vacancies and M and O interstitial atoms or ions. Vacancies are written V with a subscript M or O referring to vacant metal or oxygen sites, respectively. Interstitial ions or sites are described with a sub i. Correspondingly, an unoccupied or vacant interstitial site is written V_i.

The point defects often occur in ionized form. In considering their charges, one may describe their actual charges or valence. However, it is generally more convenient in writing defect reactions to consider the charge on the defects relative to the perfect crystal. This relative charge is termed the effective charge of the defect.

In addition to the structural defects, crystals also contain electronic imperfections, i.e., electrons and holes, which are relatively free to move in the crystal. Free electrons and holes are usually indicated by e' and $h^{\cdot}$, e and h standing for electron

and hole respectively, the aded dash and dot indicating the effective negative and positive charge.

More complex defect species may be encountered, for instance, from an association of two or more single point defects, valence defects, etc. In this paper, however, for the sake of simplicity, and because this actually applies to a great number of pure inorganic compounds at higher temperatures, we shall assume complete absence of association of imperfections. Therefore, for an oxide MO_y with a Schöttky disorder, the only allowed oxygen vacancies will be written $V_O^{\cdot\cdot}$, with two positive effective charges. That doubly charged oxygen vacancies predominate relatively to neutral or singly charged ones at high temperatures is a very well illustrated aspect in papers dealing with the individual oxides.

2 — CALCULATION OF DEFECT CONCENTRATIONS

If a simple MO_y oxide contains simultaneously several of the imperfections referred in the previous section, their concentrations are interrelated. Since both the stoichiometric and nonstoichiometric defect structure situations may apply to the same binary metal oxide, depending on the oxygen partial pressure of the gas phase in equilibrium with the oxide, we will begin by considering a Schöttky defect structure situation in stoichiometric MO_y oxides, and then, two defect structure situations in nonstoichiometric MO_y oxides, in which predominate either oxygen or metal vacancies. It should be noted that the subscript y in the MO_y formula may be equal to 1/2, 1, 3/2, 2, etc., depending on the valence of the metal associated with the oxygen component.

Stoichiometric MO_y oxides. A stoichiometric compound MO_y with Schöttky disorder contains y oxygen vacancies per metal vacancy. The overall formation of such a defect situation within the crystal involves the transfer of an equivalent number of cations and anions on regular lattice sites from the bulk to the surface. The overall defect equation may thus be written

$$0 = V_M^{2y\,|} + y\,V_O^{\cdot\cdot}$$

where 0 designates a perfect crystal.

Applying equilibrium thermodynamics to this net reaction the corresponding defect equilibrium may, at low defect concentrations, be written

$$[V_O^{\cdot\cdot}]^y \; [V_M^{2y\prime}] = K_S$$

where K_S is the equilibrium constant. The square brackets indicate that the structure elements are expressed in terms of concentrations. It is obvious that the value of the equilibrium constant depends on the units of concentration employed, but it is a simple matter to convert values of the equilibrium constant from one system to another (Kröger 1974).

Oxygen-deficient MO_{y-x} oxides. For the oxides treated in this paper interstitial defects are supposed to be absent, so the composition of a oxygen-deficient MO_y oxide may be written MO_{y-x}, to emphasize that the defects represent a deficit of oxygen relative to the stoichiometric composition.

In these oxides, an oxygen vacancy is formed by the transfer of an oxygen atom on a normal site to the gaseous state, without any change in the number of sites. This defect reaction may be written

$$O_O = V_O^{\cdot\cdot} + 1/2 \; O_2 + 2\, e^\prime$$

where O_O designates the oxygen ions on normal lattice sites. The defect equilibrium may accordingly be written

$$[V_O^{\cdot\cdot}] \; P(O_2)^{1/2} \; n^2 = K' \; [O_O]$$

where $n = [e^\prime]$ designates the concentration of electrons.

Metal-deficient $M_{1-x} O_y$ oxydes. In a metal-deficient MO_y oxide a charged metal vacancy may be formed through the reaction of oxygen with the oxide

$$y/2 \; O_2 = V_M^{2y\prime} + 2\, y \; h^{\cdot} + y \; O_O \quad ;$$

in this reaction both a cation and y anion sites are created in MO_y.

The defect equilibrium may, for small defect concentration, be written

$$[V_M^{2y\prime}] \; p^{2y} \; [O_O]^y = K'' \; P(O_2)^{y/2}$$

where $p = [h^{\cdot}]$ denotes the concentration of electron holes.

Intrinsic electronic equilibrium. This process, of thermal excitation of electrons from the valence band to the conduction band, can be formulated by the reaction

$$0 = e' + h^{\cdot}$$

and leads to the following equilibrium concentration of electrons and holes

$$n\,p = K_i$$

Brouwer's method of approximation. Summarizing the preceding considerations, it can be stated that for a pure MO_y crystal in equilibrium with its vapour phase, in which are present in the solid phase atoms M and O, ionized metal and oxygen vacancies, electrons, holes, and molecules O_2 only in the vapour phase, the following reactions and relations will hold:

$$0 = V_M^{2y\,\prime} + y\ V_O^{\cdot\cdot} \qquad [V_O^{\cdot\cdot}]^y\ [V_M^{2y\,\prime}] = K_S \tag{1}$$

$$y/2\ O_2 = V_M^{2y\,\prime} + 2\,y\,h^{\cdot} + y\,O_O \qquad [V_M^{2y\,\prime}]\ p^{2y} = K\,P(O_2)^{y/2} \tag{2}$$

$$0 = e' + h^{\cdot} \qquad n\,p = K_i \tag{3}$$

It should be noted that the formulations for nonstoichiometric MO_{y-x} and $M_{1-x}O_y$ oxides are equivalent and, as a result, only the defect reaction (2) is taken into account at this stage.

Another basic requirement for treating defect equilibria and for evaluating defect concentrations in crystals is the electroneutrality condition. Therefore:

$$2\,y\,[V_M^{2y\,\prime}] + n = 2\,[V_O^{\cdot\cdot}] + p \tag{4}$$

Since all the constants K are functions of temperature only, the four unknown concentrations n, p, $[V_O^{\cdot\cdot}]$ and $[V_M^{2y\,\prime}]$ can be calculated from relations (1)-(4). At any temperature the problem is completely determined. However an analytical solution is not possible; for instance eqs. (1)-(4) lead to a non-linear equation for the hole concentration p

$$p^{2y-1}\,[2\,K_S^{1/y}\,K^{-1/y}\,p^3\,P(O_2)^{-1/2} + p^2 - K_i] = 2\,y\,K\,P(O_2)^{y/2}\ .$$

Whereas precise calculation of all the concentrations is a rather tedious affair, approximate solutions are easily obtained if the neutrality condition is approximated by its dominant members; this method which is to be our next task, was first proposed by Brouwer (1954) for exactly this type of problem. The neutrality condition can be approximated in four ways: $n = 2[V_O^{\cdot\cdot}]$; $n = p$; $[V_O^{\cdot\cdot}] = y[V_M^{2y\,|}]$; $p = 2y[V_M^{2y\,|}]$.

The first approximation holds at small values of the oxygen partial pressure, corresponding to the predomination of oxygen vacancies and the complementary electrons in the oxygen-deficient oxide. In this case (range I) the various concentrations are given by

$$\begin{aligned} n &= 2^{1/3}\,(K_i\,K^{-1/2y}\,K_S^{1/2y})^{2/3}\,P(O_2)^{-1/6} \\ p &= 2^{-1/3}\,(K_i^{-1/2}\,K^{-1/2y}\,K_S^{1/2y})^{-2/3}\,P(O_2)^{1/6} \\ [V_O^{\cdot\cdot}] &= 2^{-2/3}\,(K_i\,K^{-1/2y}\,K_S^{1/2y})^{2/3}\,P(O_2)^{-1/6} \\ [V_M^{2y\,|}] &= 2^{2y/3}\,(K_i^{-y}\,K^{1/2}\,K_S)^{2/3}\,P(O_2)^{y/6} \end{aligned} \tag{5}$$

Thus n and $[V_O^{\cdot\cdot}]$ will decrease with increasing oxygen pressure, and p and $[V_M^{2y\,|}]$ will increase with increasing oxygen pressure. This situation is typical of Ta_2O_5, V_2O_5, ZrO_2, etc., over at least a large part of their homogeneity ranges. The approximation $n = 2[V_O^{\cdot\cdot}]$ is no longer valid when either p or $[V_M^{2y\,|}]$ become larger than $[V_O^{\cdot\cdot}]$ or n. Which of these two possibilities will occur depends on whether, in range I, $p >$ or $< [V_M^{2y\,|}]$; and this, in turn, depends on whether $K_i >$ or $< K_S$.

For $K_i > K_S$ we get a new range (II) in which the neutrality condition is governed by $n = p$. Under this condition

$$\begin{aligned} n = p &= K_i^{1/2} \\ [V_O^{\cdot\cdot}] &= K_i\,K^{-1/y}\,K_S^{1/y}\,P(O_2)^{-1/2} \\ [V_M^{2y\,|}] &= K_i^{-y}\,K\,P(O_2)^{y/2} \end{aligned} \tag{6}$$

Thus $[V_O^{\cdot\cdot}]$ decreases and $[V_M^{2y|}]$ increases with $P(O_2)$, whereas n and p remain constant. This situation is particularly important for many oxides in which the intrinsic ionization is large and concentration of electron and holes according to eq. (3) predominates in the oxide (e.g. $CaO\text{-}ZrO_2$).

For $K_i < K_S$, n and p become smaller than $[V_M^{2y|}]$ and $[V_O^{\cdot\cdot}]$, respectively. In this case the electroneutrality condition can be approximated by $y\,[V_M^{2y|}] = [V_O^{\cdot\cdot}]$.

Under this condition (range III)

$$\begin{aligned} n &= y^{-1/2(y+1)}\, K_i\, K^{-1/2y}\, K_S^{-1/2y(y+1)}\, P(O_2)^{-1/4} \\ p &= y^{1/2(y+1)}\, K^{1/2y}\, K_S^{-1/2y(y+1)}\, P(O_2)^{1/4} \\ [V_O^{\cdot\cdot}] &= y\,[V_M^{2y|}] = (y\,K_S)^{1/(y+1)} \end{aligned} \tag{7}$$

In this range n decreases and p increases with increasing $P(O_2)$, whereas $[V_O^{\cdot\cdot}]$ and $[V_M^{2y|}]$ remain constant. This situation is typical of solid electrolytes in which the Schöttky defects predominate; a good example may be illustrated by pure thoria which exhibits predominant ionic conductivity at reduced oxygen pressures.

The last region holds at very high values of the oxygen pressure, corresponding to the predomination of metal vacancies and the complementary electron holes in the metal-deficient oxide. In this case (range IV) electroneutrality is governed by $2y\,[V_M^{2y|}] = p$, and the defect concentrations are given by

$$\begin{aligned} n &= K_i\, K^{-1/(2y+1)}\, (2y)^{-1/(2y+1)}\, P(O_2)^{-y/2(2y+1)} \\ p &= K^{1/(2y+1)}\, (2y)^{1/(2y+1)}\, P(O_2)^{y/2(2y+1)} \\ [V_O^{\cdot\cdot}] &= K_S^{1/y}\, K^{-1/y(2y+1)}\, (2y)^{2/(2y+1)}\, P(O_2)^{-1/2(2y+1)} \\ [V_M^{2y|}] &= K^{1/(2y+1)}\, (2y)^{-2y/(2y+1)}\, P(O_2)^{y/2(2y+1)} \end{aligned} \tag{8}$$

These relations are similar to those for range I. Some examples of oxides which are metal-deficient at higher partial pressures of

oxygen are V_2O_3, Cu_2O, NiO, etc. It should be noted that NiO is approximately stoichiometric at lower partial pressures of oxygen, which, as mentioned earlier, is in agreement with the fact that, depending on the oxygen gas pressure, different defect situations may apply to the same high-temperature oxide.

The advantages of the Brouwer's compensation mechanism, which is typical of all practical discussions about defect chemistry, become apparent when more intricate problems are described, in particular if solutions under a variety of circumstances are to be obtained, and graphical methods (logarithmic plots) can be used. In the present case, although the defect chemistry is quite simple, the discussion was facilitated by the approximation possibilities, leading to equations (5) to (8) which were readily derived.

REFERENCES

G. BROUWER, *Philips Res. Rep.*, **9**, 366 (1954).

F. A. KRÖGER, "*The Chemistry of Imperfect Crystals*", North-Holland Publ. Co., Amsterdam, and Wiley, New York (1964)

F. A. KRÖGER, "*The Chemistry of Imperfect Crystals*", vol. **2**, North-Holland (1974).

F. A. KRÖGER and H. J. VINK, "*Solid State Physics*", ed. by F. Seitz and D. Turnbull, vol. **3**, 307, Academic Press, New York (1956).

A. G. REES, "*Chemistry of the Defect Solid State*", Methuen, London (1954).

W. SCHÖTTKY, "*Halbleiterprobleme*", ed. by W. Schöttky, vol. **4**, 235, Vieweg und Sohn, Braunschweig (1959).

C. WAGNER and W. SCHÖTTKY, *Z. Physik. Chem.*, B. II, 163 (1930).

Composto e impresso na *Imprensa Portuguesa* • Rua Formosa, 108-116 • 4000 PORTO

SOCIEDADE PORTUGUESA DE FÍSICA
AV. REPÚBLICA 37-4.º, 1000 LISBOA, PORTUGAL

PORTUGALIAE PHYSICA publishes articles or research notes with original results in theoretical, experimental or applied physics; invited review articles may also be included.

Manuscripts, with an abstract, may be written in English or French; they should be typewritten with two spaces and in duplicate. Figures or photographs must be presented in separate sheets and be suitable for reproduction with eventual reduction in size; captions should make the figures intelligible without reference to the text. Authors are requested to comply with the accepted codes concerning references.

There is no page charge. Author(s) will get 50 free reprints (without covers); these are to be shared among all the authors of the article. Authors interested in more reprints should say so when sending their manuscripts; quotations shall be sent with the proofs.

Subscription rates for volume 15:

3,600 Escudos (US$24) — individuals
9,000 Escudos (US$60) — libraries

PORTUGALIAE PHYSICA may also be sent on an exchange basis; we wellcome all suggestions to such effect.

All mail to be addressed to

PORTUGALIAE PHYSICA

C/O LABORATÓRIO DE FÍSICA, FACULDADE DE CIÊNCIAS
PRAÇA GOMES TEIXEIRA
4000 PORTO PORTUGAL

PORTUGALIAE PHYSICA

VOL. 15 · NUMB 1/2 · 1984

CONTENTS

GENERAL AND MATHEMATICAL PHYSICS

Les Transitions de Connectivité
P. G. DE GENNES 1

Frustrated Spin Systems (a review)
A. ERZAN 9

ATOMIC AND NUCLEAR PHYSICS

The LX-Ray Spectrum of Argon, Krypton and Xenon
M. T. RAMOS, J. G. FERREIRA, M. L. CARVALHO and L. SALGUEIRO 55

$\beta+$/EC Decay of ^{181}Au : γ-Ray Identification
F. BRAGANÇA GIL, C. BOURGEOIS, P. KILCHER, G. PAROT, M. G. PORQUET, B. ROUSSIÈRE, J. SAUVAGE-LETESSIER and the ISOCELE Collaboration 59

D-State and Nuclear Structure Effects in (d, α) Reactions
F. D. SANTOS and A. M. EIRÓ 65

Nuclear Hydrodynamics
J. P. DA PROVIDÊNCIA 89

Effects of the Magnetic Field Shape in the Characteristics of a Double Focusing Electron Spin Polarimeter
P. AMORIM and J. P. RIBEIRO 99

CONDENSED MATTER PHYSICS

Approximate Solution for the Concentrations of Imperfections in a Pure Metal Oxide MO_y with Schöttky Disorder
C. A. C. SEQUEIRA 111

ISSN 0048-4903 POPYA4 15 (1/2) 1-118 (1984)

PORTUGALIAE PHYSICA

VOLUME 15
FASCÍCULO 3-4
1984

SOCIEDADE PORTUGUESA DE FÍSICA

PORTUGALIAE PHYSICA

Fundada em 1943 por A. Cyrillo Soares, M. Telles Antunes, A. Marques da Silva e M. Valadares

Publicação subsidiada pelo INSTITUTO NACIONAL DE INVESTIGAÇÃO CIENTÍFICA

ISSN 0048 - 4903

PORTUGALIAE PHYSICA

VOLUME 15
FASCÍCULO 3-4
1984

A COMPENDIUM ON DIRECTED AND 3-D UNDIRECTED LATTICE DATA

J. A. M. S. DUARTE

Departamento de Física — Faculdade de Ciências do Porto, 4000 Porto, Portugal

(Received 30 July 1984)

ABSTRACT — Lattice data on configurational histograms are given for three dimensional undirected bond (site) clusters according to cycle discriminations and for directed lattice animals with both perimeter and cycle discriminations.

INTRODUCTION

Configurational studies have remained one of the foundations of critical phenomena, ever since their study began, despite strong competition from transfer-matrix methods and all the various types of calculations spawned by the renormalization group theory. In this presentation we are concerned with the statistics of connected clusters relevant to the percolation and animal problems, as covered in a previous compendium of data [1]. The present summary lists results pertaining to both the normal (i.e. undirected) and directed problems, and aims to complete the previous illustration in the light of both the current knowledge and the significant theoretical advances that have occurred in the intervening three years. In the domain of normal percolation and normal lattice animals these are non-existent (but see [5]). However, for directed percolation and the relevant animals exact results now include the dominant and sub-dominant singularities for dimensions 2 and 3, their connection in all dimensions to the value of the Yang-Lee edge singularity [2], [3], as well as some multiplicities for the most significant lattices in 2 and 3 dimensions [3].

In this paper, the normal models are only listed in 3 dimensions and we have run as close a parallel as possible with the earlier

presentation. The data are therefore divided into 4 groups: cyclomatic number distributions (in normal percolation), fixed size cycle groupings (normal animals), fixed size directed percolation groupings and cyclomatic number distributions (directed animals). The notation conforms to the one applied throughout the previous paper, so that

s — denotes the number of cluster sites
b — denotes the number of cluster bonds
$c = b - s + 1$ denotes the cyclomatic number of a connected cluster
e — denotes the external bond ("energy") perimeter
t — denotes the perimeter in the percolation sense

A — *Cyclomatic number distributions in percolation*

In 3 dimensions the weighting of configurations by its cyclomatic number continues to be of interest. In normal percolation the weighted Euler's law acts as a sum rule for configuration derivations that include the three indices *b*, *s*, and *t*. In fact from the expansions of the moments of the cluster size distribution for bond

$$< s^k > = \sum_{s,\,b,\,t} s^k \, g_{sbt} \, p^b \, (1-p)^t \qquad \text{A1}$$

and site percolation

$$< b^k > = \sum_{s,\,b,\,t} b^k \, g_{sbt} \, p^s \, (1-p)^t \qquad \text{A2}$$

one has for $k = 1$

$$< s^1 > = 1-(1-p)^z \qquad \text{A3}$$

and

$$< b^1 > = 1/2 \; z \; p^2 \qquad \text{A4}$$

with *z* the coordination number of the lattice.

Our results are for the sets of histograms $\Sigma_b \; b \; g_{sbt}$ for the simple cubic, body-centred cubic and face-centred cubic site animals, and for $\Sigma_s \; s \; g_{sbt}$ on the diamond, simple cubic, and face-centred

cubic lattices. For the first set we have managed to complete valence discriminations on all three lattices (a particularly lengthy task for the face-centred cubic lattice). From these the number of bonds in a cluster follows through the laws

$$\sum_{v} s_v = s \qquad \text{A5}$$

$$\sum_{v} v\, s_v = 2\, b \qquad \text{A6}$$

where s_v is the number of sites with alence v and the summations run from 1 to z. Rather than pursue the same line for bond percolation we have partitioned the data in [4] according to the number of sites in each cluster and weighted them accordingly. Equation A3 provides, as usual, a consistency check on such manipulations. The task is very easy. On the lower coordination number side it can be supplemented, if required, with analyses of those few space types whose contribution to the added perimeter through the yield factor technique stretches long enough to involve an overlap with the contribution of strongly embedded clusters of the following cyclomatic number. The cardinal rules of this derivation are stated in [1], section D.

B — *Fixed size energy groupings (normal animals)*

The most relevant result applicable is ref. [5], which throws light on the structure of the dominant singularities for fixed cycle animals. We complete the simple cubic results of ref. [5] with the rest of the possible cycle values and add the diamond site results for animals.

Since our previous comments in [1] were written in the light of the then current ideas, that basically relied on a logmultiplicity for the histogram that would ultimately be linear in the cluster size, it is now clear from [5] that only the prefactor and the exponent can make the shape of these histograms evolve (the multiplicity associated with each cycle value is constant and equal to the tree multiplicity). As could be expected, the diamond lattice gives no more than a rather faint support to this rule.

C — *Fixed size directed percolation groupings*

Directed lattice animals have greatly benefited from the attention of Deepak Dhar and his collaborators [2], [3], and K. De'Bell has derived unpublished 3 and 2 dimensional perimeter polynomials as a basis for his calculations of the usual critical exponents in directed percolation [6], [7]. In this section we list results on the simple quadratic, triangular, simple cubic and hypercubic 4-dimensional lattices (site problem). These typically add two to three more terms to the susceptibility-like exponent series, although further efforts are necessary for a significant refining of the p_c estimates and the γ values in refs. [6] and [7].

These susceptibility series provide consistency checks on the present data, while for the total number of clusters [2] and [3] furnish further numbers, on the totals of lattice animals with a given size.

Ref. [3] is particularly interesting, since a good alternative derivation relies on the use of compact source clusters. Although a recursion relation with the generality of that in ref. [3] valid for the total number of clusters has not been proposed, the two index discriminations required for the perimeter polynomials can be written through inspection. Putting $g^{(i)}_{s,t}$ as the total number of animals from a compact source cluster with length i, and using the simple quadratic lattice

$$g_{s\,t} = 2\, g_{s-1,\,t-1} + g^{(2)}_{s\,t} \qquad \text{C1}$$

$$g^{(2)}_{s\,t} = 3\, g_{s-3,\,t-2} + g^{(3)}_{s+1,\,t-1} + g^{(3)}_{s\,t} + 2\, g_{s-2,\,t-1} \qquad \text{C2}$$

$$\sum_{s,\,t} g^{(i)}_{s\,t}\, p^{s}\, (1-p)^{t} = p^{\sum_1^i m} \qquad \text{C3}$$

This last equation is very useful. For $i = 1$, it is no more than the sum rule for the primary species in directed percolation. For higher values of i additional sets of perimeter polynomials can be used to either check or substitute the lengthier complete polynomials. The configurational work is therefore lessened while

parallel series for the moments of the cluster size distribution can be obtained by the formula

$$< s^k > = \sum_{s,\,t} s^k \, g_{s\,t}^{(i)} \, p^s \, (1-p)^t \qquad \text{C4}$$

where equation C3 is implicity contained for $k = 0$, $k = 1$ leads to susceptibility series (for the exponent γ) and the sum rule C3 provides further coefficients.

D — *Cyclomatic number distributions (directed animals)*

There is no available information on cycle discrimination for directed lattice animals and critical properties have only one significant point of reference: the result on the correlation exponent for two-dimensional trees obtained by Nadal et al. [8], by the transfer-matrix technique to a high degree of precision. For our studies on the cyclomatic structure of directed animals we have combined straightforward counting, compact source generation and valence discrimination. Note that unlike the undirected models, in the present instance, the bond expectancy rule for site percolation and the site expectancy rule for bond percolation cannot be used. There are no closure sum rules that conveniently test the overall consistency of the discriminations. Unlike earlier valence studies there are 3 possible options in directed models: incoming valence, outgoing valence and total valence. We have made extensive studies — not listed here — on outgoing valence and in terms of these the linkage rule for cyclomatic number calculations is

$$\sum_{v=0}^{z/2} v \, s_v = b \qquad \text{D1}$$

We have used outgoing valence studies on all the simple quadratic site problem histograms. For the simple cubic site problem only the last two terms have not been checked in this way. The data are here presented in a combination of the various references presented: thus, the generation of complete bond

discriminations from compact sources of length 2 on the simple quadratic lattice is obtained by the law

$$g_{s\,b} = g^{(2)}_{s\,b} + 2\, g_{s-1,\,b-1} \qquad \text{D2}$$

and other linkage rules can be related in a similar manner (for example, on the simple cubic, they will involve the embedding of compact sources $g^{(2)}_{s\,b}$, expanding three-dimensionally, and of $g^{(3)}_{s\,b}$).

This research was funded at various stages by the Royal Society, Academia das Ciencias and INIC (Portugal). The author is indebted to N. Rivier for discussions, Prof. J. M. Araújo for help with the manuscript and the École Normale Supérieure Group for hospitality during part of the writing.

APPENDIX

CYCLOMATIC NUMBER DISTRIBUTION IN PERCOLATION

A — *Simple cubic site problem*

	$s=2$	$\Sigma_b\ bg_{sbt}$		$s=7$	
10		3	25		240
	$s=3$		26		15
13		24		$s=7$	
14		6	18		6
	$s=4$		21		480
15		24	22		4500
16		156	23		16440
17		72	24		31488
18		9	25		39816
	$s=5$		26		34404
17		48	27		15408
18		420	28		3240
19		936	29		360
20		624	30		18
21		144		$s=8$	
22		12	21		96
	$s=6$		22		42
18		30	23		2304
20		1536	24		17196
21		3864	25		65904
22		5808	26		154050
23		4824	27		245040
24		1620	28		284028
			29		245676

30	129660
31	36816
32	5712
33	504
34	21
s = 9	
23	456
24	852
25	12144
26	71448
27	283704
28	706248
29	1332984
30	1902468
31	2069100
32	1770576
33	1033824
34	362904
35	74520
36	9216
37	672
38	24
s = 10	
25	2352
26	8181
27	58224
28	352020
29	1232616
30	3303642
31	6821196
32	11207616
33	14634960
34	15332598
35	12894384
36	8024256
37	3284916
38	842694
39	136176
40	13932
41	864
42	27

A — *Body-centred cubic site problem*

	$\Sigma_b\ bg_{sbt}$
s = 2	
14	4
s = 3	
17	24
19	24
20	8
s = 4	
20	132
22	240
23	96
24	108
25	72
26	12
s = 5	
21	24
23	680
24	120
25	1752
26	752
27	1560
28	1344
29	576
30	432
31	144
32	16
s = 6	
24	288
25	120
26	3736
27	1200
28	11544
29	7144
30	14436
31	13128
32	10684
33	10104
34	5220
35	2400
36	1080
37	240
38	20
s = 7	
25	72
26	96
27	2472
28	1080

29		22608	45		129048
30		14664	46		47460
31		70968	47		15792
32		58032	48		3780
33		119376	49		504
34		115872	50		28
35		129744		s = 9	
36		127224	26		8
37		90912	29		504
38		67320	31		14280
39		40560	32		15400
40		16920	33		163152
41		6888	34		191016
42		2160	35		909392
43		360	36		1058856
44		24	37		3093864
	s = 8		38		3628232
26		56	39		6992304
28		924	40		8188248
29		864	41		11147440
30		21288	42		12390048
31		17328	43		12844488
32		139260	44		12532480
33		129960	45		10577016
34		457020	46		8330232
35		455128	47		5920960
36		926712	48		3536496
37		997656	49		1925496
38		1259788	50		930536
39		1303104	51		354264
40		1183764	52		113568
41		1049648	53		31296
42		757584	54		6048
43		472896	55		672
44		282244	56		32

A — *Face-centred cubic site problem*

		$\Sigma_b\ bg_{sbt}$			
	s = 2		27		192
18		6	28		360
	s = 3		29		432
22		24	30		474
23		24		s = 5	
24		60	28		192
	s = 4		29		48
24		12	30		888
26		132	31		1560

32		2340	39		48504
33		3840	40		139044
34		5352	41		227424
35		4848	42		523392
36		3384	43		894624
	s = 6		44		1529868
30		66	45		2518632
31		264	46		3795504
32		1452	47		5293128
33		1512	48		7015092
34		7938	49		8158740
35		10152	50		8553690
36		19608	51		8040408
37		33792	52		5828280
38		44460	53		3198216
39		58896	54		1049538
40		60828		s = 9	
41		45840	37		120
42		23310	38		3096
	s = 7		39		9624
33		504	40		30264
34		1056	41		117120
35		3696	42		238488
36		14448	43		585000
37		21672	44		1324284
38		56400	45		2472480
39		99312	46		4922808
40		173712	47		8433096
41		264216	48		14548080
42		427296	49		23360916
43		567432	50		35586816
44		658944	51		51293712
45		732672	52		68905152
46		619608	53		86741136
47		394200	54		101184072
48		157092	55		105531120
	s = 8		56		99223488
35		408	57		81340632
36		1008	58		51984224
37		9192	59		24993376
38		16560	60		6972840

A — *Diamond bond problem*

	b = 1	Σ_s sg_{sbt}		b = 3	
6		4	10		88
	b = 2			b = 4	
8		18	12		455

	b = 5		19		10380
13		72	20		99780
14		2376	21		22528
	b = 6		22		416196
12		12	23		4152720
15		1008	24		9489062
16		12474		b = 11	
	b = 7		17		120
14		168	18		1020
17		9984	20		10560
18		65488	21		130152
	b = 8		22		683232
16		1656	23		319968
18		1728	24		4187592
19		82080	25		27118656
20		343791	26		49936536
	b = 9			b = 12	
17		540	16		10
18		13572	19		2112
19		1280	20		12606
20		33180	22		148608
21		605040	23		1309032
22		1805440	24		4556844
	b = 10		25		3828032
16		54	26		36671700
18		600	27		170927328
			28		263195972

A — *Simple cubic bond problem*

		Σ_s sg_{sbt}			
	b = 1			b = 6	
10		6	23		756
	b = 2		24		2976
14		45	27		2800
	b = 3		28		39900
17		48	29		123312
18		332	30		131236
	b = 4			b = 7	
16		12	22		108
21		960	26		1848
22		2430	27		18732
	b = 5		28		30576
20		240	29		3072
24		1620	31		128832
25		11952	32		591216
26		17802	33		1166976
			34		973800

	b = 8	27	1696
25	504	29	23136
26	2646	30	38832
28	3264	32	88128
30	86112	33	226908
31	278256	34	1815912
32	288216	35	3330288
33	82944	36	2928828
34	263520	37	1677600
35	2695248	38	9708450
36	7069032	39	39865920
37	10558944	40	76089120
38	7266429	41	92969640
	b = 9	42	54472030
24	56		

A — *Face-centred cubic bond problem*

	b = 1 Σ_s sg_{sbt}	57	103536
22	12	58	215280
	b = 2	59	286704
31	72	60	393300
32	126	61	321840
	b = 3	62	145404
30	24		b = 6
39	128	36	8
40	768	46	4080
41	1488	47	3240
42	1304	48	2520
	b = 4	54	4440
38	120	55	62928
39	480	56	150480
40	492	57	255600
48	6150	58	261216
49	9480	59	247788
50	20880	60	105888
51	22920	63	94192
52	13695	64	237720
	b = 5	65	1172304
37	48	66	2373616
38	96	67	3740352
47	7320	68	5592804
48	8640	69	6170472
49	13080	70	6544944
50	7560	71	4284000
55	2304	72	1557962
56	37008		

	b = 7
45	1200
46	480
53	4464
54	54288
55	106416
56	138528
57	94752
58	46620
62	227976
63	523824
64	2284800
65	4064928
66	5450424
67	6644232
68	5663280
69	4138092
70	1406328
71	1619520
72	3240960
73	13946112
74	27036480
75	52254336
76	75166848
77	100550400
78	119089344
79	116656896
80	100660752
81	55223040
82	16817664

FIXED SIZE ENERGY GROUPINGS (NORMAL ANIMALS)

B — *Simple cubic bond animals*

	b = 1 g_{sb}
2	3
	b = 2
3	15
	b = 3
4	95
	b = 4
4	3
5	678
	b = 5
5	48
6	5229
	b = 6
6	622
7	42464
	b = 7
6	18
7	7308
8	357987
	b = 8
7	450
8	81981
9	3104013
	b = 9
7	8
8	7958
9	895536
10	27511300

B — *Diamond lattice site animals*

	s = 1 g_{sb}
0	1
	s = 2
1	2
	s = 3
2	6
	s = 4
3	22
	s = 5
4	91
	s = 6
5	396
6	2
	s = 7
6	1782
7	24

s = 8	
7	8186
8	207
s = 9	
8	38199
9	1508
10	6
s = 10	
9	180544
10	9978
11	102
12	1
s = 11	
10	862642
11	62112
12	1146
13	16
s = 12	
11	4161378
12	371001
13	10434
14	198

FIXED SIZE DIRECTED PERCOLATION GROUPINGS

C — *Simple quadratic site problem*

	g_{st}
s = 1	
2	1
s = 2	
3	2
s = 3	
3	1
4	4
s = 4	
4	5
5	8
s = 5	
4	2
5	17
6	16
s = 6	
4	1
5	13
6	50
7	32
s = 7	
5	10
6	58
7	135
8	64
s = 8	
5	5
6	57
7	214
8	346
9	128
s = 9	
5	2
6	45
7	259
8	707
9	854
10	256
s = 10	
5	1
6	28
7	267
8	1023
9	2163
10	2052
11	512
s = 11	
6	20
7	218
8	1269
9	3681
10	6264
11	4827
12	1024
s = 12	
6	10
7	181
8	1278
9	5291
10	12360
11	17383

12		11170	12		242203
13		2048	13		352343
	s = 13		14		311262
6		5	15		128726
7		131	16		16384
8		1219		s = 16	
9		6290	7		36
10		20136	8		681
11		39329	9		6428
12		46661	10		37451
13		25498	11		148186
14		4096	12		411505
	s = 14		13		784420
6		2	14		1005138
7		90	15		779932
8		1069	16		285572
9		6805	17		32768
10		27455		s = 17	
11		71686	7		20
12		119848	8		508
13		121873	9		5741
14		57564	10		39233
15		8192	11		183464
	s = 15		12		610686
6		1	13		1462141
7		56	14		2452215
8		881	15		2794187
9		6837	16		1922948
10		33337	17		629100
11		109887	18		65536

C — *Triangular site problem*

	s = 1	g_{st}	8		6
3		1	9		1
	s = 2			s = 5	
4		2	6		6
5		1	7		31
	s = 3		8		51
5		5	9		29
6		4	10		8
7		1	11		1
	s = 4			s = 6	
5		1	6		2
6		12	7		22
7		15	8		93

9		162	14		23596
10		125	15		18901
11		47	16		10084
12		10	17		3663
13		1	18		921
	s = 7		19		159
7		15	20		18
8		77	21		1
9		293		s = 11	
10		523	8		6
11		485	9		142
12		241	10		925
13		69	11		4370
14		12	12		14317
15		1	13		35970
	s = 8		14		66029
7		5	15		84536
8		65	16		74390
9		291	17		45287
10		934	18		19350
11		1725	19		5891
12		1800	20		1285
13		1098	21		197
14		407	22		20
15		95	23		1
16		14		s = 12	
17		1	8		2
	s = 9		9		75
7		1	10		761
8		40	11		4144
9		265	12		17096
10		1078	13		52340
11		3086	14		125301
12		5739	15		228005
13		6555	16		302428
14		4659	17		286950
15		2114	18		194685
16		631	19		95281
17		125	20		34057
18		16	21		8960
19		1	22		1731
	s = 10		23		239
8		20	24		22
9		199	25		1
10		1094		s = 13	
11		3925	9		40
12		10452	10		522
13		19345	11		3736

12	17850	11	2990
13	66212	12	17429
14	191545	13	74526
15	441060	14	255149
16	794995	15	701740
17	1083076	16	1565490
18	1091816	17	2796170
19	810484	18	3886667
20	444953	19	4116618
21	182225	20	3294610
22	56161	21	1994447
23	13048	22	918464
24	2267	23	324019
25	285	24	88006
26	24	25	18349
27	1	26	2901
s = 14		27	335
9	15	28	26
10	348	29	1

C — *Simple cubic site problem*

s = 1	g_{st}	11	168
3	1	12	571
s = 2		13	1512
5	3	14	2334
s = 3		15	729
6	3	s = 8	
7	9	10	12
s = 4		11	36
6	1	12	394
8	24	13	1554
9	27	14	4131
s = 5		15	8598
8	9	16	9099
9	21	17	2187
10	126	s = 9	
11	81	10	3
s = 6		11	3
9	15	12	198
10	69	13	798
11	219	14	4062
12	567	15	12285
13	243	16	26619
s = 7		17	43605
9	3	18	34113
10	22	19	6561

	s = 10
10	1
12	45
13	426
14	2400
15	10122
16	34907
17	86118
18	155874
19	204408
20	124362
21	19683
	s = 11
12	13
13	153
14	1029
15	6852
16	27480
17	98232
18	265065
19	548817
20	846369
21	905424
22	443484
23	59049
	s = 12
13	48
14	477
15	3156
16	17535
17	82128
18	274809
19	809265
20	1832232
21	3250473
22	4323981
23	3838500
24	1554633
25	177147

C — *Hypercubic 4 - dimensional site problem*

	s = 1 g_{st}
4	1
	s = 2
7	4
	s = 3
9	6
10	16
	s = 4
10	4
12	66
13	64
	s = 5
10	1
13	52
14	84
15	474
16	256
	s = 6
13	14
15	132
16	514
17	1236
18	2904
19	1024
	s = 7
15	36
16	169
17	286
18	2100
19	5336
20	11922
21	16218
22	4096
	s = 8
16	28
17	82
18	900
19	1770
20	7244
21	25224
22	51254
23	93918
24	85560
25	16384
	s = 9
16	4
18	183
19	686

20	2274	20	224
21	13746	21	4536
22	29603	22	13586
23	103320	23	53986
24	259638	24	177514
25	450758	25	439916
26	655770	26	1196838
27	433320	27	2413458
28	65536	28	3640140
s = 10		29	4214016
18	30	30	2130912
19	216	31	262144

CYCLOMATIC NUMBER DISTRIBUTIONS (DIRECTED ANIMALS)

D — *Simple quadratic cycle groupings*

	$g_{sb}^{(2)}$		
s = 3		12	105
2	1	13	18
s = 4		s = 11	
3	2	10	1818
4	1	11	1860
s = 5		12	1073
4	5	13	356
5	4	14	98
s = 6		15	6
5	14	s = 12	
6	10	11	4790
7	2	12	5307
s = 7		13	3308
6	38	14	1277
7	26	15	368
8	11	16	63
s = 8		17	2
7	100	s = 13	
8	77	12	12633
9	34	13	15084
10	5	14	10087
s = 9		15	4406
8	262	16	1357
9	228	17	320
10	102	18	36
11	30	s = 14	
12	1	13	33364
s = 10		14	42670
9	690	15	30638
10	653	16	14532
11	334	17	5094

18		1291
19		250
20		15
	s = 15	
14		88211
15		120348
16		92290
17		47130
18		18293
19		5126
20		1182
21		164
22		5
	s = 16	
15		233460
16		338642
17		275698
18		151301
19		63146
20		19994
21		4988
22		955
23		98
24		1
	s = 17	
16		618500
17		950692
18		818594
19		479578
20		213949
21		74466
22		20508
23		4476
24		734
25		48

D — *Simple cubic site problem*

		g_{sb}
	s = 1	
0		1
	s = 2	
1		3
	s = 3	
2		12
	s = 4	
3		49
4		3
	s = 5	
4		204
5		33
	s = 6	
5		870
6		228
7		15
	s = 7	
6		3787
7		1344
8		201
9		7
	s = 8	
7		16722
8		7467
9		1641
10		180
12		1
	s = 9	
8		74643
9		40245
10		11119
11		2037
12		108
13		15
	s = 10	
9		336108
10		212505
11		70752
12		16686
13		2097
14		180
15		18
	s = 11	
10		1524438
11		1105692
12		427305
13		119091
14		22386
15		2740
16		294
17		21

$s = 12$		15	186237
11	6956214	16	32493
12	5692404	17	3927
13	2498400	18	555
14	794151	20	3

REFERENCES

[1] DUARTE, J. A. M. S., *Portgal Phys.*, **12**, 99 (1981).

[2] DHAR, D., PHANI, M. K., BARMA, M., *J. Phys.*, **A15**, L279 (1982).

[3] DHAR, D., *Phys. Rev. Letters*, **21**, 853 (1983).

[4] SYKES, M. F., GAUNT, D. S., GLEN, M., *J. Phys.*, **A14**, 287 (1981).

[5] WHITTINGTON, S. G., TORRIE, G. M., GAUNT, D. S., *J. Phys.*, **A16**, 1695 (1983).

[6] DE'BELL, K., ESSAM, J. W., *J. Phys.*, **A16**, 385 (1983).

[7] DE'BELL, K., *J. Phys.*, **A16**, 3553 (1983).

[8] NADAL, J. P., DERRIDA, B., VANNIMENUS, J., *J. Physique* (Paris), **43**, 1561 (1982).

ERRATA AND ADDENDA: FRUSTRATED SPIN SYSTEMS

(Portgal. Phys. 15, 9-54 (1984))

AYSE ERZAN

Laboratório de Física, Faculdade de Ciências,
4000 Porto, Portugal

(Received 19 October 1984)

The relevant set of symmetry operations on the Potts spins, taking q possible values, is not the whole permutation group of q objects but the q dimensional cyclic group (see paragraph preceding eq. 3.4) which is abelian, and which has the desired property that all elements are traceless except for the identity, in a q-dimensional matrix representation (see paragraph following eq. 3.8).

One should stress that the simplest gauge invariant object that can be constructed from the gauge variables ψ ($\mathbf{r}$, $\mathbf{r}'$) is the plaquette function $\Pi_p \psi$, or the matrix product of the gauge variables taken around a plaquette. The trace of this object (or the quantity ϕ_p , eq. 3.11) is only one of the q - 1 independent scalar quantities that can be constructed from $\Pi_p \psi$. The partition function, however, will depend upon all such gauge invariant quantities.

Define the vector

$$f_p^{\alpha} = (1/q) \sum_{\beta,\gamma} \delta_{\beta,\gamma+\alpha-1} (\Pi_p \psi)_{\beta\gamma} \qquad \alpha, \beta, \gamma = 1, \ldots q .$$

Note that the first element is just $1/q$ times the trace itself, and $\Sigma f_p^{\alpha} = 1$. In specifying the frustration configuration, one may now specify each of these vectors, as, say, taking the values $\hat{\phi}_p$.

Thus, in eq. (3.14) $\hat{\phi}_p$ should be substituted for the scalar ϕ_p that appears there. Similiarly, eq. (3.17) should read,

$$Z \{ \hat{\phi}_p \} = \Omega_M \sum_{\{\psi\}} \prod_p \delta (\hat{\phi}_p , \mathbf{f}_p) \exp [k \sum_{(\mathbf{r},\mathbf{r}')} \psi_{00} (\mathbf{r} , \mathbf{r}')]$$

The Kroenecker delta $\delta (\hat{\phi}_p , \mathbf{f}_p)$ can be expressed conveniently as

$$\delta (\hat{\phi}_p , \mathbf{f}_p) = \hat{\phi}_p^\dagger \mathbf{f}_p$$

and, up to an infinite constant factor, as

$$\lim_{K_p \to \infty} \exp [K_p \phi_p^\dagger \mathbf{f}_p]$$

giving, in place of eq. (3.19), (3.20),

$$Z \{ \hat{\phi}_p \} = \Omega_M \lim_{K_p \to \infty} \sum_{\{\psi\}} \exp [K \sum_{\mathbf{r},\mathbf{r}'} \psi_{00} (\mathbf{r} \ \mathbf{r}') + K_p \Sigma \hat{\phi}_p^\dagger \mathbf{f}_p]$$

The Duality Transformation given in the Appendix is correct for the unfrustrated case (setting all $\phi_p = 1$ in the notation used there). The generalization to the frustrated case, however, does not follow along the same lines as the Ising model. In particular, the statement that it can be accomplished by the replacement $K_p \to -K_p / (q - 1)$ turns out to be incorrect in general. Instead of eq. (4.15) one should have, using the following parameterization of

$$\hat{\phi}_p^\alpha = \delta_{\alpha, r_p + 1} \quad , \quad r_p = 0 , \ldots q - 1 \quad \text{and} \quad - r_p \equiv q - r_p \ ,$$

that: i) in the case of one frustration at a plaquette p dual to the site $\tilde{i}$

$$(q - 1)^{-1} < q \ \delta_{\sigma_{\tilde{i}}, 1} - 1 >_{k^*}$$

$$= \lim_{K_p \to \infty} \frac{Z \{ r_p \neq 0 , \text{ all } r_q \ (q \neq p) = 0 \}_{k, k_p}}{Z \{ \text{all } r = 0 \}_{k, k_p}}$$

ii) in the case of two frustrations at plaquettes p, q dual to sites $\tilde{i}$, $\tilde{j}$:

$$(q-1)^{-1} < (q\,\delta_{\tilde{i},1} - 1)\,(q\,\delta_{\tilde{j},1} - 1) >_{k^*} =$$

$$\lim_{K_p \to \infty} [Z_{k,k_p}\{r_p \neq 0, r_q = -r_p, r_s (s \neq p, q) = 0\} + (q-2) \cdot$$

$$\cdot Z_{k,k_p}\{r_p \neq 0,\ r_q \neq -r_p, r_s (s \neq p, q) = 0\}] / Z_{k,k_p}\{\text{all } r = 0\}$$

iii) in the case of three frustrations at p, q, s dual to $\tilde{i}$, $\tilde{j}$, $\tilde{k}$

$$(q-1)^{-1} < \prod_{\mu = \tilde{i}, \tilde{j}, \tilde{k}} (q\,\delta_{\sigma_\mu, 1} - 1) > =$$

$$\lim_{K_p \to \infty} [(q-2)\, Z_{k,k_p}\{r_p + r_q + r_s = 0, r_t\ (t \neq p, q, s) = 0\}$$

$$+(q-1)\,(Z_{k,k_p}\{r_p + r_q = 0, r_s \neq 0, r_t\,(t \neq p, q, s) = 0\} + \text{permutations})$$

$$+(q^2 - 6q + 6)\,(Z_{k,k_p}\{r_p + r_q + r_s \neq 0, r_p + r_q \neq 0, r_s \neq 0, r_t\,(t \neq p, q, s)$$

$$= 0\} + \text{permutations})] / Z_{k,k_p}\{\text{all } r = 0\}$$

The cases with more than three frustrations are even more complicated. One should be able to invert these equations for the partition functions, but this has not yet been accomplished.

I would like to thank Drs. E. J. S. Lage, L. Banyai and Prof. Wegner for their useful comments.

MISFIT DISLOCATIONS IN CRYSTALLINE INTERFACES

M. A. FORTES

Departamento de Metalurgia, Instituto Superior Técnico
Centro de Mecânica e Materiais da Universidade Técnica de Lisboa
Av. Rovisco Pais, Ed I. S. T. — 1096 Lisboa Codex, Portugal

(Received 13 April 1984)

ABSTRACT — The equations that give the misfit dislocation content of an arbitrary interface are derived from a general formulation of the coincidence site lattice model of crystalline interfaces. The equations are solved, by introducing a "dislocation content lattice", to determine the orientation and spacing of the dislocations. The results are amenable to a simple geometrical interpretation. Grain boundaries are discussed as an application.

1 — INTRODUCTION

Arrays of misfit dislocations [1, 2] appear in grain boundaries between crystals with relative orientations deviating slightly from a coincidence site lattice (c. s. l.) orientation. At such special orientations the lattices in the two crystals admit a sub-lattice of coincidence points. The dislocations are grouped in one or more families of approximately straight, parallel and equidistant dislocations. Misfit dislocations have been observed by various techniques, particularly by transmission electron microscopy, in low [3] and high angle [4-6] grain boundaries, mainly in cubic metals. In the case of low angle boundaries, the near c. s. l. orientation is the perfect crystal. Bollmann [2] distinguishes between primary and secondary dislocations; the former occur in low angle boundaries and the latter in (other) near c. s. l. boundaries. This distinction will not be made here.

At the exact c. s. l. orientations, particularly when the degree of coincidence Σ is low (high coincidence; Σ is defined as the

reciprocal fraction of coincidence points) boundaries exist which are built up of low energy atom groups ("structural units") periodically repeated along the boundary [7, 8]. The corresponding short period boundaries have therefore a low energy and other special properties. The misfit dislocations introduced as a result of small deviations from those special or "favoured" orientations permit that in most of the boundary area the low energy atom groups are maintained [9]. Misfit dislocations can be regarded as lattice defects in the so-called DSC lattice; this is defined as the coarsest lattice that contains both crystal lattices (in a c. s. l. orientation) as sub-lattices [2]. The Burgers vectors of the (perfect) misfit dislocations are therefore among the DSC lattice vectors.

These ideas are inspired by the model of Read and Shockley [10] for low angle boundaries. In this case, the special, reference orientation is the perfect crystal and the misfit dislocations have Burgers vectors which are lattice vectors. The dislocation content of small angle boundaries, that is, the direction and spacing of the dislocations in each family, can be obtained from the well-known Frank's formula [10, 11] for a given set of three independent Burgers vectors. This formula is easily generalized to determine the dislocation content of any grain boundary between two crystals which deviate slightly from a c. s. l. orientation [5, 12, 13]. When the dislocation content is known, the contribution of the misfit dislocations to the boundary energy can be evaluated , and this may be sufficient to determine the variation of energy with the deviation away from a given c. s. l. orientation [14].

Dislocations with the same role of maintaining as much as possible low energy atomic configurations at the interface, may also occur at an interface between two different crystals [2, 15-21]. The basic ideas of the c. s. l. model can be adapted to such general interfaces, the only difficulty being that c. s. l. orientations between two different crystals (and in fact also between two non-cubic identical crystals) only occur if the lattice parameters satisfy particular metric relations [22]. Formally, a c. s. l. model of interfaces can then be based on the following points:

1 — Low energy interfaces should occur for particular values of the lattice parameters and of the parameters defining

the relative orientation of the two crystals, which correspond to a c. s. l. relation between the two crystal lattices.

2 — When the lattice parameters and/or the relative orientation deviate from the exact c. s. l. values, interfacial misfit dislocations are incorporated in the interface structure.

3 — The Burgers vectors of the interfacial dislocations are among the vectors of the DSC lattice associated with the reference c. s. l..

In this paper we derive, from the point of view of the c. s. l. model, the equations that give the dislocation content of a general interface between two crystals. To do this it is of course necessary to choose a definite reference c. s. l. relation between the two crystals or between two other crystals with different lattice parameters. The choice of the reference state is not unique and in the derivation we shall not require that the actual parameters (lattice and orientation) deviate slightly from those of the reference state. However, if the deviation is too large, the spacing between the dislocations will be so small to question their individuality. The equation derived for the total dislocation content is formally identical to the one first obtained by Bullough and Bilby [23] for a continuous distribution of surface dislocations and subsequently adapted for discrete dislocations at crystalline interfaces [20]. The advantage of the present derivation is that it clearly indicates the possible Burgers vectors of the misfit dislocations. The equation will be solved to obtain the orientation and spacing of the dislocations in a general interface. The solution is analogous to the one found by Knowles [21] but corrects an error introduced in his derivation. The dislocation distribution is related to a "dislocation content lattice" which in turn can be related to the c. s. l. of the reciprocal lattices of the two crystals. The range of applicability of the c. s. l. model of interfaces is assessed and the continuity of dislocation lines in non-planar interfaces is proved. The particular case of grain boundaries is treated as an example of application.

2 — DISTRIBUTION OF MISFIT DISLOCATIONS

2.1 — *Basic Mathematical Concepts*

We consider two crystal lattices, L and L′, and choose vector bases $(\mathbf{e}) \equiv (\mathbf{e}_1, \mathbf{e}_2, \mathbf{e}_3)$ and $(\mathbf{e}') \equiv (\mathbf{e}'_1, \mathbf{e}'_2, \mathbf{e}'_3)$ in each. When two crystals with those lattices meet at an interface, there is a definite relation between the two sets of vectors, which we write in matrix notation as

$$[\mathbf{e}] = [\mathbf{e}']\ \mathrm{X} \tag{1}$$

where $[\mathbf{e}] = [\mathbf{e}_1, \mathbf{e}_2, \mathbf{e}_3]$ and $[\mathbf{e}'] = [\mathbf{e}'_1, \mathbf{e}'_2, \mathbf{e}'_3]$ are to be regarded as row matrices, and X is a non-singular 3×3 matrix. X defines the relative orientation of the two lattices and will be termed the orientation matrix. The relation defined by eq. (1) can be regarded in two ways. First, it defines a coincidence of vectors $\mathbf{v}$ and $\mathbf{v}'$, one in each lattice:

$$\mathbf{v}' = \mathrm{X}\ \mathbf{v} \tag{2}$$

that is, a relation between the components of $\mathbf{v}$ in the basis $(\mathbf{e})$ and those of the coincident vector $\mathbf{v}'$ in the basis $(\mathbf{e}')$. If $\{\mathbf{v}\}_{\mathbf{e}}$ is a column matrix with the $\mathbf{e}$ components of $\mathbf{v}$ then eq. (2) is equivalent to

$$\{\mathbf{v}\}_{\mathbf{e}} = \mathrm{X}^{-1}\ \{\mathbf{v}'\}_{\mathbf{e}'} \quad . \tag{3}$$

The second interpretation of eq. (1) is that it transforms a vector $\mathbf{v}$ of lattice L into another vector $\mathbf{v}_x$, the $(\mathbf{e})$ components $\{\mathbf{v}\}$ and $\{\mathbf{v}_x\}$ of the vectors being related by

$$\mathbf{v}_x = \mathrm{X}^{-1}\ \mathbf{v} \quad , \quad \{\mathbf{v}_x\}_{\mathbf{e}} = \mathrm{X}^{-1}\ \{\mathbf{v}\}_{\mathbf{e}} \quad . \tag{4}$$

It has been established [24] that a c. s. l. relation between the two lattices (that is, the existence of coincident vectors forming a 3-dimensional lattice) is defined by those matrices $\mathrm{X} = \mathrm{C}$ that are rational. As shown elsewhere [25] the c. s. l. can be determined by factorizing C in the form

$$\mathrm{C} = \mathrm{N}'\ \mathrm{N}^{-1} \tag{5}$$

where N and N′ are integral matrices with the least possible values of $|\det N|$ and $|\det N'|$. These values are the degrees of coincidence Σ and Σ' for lattices L and L′. A basis of the c. s. l. is

$$[\mathbf{e}]\, N = [\mathbf{e}']\, N' \quad . \tag{6}$$

The DSC lattice is determined by factorizing C in the form

$$C = M'^{-1}\, M \tag{7}$$

with the least possible values of $|\det M|$ and $|\det M'|$, which in fact coincide with Σ and Σ' [25]. A basis of the DSC is the set $(\mathbf{b}_0) = (\mathbf{b}_{01}, \mathbf{b}_{02}, \mathbf{b}_{03})$ defined by

$$[\mathbf{b}_0] = [\mathbf{e}]\, M^{-1} = [\mathbf{e}']\, M'^{-1} \quad . \tag{8}$$

In the following, we shall make use of the metric matrix of a lattice. For example, for lattice L this matrix is $G = (g_{ij})$, with $g_{ij} = \mathbf{e}_i \cdot \mathbf{e}_j$. The volume of the unit cell is $(\det G)^{1/2}$. Esq. (1) implies that

$$G = X^{T}\, G'\, X \tag{9}$$

and for given G and G′ there may not be rational solutions X for this equation. T denotes the transposed matrix. The reciprocal lattice of L, for example, has a basis $(\mathbf{e}^*)$ given by

$$[\mathbf{e}^*] = [\mathbf{e}]\, G^{-1} \tag{10}$$

2.2 — *Formulation of the Problem*

If the orientation matrix X is not rational, we write X in the form

$$X = D\, C \tag{11}$$

where C is a rational matrix defining a c. s. l. relation between lattice L and another lattice L'_d with basis

$$[\mathbf{e}'_d] = [\mathbf{e}']\, D \quad . \tag{12}$$

L'_d deviates slightly from lattice L′ and is in a c. s. l. relation with lattice L:

$$[\mathbf{e}] = [\mathbf{e}'_d]\, C \quad . \tag{13}$$

More generally, we could write X in the form $X = D' C D^{-1}$, by considering two auxiliary lattices $[\mathbf{e}_d] = [\mathbf{e}]\, D$ and $[\mathbf{e}'_d] = [\mathbf{e}']\, D'$, associated respectively with L and L′, in a c. s. l. relation: $[\mathbf{e}_d] = [\mathbf{e}'_d]\, C$. This is the type of decomposition used by Christian [20]. However, for a given X and a chosen C, it is always possible to write X in the simpler form eq. (11), which we shall use in the following analysis. There are, of course, infinite choices for the matrices C and D satisfying eq. (11). As a general rule, the physically best choice should be the one for which the degrees of coincidence (Σ and Σ') defined by C are small and the deviation defined by D is small (that is, $D \simeq I$, I being the identity matrix). For a given choice of C, we find a basis $(\mathbf{b}_0) = (\mathbf{b}_{01}, \mathbf{b}_{02}, \mathbf{b}_{03})$ of the DSC lattice in the way described above (eqs. (7) and (8)) and choose three arbitrary non-coplanar vectors $(\mathbf{b}) = (\mathbf{b}_1, \mathbf{b}_2, \mathbf{b}_3)$ of this lattice. We shall find the dislocation content of an interface with unit normal $\mathbf{n}$, assuming that the dislocations have Burgers vectors $\mathbf{b}_1$, $\mathbf{b}_2$, $\mathbf{b}_3$.

We take lattice L as fixed and consider a reference state with lattices L and L'_d in the c. s. l. orientation, C. As in the derivation of Frank's formula [11] we take an arbitrary vector $\mathbf{v}$ in the plane of the interface between L and L'_d. This plane has a definite orientation in lattice L, so that no ambiguity occurs. When L'_d is transformed into L′ by means of the operator D, the vector $\mathbf{v}$ is transformed into $D^{-1}\mathbf{v}$ (eq. 4). We now state that the difference between the two vectors $\mathbf{v}$ and $D^{-1}\mathbf{v}$ is the sum, $\mathbf{B}$, of the Burgers vectors of all dislocations cut by $\mathbf{v}$:

$$\mathbf{B} = (I - D^{-1})\, \mathbf{v} \quad . \tag{14}$$

This is the basic equation of the formal theories of surface and interface dislocations [20, 23]. In the following we shall find the solution of this equation in order to determine the detailed dislocation content of the interface. The method of solution is similar to that of Knowles [21] but a correction is made to an error in his derivation, which is in fact valid only when the reference lattice is cubic (see below).

The interface will in general contain several families of dislocations, each family having the same Burgers vector. An argument similar to the one used by Read [11] would show that the dislocations of a given Burgers vector are parallel and equally spaced. Adopting the procedure of Sargent and Purdy [18] we therefore define vectors $\mathbf{N}_i$, perpendicular to the family of dislocations $\mathbf{b}_i$ and such that the spacing d_i between the dislocations in the family is

$$d_i = |\mathbf{N}_i|^{-1} \quad . \tag{15}$$

The number of dislocations $\mathbf{b}_i$ cut by $\mathbf{v}$ is $\mathbf{v} \cdot \mathbf{N}_i$ and their contribution to the total Burgers vector $\mathbf{B}$ is $(\mathbf{v} \cdot \mathbf{N}_i)\, \mathbf{b}_i$. Therefore

$$(I - D^{-1})\, \mathbf{v} = \sum_i (\mathbf{v} \cdot \mathbf{N}_i)\, \mathbf{b}_i \quad . \tag{16}$$

This relation holds for any $\mathbf{v}$ such that

$$\mathbf{v} \cdot \mathbf{n} = 0 \quad . \tag{17}$$

2.3 — *Determination of the Dislocation Content*

To solve eqs. (16) and (17) we introduce the reciprocal vectors $\mathbf{b}_i^*$ of the $\mathbf{b}_i$, defined by (cf. eq. 10)

$$[\mathbf{b}^*] = [\mathbf{b}]\, G_b^{-1} \tag{18}$$

where G_b is the metric matrix of the $\mathbf{b}_i$. The vectors $\mathbf{b}_i^*$ belong to the reciprocal lattice of the $(\mathbf{b}_o)$, with basis $(\mathbf{b}_o^*)$ given by (cf. eqs. (9) and (10))

$$[\mathbf{b}_o^*] = [\mathbf{b}_o]\, M\, G^{-1}\, M^T \quad . \tag{19}$$

The lattice $(\mathbf{b}_o^*)$ is the c. s. l. of the reciprocal lattices of $(\mathbf{e})$ and $(\mathbf{e}')$ (e.g. [25]). Taking the scalar product of eq. (16) by $\mathbf{b}_i^*$, we obtain

$$\mathbf{b}_i^* \cdot (I - D^{-1})\, \mathbf{v} = \mathbf{v} \cdot \mathbf{N}_i \quad . \tag{20}$$

Next we introduce the adjoint operator of $(I - D^{-1})$ which is represented in the basis $(\mathbf{e})$ by the matrix

$$Q = G^{-1} (I - D^{-1})^{T} G \quad . \tag{21}$$

This allows us to write eq. (20) in the form

$$(\mathbf{N}_i - Q\,\mathbf{b}_i^*) \cdot \mathbf{v} = 0 \quad . \tag{22}$$

The vector in brackets in then parallel to $\mathbf{n}$, and since $\mathbf{N}_i$ is perpendicular to $\mathbf{n}$, we finally obtain

$$\mathbf{N}_i = Q\,\mathbf{b}_i^* - (Q\,\mathbf{b}_i^* \cdot \mathbf{n})\,\mathbf{n} \tag{23}$$

with Q defined by eq. (21). The vector $\mathbf{N}_i$ is the projection of $Q\,\mathbf{b}_i^*$ in the plane of the boundary. In matrix notation, eq. (23) is written as

$$\{\mathbf{N}_i\} = Q\{\mathbf{b}_i^*\} - \{\mathbf{n}\}^{T} (GQ\{\mathbf{b}_i^*\})\{\mathbf{n}\} \tag{24}$$

where $\{\ \}$ denotes a column matrix. This derivation leads to the same equations obtained by Knowles [21] except for the presence of the metric matrix G in the definition of Q. In fact, Knowles' result is only valid when $G = I$. This becomes apparent from inspection of eq. (17) in his paper.

The general procedure to obtain the orientation and spacing of misfit dislocations can be summarized in the following steps:

1 — Decomposition of the orientation matrix X (eq. 11).

2 — Determination of the DSC lattice associated with C (eq. 8): vector basis $(\mathbf{b}_o)$.

3 — Determination of the matrix Q (eq. 21) and vectors $Q\,\mathbf{b}_o^*$

$$[\mathbf{b}_o^*]\ Q = [\mathbf{b}_o]\ M\ G^{-1} M^{T} Q = [\mathbf{e}]\ G^{-1} M^{T} Q \quad . \tag{25}$$

To each Burgers vector $\mathbf{b}$ we may therefore associate a vector $Q\,\mathbf{b}^*$.

4 — Choice of three non-coplanar Burgers vectors $\mathbf{b}$ in the lattice $(\mathbf{b}_o)$.

5 — The direction and spacing of the dislocations with **b** is determined from the projection of the corresponding Q **b*** in the plane of the interface: the dislocations are perpendicular to the projected vector and their reciprocal spacing is the modulus of that vector (Fig. 1).

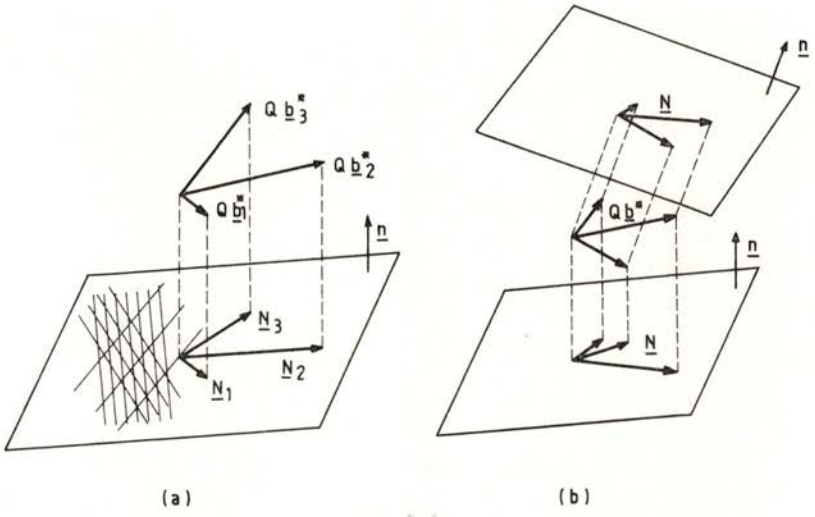

Fig. 1 — *a*) The directions and spacing of the misfit dislocations is determined by the projection $\mathbf{N}_i$ of the three vectors $Q\mathbf{b}_i^*$ in the plane of the interface. *b*) Effect of orientation of the interface on the distribution of dislocations defined by vectors **N**.

If the rank of Q is three, the vectors Q **b*** form a 3-dimensional lattice with the basis (25). This lattice can be termed the dislocation content lattice. Three families of dislocations with any non-coplanar **b**'s can accommodate the deviation from the c. s. l., for any orientation of the interface (Fig. 1). When a particular near c. s. l. relation and a particular interface orientation are considered, it is clear that larger Burgers vectors, **b**, correspond to larger Q **b*** vectors and therefore to larger dislocation spacings. However, if the energy per unit length of the dislocations increases more than linearly with b, the energy of the interface should increase as b

increases. Small Burgers vectors are therefore preferred. This is a general tendency, but in particular cases (e.g. for particular orientations of the interface) larger Burgers vectors may be energetically favourable. Various criteria that can be used to choose the more convenient matrix D have been discussed by Knowles [19, 21]. As a guide to decide the more favourable near c. s. l. relation, that is, the one for which the interface structure has lower energy, we can use the following simple argument. From eq. (25) and the relation between metric matrices, eq. (9), it is easily concluded that the volume of the unit cell of the $Q\,\mathbf{b}^*$ vectors is $\Sigma\,|\det Q|\,/\,\Omega$, where Ω is the volume of the unit cell of lattice L. This quantity is a measure of the average dislocation density at interfaces for that particular reference c. s. l. relation. Therefore, the best choice of the decomposition (eq. 11) of the orientation matrix should be the one for which $\Sigma\,|\det Q|$ has the smallest value. Broadly, low Σ values and $D \simeq I$ should be favoured. However, the energy of the interface is not a simple function of the dislocation density, so that the rule has to be regarded carefully. Finally, the above result shows that as the deviation from a given c. s. l. relation increases, or the value of Σ increases, the average dislocation spacing $(\Sigma\,|\det Q|\,/\,\Omega)^{-1/3}$ decreases; the c. s. l. model fails when $\Sigma\,|\det Q|$ is of the order of unity.

If the rank of Q is two, the vectors $Q\,\mathbf{b}^*$ are all in the same plane, but do not form a lattice except in special cases (see an example below). If there is a vector $\mathbf{b}^*$ such that $Q\,\mathbf{b}^* = 0$ (and this may be possible if the rank of Q is two), interfaces of any orientation can be described with just two families of dislocations.

Similar considerations apply when the rank of Q is one.

2.4 — *Continuity of Dislocations Lines*

It is interesting to point out that eq. (23) ensures the physically necessary continuity of the dislocation lines, of a given Burgers vector, as the plane of the interface changes (Fig. 2). This question is important in relation to interface faceting. Consider two planes with unit normals $\mathbf{n}$ and $\mathbf{n}'$. Their intersection is parallel to $\mathbf{n} \times \mathbf{n}'$. The orientation and spacing of dislocations in each plane is defined by $\mathbf{N}_i$ and $\mathbf{N}'_i$ for each Burgers vector $\mathbf{b}_i$.

It is assumed that the same Burgers vectors appear in both planes, although this is not strictly necessary. Continuity of the dislocations $\mathbf{b}_i$ implies that

$$d_i / \cos\theta = d'_i / \cos\theta' \tag{26}$$

where θ and θ' are defined in Fig. 2. Eq. (26) is equivalent to

$$| \mathbf{N}_i \cdot (\mathbf{n} \times \mathbf{n}') | = | \mathbf{N}'_i \cdot (\mathbf{n} \times \mathbf{n}') | . \tag{27}$$

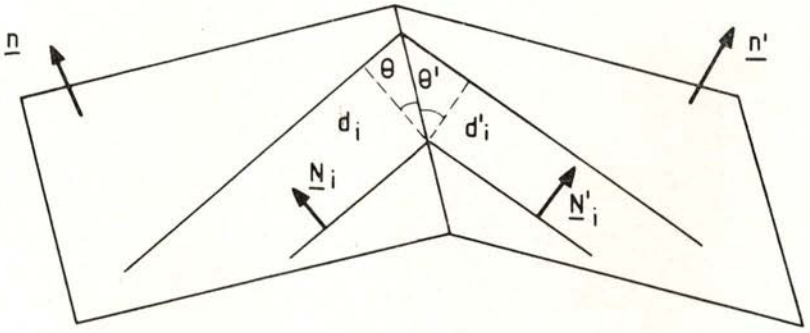

Fig. 2 — The dislocations of a given Burgers vector are continuous when the plane of the interface changes from the orientation **n** to **n'**.

It is immediately seen from eq. (23), that this relation holds for any **n**, **n'**. The dislocations are therefore continuous, even when the plane of the interface changes abruptly.

3 — APPLICATION TO GRAIN BOUNDARIES

The orientation matrix X is in this case a rotation matrix. Then D is also a rotation matrix and the rank of Q is necessarily two. The Q **b*** vectors are all in the same plane. If the rotation axis for D is defined by the unit vector **u**, the plane of the Q **b*** vectors is perpendicular to **u**. When the rotation angle θ in D is small, the matrix Q is equivalent to the operation defined by

$$Q = \theta\, \mathbf{u} \times \tag{28}$$

where $\times$ denotes the cross product.

The $Q\,\mathbf{b}^*$ vectors form a lattice in the plane $\mathbf{u}$ if and only if $\mathbf{u}$ is parallel to a lattice direction and perpendicular to a lattice plane of the two lattices in the c. s. l. orientation. This is immediately seen when Q has the form (28), since in this case the operation Q is directly related to the projection on the plane $\mathbf{u}$. Those conditions are in general only met in cubic crystals. More generally, the $Q\,\mathbf{b}^*$ vectors may have their extremities on a family of parallel equidistant straight lines or they may fill the whole plane when placed at a common origin.

When $\mathbf{u}$ is perpendicular to a lattice plane of the two crystal lattices in the c. s. l. orientation, there is a reciprocal $\mathbf{b}^*$ parallel to $\mathbf{u}$ and for this $Q\,\mathbf{b}^* = 0$. In this case all grain boundaries may contain just two families of dislocations with Burgers vectors in the plane $\mathbf{u}$.

As for a general crystalline interface, the actual dislocation content of a grain boundary can only be decided, among all possible choices of the reference c. s. l. and the corresponding combinations of Burgers vectors, after calculating the energy of the boundary for each set of Burgers vectors. The variation of the energy of the boundary with its orientation can then be determined, and the so called γ - plot constructed. Special orientations, possibly associated with cusps in the γ - plot, will occur when one family of dislocations is missing, relative to neighbouring orientations. The special orientations are those for which the boundary plane is normal to a $Q\,\mathbf{b}^*$ vector, which in turn implies that the deviation from the c. s. l. orientation is a pure tilt rotation.

4 — DISCUSSION

Although misfit dislocations have been observed in a variety of interfaces, it is not certain whether they are a general feature of crystalline interfaces. The formal theory outlined in this paper plausibly admits that they should occur at interfaces which deviate slightly from special or favoured orientations containing a high density of coincidence points. The misfit dislocations can be regarded as line defects in the DSC lattice but this lattice can only be defined for c. s. l. orientations. In most cases, such orientations only occur if we allow for changes in the metric of the two crystals. However, it is difficult to physically legitimate

these changes since they interfere with the stability of the crystals; the favoured interfaces are then purely conceptual.

When coincidence of lattice points does not occur, it is still possible to define a coincidence of equivalent points in the two crystal lattices [2]. These are the 0 - points and form a translation lattice — the 0 - lattice. Bolmann [2] suggested that special interfaces are those that contain a high density of 0 - points, but the physical basis for this is weak: the 0 - lattice theory is "too" geometrical.

Nevertheless, the concept of favoured or special interfaces of low energy is useful and can possibly be generalized to include all those interfaces correlated with cusps in the energy plots (or γ - plots) as a function of the orientation of the interface for any relative orientation of the two crystals. A difficulty arises in such cases, in that there is not, as there is in the case of c. s. l. interfaces, an obvious crystallographic "state" in relation to which dislocations can be defined, although they could still be regarded as line singularities in the atomic configuration at the interface.

The formal theory discussed in this paper and the equations derived allow a correct interpretation of the structure of interfaces in simples cases, but it is unlikely that their applicability is general. Besides, the theory does not identify unambiguously the Burgers vectors of the intervening dislocations. The alternative approach to the structure of interfaces is the direct calculation by computer of the atomic positions, using adequate interatomic potentials. A considerable amount of work along this line has been undertaken in recent years for grain boundaries [26, 27]. But, as expected, the approach has little predictive value and the c. s. l. theory of interfaces remains the most rational and simple (although not entirely satisfactory) framework to discuss the structure and properties of interfaces.

REFERENCES

[1] D. G. BRANDON, B. RALPH, S. RANGANATHAN and M. S. WALD, *Acta Met.* 12, 813 (1964); see also P. H. PUMPHREY, «*Grain Boundary Structure and Properties*», Chap. 5, ed. G. A. CHADWICK and D. A. SMITH, (Academic Press, 1976).

[2] W. BOLLMANN, «*Crystal Defects and Crystalline Interfaces*», (Springer--Verlag, Berlin, 1970).

[3] S. AMELINCKX, «*Dislocations and Mechanical Properties of Crystals*», (Wiley, New York, 1957).

[4] B. LOBERG and H. NORDEN, «*Grain Boundary Structure and Properties*», Chap. 1, ed. G. A. CHADWICK and D. A. SMITH, (Academic Press, 1976).

[5] L. M. CLAREBROUGH and C. T. FORWOOD, *Phys. Stat. Sol.* (a), **58**, 597 (1980).

[6] L. M. CLAREBROUGH and C. T. FORWOOD, *Phys. Stat. Sol.* (a) **59**, 263 (1980).

[7] G. H. BISHOP and B. CHALMERS, *Scripta Met*, **2**, 133 (1968).

[8] A. P. SUTTON and V. VITEK, *Scripta Met.* **14**, 129 (1980).

[9] A. P. SUTTON, R. W. BALLUFFI and V. VITEK, *Scripta Met.* **15**, 989 (1981).

[10] W. T. READ and W. SHOCKLEY, *Phys. Rev.* **78**, 275 (1950).

[11] W. T. READ, «*Dislocations in Crystals*» (McGraw Hill, 1953).

[12] S. AMELINCKX and W. DEKEYSER, *Solid State Phys.* **8**, 325 (1959).

[13] M. A. FORTES, *Philos. Mag.* **28**, 1165 (1973).

[14] P. H. PUMPHREY, *Scripta Met.* **9**, 151 (1975).

[15] J. H. VAN DER MERWE, *Proc. Phys. Soc.* **A63**, 616 (1950).

[16] G. BARO and H. GLEITER, *Acta Met.* **21**, 1405 (1973).

[17] J. M. RIGSBEE and H. I. AARONSON, *Acta Met.* **27**, 351 (1979).

[18] C. M. SARGENT and G. R. PURDY, *Philos. Mag.* **32**, 27 (1975).

[19] K. M. KNOWLES and D. A. SMITH, *Acta Cryst.* **A38**, 34 (1982).

[20] J. W. CHRISTIAN, «*The Theory of Transformation in Metals and Alloys*» (Oxford: Pergamon Press) Chap. 8, 1976.

[21] K. M. KNOWLES, *Philos. Mag.* **A46**, 951 (1982).

[22] M. A. FORTES, *Phys. Stat. Sol.* (b), **82**, 377 (1977).

[23] R. BULLOUGH and B. A. BILBY, *Proc. Phys. Soc.* **69**, 1276 (1956).

[24] H. GRIMMER, *Acta Cryst.*, **A32**, 783 (1976).

[25] M. A. FORTES, *Acta Cryst.*, **A39**, 351 (1983).

[26] L. J. HARRISON, G. A. BRUGGEMAN and C. H. BISHOP «*Grain Boundary Structure and Properties*», Chap. 2, ed. G. A. CHADWICK and D. A. SMITH (Academic Press, 1976).

[27] A. BROKMAN and R. W. BALLUFFI, *Acta Met.* **29**, 1703 (1982).

COUPLING IN ONE ELECTRON TRANSFER PROCESSES +

A. M. C. MOUTINHO *

Centro de Física Molecular das Universidades de Lisboa (INIC)
Av. Rovisco Pais, Complexo I, I. S. T., 1000 Lisboa — Portugal

(Received 27 January 1984; revised version in 29 May 1984)

ABSTRACT — The correlation between the adiabatic splitting $\Delta V\ (R_c)$ and the crossing distance R_c for one electron transfer processes is analysed. This is based upon a selection of the experimental and computational data actually available, the test of several reduced variables and the correct asymptotic behaviour. A simple semi-empirical formula is proposed.

1 — INTRODUCTION

The calculation of the transition probability for electron transfer collisions of the type

$$A + B^{+n} \rightleftarrows A^{+} + B^{+(n-1)} \qquad (1)$$

requires the estimation of the coupling between the two states. This applies to many inelastic processes such as charge transfer, formation and recombination of ion pairs, chemi-ionization, an important part of chemical reactions, collisional excitation, quenching and dissociation. The adiabatic splitting $\Delta V\ (R_c)$ between the initial and final states is the fundamental parameter required to describe these interactions which involve curve

---

+ Results partially presented at the Third General Conference of the Portuguese Physical Society (Coimbra, June 1982).

* Dept de Física, Faculdade de Ciências e Tecnologia (U.N.L.), Quinta da Torre, 2825 Monte da Caparica, Portugal.

crossings. The splitting is directly related to the coupling matrix element H_{12} through [1]

$$\Delta V(R_c) = 2 \, | H_{12} - S H_{11} | / (1 - S^2) \qquad (2)$$

where S is the overlap integral and $H_{ij} = < \phi_i^0 | \hat{H}_{el} | \phi_j^0 >$ are the matrix elements of the electronic Hamiltonian in the diabatic representation, ϕ_1^0 and ϕ_2^0. When $S \simeq 0$, then $\Delta V(R_c) \simeq 2 H_{12}$.

Once one knows the coupling matrix element, the calculation of the cross section for the electron transfer process can be performed using the Landau-Zener formula

$$p_l = \exp(-v_{cr} / v_l) \quad \text{where} \quad v_{cr} = 2\pi H_{12}^2 (R_c) / | F_{11} - F_{22} |_{R_c} . \qquad (3)$$

F_{ii} are the derivatives dH_{ii} / dR and v_l is the radial velocity for the angular momentum l, all the quantities being evaluated at the crossing point R_c.

Atomic units are used throughout this work.

2 — CORRELATION $\Delta V(R_c) - R_c$

Estimations of the splitting $\Delta V(R_c)$ or the term $H_{12}(R_c)$ have been obtained either from experimental or theoretical work.

Experimentally these splittings can be deduced from the behaviour of the total, as well as, from the differential cross section. However the initial and final states involved have to be inequivocally identified. The velocity where the maximum of the total cross section occurs is directly related to the coupling term [2]. The differential cross section is very sensitive to the transition probability and therefore also contains information on the coupling but the determination is not so straightforward.

From the analysis of spectroscopic data, using the Rydberg-Klein-Rees (R. K. R.) method, the adiabatic potential curves can be derived. These potentials in the neghbourhood of the diabatic crossing point allow one to estimate the splitting [3, 4].

Theoretically three methods have been used to obtain these parameters.

Calculations using variational methods have been mainly performed by Bates and associates in the fifties [5-9]. They studied

several charge transfer and ion pair recombination processes. At large R_c distances, where the multipole interactions are dominant the calculations are incorrect [10].

The Heitler-London L. C. A. O. method has been also widely used. It predicts an asymptotic behaviour of the type $\Delta V_{LCAO} \sim \exp\,[-(\nu + \gamma)\,R_c]$ where $\nu = \sqrt{2\,I}$ and $\gamma = \sqrt{2\,EA}$, I and EA being respectively the ionization potential and the electron affinity or, in general, the higher and lower electron binding energy of the collision partners. At large crossing distances this method becomes also incorrect since the perturbation is as important as the zero order interaction [1].

In the Landau-Herring method, the exchange interaction $\Delta = 2\,|\,H_{12} - SH_{11}\,|$ is expressed as a surface integral of the transient particle flux in the configuration space of electronic coordinates. Several calculations have been performed using this asymptotic method [10-12]. They differ in the choice of the integration conditions and characteristics of the collisional systems. This method provides the means of obtaining the asymptotic behaviour [10] of the correlation $\Delta V - R_c$ which turned out to be $\Delta V_{LH} \sim \exp\,(-\nu R_c)$.

The first correlation $H_{12} - R_c$ was presented by Hasted and Chong [13]. Table I shows several theoretical and semi-empirical relations which, since then, have been forwarded. Of these, the formula of Olson, Smith and Bauer (O. S. B.) [16] is the one which has been the most extensively used although it does not have the correct asymptotic behaviour. The expression was obtained from a fit with almost one hundred theoretical and experimental points available in the literature up to 1971.

The relation proposed by Hubers, Klein and Los (H. K. L.) [17] is a generalization of O. S. B. but it has been derived from experimental fits only for alkali atom-halogen molecules. It has more adjustable parameters than the O. S. B. expression, however the exponential dependence only on νR_c resulted from the best fit.

Actually the data available for electron transfer, both in atom-atom and atom-molecule, rose to more than two hundred points. Most of them are theoretically estimated. Those experimentally derived are about one fifth of the total and are confined to high ΔV i.e. large coupling and small crossing distances. The collision processes analysed are listed in Table II and plotted in

Fig. 1. The adiabatic splitting ranges for about 10 orders of magnitude when R_c ranges only less than two orders. From the theoretical data available were excluded those splittings extrapolated from formulas although some of them were taken in the

TABLE I — Proposed relations for the H_{12} or ΔV dependence on R_c (atomic units) $\quad \nu = \sqrt{2\,I} \qquad \gamma = \sqrt{2EA}$

$H_{12} = R_c\,(\nu^2/2)\,\exp\,(-\nu R_c/\sqrt{2}) \qquad$ (for $H^+ + H$)

RAPP and FRANCIS [14]

$$H_{12} = A\left[\frac{\gamma\,\nu^2}{2}\left(\frac{4}{e}\right)^{1/\gamma}\frac{\nu^{2/\nu}\,(2l+1)}{\Gamma\,[(1/\nu)+l+1]\;\Gamma\,[(1/\nu)-l]}\right]^{1/2} \cdot R_c^{\,1/\nu-1}\,\exp\,[-(\nu+\gamma)\,R_c/2]$$

SMIRNOV [12]

(A is a constant and l is the orbital angular momentum)

$$H_{12} = \frac{\nu}{\Gamma(1/\nu)}\,(2\nu)^{1/\nu+1/2}\;R_c^{\,1/\nu-1}\,\exp\,(-\nu R_c)$$

KOMAROV [11]

$H_{12} = \gamma^2\,[8.0\,\exp(-0.91\,\gamma R_c) - 7.5\,\exp(-0.99\,\gamma R_c)]$

OLSON, PETERSON and MOSELEY [15]

$H_{12}^* = 1.0\,R_c^*\,\exp(-0.86\,R_c^*)\;,\quad H_{12}^* = H_{12}/\nu\gamma\;,\quad R_c^* = (\nu+\gamma)\,R_c/2$

OLSON, SMITH and BAEUR [16]

$\Delta V = \exp\,[(R_c^{\circ} - R_c)/\Delta R]$ (R_c, ΔR are parameters)

GRICE and HERSCHBACH [3]

$H_{12}^{**} = 1.73\,R_c^{**}\,\exp(-0.875\,R_c^{**})\;,\quad H_{12}^{**} = 2\,H_{12}/\nu\gamma\;,\quad R_c^{**} = \nu R_c$

HUBERS, KLEYN and LOS [17]

TABLE II — One electron transfer processes analysed

n	$A + B^{+n} \rightleftarrows A^{+} + B^{+(n-1)}$	References
0	$M(n,1) + H(ls) \rightleftarrows M^{+} + H^{-}$	M = H [4, 7, 10] Li [4, 8, 10] Na [4, 8, 10, 18] K [4, 8, 10, 18] Rb [4, 10] Cs [4, 10]
0	$M + X \rightleftarrows M^{+} + X^{-}$	M = Li [3, 10, 19a, 20, 21, 22] Na [3, 10, 19b, 20, 23] K [3, 10, 19c, 23, 24] Rb [3, 10, 19d, 23] Cs [3, 10, 19e, 23] X = H [3, 10, 21, 22] O [10, 23] F [3, 19a-c] Cl [3, 19a-c] Br [3, 19a-d] I [3, 19, 20, 24]
0	$M + X_2 \rightleftarrows M^{+} + (X_2)^{-}$	M = Li [3] Na [3, 17] K [3, 17, 25] Rb [3] Cs [3, 17, 25] X = Cl [3, 17] Br [3, 17] I [3, 17] O [25]
0	$M + XY \rightleftarrows M^{+} + (XY)^{-}$	M = Na [17] K [17] XY = ICl [17] IBr [17]
2	$A + B^{2+} \rightleftarrows A^{+} + B^{+}$	A = H [5, 6] He [26] Ne [13, 26] B = Li [6] Be [5] B [6] N [26] Mg [5] Al [6] Si [5] Ar [26] Kr [13]
3	$A + B^{3+} \rightleftarrows A^{+} + B^{2+}$	A = H [6] He [9, 13] Ne [13, 26, 27] B = Li [9] Be [9] Mg [9] Al [6, 9] Kr [13] Xe [27]
4	$A + B^{4+} \rightleftarrows A^{+} + B^{3+}$	A = He [13] Ne [13, 27, 28] B = Kr [13, 28] Xe [27]

work of Olson et al. Although an exponential decrease is in general observed, one notes a divergence with increasing R_c that depends mainly on the electron affinity. This divergence is not clear in the experimental data plot and therefore it is probably related to the method of calculation (Fig. 1).

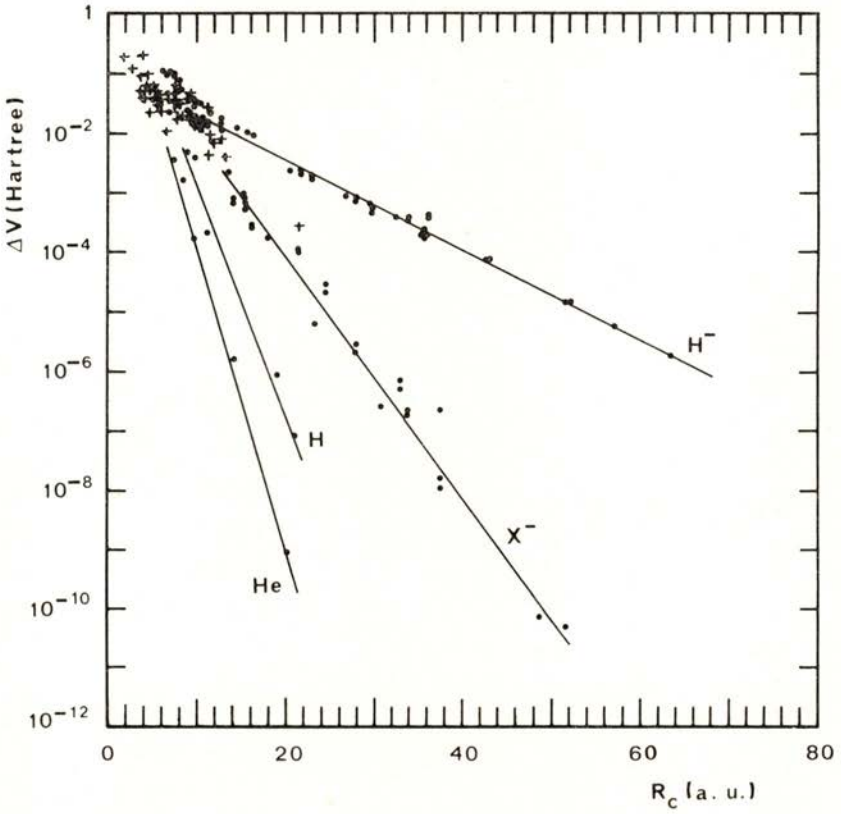

Fig. 1 — Experimental (+) and theoretical (•) splittings, ΔV, as function of the crossing distance R_c.

In order to get a simple relationship, several reduced variables (X, Y) have been tested. This was done assuming always an exponential relation

$$Y = a \exp(-b X) \qquad (4)$$

TABLE III — Correlation $\Delta V - R_c$ with reduced variables

$Y = a \exp(-bX)$ σ – standard deviation (atomic units)

Pair (X, Y)	X	Y	Set 1			Set 2			Set 3			Obs.
			a	b	σ	a	b	σ	a	b	σ	
I	νR_c	$\Delta V/\nu$	5.95	0.86	0.521	0.69	0.52	0.366	0.14	0.26	0.308	
II	νR_c	$\Delta V/\nu^2$	9.16	0.85	0.509	1.48	0.59	0.345	0.25	0.32	0.265	Simple expression
III	νR_c	$\Delta V/\nu X$	1.54	0.94	0.479	0.25	0.64	0.363	0.054	0.39	0.311	
IV	νR_c	$\Delta V/\nu^2 X$	2.37	0.93	0.463	0.54	0.71	0.341	0.093	0.45	0.271	
V	νR_c	$\Delta V/(\nu^2 R_c^{1/\nu - 1})$	2.26	0.96	0.981	0.18	0.45	0.563	0.045	0.17	0.510	Komarov type
VI	νR_c	$\Delta V/\gamma$	12.0	0.89	0.492	1.93	0.60	0.369	0.34	0.32	0.315	
VII	νR_c	$\Delta V/\gamma^2$	37.3	0.91	0.504	11.7	0.75	0.425	1.36	0.45	0.400	
VIII	νR_c	$\Delta V/\gamma X$	3.10	0.97	0.458	0.70	0.72	0.370	0.13	0.45	0.321	
IX	νR_c	$\Delta V/\nu^2 X$	9.64	0.99	0.478	4.22	0.87	0.428	0.51	0.58	0.409	
X	νR_c	$\Delta V/\nu\gamma$	18.5	0.88	0.497	4.16	0.67	0.375	0.58	0.39	0.322	
XI	νR_c	$\Delta V/\nu\gamma X$	4.77	0.96	0.460	1.50	0.79	0.375	0.22	0.52	0.330	H. K. L. revised
XII	γR_c	$\Delta V/\gamma^2$	4.18	0.89	0.433	1.71	0.67	0.336	0.59	0.45	0.316	
XIII	$\frac{\nu+\gamma}{2} R_c$	$\Delta V/\nu\gamma$	6.43	0.87	0.458	1.70	0.64	0.337	0.41	0.39	0.290	
XIV	$\frac{\nu+\gamma}{2} R_c$	$\Delta V/\nu\gamma X$	2.00	0.96	0.412	0.76	0.78	0.342	0.18	0.54	0.311	O. S. B. revised

Set 1 — Computational and experimentally derived data;
Set 2 — Partial set (see text); Set 3 — Experimental derived data.

the constants being derived by least square fits (Table III). The standard deviations, σ, were used to compare the different fits. The exponential dependence of ΔV upon R_c is suggested by the exponential tails of the orbitals.

Although the experimental points (set 3) are not numerous and are confined to splittings larger than 10^{-4} Hartree and R_c smaller than 20 a.u., they show a general exponential decrease expressed by

$$\Delta V = 0.21 \exp(-0.29\ R_c) \qquad (5)$$

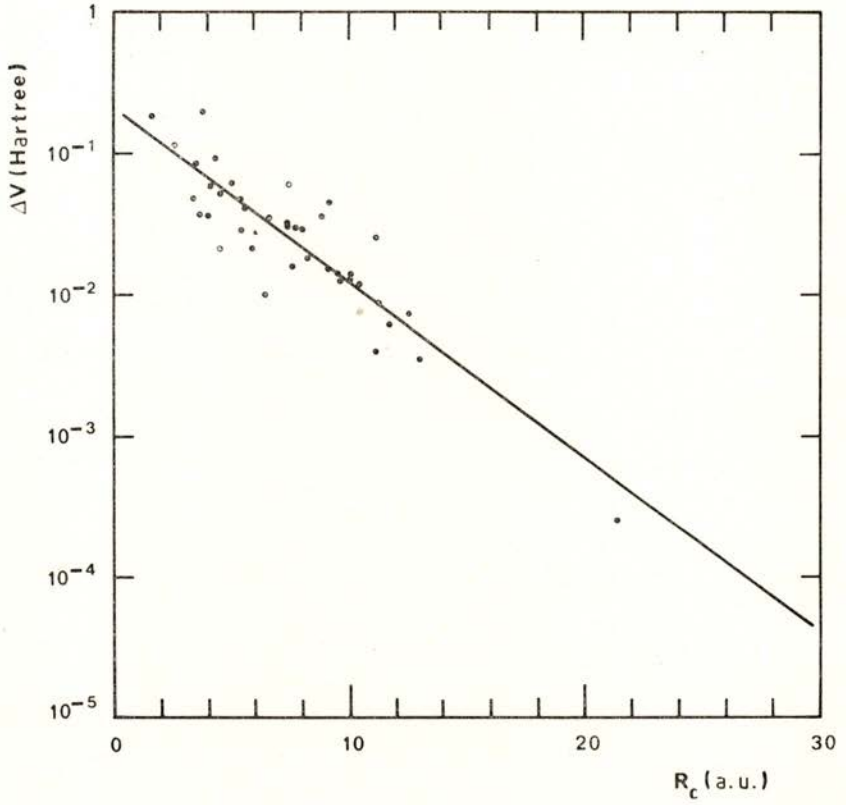

Fig. 2 — Correlation $\Delta V - R_c$ obtained with the available experimental data.

The fit (Fig. 2) has a standard deviation of 0.222. It is smaller than the other ones obtained with reduced variables for the set

of experimental derived data. Almost all the points lie within a factor of three to the average line.

Most of our effort was focused on relations with the correct asymptotic behaviour because, to our knowledge, general fits of this type have not yet been obtained. Also with that in mind a selection of theoretical data has been tried. In fact, at very large distances either the L. C. A. O. or the old variational data seem to be incorrect. Therefore, fits have been obtained with a partial set of experimental and theoretical data (set 2) which excluded those points computed by the referred methods and corresponding to crossings larger than 8 Å. This limit was arbitrarily chosen but it is reasonable since at larger distances the relative errors increase [1].

The so much used O. S. B. relation has been also revised, although it misrepresents the asymptotic behaviour as was already referred. Indeed it is interesting to include all the data, which doubled after that work. One can see that, both the total set and the partial one give clearly good fits but the exponential constant has to be somewhat changed. With the total set the expression is now

$$\frac{\Delta V}{\nu \gamma X} = 2.0 \exp(-0.96\ X) \text{ with } X = \frac{\nu + \gamma}{2} R_c \qquad (6)$$

and is represented in Fig. 3. About 90 % of the data lie within a factor of three, as in the early fit.

Fits with small deviation were obtained with ($X = \gamma R_c$, $Y = \Delta V / \nu^2 X$) or ($X = \gamma R_c$, $Y = \Delta V / \nu \gamma$) but they have the drawback of a wrong asymptotic behaviour.

The H. K. L. relation [17] has been derived only for the systems $M + X_2$ and $M + XY$ (13 points) and gives an excellent fit. Moreover it has the advantage of having the correct behaviour at large R_c. However, when tested with the complete and partial sets of data, the constants have to be changed and the deviations become larger.

For the selected set of data. the other fits with $X = \nu R_c$ show deviations almost of the same order (except for the Komarov type expression) being slightly smaller for the reduced variables $Y_{IV} = \Delta V / \nu^2 X$ and $Y_{II} = \Delta V / \nu^2$. These pairs of reduced

variables have also the advantage of avoiding the use of electron affinity which is of particular importance for molecular systems with near zero or negative electron affinity. The second pair has

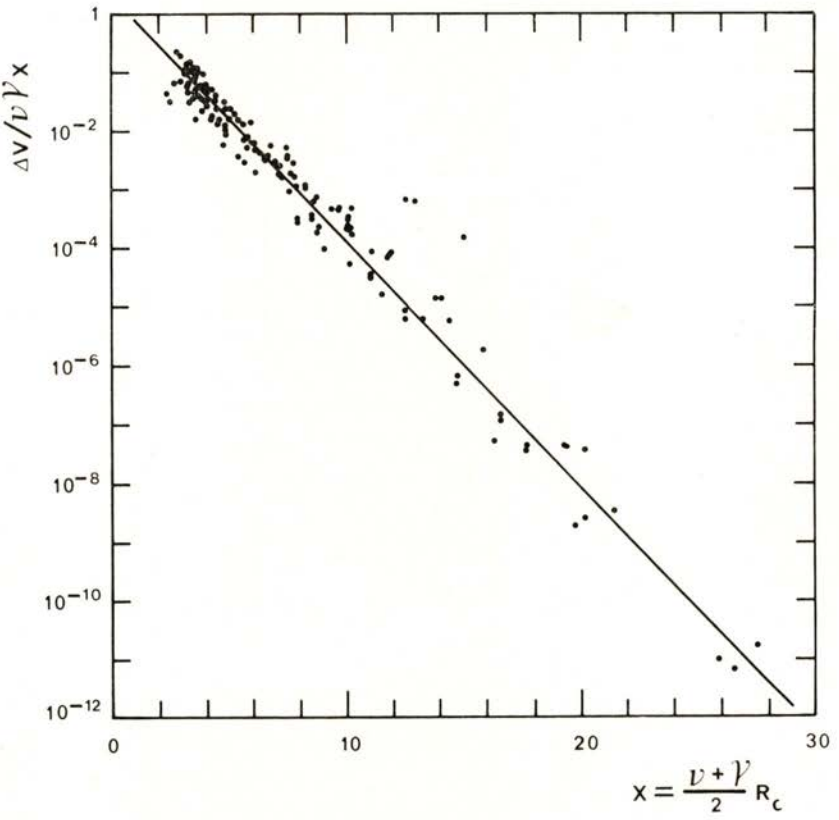

Fig. 3 — Fit with Olson, Smith and Bauer (O. S. B.) reduced variables, using the total set of data.

the advantage of being quite simple and also has a small deviation when tested with the experimental set. With the partial set of data it corresponds to the relation

$$\Delta V = 1.48\ \nu^2\ \exp\ (-0.59\ \nu\ R_c) \qquad (7)$$

The simple relation (7) is shown in Fig. 4 together with the selected set of data. One notes that it is a reasonable one and, like the O. S. B. expression, most of the data are within a factor of three.

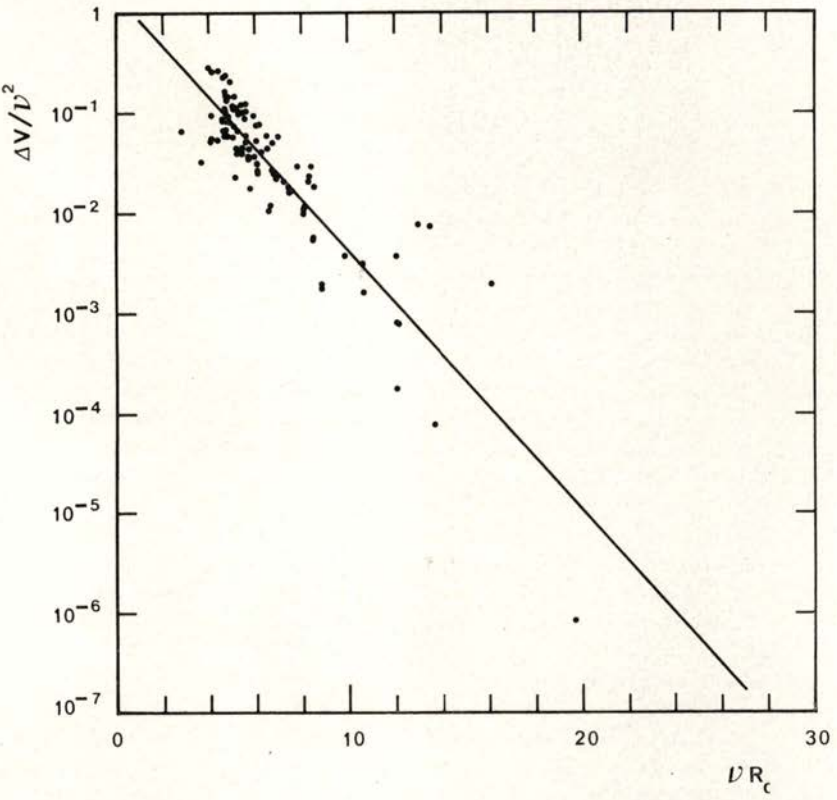

Fig. 4 — Plot with the reduced variables (νR_c , $\Delta V/\nu^2$) for the selected set of data.

3 — CONCLUDING REMARKS

Exponential relations involving reduced variables are particularly suitable to represent the correlations $\Delta V - R_c$. The experimental derived data show a general exponential decay which is acceptable within errors. From several variables tested, one

concludes that, within the errors, they do not differ so much. From those with the correct asymptotic behaviour the set $(\nu R_c, \Delta V / \nu^2)$ is favoured because it is the simplest.

The autor thanks Prof. M. F. Laranjeira, as well as Dr. M. J. P. Maneira and Eng.º A. J. F. Praxedes for their interest in this work.

REFERENCES

[1] R. K. JANEV, *Adv. At. Mol. Phys.* **12** (1976), 1.
[2] D. R. BATES, H. C. JOHNSTON and I. STEWART, *Proc. Phys. Soc.* (London), **84** (1964), 517.
[3] R. GRICE and D. R. HERSCHBACH, *Mol. Phys*, **27** (1974), 159.
[4] S. A. ADELMAN and D. R. HERSCHBACH, *Mol. Phys.* **33** (1977), 793.
[5] D. R. BATES and B. L. MOISEIWITSCH, *Proc. Phys. Soc.* (London), **A67** (1954), 805.
[6] A. DALGARNO, *Proc. Phys. Soc.* (London), **A67** (1954), 1010.
[7] D. R. BATES and J. T. LEWIS, *Proc. Phys. Soc.* (London), **A68** (1955), 173.
[8] D. R. BATES and T. J. M. BOYD, *Proc. Phys. Soc.* (London), **A69** (1956), 910.
[9] T. J. M. BOYD and B. L. MOISEIWITSCH, *Proc. Phys. Soc.* (London), **A70** (1957), 809.
[10] R. K. JANEV, *J. C. P.*, **64** (1976), 1981.
[11] I. V. KOMAROV, Abstr. papers VI ICPEAC, Cambridge U.S.A. (1969), 1015.
[12] B. M. SMIRNOV, *Sov. Phys. Dokl.*, **10** (1965), 218; **12** (1967), 242.
[13] J. B. HASTED and A. Y. J. CHONG, *Proc. Phys. Soc.* (London), **80** (1962), 441.
[14] D. RAPP and W. E. FRANCIS, *J. C. P.*, **37** (1962), 2631.
[15] R. E. OLSON, J. R. PETERSON and J. MOSELEY, *J. C. P.*, **53** (1970), 3391.
[16] R. E. OLSON, F. T. SMITH and E. BAEUR, *Appl. Optics*, **10** (1971), 1848.
[17] M. M. HUBERS, A. W. KLEYN and J. LOS, *Chem. Phys.*, **17** (1976), 303.
[18] R. W. NUMRICH and D. G. TRUHLAR, *J. Phys. Chem*, **79** (1975), 2745.
[19] J. J. EWING, R. MILSTEIN and R. S. BERRY, *J. C. P.*, **54** (1971), 1752.
[20] A. M. C. MOUTINHO, J. A. ATEN and J. LOS, *Physica*, **53** (1971), 471.
[21] R. BROWN and H. SHULL, *Int. J. Quant. Chem*, **2** (1968), 263.
[22] K. DOCKEN and J. HINZE, *J. C. P.*, **57** (1972), 4928.
[23] J. VAN DEN BOS, *J. C. P.*, **52** (1970), 3254.
[24] M. A. D. FLUENDY, D. S. HORNE, K. P. LAWLEY and A. W. MORRIS, *Mol. Phys.* **19** (1970), 659.
[25] A. W. KLEYN, M. M. HUBERS and J. LOS, *Chem. Phys.*, **34** (1978), 55.
[26] J. B. HASTED and R. A. SMITH, *Proc. Roy Soc.* (London), **A235** (1956), 354.
[27] G. N. OGURTSOV and I. P. FLAKS, *Sov. Phys. J.E.T.P.*, **15** (1962), 502.
[28] J. B. HASTED and M. HUSSAIN, *Proc. Phys. Soc.* (London), **83** (1964), 911.

TRANSPORT PROPERTIES OF n-TYPE FERROMAGNETIC SEMICONDUCTOR $HgCr_2Se_4$ (*)

J. L. RIBEIRO (1), M. RENATA CHAVES (2), J. M. MOREIRA (2), J. BESSA E SOUSA (2), A. SELMI (3) and P. GIBART (3)

(Received 8 November 1984)

ABSTRACT — Temperature dependence of the electrical resistivity (ρ), its temperature derivative and Seebeck effect were used to study the ferromagnetic transition in a $HgCr_2Se_4$ sample with n-type impurity. The Hall voltage has been separated in the so-called normal and extraordinary Hall contributions.

1 — INTRODUCTION

The chalcogenide spinel $HgCr_2Se_4$ is a ferromagnetic semiconductor in which the Cr^{3+} ions occupy the octahedral sites and the Hg^{2+} ions occupy the tetrahedral sites [1-4]. It undergoes a ferro-paramagnetic transition at about 110 K [1, 3]. The magnetic properties arise from the interaction of localised Cr^{3+} electrons with free electrons [1]. A competition between the opposing ferromagnetic super-exchange Cr-Se-Cr and antiferromagnetic super-exchange Cr-Se-Hg-Se-Cr also plays an important role in the magnetic properties of $HgCr_2Se_4$ [5]. One of the most striking features of ferromagnetic chalcogenide spinels is that their absorption edge shows anomalously large shifts as the

(*) This work was partially supported by Junta Nacional de Investigação Científica e Tecnológica under research contract n.° 160.79.27, by Instituto Nacional de Investigação Científica and Gesellschaft für Technische Zusammenarbeit (German Federal Republic).

(1) Departamento de Física, Universidade do Minho, 4700 Braga, Portugal.

(2) Laboratório de Física, Universidade do Porto, 4000 Porto, Portugal.

(3) Laboratoire de Magnétisme, CNRS, 1 Place Aristide Briand 92190 Meudon Bellevue, France.

temperature falls very low [6-8]; for example $HgCr_2Se_4$ absorption edge is 0.80 eV at room temperature and shifts to 0.27 eV at liquid helium temperature [7]. The temperature dependence of the absorption edge is non-linear, being remarkably high around the critical temperature (T_c) and nearly constant in the temperature range 180-300 K [7]. $HgCr_2Se_4$ exhibits anomalous electrical properties strongly dependent on the heat treatment of the sample [1]. $HgCr_2Se_4$ can be obtained by vapour transport reaction using Al + Cl as transport agent. $HgCr_2Se_4$ annealed in Hg is a n-type semiconductor in the whole temperature range studied [1]. In the following we present an experimental study of transport properties (electrical resistivity, Hall effect and Seebeck effect) as a function of the temperature in a n-type $HgCr_2Se_4$ sample with a very high concentration of free electrons. This study aims at correlating the electronic properties of $HgCr_2Se_4$ with the anomalous temperature dependence of its gap width in order to obtain a better insight into the magnetic properties of that system.

2 – EXPERIMENTAL

The n-type $HgCr_2Se_4$ sample we have studied was annealed in Hg. Its dimensions are $2.5 \times 2 \times 1.2$ mm and its resistivity is 202 mΩcm at 273 K.

Very accurate measurements of electrical resistivity were obtained with a 4 wire potentiometer method using a d. c. current with stability better than $5/10^6$ [9]. The voltage resolution in the detector was $\pm 10^{-2}$ μV. The Hall effect was measured with a lock' in a. c. technique [10]. The Seebeck coefficient was measured by the hot-point method using a copper-constantan thermocouple with a measuring junction of 0.1 mm in diameter [11]. The voltage resolution in the detectors is $\pm 10^{-2}$ μV.

3 – DATA ANALYSIS

As shown in figure 1(a) the electrical resistivity (ρ)of the n-type $HgCr_2Se_4$ crystal has an unusual temperature dependence, increasing as the temperature rises. The temperature derivative ($d\rho / dT$) of the resistivity is obtained by a sliding average rule [12]. This derivative reaches a maximum value at about 124 K

and as usual we take this temperature as the critical temperature (T_c) – figure 1(b). A minimum in $d\rho / dT$ occurs at around 180 K,

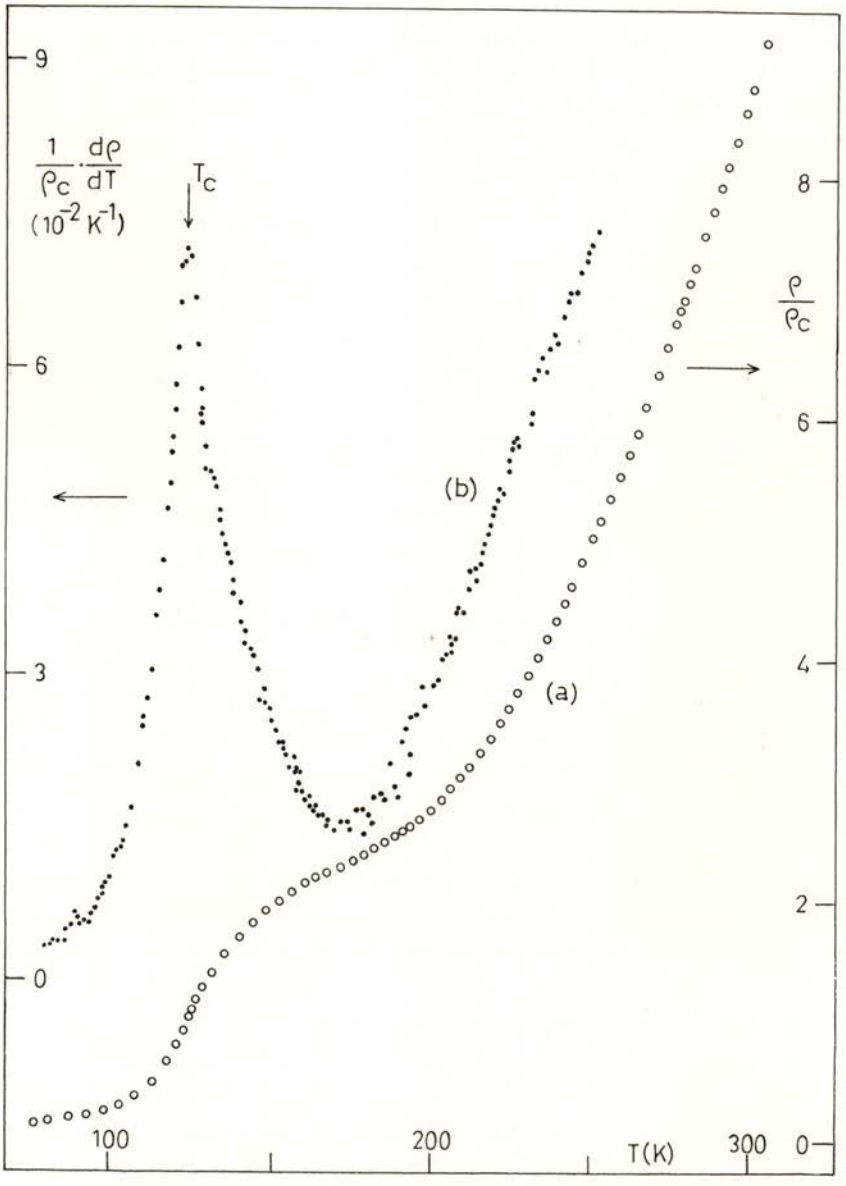

Fig. 1 — Temperature dependence of reduced resistivity (a) and thermal derivative of resistivity (b) of $HgCr_2Se_4$.

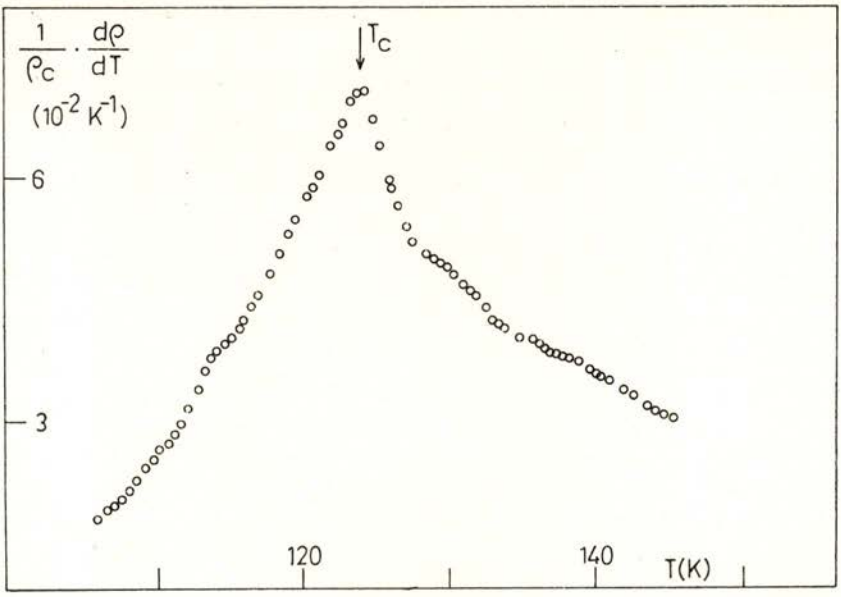

Fig. 2 — Temperature dependence of thermal derivative of resistivity near the critical temperature, $T_c = 124$ K, in an enlarged scale.

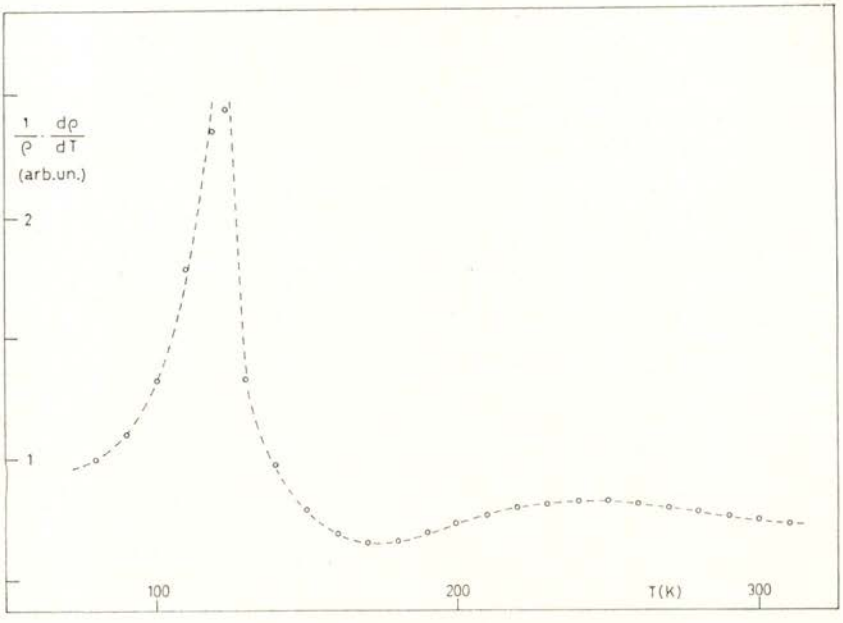

Fig. 3 — Temperature dependence of thermal derivative of log of resistivity ( ) of $HgCr_2Se_4$.

followed by a pronounced increase in $d\rho / dT$. The temperature derivative of ρ displays a striking asymmetric behaviour around T_c (figure 2). These results are quite similar to those previously reported although this asymmetric behaviour was not explicitly referred [13].

According to a model of spin-polarized bands, the exchange interaction between localized and band electrons results in a spin splitting of the conduction and valence bands [14]. In a first approximation the corresponding energy changes for each band are given by:

$$\Delta E_b^{\pm 1} = \mp \frac{1}{2} S J_b \frac{M(T)}{M(0)}$$

where S is the localized spin, J_b the exchange parameter for the b-labelled band, $M(T)$ the magnetization at the temperature T and ± 1 refers to the spin up or down. Let us suppose that changes in free carrier mobility are relatively small and so the anomalous variation in the electrical resistivity at the critical region is mainly due to concentration variation. Using this assumption and assuming the existence of a donor level of activation energy $E_d(T)$ we have

$$\rho(T) = \rho_0 \exp(-E_d / k_B T)$$

It seems plausible to assume that the activation energy of impurity levels varies with the temperature, accompanying the variation of the gap width. For simplicity sake let us suppose that $E_d(T) = E_0 - E_1 M(T)$, E_0 and E_1 constants. The temperature derivative of $\log \rho$ becomes

$$\frac{1}{\rho} \frac{d\rho}{dT} = \frac{1}{k_B T^2} (E_0 - E_1 M) + \frac{E_1}{k_B T} \frac{dM}{dT}$$

Near the critical temperature $M(T) \simeq 0$ and then we have approximately

$$(1/\rho)\, d\rho/dT \propto dM/dT$$

An anomalous behaviour of $(d\rho/dT) \cdot (1/\rho)$ similar to $|dM/dT|$ is predictable in the critical region and so the asymmetric behaviour in $d\rho/dT$ must be closely related to the asymmetric behaviour in dM/dT. In figure 3 we have a plot of $(d\rho(T)/dT)\,(1/\rho(T))$ versus T.

As the gap width (E_g) variation follows the magnetization variation, related to $E_d(T)$, it is natural to expect that ρ (T) is associated with E_g. In fact log ρ has a roughly linear dependence on E_g from 90 to 200 K, as can be seen in figure 4.

A fitting of the experimental values in the ferromagnetic region to the expression $(d\rho / dT) = A - B \log |\varepsilon|$ where A

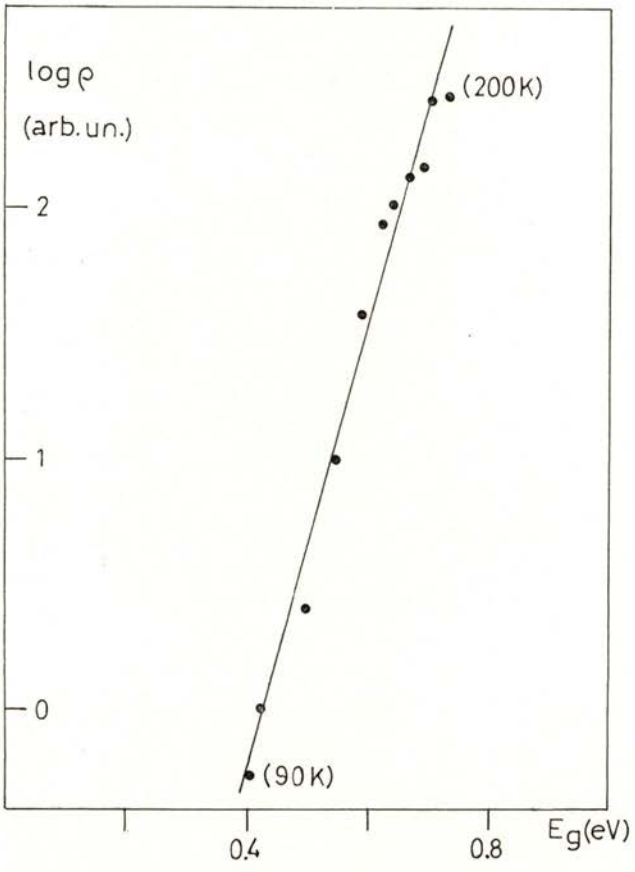

Fig. 4 — A plot of log ρ versus the gap width (E_g).

and B are constants and $\varepsilon = (T - T_c) / T_c$, defines $T_c = 123.7$ K, but it was not possible to fit the experimental data in the paramagnetic region near T_c, to such an expression. The log ρ as a function of the reciprocal of the temperature (figure 5) exhibits a complicated behaviour. In the high temperature region ($T \gtrsim 200$ K),

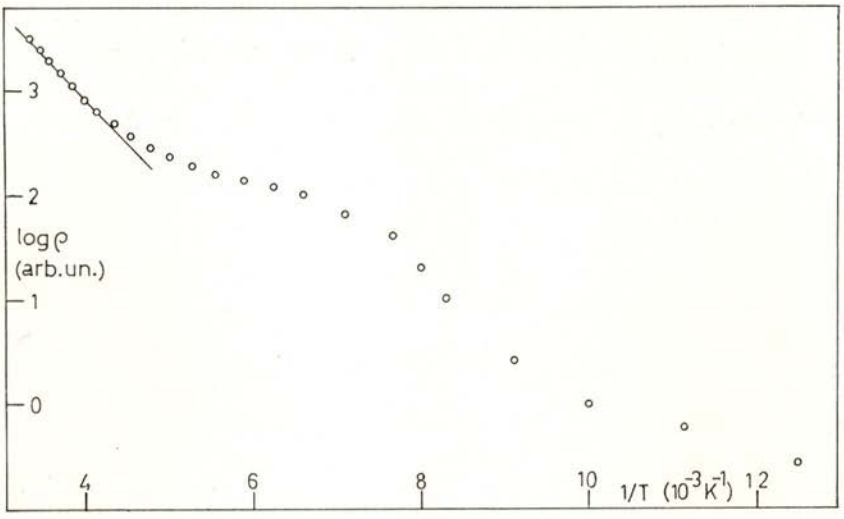

Fig. 5 — A plot of log ρ versus the reciprocal of the temperature.

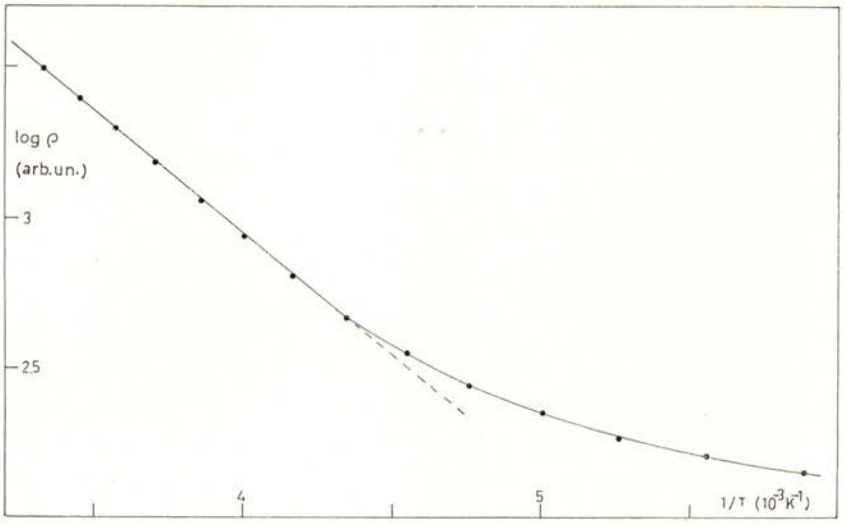

Fig. 6 — A plot of log ρ versus the reciprocal of the temperature in the range 170-300 K.

from the slope of the straight line we deduce a value of 0.071 eV for the activation energy of impurity levels in the 200-300 K temperature range (figure 6).

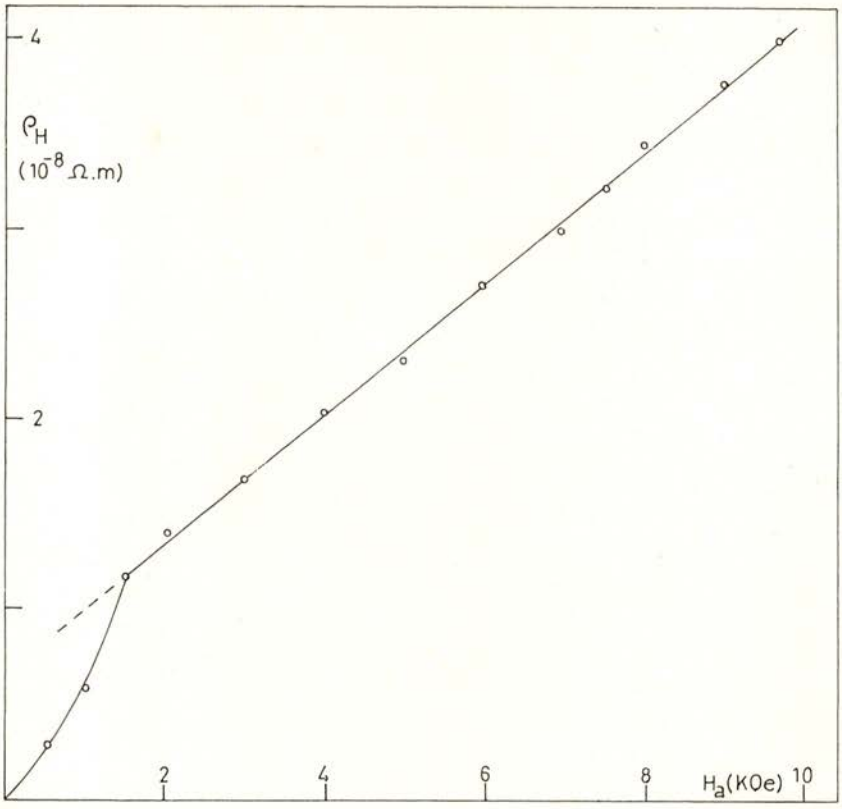

Fig. 7 — A plot of the Hall resistivity (ρ_H) versus the applied magnetic field for $HgCr_2Se_4$ at 77 K.

We consider now the Hall voltage measurements performed in the same $HgCr_2Se_4$ sample. As is well known, in an applied magnetic field (H_a) and for a magnetic single carrier semiconductor the Hall voltage is given by $V_H = (R_0 B + R_s \mu_0 M) I/d$, where R_0 is the ordinary Hall coefficient $R_0 = (ne)^{-1}$, n being the effective density of conduction electrons, B the magnetic field inside the sample, R_s the extraordinary Hall coefficient, M the magnetization, I the intensity of the electric current, d the thickness of the sample and μ_0 the magnetic permeability of vacuum [15]. In figure 7 we have a plot of the Hall resistivity

($\rho_H = V_H\ d/I$) as a function of the applied magnetic field when the sample is at 77 K. The onset of the saturation of the extraordinary Hall effect occurs for $B_d = 0.15$ Tesla. This is the typical behaviour for the magnetic field dependence of the Hall voltage in the spinel system. An order of magnitude of the free electron concentration (n) at 77 K can be calculated from the slope of the straight line of figure 6; its value is approximately 1.9×10^{19} cm^{-3} (the corresponding mobility for free electrons is 31 $cm^2\ V^{-1}\ s^{-1}$). That value agrees with 3×10^{19} cm^{-3} predicted for $T_c \simeq 124$ K from the law $T_c \propto n^{1/3}$ [4].

We have plotted the Hall resistivity (ρ_H) as a function of the temperature in figure 8, for an applied field of 0.97 Tesla.

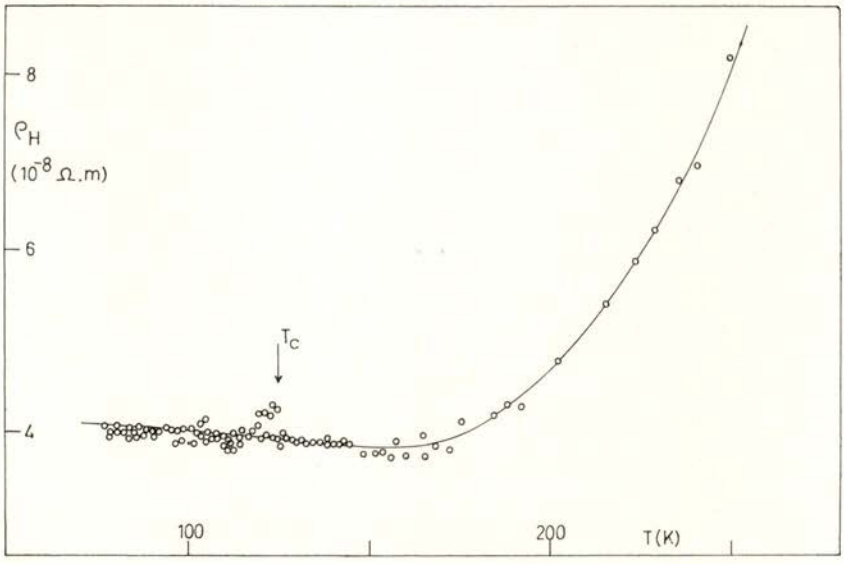

Fig. 8 — Temperature dependence of Hall resistivity (ρ_H) for $HgCr_2Se_4$ under an applied magnetic field of 0.97 Tesla.

ρ_H is approximately constant between 77 and 180 K and there is no significant anomaly around T_c, although appreciable 'noise' exists near this temperature. These instabilities can not be associated with experimental errors. A plot of ρ_H versus ρ

(figure 9) shows that above 160 K the Hall resistivity is proportional to ρ. This is due to the fact that in the higher temperature region the total Hall voltage is essentially equal to the ordinary voltage ($M(T) \simeq 0$) and according to the previous assumption, the mobility variation with the temperature is not relevant (at least for $T > 160$ K). For $T = 250$ K we obtain, $n = 8 \times 10^{17}$ cm^{-3} and $\mu = 28$ cm^{-2} V^{-1} s^{-1}, using the experimental values of R_0 and ρ, and the formulae $R_0 = 1/ne$, $\rho = R_0/\mu$.

Assuming, as before, that in all the temperature range studied mobility variation is much smaller than the variation of free

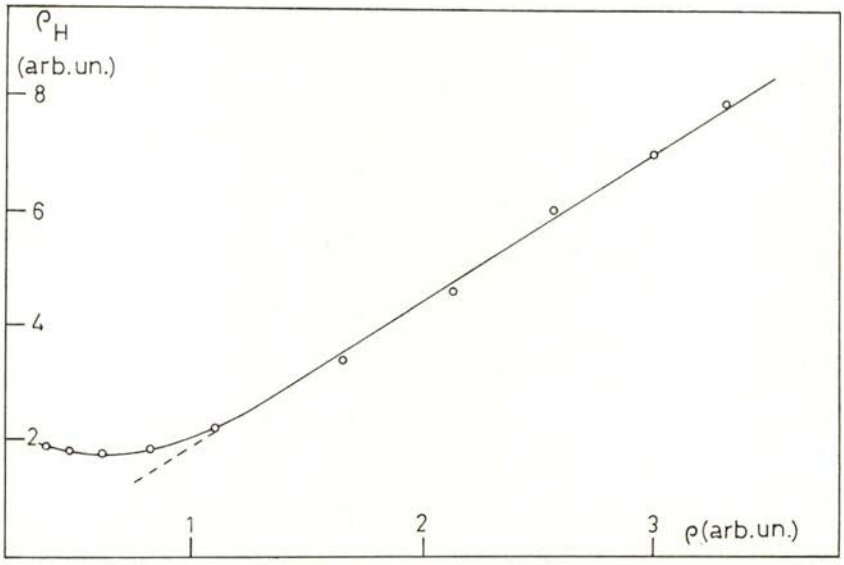

Fig. 9 — A plot of Hall resistivity (ρ_H) versus resistivity (ρ) for $HgCr_2Se_4$.

electron concentration [16], we have made a rough calculation to separate the extraordinary from the ordinary Hall resistivities. We have taken the ordinary Hall resistivity as proportional to the electrical resistivity; extraordinary Hall resistivity was derived by subtraction. The extraordinary Hall voltage as a function of

the temperature is shown in figure 10(a). An occasional cancellation of the ordinary and extraordinary Hall effects overshadows an anomalous behaviour of the sample around T_c. We have also used the law of variation of electron concentration with the

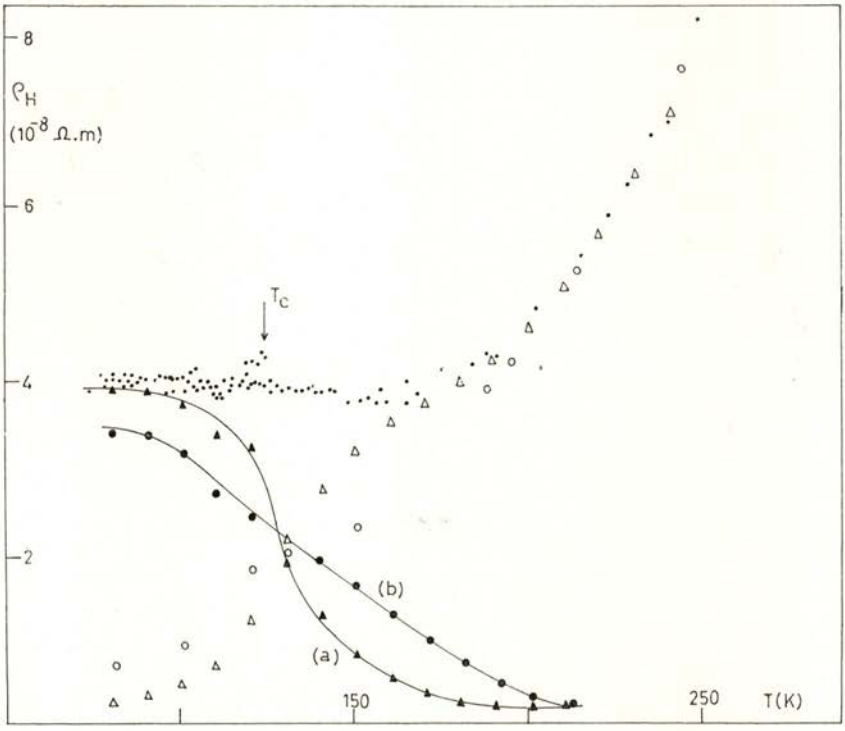

Fig. 10 — Temperature dependence of Hall resistivity (·); ordinary (Δ) and extraordinary (▲, curve a) Hall resistivities calculated from electrical resistivity and total Hall resistivity data; ordinary (o) and extraordinary (•, curve b) Hall resistivities from optical measurements.

temperature, determined by optical measurements in a n-type $HgCr_2Se_4$ [16], to separate the extraordinary and normal Hall resistivities. By using that law we derived the extraordinary Hall resistivity seen in figure 10(b). The results obtained are similar to

each other and clearly point to the existence of an appreciable magnetization in a large temperature range above T_c.

Fig. 11 displays the Seebeck coefficient (S) as a function of temperature for $HgCr_2Se_4$. It is negative in the whole temperature range studied, as expected, and $|S|$ increases as the temperature increases. $|S|$ is rather low and an order of magnitude smaller that the value reported for $CdCr_2Se_4$ [17]. The room temperature value we found agrees quite well with corre-

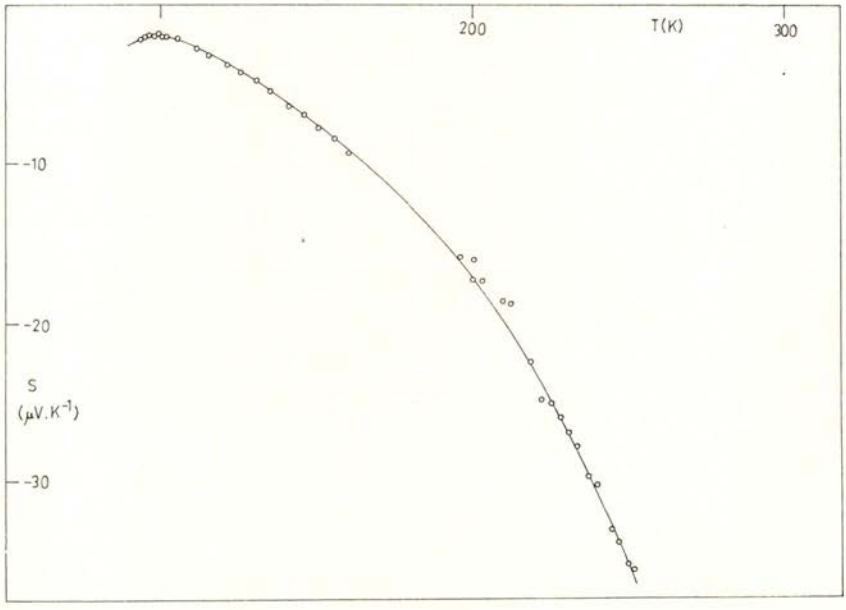

Fig. 11 — Seebeck effect (S) as a function of the temperature.

sponding values previously reported for $HgCr_2Se_4$ [2]. As we shall see, the values obtained for S can be well understood by assuming that, above 200 K, $HgCr_2Se_4$ is a semiconductor and below this temperature it behaves like a metallic system.

For a metallic system $S(T) = -(3/2 + q)\,\pi^2 k_B^2 T/(3\eta|e|)$, where η is the Fermi level and q is associated with the relaxation time [18]. As $\eta = (\hbar^2/2m)\,(3\pi^2 n)^{2/3}$ we have $\log n(T) = -3/2$

log $|S(T)|$ + const, by neglecting q. In figure 12 a plot of the experimental values of log ρ versus log $|S|$ gives a straight line, below 150 K, with a slope 1.6, approaching the theoretical value 1.5 (predicted in the above model) fairly well. Accordingly, for T = 150 K we have $\eta \simeq 0.5$ eV. Above 180 K, log ρ varies

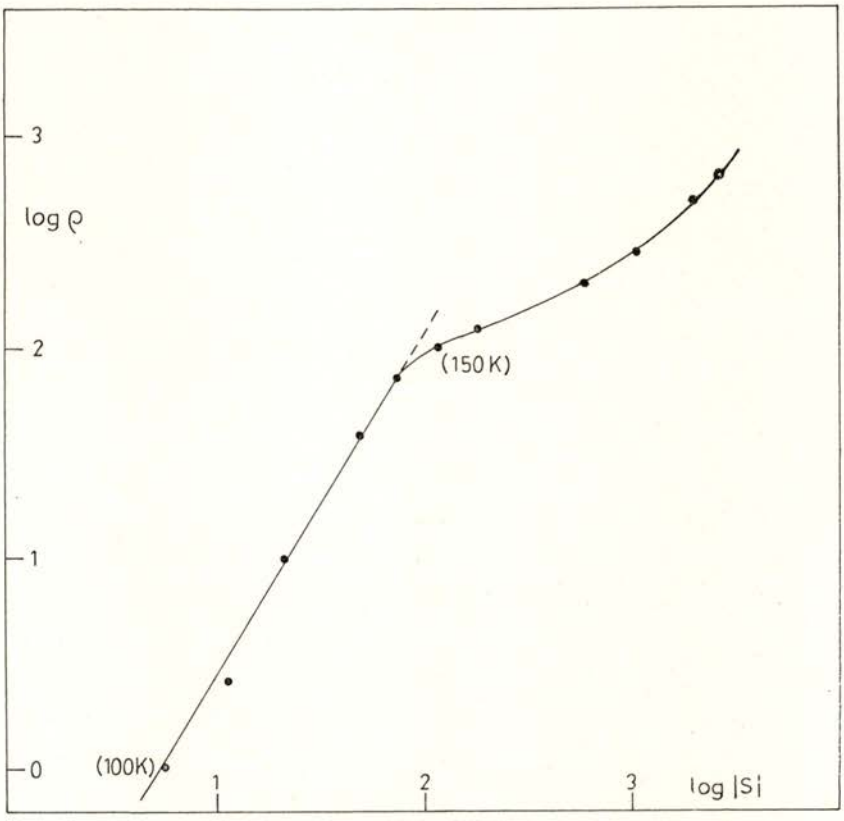

Fig. 12 — A plot of log ρ versus log $|S|$.

linearly with $|S|$ as we can see in figure 13. This is the result obtained from a simple model used in the study of a non-degenerate single carrier semiconductor with parabolic bands. In this case the Seebeck coefficient is given by [19]:

$$S(T) = -(k_B/|e|)\,|(5/2 + q) + \eta/(k_B T)| \qquad (1)$$

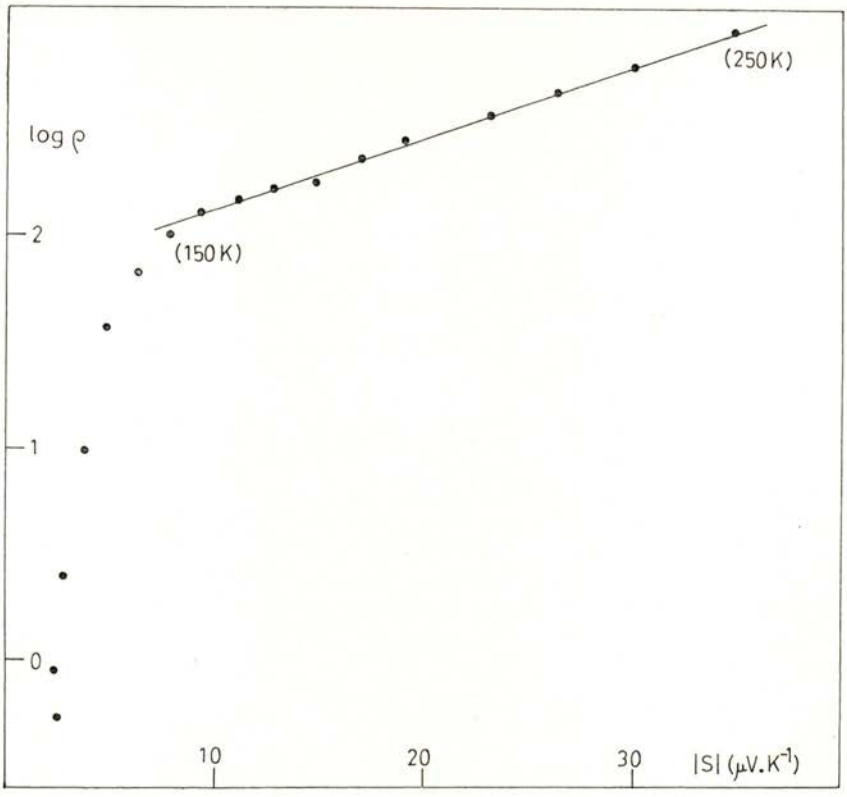

Fig. 13 — A plot of log ρ versus the Seebeck coefficient ($|S|$).

where $q = -1/2$ for acoustic mode scattering, while $q = 3/2$ for scattering by impurities. If $g(E)$ represents the state density for electrons and $f(E)$ the Fermi distribution

$$n(T) = \int_0^\infty g(E)\, f(E)\, dE = 4\pi\,(2m/\hbar^2)^{3}\sqrt{\pi/2}\,\exp(-\eta/k_B T) \tag{2}$$

Replacing (2) into (1) we have:

$$S(T) = -(k_B/|e|)\cdot|(5/2+q) - \log n(T) + \text{const}|$$

Using the assumption $\rho(T) \propto n(T)^{-1}$, we obtain

$$S(T) \simeq C \log \rho(T) + \text{const},$$

where C is constant.

It is quite interesting to remark that the variation of the Fermi level, which is associated with the Seebeck coefficient as we have just seen, follows the variation of the gap width (figure 14).

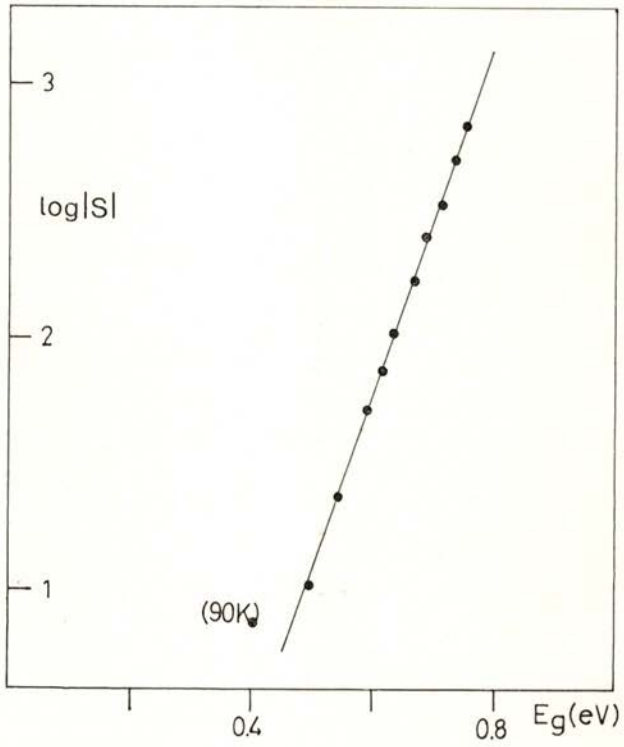

Fig. 14 — A plot of log | S | versus the gap width (E_g).

Log | S | versus E_g is a straight line between 90 and 200 K. The results concerning the Seebeck coefficient confirm the major importance of the electron concentration on the electrical properties of the n-type semiconductor $HgCr_2Se_4$. The small values of | S | may be explained by assuming that the Fermi level is very close to the bottom of the conduction band.

The technical assistance of José Magalhães is gratefully acknowledged.

REFERENCES

[1] L. GOLDSTEIN, P. GIBART, A. SELMI, *J. Appl. Phys.*, **49**, 1474 (1978).

[2] K. MINEMATSU, K. MIYATANI and T. TAKAHASHI, *J. of Phys. Soc. of Japan*, **31**, 123 (1971).

[3] A. SELMI, R. LE TOULEC, R. FAYMONVILLE, *Phys. Stat. Sol.* (b), **114**, K97 (1982).

[4] A. SELMI, P. GIBART, L. GOLDSTEIN, *J. of Magnetism and Magnetic Materials*, **15-18**, 1285 (1980).

[5] P. K. BALTZER, P. J. WOJTOWICZ, M. ROBBINS and E. LOPATAN, *Phys. Rev.*, **151**, 367 (1966).

[6] I. BALBERG, A. MAMAN and H. HÉRITIER, *Physica*, **117-118 B**, 482 (1983).

[7] T. ARAI, M. WAKAKI, S. GNARI, K. KUDO, T. SATOH and T. TSUSHIMA, *J. of the Phys. Soc. Japan*, **34**, 68 (1973).

[8] M. WAKAKI, K. YAMAMOTO, S. GNARI and T. ARAI, *Sol. Stat. Commun.*, **43**, 957 (1982).

[9] M. P. KAWATRA, J. A. MYDOSH and J. I. BUDNICK, *Phys. Rev.* B, **2**, 665 (1970).

[10] J. B. SOUSA, J. M. MOREIRA, *Port. Phys.*, **13**, 137 (1982).

[11] L. MARTON - editor in chief, *Methods of Experimental Physics*, vol. **6B**, Academic Press, 1959.

[12] F. C. ZUMSTEG and R. D. PARKS, *Phys. Rev. Letters*, **24**, 520 (1970).

[13] A. SELMI, *Propriétés galvanomagnétiques du semiconducteur* $HgCr_2Se_4$, Thèse 3ème cycle, Paris 1979.

[14] M. ILIEV, *J. de Physique*, Colloque C5 Supplément au n.° 6, **41**, C5-23, 1980.

[15] A. HERPIN, *Theorie du Magnétisme*, Presses Universitaires de France, Paris, 1968.

[16] A. A. SAMOKHALOV, B. A. GIZHEVSKII, N. N. LOSHKAREVA, T. I. ARBUZOVA, M. I. SIMONOVA and N. M. CHEBOTAEV, *Sov. Phys. Sol. State*, **23**, 2016 (1981).

[17] A. AMITH, L. FRIEDMAN, *Phys. Rev.* B, **2**, 434 (1970).

[18] R. D. BARNARD, *Thermoelectricity in metals and alloys*, Taylor & Francis Ltd., London, 1972.

[19] F. J. BLATT, *Physics of Electronic Conduction*, McGraw-Hill Book Company, London, 1968.

POLARIZATION REVERSAL OF SbSI (*)

A. GONÇALVES DA SILVA

Faculdade de Engenharia, Universidade do Porto, 4000 Porto, Portugal

M. RENATA CHAVES, A. ALMEIDA, M. HELENA AMARAL

Laboratório de Física, Universidade do Porto, 4000 Porto, Portugal

S. ZIOLKIEWICZ

Laboratoire d'Ultrasons (1), Université Pierre et Marie Curie, Tour 13, Place Jussieu 75230 Paris Cedex 05, France

(Received 8 November 1984)

ABSTRACT — The ferro-paraelectric phase transition of SbSI has been studied by using very accurate measurements of spontaneous polarization and dielectric constant as a function of the temperature. There is strong evidence of a large discrepancy between the Curie temperature as determined from data above or below T_c.

1 – INTRODUCTION

The Landau theory for a second order phase transition is valid when the fluctuations of the order parameter are not too strong, i.e. for temperatures not too close to the critical temperature T_c, which coincides with the Curie temperature T_0. Ginzburg [1] has given a criterion which allows an estimate of the

---

(*) This work was partially supported by Junta Nacional de Investigação Científica e Tecnológica under research contract n.° 106.79.27; by Instituto Nacional de Investigação Científica; by NATO research grant 1824 and by Gesellschaft für Technische Zusammenarbeit (German Federal Republic).

(1) Associated with the Centre National de la Recherche Scientifique, France.

temperature range (around T_0) where this theory is not valid. When electric dipolar interactions are responsible for a phase transition, this should obey Landau theory except in a narrow "critical region" close to T_c, typically of the order of $\varepsilon = 10^{-4}$ to 10^{-5} where $\varepsilon = |T - T_0| / T_0$. For a first order transition the change of phase occurs at a temperature T_c which is different from T_0 The critical temperature T_c is higher than the temperature T_0 (stability limit of the paraelectric phase) and lower than the stability limit of the ferroelectric phase, T_0^- [2].

In a previous paper [3] we used the critical exponent associated with the spontaneous polarization of SbSI to test Landau theory in that compound. Here we have fitted experimental data on SbSI to the correct expressions of spontaneous polarization obtained from Landau theory. Experimental spontaneous polarization is obtained through pyroelectric effect and D-E hysteresis loops studies. Dielectric constant measurements as a function of the temperature were carried out in order to obtain the values of all parameters of Gibbs free energy in Landau theory.

2 – EXPERIMENTAL PROCEDURE

The pyroelectric coeficient (λ) is determined by measuring the d. c. discharge current (i) from a sample of known electrode area (s) subjected to a controlled rate of change of temperature (dT/dt). The pyroelectric coefficient is given by $\lambda = (i/s)(dT/dt)^{-1}$. The potential difference across a short circuiting resistor arising from the discharge current was measured with a P. A. R. model 134 electrometer [3]. The spontaneous polarization as a function of the temperature was also derived from 50 cps hysteresis loops obtained with a modifiel Sawyer-Tower circuit [4]. Dielectric loss (ε'') and dielectric constant (ε') were measured with a model 745 LEADER LRC meter. SbSI was polarized with a d. c. electric field while being cooled down through the transition temperature. The temperature was measured with a copper-constantan thermocouple with a precision better than 0.02 K. Samples were cut from thin rectangular prisms 10-20 mm long and about 0.4 mm^2 cross section. SbSI crystals were grown by vapour

transport reaction, the polar axis being along the long edge. Silver paste contacts were used as electrodes.

3 – EXPERIMENTAL RESULTS AND DISCUSSION

Experimental results of pyroelectric effect measured at an uniform heating rate of 4 mK s^{-1} in one sample of SbSI, here refered as sample (a), are shown in figure 1. As the temperature rises the current passes through a sharp maximum at $T_m = 288.9$ K and then gradually approaches zero. The temperature dependence of spontaneous polarization deduced from figure 1 can be seen in

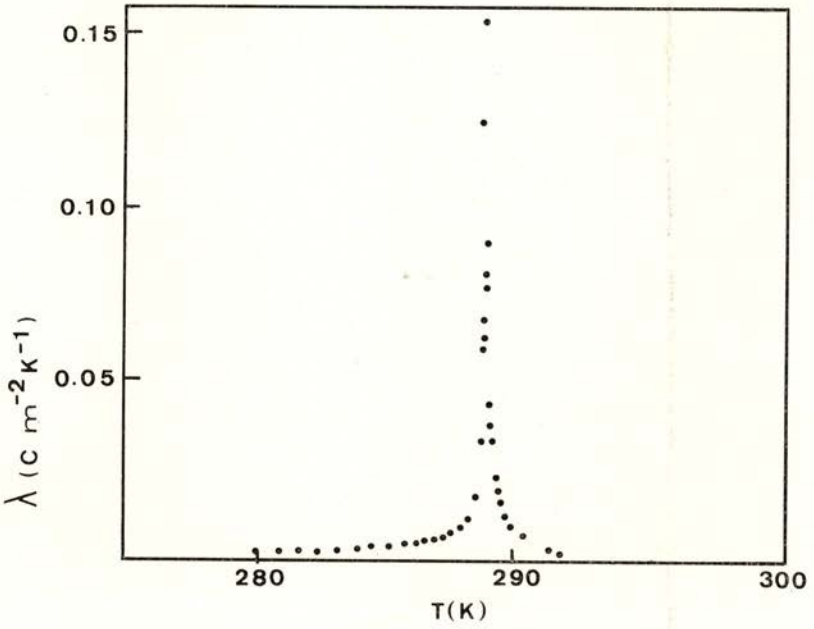

Fig. 1 — Temperature dependence of pyroelectric coefficient λ for SbSI (sample (a)).

figure 2. In figures 3 and 4 we can see pyroelectric coefficient and spontaneous polarization as a function of the temperature for another sample of SbSI, sample (b). For this sample the pyro-

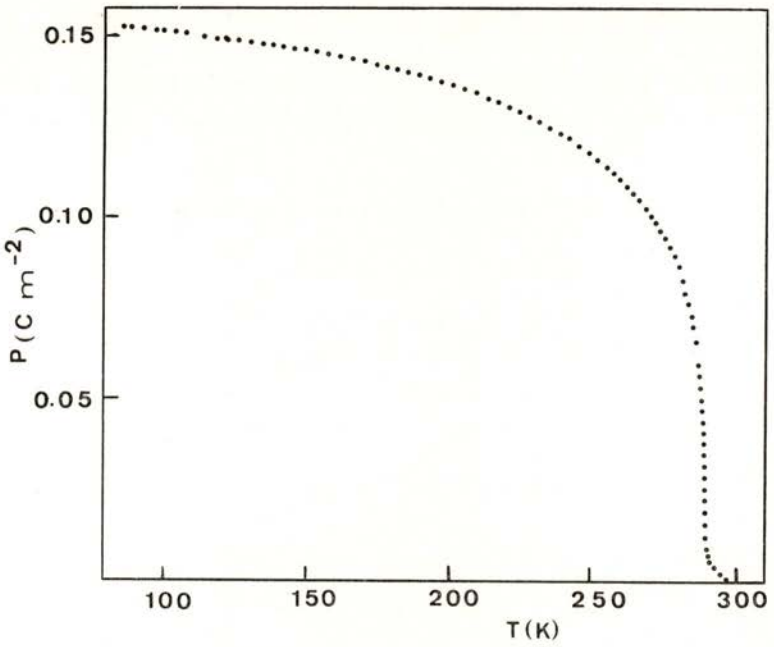

Fig. 2 — Temperature dependence of spontaneous polarization P_s for SbSI (sample (a)) obtained from pyroelectric coefficient data of figure 1.

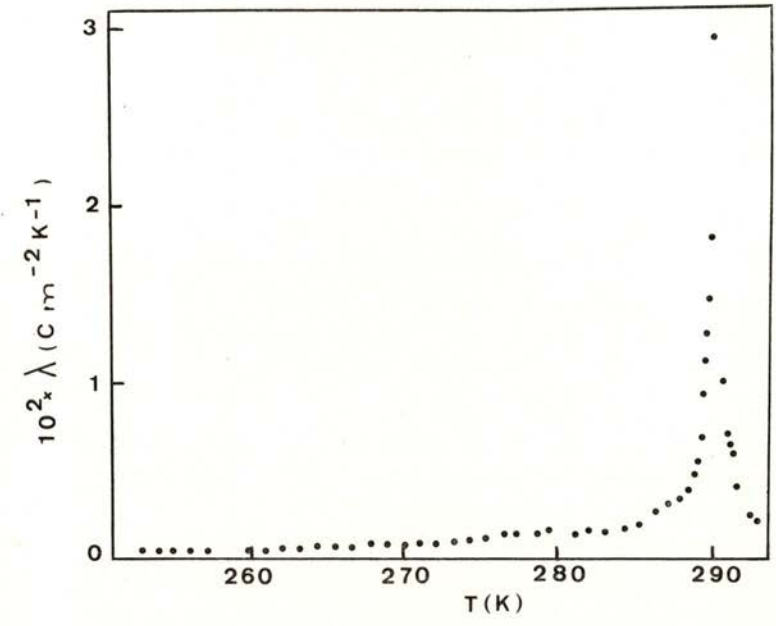

Fig. 3 — Temperature dependence of pyroelectric coefficient λ for SbSI (sample (b)).

electric coefficient shows a more pronounced tailing-off above $T_m = 290.1$ K. As is well known, Landau's theory for a first order

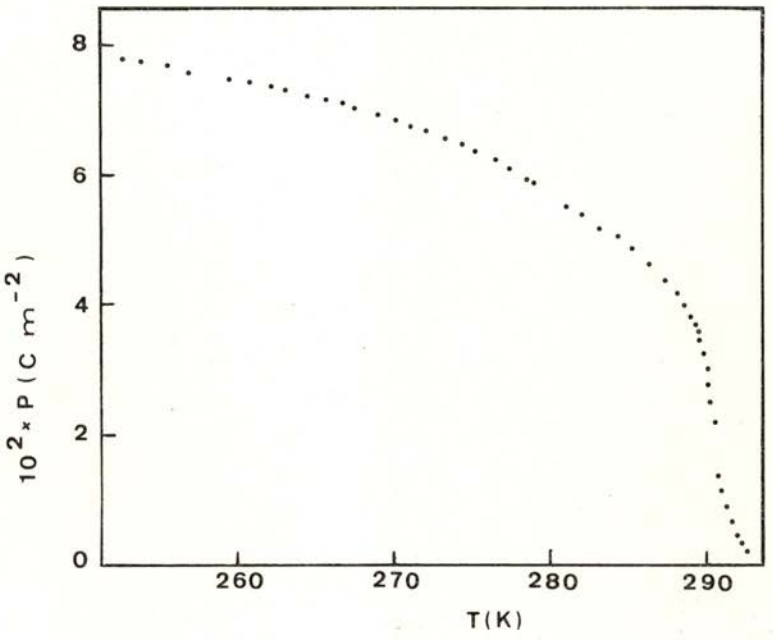

Fig. 4 — Temperature dependence of spontaneous polarization P_s for SbSI (sample (b)) obtained from pyroelectric coefficient data of figure 3.

transition requires the Gibbs free energy density to be expanded up to the sixth power of the order parameter P [2, 4] :

$$G = G_0 + a\ (T - T_0)\ P^2/2 + b\ P^4/4 + c\ P^6/6 \qquad (1)$$

The coefficient *a* and *c* are positive and *b* is negative. Standard calculations based on minimisation of the free energy give the following result :

$$a\ (T - T_0) + b\ P^2 + c\ P^4 = 0 \quad \text{for} \quad T < T_c = T_0 + 3\ b^2/16\ a\ c \qquad (2)$$

$$P = 0 \qquad \text{for} \quad T > T_c \qquad (3)$$

For a sample under an uniform electric field E_b expression (2) must be replaced by the following one :

$$a\,(T - T_0)\;P + b\,P^3 + c\,P^5 - E_b = 0 \qquad (4)$$

The reciprocal of the electrical susceptibility is given by

$$(\chi_T)^{-1} = 4\,a\,(T_0 - T) + (b^2/c)\,\{1 + [(\tilde{T} - T)/(\tilde{T} - T_0)]^{1/2}\} \quad \text{for} \quad T < T_c \qquad (5)$$

$$(\chi_T)^{-1} = a\,(T - T_0)\,, \quad \text{for} \quad T > T_c \qquad (6)$$

where

$$\tilde{T} = T_0 + b^2/4\,a\,c\,. \qquad (7)$$

Using a least squares method, data were fitted on a computer to expression (2). The best fitting to this expression yields the values

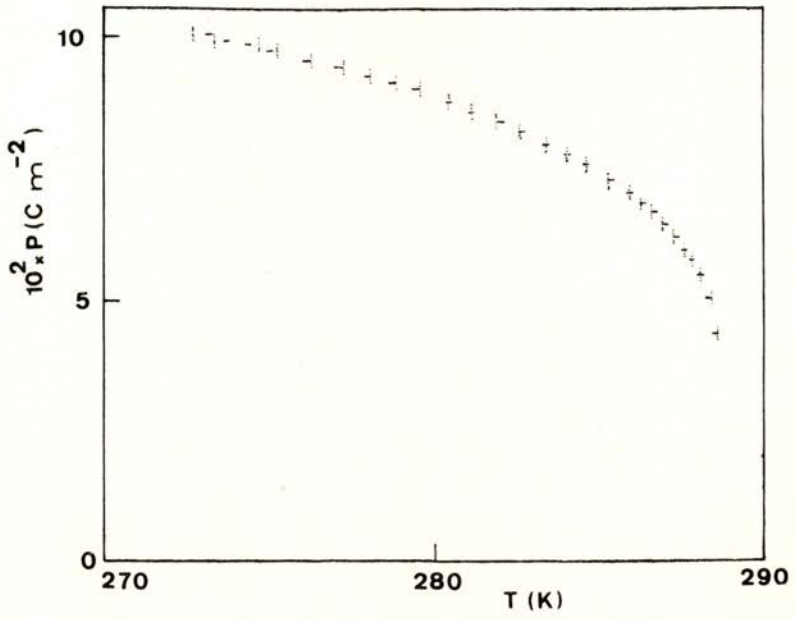

Fig. 5 — Theoretical fitting of P_s versus T (horizontal dashes) for SbSI (sample (a)). Vertical dashes: experimental data obtained from pyroelectric effect.

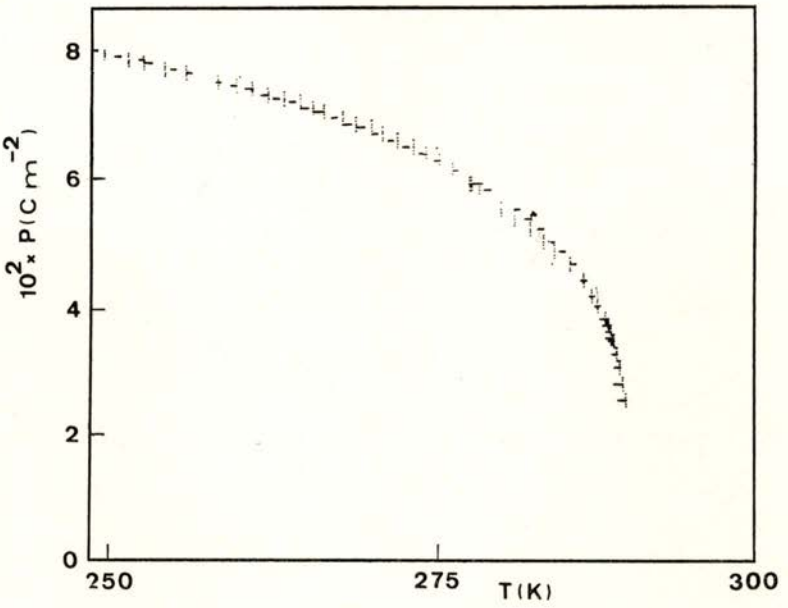

Fig. 6 — Theoretical fitting of P_s versus T (horizontal dashes) for SbSI (sample (b)). Vertical dashes: experimental data obtained from pyroelectric effect.

of b/a, c/a, T_0 and T_c listed in Table I. The horizontal dashes of figures 5 and 6 are drawn using those values. Vertical dashes represent experimental data.

TABLE I

	Sample (a)		Sample (b)
	Pyroelec. eff.	Hyst. loop	Pyroelec. eff.
b/a [$C^{-2}m^4K$]	-6.3×10^2	-1.4×10^2	-9.0×10^2
c/a [$C^{-4}m^8K$]	2.1×10^5	5.4×10^4	12×10^5
T_o [K]	288.2	289.4	289.5
T_c [K]	288.5	289.5	289.6
T_m [K]	288.9	—	290.1

The results obtained seem to show that SbSI follows Landau's theory for a first order transition. As the difference $T_c - T_0$ is very small the phase transition is very nearly a continuous one, as referred

by Glass and Lines [4]. By assuming that the tailing off in the pyroelectric effect above T_c could be explained by an internal electric bias field (E_b) we have also fitted the data to expression (4). The values of b/a , c/a , T_o , T_m and E_b/a obtained by a method similar to that referred above are listed in Table II. The horizontal dashes of figures 7 and 8 are drawn accordingly.

TABLE II

	Sample (a)		Sample (b)
	Pyroelec. eff.	Hyst. loop	Pyroelec. eff.
b/a [$C^{-2}m^4K$]	-4.3×10^2	-3.6×10^1	-6.9×10^2
c/a [$C^{-4}m^8K$]	2.0×10^5	0.64×10^5	9.2×10^5
T_o [K]	288.7	288.3	289.9
T_m [K]	288.9	—	290.1
E_b/a [$Cm^{-2}K$]	6.9×10^{-3}	3.35×10^{-2}	9.1×10^{-3}

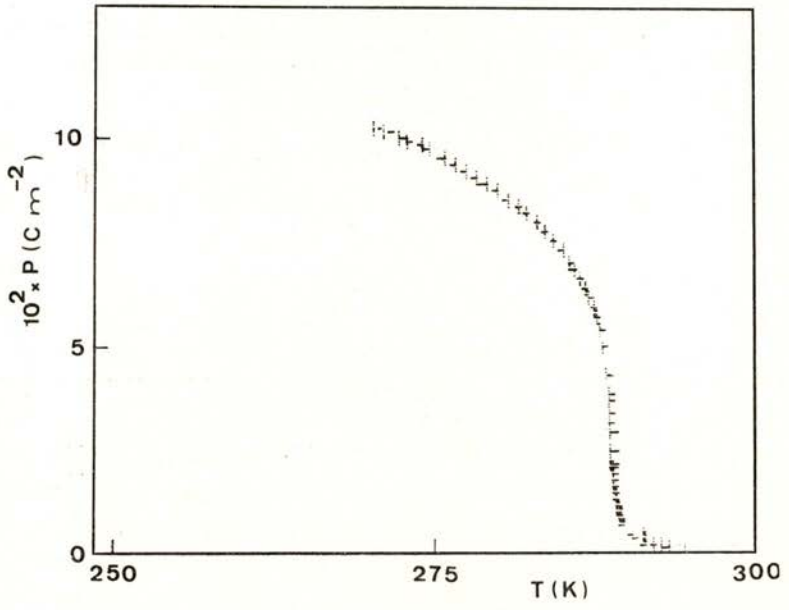

Fig. 7 — Theoretical fitting of P_s versus T including a bias internal electrical field E_b (horizontal dashes) for SbSI, (sample (a)). Vertical dashes: experimental data obtained from pyroelectric effect.

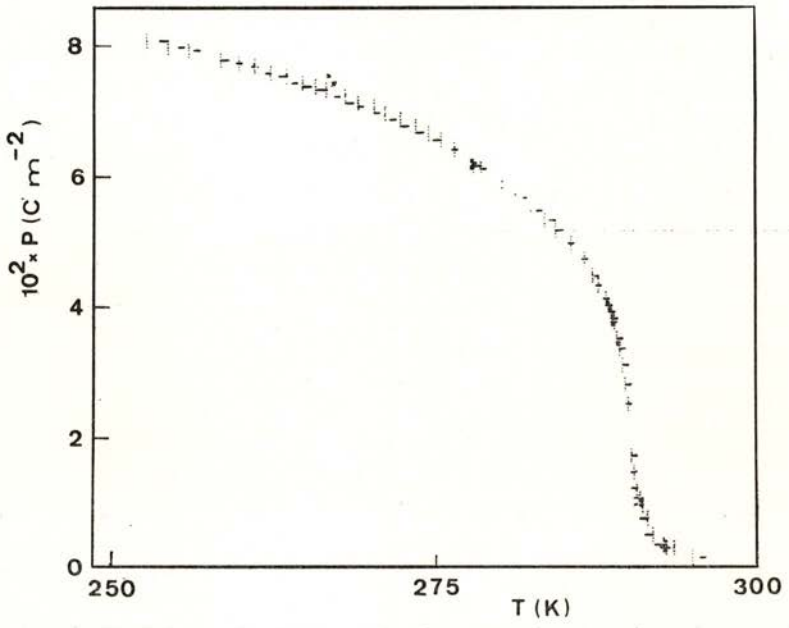

Fig. 8 — Theoretical fitting of P_s versus T including a bias internal electrical field E_b (horizontal dashes) for SbSI (sample (b)). Vertical dashes: experimental data.

In figure 9 we can see some hysteresis loops, at different temperatures, for sample (a). We have not observed double hysteresis loops as reported by S. Kawada [5] in SbSI samples with a critical temperature higher than in our samples. Vapour grown non-stoichiometric crystals with a slight excess of sulfur together with oxygen impurities show a transition temperature around 24.7 C [6]. The results we obtained are very similar to those reported by Fattuzo and Merz [7]. Spontaneous polarization obtained from hysteresis loops is seen in figure 10. The results exhibited in figure 11 for increasing and decreasing temperature do not show appreciable thermal hysteresis, which is consistent with the small difference between T_0 and T_c. Table I also lists the values of b/a, c/a, T_0 and T_c obtained by fitting the polarization obtained from hysteresis loops for sample (a) to expression (2); and in Table II are presented the corresponding values by fitting

the same data to expression (4). In figure 12 the horizontal dashes represent the fitting of the experimental data to expression (2) and in figure 13 the horizontal dashes represent the fitting of the experimental data to expression (4).

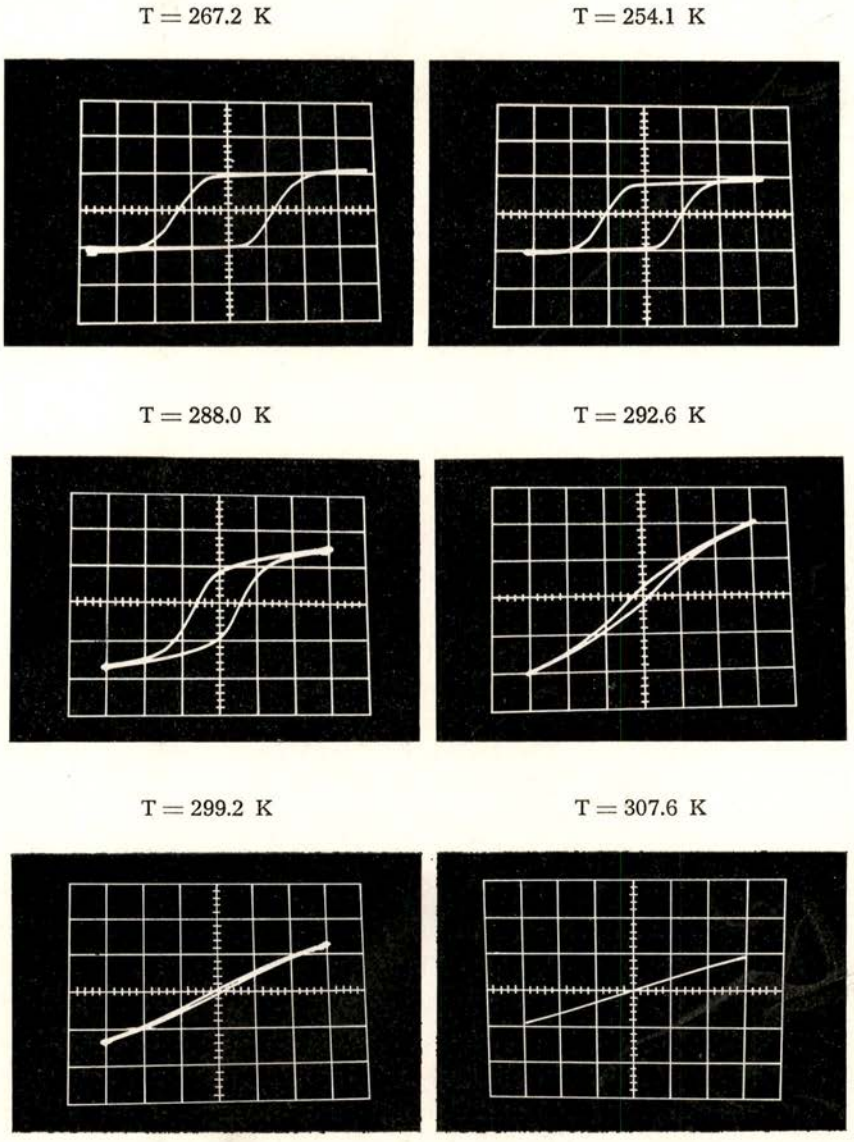

Fig. 9 — SbSI hysteresis loops, at different temperatures, for SbSI (sample (a)).

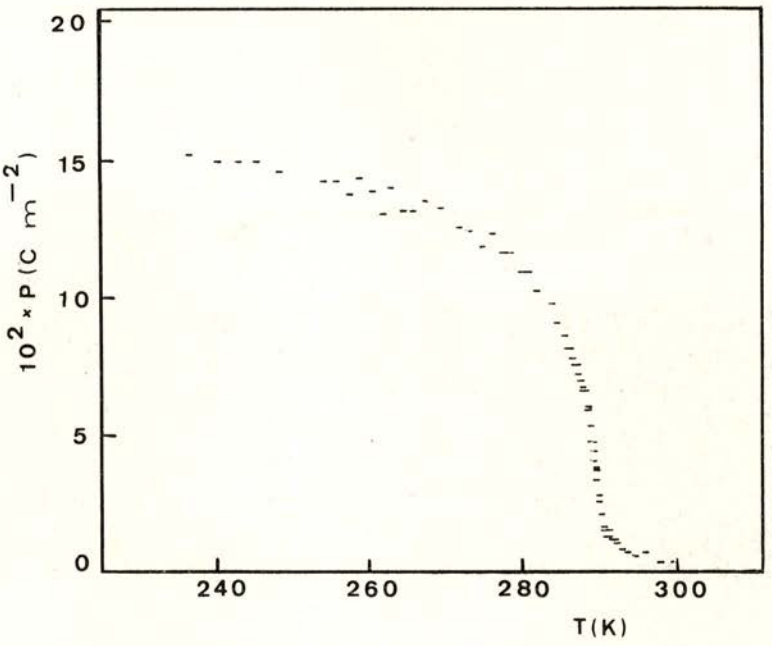

Fig. 10 — Temperature dependence of spontaneous polarization of SbSI (sample (a)) obtained from hysteresis loops.

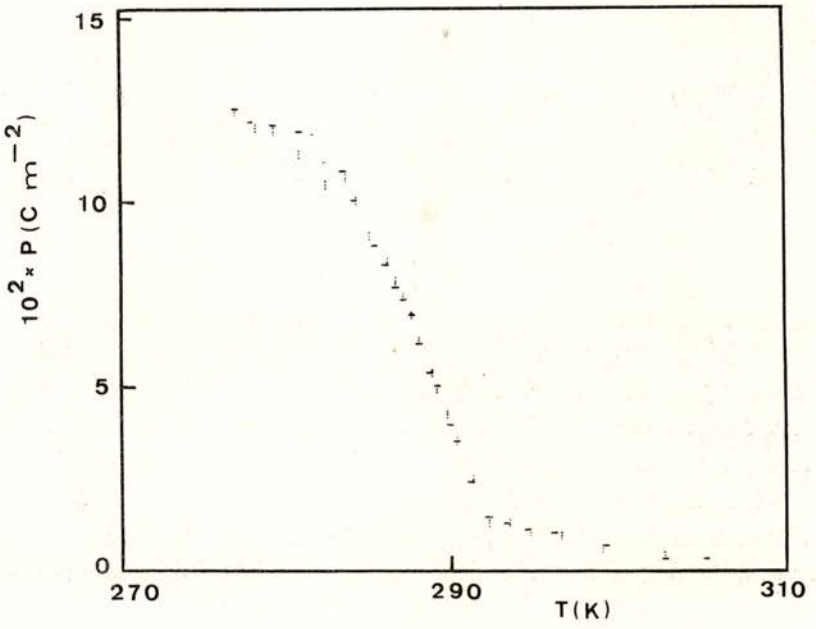

Fig. 11 — Temperature dependence of spontaneous polarization of SbSI (sample (a)), determined for increasing temperatures (vertical dashes) and decreasing temperatures (horizontal dashes).

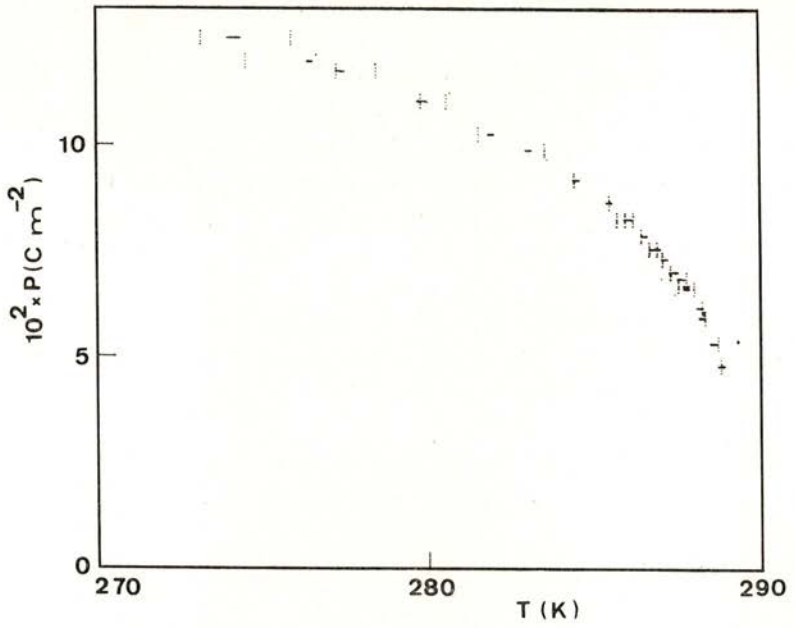

Fig. 12 — Theoretical fitting of P_s versus T (horizontal dashes) for SbSI (sample (a)). Vertical dashes: experimental data obtained from hysteresis loops.

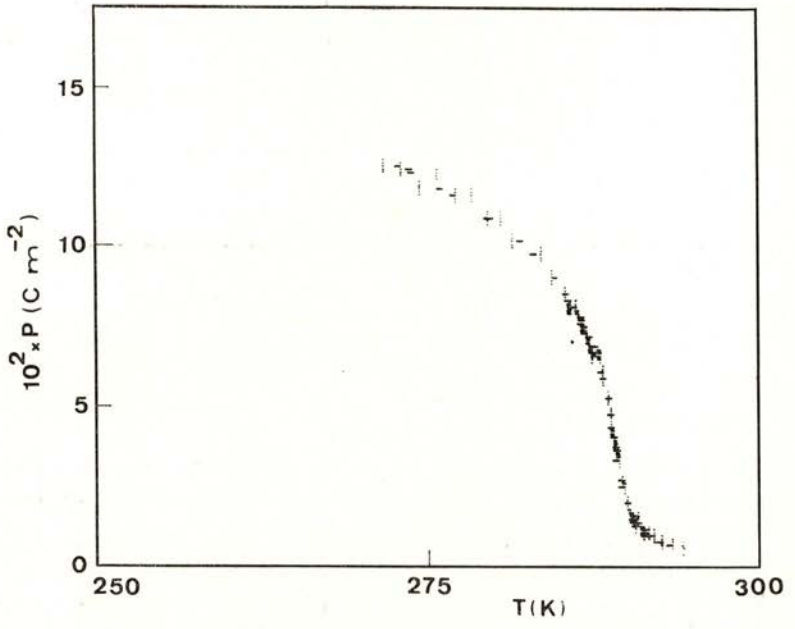

Fig. 13 — Theoretical fitting of P_s versus T including a bias internal electrical field E_b (horizontal dashes) for SbSI (sample (a)). Vertical dashes: experimental data obtained from hysteresis loops.

We have also measured dielectric loss (ε'') and dielectric constant (ε') as a function of the temperature in sample (a) (figure 14). ε' has a maximum value at $T_m = 288.2$ K. The reciprocal of dielectric constant is approximately described by $(\varepsilon')^{-1} \simeq a'(T - T'_0)$ with $a' = 1.66 \times 10^5\ F^{-1}\,K^{-1}m$ and $T'_0 = 277.3$ K for $T > T_c$ (figure 15). For $T < T_c$, we have $(\varepsilon')^{-1} = a''(T - T''_0)$ with $a'' = 1.26 \times 10^6\ F^{-1}\,K^{-1}m$ and $T''_0 = 290.3$ K (figure 15). Measurements of dielectric constant with increasing and decreasing temperature show a very small thermal hysteresis as can be seen in figures 16 and 17.

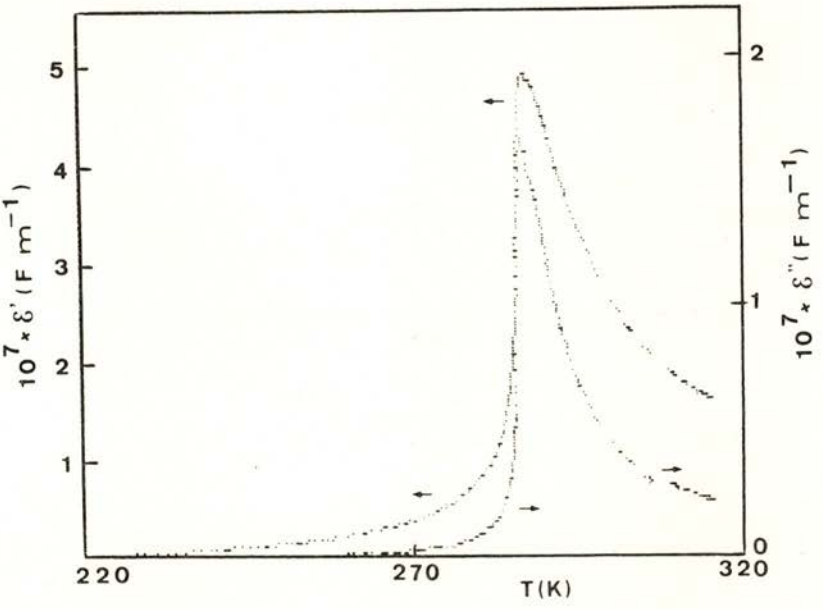

Fig. 14 — Temperature dependence of dielectric constant, ε', and dielectric loss, ε'', for SbSI (sample (a)).

As we can see in figure 18 the reduced dielectric susceptibility obtained with the values listed in Table II (pyroelectric effect) for sample (a) and using expression (5) are in fair agreement with the experimental data.

Landau's theory predicts that $T'_0 = T_0$. Previous results reported for SbSI gave a value of the order of 10 K [8-10] for

the difference $T_c - T'_0$ which is consistent with the result we have obtained for SbSI. To identify T'_0 with T_0, as it is sometimes done, does not seem consistent with the small thermal hysteresis observed in SbSI. Given the large value of 10 K for $T_c - T'_0$ the difference of the stability limits of ferro and paraelectric phase ($T_0 - T_0^-$) would be of the same order of magnitude and so a

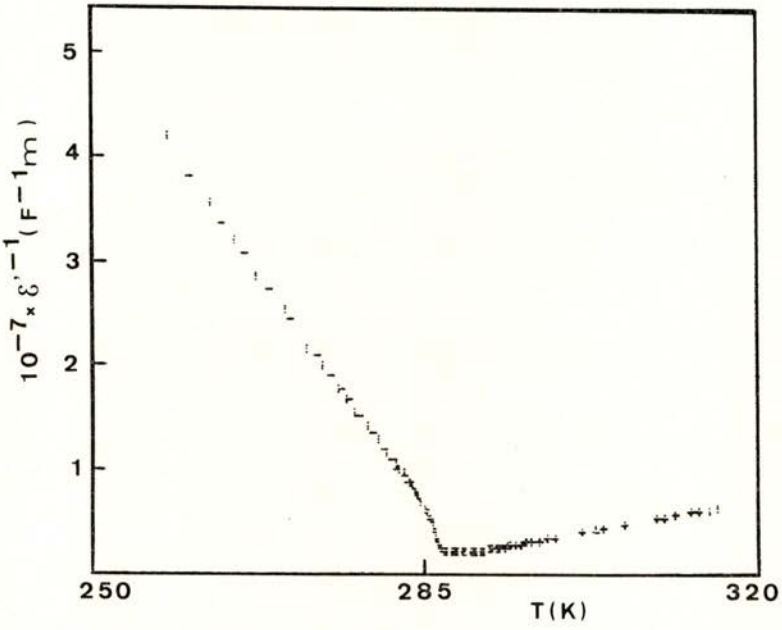

Fig. 15 — Temperature dependence of the reciprocal of dielectric constant for SbSI (vertical dashes). Theoretical fittings (horizontal dashes): see text.

much larger thermal hysteresis should be observed. Stokka *et al* [11], in measurements of specific heat for increasing temperatures, in SbSI, found $T_m - T_0 \sim 1$ K, and a thermal hysteresis of the order of magnitude of 1 K. These results are consistent with those we obtained.

It is not easy to understand the large difference between T_0 and T'_0. As is well known, some ferroelectric properties of SbSI and ABO_3 perovskites, namely the temperature dependence of the soft mode, can be well understood by assuming an anisotropic polarizability of the oxygen and sulfur ions [12].

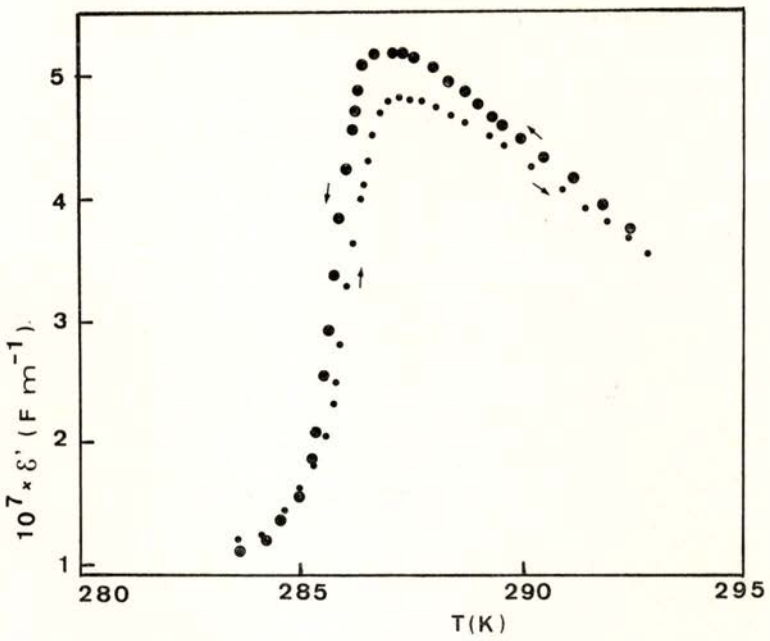

Fig. 16 — Temperature dependence of dielectric constant for sample (a); dots: increasing temperatures; circles: decreasing temperatures.

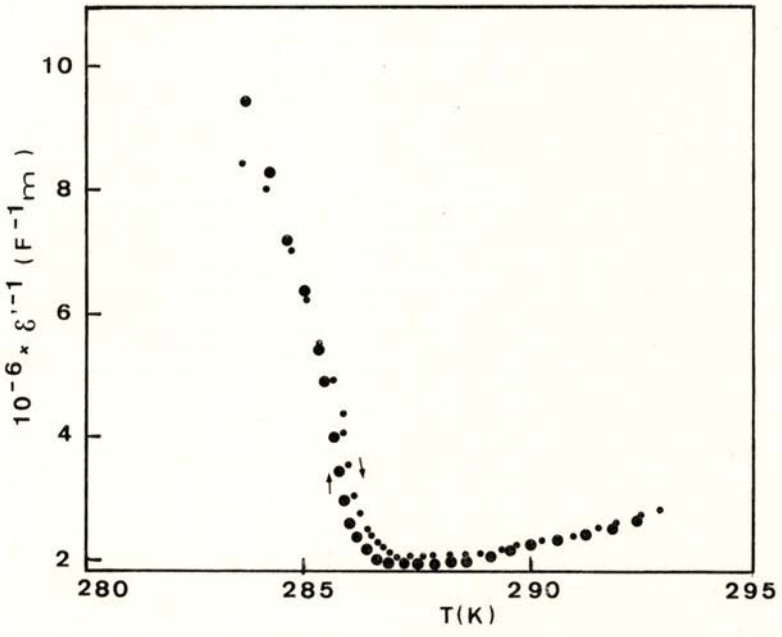

Fig. 17 — Temperature dependence of the reciprocal of dielectric constant for sample (a); dots: increasing temperatures; circles: decreasing temperatures.

Bilz *et al.* consider a quasi-one dimensional shell model, where one sublattice with rigid cations (Sb) is interacting with another sublattice of polarisable anions (S). The third lattice component (I) may be neglected in a first approximation. All long range forces are simulated by nearest neighbor forces, while the

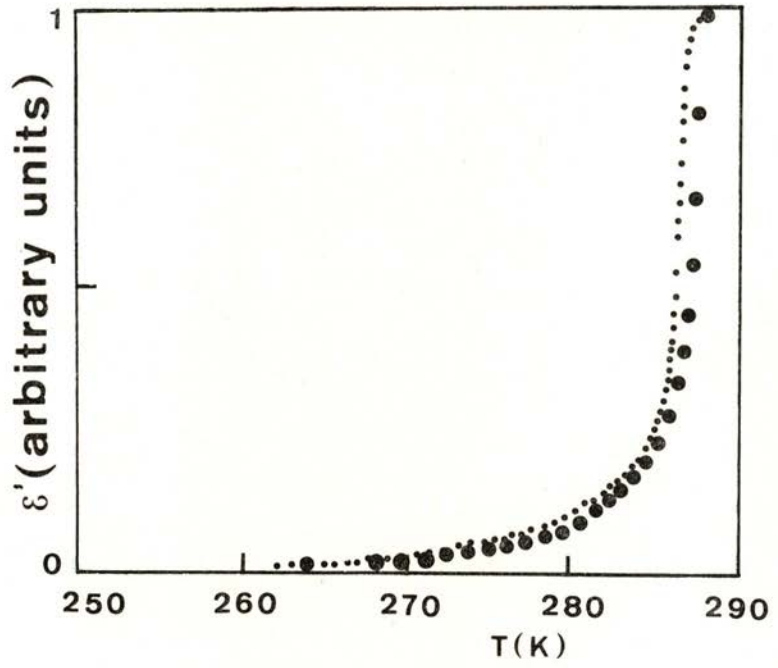

Fig. 18 — Circles: temperature dependence of reduced dielectric susceptibility obtained with values listed in table II for sample (a) ; dots: temperature dependence of reduced dielectric constant exhibited in figure 14.

non-linear polarisability of the anions is described by a quartic (electronic) shell-ion coupling [13]. This model leads to the following expression for dielectric constant as a function of the temperature (Barret formula) :

$$B / (\varepsilon' - A) = (T_f / 2) \coth (T_f / 2T) - T_c \qquad (7)$$

where A and B are parameters, T_f the temperature equivalent to the frequency (ω_f) of the soft mode at the zone boundary in the disperson relation $\omega_f (\mathbf{q})$.

By taking $T_c = 288\,K$ and for different values of T_f we can see in figure 19 a plot of $(T_f/2)\coth(T_f/2T) - T_c$ as a function of T. For $T_f = 200\,K$ we found $T_c - T_0' \simeq 10\,K$, but the value $T_f = 200\,K$ corresponds to a wave number $140\,cm^{-1}$ which is too high compared to the known values of the soft mode frequencies [10]. That model does not give a complete explanation for the observed behaviour in the critical region and so we must find an additional reason for the existence of such a difference between T_0' and T_c.

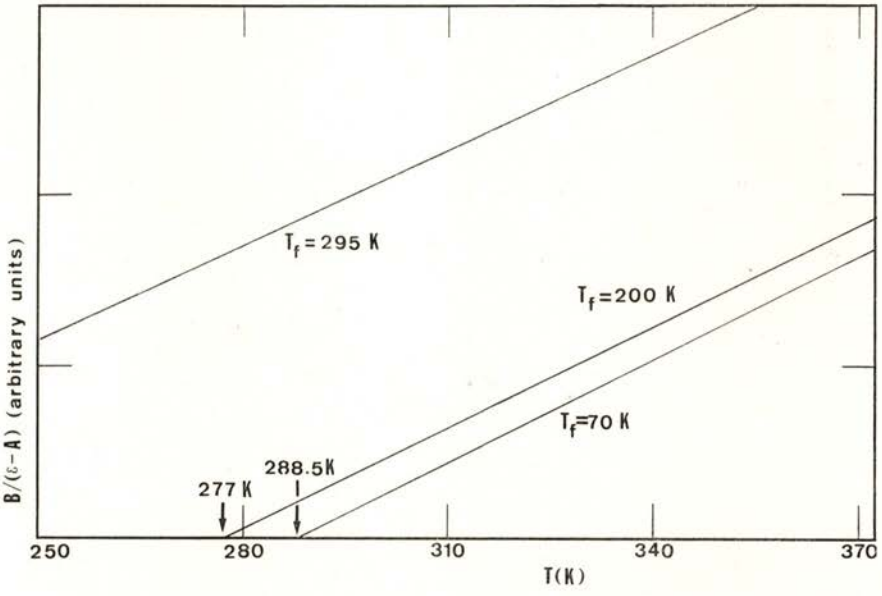

Fig. 19 — A plot of $B/(\varepsilon' - A) = (T_f/2)\coth(T_f/2T) - T_c$ with $T_c = 288\,K$, for several values of T_f.

As there exists strong experimental evidence for a mixing of the soft mode with higher vibration modes, leading to the observation of interesting optical properties in SbSI, it seems that (figure 20) the softening of the low frequency mode is driven by one or two other modes coupled with it [14]. The transition actually occurs when the frequency of the soft mode vanishes at T_c, a few degrees above the paraelectric Curie temperature. The transition

is somewhat "clamped" between T_0' and T_c and this might result from a strong phonon-phonon interaction. This interpretation is well supported by the study of Raman spectra of the ferroelectric transition in SbSI induced by hydrostatic pressure, where one observes a tailing-off of the soft mode above a crossing point, due to a strong interaction between phonons [14]. It might also be possible that a diffuse character in the SbSI transition could explain the large difference between T_0 and T_0'.

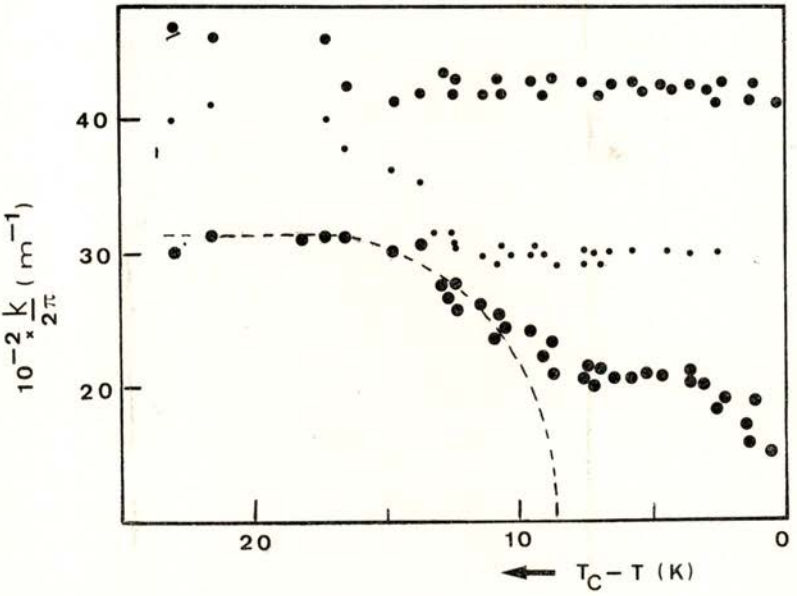

Fig. 20 — A plot of wave numbers versus $T_c - T$ for SbSI. Dots and circles: experimental data taken from reference [14]. The dashed line is a possible curve for the temperature dependence of the uncoupled soft mode wave number.

The authors wish to express their gratitude to Prof. M. Balkanski, Prof. M. K. Teng, Dr. A. Levelut and Dr. M. Massot, for valuable discussions and to Dr. J. M. Brochado for invaluable help. Financial support from the "Service Culturel, Scientifique et de Coopération Technique de l'Ambassade de France au Portugal" is gratefully acknowledged. The technical assistance of José Magalhães is also gratefully acknowledged.

REFERENCES

[1] V. L. GINZBURG, *Sov. Phys. Solid State*, **2**, 1824 (1961).

[2] R. BLINC and B. ZEKS, *Soft modes in ferroelectrics and antiferroelectrics*, North-Holland Publishing Company, Amsterdam, 1974.

[3] R. CHAVES, H. AMARAL and S. ZIOLKIEWICZ, *J. Physique*, **41**, 259 (1980).

[4] M. E. LINES and A. M. GLASS, *Principles and applications of ferroelectrics and related materials*, Clarendon Press, Oxford, 1977.

[5] S. KAWADA, *J. Phys. Soc. Japan*, **25**, 919 (1968).

[6] A. S. BHALLA, R. E. NEWNHAM, L. E. CROSS, J. P. DOUGHERTY and W. A. SMITH, *Ferroelectrics*, **33**, 3 (1981).

[7] E. FATUZZO, G. HARBEKE, W. J. MERZ, R. NITSCHE, H. ROETSCHI and W. RUPPEL, *Phys. Rev.*, **127**, 2036 (1962).

[8] T. A. PIKKA and V. M. FRIDKIN, *Sov. Phys. Solid State*, **10**, 2668 (1969).

[9] K. JRIE, *Ferroelectrics*, **21**, 395 (1978).

[10] M. MASSOT, M. K. TENG, J. F. VITTORI, M. BALKANSKI, S. ZIOLKIEWCZ, F. GERVAIS and J. L. SERVOIN, *Ferroelectrics*, **45**, 237 (1982).

[11] S. STOKKA, F. FOSSHEIM and S. ZIOLKIEWICZ, *Phys. Rev.* B, **24**, 2807 (1981).

[12] H. BILZ, A. BUSSMANN, G. BENEDEK, H. BÜTTNER, D. STRAUCH, *Ferroelectrics*, **25**, 339 (1980).

[13] M. BALKANSKI, M. K. TENG, M. MASSOT and H. BILZ, *Ferroelectrics*, **26**, 737 (1980).

[14] M. K. TENG, M. BALKANSKI and M. MASSOT, *Phys. Rev.*, **B5**, 1031 (1972).

INTERSYSTEM CROSSING IN HEXAFLUOROBENZENE AND BENZENE VAPOURS. THE ROLE OF LOCAL MODES ON THE NONSTATISTICAL BEHAVIOUR OF BENZENE

SEBASTIÃO J. FORMOSINHO and ABÍLIO M. DA SILVA

Department of Chemistry, University of Coimbra, 3000 Coimbra, Portugal

ABSTRACT — Previous work on decay of triplet states of aromatic molecules in the vapour phase is reviewed and the possible role of local modes in the decay of such systems is followed by studying triplet yields of C_6F_6 as a function of pressure and comparing the behaviour with that of C_6H_6. Measurements of the triplet yield of C_6F_6 using but-2-ene sensitized isomerization reveal that ϕ_T may show a weak increase (ca. 10 %) from pressures of 15 Torr ($\phi_T^{\infty} = 0.84 \pm 0.08$) down to 0.16 Torr ($\phi_T^{o} = 0{,}92 \pm 0.08$). This behaviour contrasts with the strong decrease (4 times) observed in ϕ_T for C_6H_6 within the same pressure range. For C_6H_6 these observations are interpreted in terms of a nonstatistical intersystem crossing allowed by a slow intramolecular vibrational randomization process for the CH local modes, which are populated via a large electronic energy gap radiationless transition. The normal mode character of the CF stretches provides a faster intramolecular vibrational redistribution in T_1 and appears to be responsible for the statistical behaviour of C_6F_6. These features are supported by the vibrational energy dependence of hot triplet decay rates in protonated aromatic and heterocyclic molecules which are attributed to $T_1 \rightsquigarrow S_0$ transitions in the low energy region and to $T_1 \rightsquigarrow S_1$ transitions in the high energy region. The population of one CC promoting mode in the intersystem crossing process in C_6H_6 accounts for the small triplet yield in the isolated molecule. Comparison with the pressure dependence of triplet formation in protio - naphthalene and anthracene supports the view of a nonstatistical intersystem crossing from S_1 in these molecules.

1 – INTRODUCTION

Studies of the effect of pressure on the formation and decay of triplet states of aromatic molecules in the vapour phase may help to unravel the detailed fate of such molecules following optical excitation. Early work by Porter and Wright [1] on the

flash photolysis of naphthalene and anthracene in the vapour phase noted a decrease in the amount of triplet (T_1) formed as the pressure of added buffer gas was reduced. Subsequent work by Porter and coworkers [2] using better experimental conditions confirmed these previous findings for a pressure region between 0.05 to 10 Torr. With the advent of laser flash photolysis relevant work was carried out to elucidate the mechanism of the population of triplet states via intersystem crossing (i. s. c.) from S_1 [3-6]. However, it is only recently that molecular beam with multicolor photoionization techniques has allowed the direct observation of triplet states under isolated conditions at several energies of excitation [7-11]. Smalley and coworkers have found that the vibrational energy, E_v , dependence of the hot triplet, T_1^v , decay rates in pyrazine, pyrimidine [10], toluene [9], benzene [8, 11] and naphthalene [7] is very strong at low energies (S_0 region), but becomes very weak at high energies, when the total energy is larger than the electronic energy of S_1 (S_1 region) . In each region the relation between the triplet decay rates and E_v is virtually exponential, but the intercept at $E_v = 0$ in the S_1 region is 3 to 5 orders of magnitude higher than the intercept in the S_0 region. Such vibrational energy effects were initially interpreted by considering that the T_1 decay was only caused by i. s. c. to S_0 . A dilution of the good acceptor modes due to a fast intramolecular vibrational relaxation (IVR) was responsible for the weakening of the dependence of $k_{T_1^v \rightsquigarrow S_0}$ at high E_v [9]. However recently Smalley and coworkers [12] have shown that this saturation effect of i. s. c. at high energies cannot be explained by a radiationless transition $T_1^v \rightsquigarrow S_0$ associated with IVR .

Pyrazine and pyrimidine have long been recognized as examples of molecules in the intermediate coupling situation [13, 14] for $S_1 \rightsquigarrow T_1$. This i. s. c. can be represented kinetically by a reversible process [15]

$$\begin{array}{ccc} & k_T & \\ S_1 & \rightleftarrows & T_1^{v'} \\ \Big\downarrow k_i & k_S & \Big\downarrow k_j \end{array}$$

where k_i and k_j are the rates of irreversible and k_T and k_S are the rates of reversible crossing. The vibrationally hot $T_1^{v'}$ state,

upon a short pulse excitation in S_1, rises with a first order rate constant λ_1 and decays with a rate constant λ_2

$$2\lambda_{1,2}=k_i+k_T+k_j+k_S \pm [(k_i+k_T-k_j-k_S)^2 + 4k_Tk_S]^{1/2} \qquad (1)$$

In molecules such as pyrazine and pyrimidine $k_i+k_T-k_j-k_S >> (4k_Tk_S)^{1/2}$ and consequently $\lambda_2 \simeq k_S+k_j$; in the isolated molecules k_j is very small and $\lambda_2 \simeq k_S$. Consequently the triplet decay rates in the S_1 region can be attributed to the i. s. c. $T_1^{v'} \rightsquigarrow S_1$, whereas at lower vibrational energies the triplet decay is due to $T_1^{v} \rightsquigarrow S_0$. This would explain why the intercept of the triplet decay rates in the S_1 region in $3 - 6 \times 10^3$ times larger than the cold triplet decay rate [10]. The dependence of the decay rates on E_v depends on the electronic energy gap between the states involved in the transition [14]. For small electronic energy gaps, as is the case for a $S_1 \rightsquigarrow T_1$ process it is a weak dependence, while for a large electronic energy gap as in the $T_1 \rightsquigarrow S_0$ process it is a strong dependence.

Owing to the similarity in the dependence of the triplet decay rates with E_v of benzene [8, 11] toluene [9] and naphthalene [7] and the above mentioned heterocyclic molecules, the same interpretation is foreseeable for these aromatic molecules. The pressure dependence of triplet formation of benzene [16, 17], naphthalene [2, 5], anthracene [2, 4, 6] and acridine [18] has been extensively studied by several authors and nonstatistical behaviour has been claimed for the i. s. c. process from S_1 [2, 6, 17, 18]. Strong support for such a claim comes from recent molecular beam experiments which allowed the observation of quantum beats in the fluorescence decay of anthracene [19] when excited into several levels in S_1. Previously such effects have only been observed in much smaller molecules, pyrimidine, biacetyl and methylglyoxal [20, 21], classified as intermediate case molecules with respect to i. s. c. from S_1.

For radiationless transitions between two electronic states, a nonstatistical behaviour requires that the density of coupled levels in the final state is comparable to that in the initial state. For the i. s. c. process $S_1 \rightsquigarrow T_1$ in aromatic molecules a suggestion was made that such a low density of states can only be provided by the CH vibrational levels [18] which are good accepting modes for the nonradiative transition $S_1 \rightsquigarrow T_1$ and which have a strong

local mode character [22-24]. Such local modes interact strongly between themselves, but are weakly coupled with the bath of normal modes [24, 25]. In these conditions the intramolecular vibrational redistribution process into the quasi-continuum bath of the normal modes is slow and can determine the rate of the overall nonradiative transition. In contrast normal modes are strongly coupled with their own bath and provide a fast redistribution of vibrational energy. To investigate the role of local and normal modes on i. s. c. we decided to study the effect of pressure on the triplet yield of C_6F_6 and compare it with the well established behaviour of the C_6H_6 triplet state [16, 17]. C_6F_6 is a convenient molecule, because it has the same size as benzene, has stretching modes (CF) with a normal mode character [23, 24] and an electronic $S_1 - T_1$ energy gap ($\sim 9500\ cm^{-1}$) that is virtually identical to that of C_6H_6, judging from the fluorescence [26] and phosphorescence spectra [27].

2 – EXPERIMENTAL

Spectrograde perfluorobenzene (Aldrich) was employed and its purity, checked by vapour phase gas chromatography, was 99 %. Cis-butene (Fluka) had a percentage of trans-butene of 0.3 %. Mixtures of C_6F_6 and cis-butene were prepared on a mercury-free vacuum line and spectroscopically pure argon (Air-Liquide) was added to increase the overall pressure. Samples were irradiated with a 150 W medium pressure Hg-lamp on a wavelength region between 250-260 nm. Absolute yields were determined on irradiation at 260 ± 1 nm by a 250 W xenonlamp through a monochromator. Analysis of reactants and products was carried out on a Perkin-Elmer 900 gas chromatograph with columns filled with Durapak. The percentage of isomerization was always $\leqslant 1$ %. Further experimental details are given elsewhere [17].

3 – RESULTS

The triplet yield of C_6F_6 measured by cis-but-2-ene isomerization was found to decrease by 10 % upon addition of argon, to a pressure of 15 Torr. At the low concentrations of butene used

not all the triplet states were scavenged, but the fraction of triplets quenched by cis-butene was constant throughout the whole pressure range, because the same mixture of C_6F_6 and cis-butene (0.08 Torr C_6F_6 + 0.08 Torr cis-butene) was employed in all the experiments.

To determine absolute triplet quantum yields a pressure of cis-butene > 100 Torr is required to ensure the scavenging of all the triplet molecules [27]. Mixtures of 0.08 Torr C_6F_6 and cis-butene, with pressures of 100 Torr and 400 Torr, were employed. The quantum yield of isomerization was 0.18 and 0.38 respectively. Assuming that all triplets are scavenged at 400 Torr of butene, an absolute yield of $\phi_T^\infty = 0.84 \pm 0.08$ is estimated from the stationary state ratio $[\,t\text{-}Bu\,]_s / [\,c\text{-}Bu\,]_s = 2.2$, determined for C_6H_6 at high pressures [17]. The small increase in the yield of triplet with a decrease in pressure ($\phi_T^0 = 0.92 \pm 0.08$) is in agreement with the small decrease in the fluorescence yield with pressure, attributed to vibrational relaxation in S_1 [27]. The fluorescence yield from the thermally equilibrated S_1 state is $\phi_F^\infty = 0.019 \pm 0.001$ and, consequently, triplet and fluorescence yields do not add up to unity (0.86). In the isolated molecule, upon excitation at 260 nm, $\phi_F^0 \simeq 0.005$ [27] and $\phi_T^0 + \phi_F^0 \simeq 0.93$.

4 – DISCUSSION

Intramolecular Vibrational Relaxation

The contrast between the pressure dependence of C_6F_6 and C_6H_6 triplets is illustrated in Fig. 1. The latter shows a nonstatistical behaviour whereas the former behaves statistically with respect to i.s.c.. C_6F_6 and C_6H_6 differ through few electronic and vibrational features. Electronically the presence of lone pair electrons in C_6F_6 can increase spin-orbit coupling and this can explain why ϕ_T^∞ is higher in this molecule than in C_6H_6. However such differences in spin-orbit coupling do not affect the relative yields as a function of pressure. The different behaviour of the two molecules should be attributed to differences in the CF and CH stretching modes. In principle the lower frequency of CF modes, compared to CH modes, increases the density of states for the triplet manifold and could place C_6F_6 in the statistical case.

However, molecules such as toluene, naphthalene and anthracene possess much higher density of states and they behave also in a nonstatistical fashion. Consequently we attribute the observed differences to the local mode character of the CH stretches in contrast with the normal mode character of the CF stretches [23, 24].

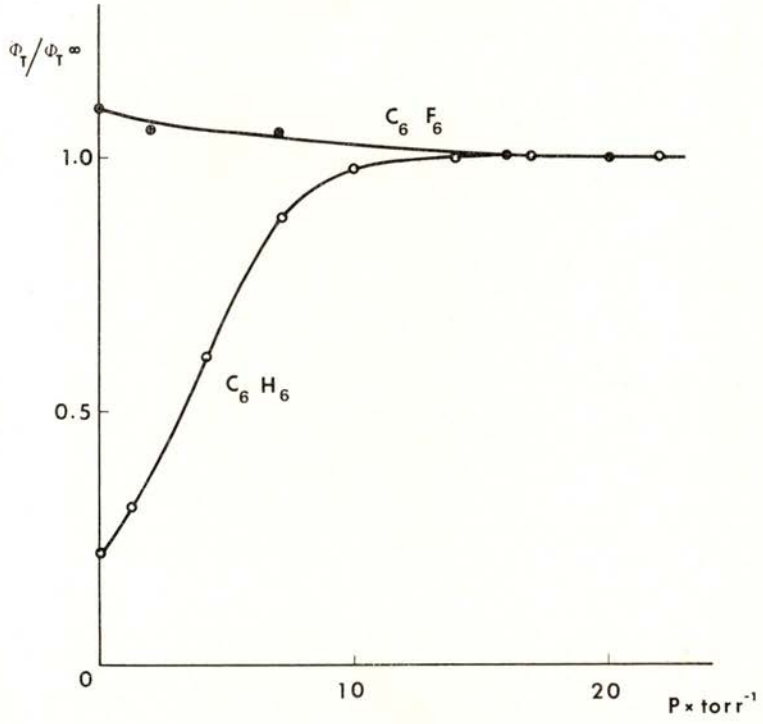

Fig. 1 — Relative triplet yields of C_6H_6 (o) and C_6F_6 (•) as a function of the pressure of added argon (0.05 Torr C_6H_6 + 0.05 Torr cis-butene; 0.08 Torr C_6F_6 + 0.08 Torr cis-butene)

On the basis of deuterium isotope effects [14] in aromatic hydrocarbons, one finds that the CH stretching modes participate significantly as accepting modes for electronic energy gaps $\geqslant 5000\ cm^{-1}$ and become the main accepting modes for electronic energy gaps $\geqslant 10\,000\ cm^{-1}$. In C_6H_6 the electronic

energy gap $S_1 - T_1$ is close to 10 000 cm^{-1} and considering that one CC promoting mode is populated, ca 75 % of the vibrational energy will go into the CH stretches after i. s. c. to T_1 [27]. A similar situation is expected in naphthalene and anthracene where the electronic energy gaps $S_1 - T_1$ are even larger.

IVR of highly vibrational CH overtone excitation in C_6H_6 vapours has been studied by Berry and coworkers [29, 30]. Vitrational relaxation is a very fast process (50-200 fs) but is highly nonstatistical. Example of such behaviour is the nearly constant bandwith in CH overtones over a vibrational energy range (up to 10 ν_{CH}) that involves 6 orders of magnitude change in the vibrational density of states. Deuteration also does not affect the overtone relaxation. These studies reveal that IVR proceeds via specific state-to-state intramolecular processes, producing a limited subset of final vibrational levels of CH stretches and possibly CH bending modes. Coupling to the bath of normal modes is a relatively slow process [25]. Evidence for the slow rate of such a relaxation process in other aromatic molecules with CH modes is given by the T - T absorption spectra of hot triplet species. Owing to the fairly restricted Franck-Condon factors governing i. s. c., only a few vibronic states are initially populated in $T_1^{v'}$ and its absorption is more structured than that of the relaxed state. Such a feature is quite evident for the nascent triplets of naphthalene [5] and anthracene [6] observed on a nanosecond time scale. In contrast normal modes such as the CF modes are strongly coupled between themselves and can very quickly populate a great manifold of vibrational levels [25] in C_6F_6 (T_1) following i. s. c. . Studies [31] of IVR in naphthalene optically populated in a few normal modes reveal that intramolecular redistribution of energy is fast and it occurs within an order of magnitude, to the bath of all the vibrational levels.

Using the concept [32] of the number of coupled states, N, and its relationship with the density of states, ρ, it can be shown that

$$N_T / N_S \simeq \rho_T k_T / (\rho_S k_S) \qquad (2)$$

Eq. (2) reveals that the weak exponential vibrational energy dependence of the triplet decay rates in the S_1 region reflects the similar dependence of the S_1 decay rates. In order to test eq. (2) in pyrimidine we have partitioned, as usual, the vibrational modes

of the molecules in S_1 and T_1 states into sets which will be treated as degenerate, with frequencies 500, 1000, 1500 and 3000 cm^{-1}. The density of states was calculated by the Haarhoff [33] equation and compared with ρ_T / ρ_S calculated through eq. (2). For such calculation the number of coupled states was estimated by direct counting, considering all possible numbers of quanta which add up to the correct energy. Table 1 presents the calculations and reveals that a fair agreement (within an order of magnitude) was found when all the vibrational modes were considered for the transition rather than just the CH stretches. Similar results were found for pyrazine. For both molecules the electronic energy gap is small (ca 2000 cm^{-1}) and CH modes are not good accepting modes. A different situation occurs for large electronic energy gap transitions. Considering the decay of the hot triplets $T_1^{v'}$ in benzene and toluene reported by Smalley and coworkers as a measure of the average k_S rates [34], ratios of density of states can also be calculated. Table 1 shows the results and in contrast with the findings for the heterocyclic molecules a fair agreement can be found if the CH local stretches were almost the only modes involved in the i. s. c. process $S_1 \rightleftharpoons T_1$. This supports the view that the nonstatistical behaviour of benzene and other aromatic molecules is due to the strong local character of the CH modes.

Triplet Yields

The pressure dependence of triplet formation in large molecules has been currently interpreted in terms of two kinds of mechanisms. One considers the i. s. c. process $S_1 \rightsquigarrow T_1$ in the statistical situation, but proposes the existence of a fast (<100 ns) i. s. c. process from the hot triplet to the ground state [5, 16]. The other considers a pressure dependent i. s. c. process such as in the intermediate coupling situation [2, 4, 6, 17].

Observations of triplet formation, at low pressures, immediately following i. s. c. can provide a clear distinction between these two kinds of mechanisms [5]. Within the fast $T_1^v \rightsquigarrow S_0$ i. s. c. mechanism the triplet concentration should decrease with time, on a nanosecond scale. Since such a decrease corresponds to the rapid loss of the high triplet levels to S_0, it should be numerically

TABLE 1 — Ratio of density of states in the Intersystem Crossing Process $S_1 \rightsquigarrow T_1$ of Heterocyclic and Aromatic Molecules.

Molecule	Vibrational Modes E/cm^{-1}	g	E_S/cm^{-1}	E_I/cm^{-1}	k_T/s^{-1}	k_S/s^{-1}	N_I/N_S		ρ_T/ρ_S					
									all modes		CH modes		n CH and 1 CC modes	
							all modes	CH modes	Haarhoff	eq. (4)	Haarhoff	eq. (4)	Haarhoff	eq. (4)
Pyrimidine	500 1000 1500 3000	6 (*b*) 9 5 4	0	2543	(*a*) 3.7×10^{8}	(*b*) 1.8×10^{6}	2.9×10^{3}	1	31	14	2.9	0.005	—	—
Pyrazine	500 1000 1500 3000	6 (*b*) 9 5 4	0	4056	(*c*) 2×10^{9}	(*b*) 3.4×10^{6}	6×10^{4}	35	182	100	4.9	0.06	—	—
Benzene	500 1000 1500 3000	6 (*f*) 12 6 6	550	9500	(*d*) 9×10^{6}	(*d*) 1×10^{6}	7×10^{5}	126	92	1×10^{5}	37	14	230	240
Toluene	500 1000 1500 3000	8 (*f*) 14 8 8	0	8600	(*e*) 8.5×10^{6}	(*e*) 3.5×10^{5}	4×10^{7}	330	3×10^{4}	1×10^{6}	44	13.5	350	300

(*a*) Reference [32]; (*b*) Reference [10]; (*c*) A. Frad, F. Lahmani, A. Tramer and C. Tric, *J. Chem. Phys.*, (1974), **60**, 4419; (*d*) Reference [8] and [34]; (*e*) Reference [9]; (*f*) C. La Lau and R. G. Snyder, *Spectrochim. Acta.* (1971), **27A**, 2073; CH_3 torsion was not included.

identical to the increase in ϕ_T of the relaxed triplet from low to high pressures. Studies of the triplet absorption spectra of anthracene (3 Torr CH_4) by nanosecond laser flash photolysis, as a function of time, reveal the opposite effect since the triplet concentration increases by a factor of 1.25 times ca. 1 μs after excitation [4, 6]. Schröder et al. [5, 35] have carried out identical studies for naphthalene at low pressures (0.07 Torr) and have found that the integrated triplet absorption decreases by a factor of 1.8 with an increase in time, a value close to the overall increase of ϕ_T (2.0 times) from low to high pressures. However the integrated absorption bands at shorter and longer times did not correspond to the same vibrational bands. When this situation is properly taken into consideration we can conclude that at most only 15 % of naphthalene triplets are lost via a $T_1^v \rightsquigarrow S_0$ process. Consequently these experimental studies support also the view that naphthalene and anthracene triplets behave nonstatistically.

Benzene [17], naphthalene [36] and anthracene [4] have small but significant triplet yields under isolated conditions. The relative triplet yields are virtually identical for these molecules $\phi_T^o / \phi_T^\infty = 0.25$. In C_6D_6 this yield decreases, $\phi_T^o / \phi_T^\infty = 0.17$. These yields can be attributed mainly to the irreversibility in the i. s. c. $S_1 \rightsquigarrow T_1$ owing to the direct population of a CC promoting mode which has a normal mode character. Under the experimental excitation conditions the energy in T_1 is $E_v = 10\,000$ cm^{-1} to 12 000 cm^{-1} for C_6H_6, $C_{10}H_8$ and $C_{14}H_{10}$ and consequently in the nonradiative transition 1 CC ($\nu_{CC} \simeq 1500$ cm^{-1}) and 3 CH ($\nu_{CH} \simeq 3000$ cm^{-1}) modes are populated. Assuming that the ratio of triplets that would not revert to S_1 is proportional to the population of the CC modes, 25 % of the triplets formed will not come back to S_1 and this is in good agreement with the experimental ratio $\phi_T^o / \phi_T^\infty = 0.25$. In C_6D_6 the i. s. c. populates 1 CC an 4 CD modes ($\nu_{CD} \simeq 2100$ cm^{-1}) in the T_1 state, leading to 20 % of irreversibility. This value is also close to the experimental ratio ϕ_T^o / ϕ_T^∞ (C_6D_6) = 0.17. Better agreement between the ratio of states was achieved for benzene and toluene when the population of a CC promoting mode was considered (Table 1).

Pressure dependent fluorescence yields and decays were found for C_6H_6 and $C_{10}H_8$ [17, 37], and agree with the pressure dependence of triplet yields. With anthracene [6] pressure dependence was also

found for the fluorescence intensity, but the fluorescence decay is exponential. We have attributed such a feature to the irregularities in the spacing and coupling constants in the $S_1 \rightsquigarrow T_1$ transitions which can lead to a variety of k_S rates. In this situation the fluorescence decay, mixture of a manifold of biexponential decays, was shown [6] to be pressure independent with a rate equal to $k_i + k_T$. However the observation of quantum beats [19] in the fluorescence of anthracene reveal that under proper experimental conditions pressure effects on the fluorescence decay can be observed.

We are grateful to Prof. G. R. Fleming for useful comments and to INIC for financial support.

REFERENCES

[1] G. PORTER and F. J. WRIGHT, *Trans. Faraday Soc.*, 1955, **51**, 1205.
[2] C. W. ASHPOLE, S. J. FORMOSINHO and G. PORTER, *Proc. Roy. Soc. A*, 1971, **323**, 11.
[3] S. J. FORMOSINHO, G. PORTER and M. A. WEST, *Chem. Phys. Letters*, 1970, **6**, 7.
[4] S. J. FORMOSINHO, G. PORTER and M. A. WEST, *Proc. Roy. Soc. A*, 1973, **333**, 289.
[5] H. SCHRÖDER, H. J. NEUSSER and E. W. SCHLAG, *Chem. Phys. Letters*, 1978, **54**, 4.
[6] S. J. FORMOSINHO and A. M. DA SILVA, *Mol. Photochem.*, 1979, **9**, 257.
[7] R. E. SMALLEY, *J. Phys. Chem.*, 1982, **86**, 3504.
[8] M. A. DUNCAN, T. G. DIETZ, M. G. LIVERMAN and R. E. SMALLEY, *J. Phys. Chem.*, 1981, **85**, 7.
[9] T. G. DIETZ, M. A. DUNCAN and R. E. SMALLEY, *J. Chem. Phys.*, 1982, **76**, 1227.
[10] T. G. DIETZ, M. A. DUNCAN, A. C. PULU and R. E. SMALLEY, *J. Phys. Chem.*, 1982, **86**, 4026.
[11] C. E. OTIS, J. L. KNEE and P. M. JOHNSON, *J. Chem. Phys.*, 1983, **78**, 2091; *J. Phys. Chem.*, 1983, **87**, 2232.
[12] M. D. MORSE, A. C. PUIRE and R. E. SMALLEY, *J. Chem. Phys.*, 1983, **78**, 3435.
[13] A. E. W. KNIGHT and C. S. PARMENTER, *Chem. Phys.*, 1976, **15**, 85.
[14] P. AVOURIS, W. M. GELBART and M. A. EL-SAYED, *Chem. Rev.*, 1977, **77**, 793.
[15] F. LAHAMANI, A. TRAMER and C. TRIC, *J. Chem. Phys.*, 1974, **60**, 4431.
[16] T. F. HUNTER and M. G. STOCK, *J. C. S. Faraday II*, 1974, **70**, 1028.
[17] S. J. FORMOSINHO and A. M. DA SILVA, *J. C. S. Faraday II*, 1976, **72**, 2044.

[18] J. L. BAPTISTA, S. J. FORMOSINHO and M. F. LEITÃO, *Chem. Phys.*, 1978, **28**, 425.

[19] W. R. LAMBERT, P. M. FELKER and A. H. ZEWAIL, *J. Chem. Phys.*, 1981, **75**, 5958.

[20] B. J. VAN DER MEER, H. TH. JONKMAN, G. M. TER HORST and J. KOMMANDEUR, *J. Chem. Phys.*, 1982, **76**, 2099.

[21] J. CHAIKEN, M. GURNICK and J. D. MCDONALD, *J. Chem. Phys.*, 1981, **74**, 106, 123.

[22] S. H. LIN, *J. Chem. Phys.*, 1966, **44**, 3759.

[23] R. WALLACE, *Chem. Phys.*, 1975, **11**, 189.

[24] B. R. HENRY in "*Vibrational Spectra and Structure*", Vol. 10, ed. R. Durig, (Elsevier, Amsterdam, 1981), p. 269.

[25] P. R. STANNARD and W. M. GELBART, *J. Phys. Chem.*, 1981, **85**, 3592.

[26] S. SPEISER and E. GRUNWALD, *Chem. Phys. Letters*, 1980, **73**, 438.

[27] D. PHILLIPS, *J. Chem. Phys.*, 1967, **46**, 4679.

[28] D. F. HELLER, K. F. FREED and W. M. GELBART, *J. Chem. Phys.*, 1972, **56**, 2309.

[29] R. G. BRAY and M. J. BERRY, *J. Chem. Phys.*, 1979, **71**, 4909.

[30] K. V. REDDY, D. F. HELLER and M. J. BERRY, *J. Chem. Phys.*, 1982, **76**, 2814.

[31] S. M. BECK, J. B. HOPKINS, D. E. POWERS and R. E. SMALLEY, *J. Chem. Phys.*, 1981, **74**, 43.

[32] K. G. SPEARS and M. EL-MANGUCH, *Chem. Phys.*, 1977, **24**, 56.

[33] P. C. HAARHOFF, *Mol. Phys.*, 1964, **7**, 101.

[34] This approximation is not valid for benzene. Since ϕ_T^o in the isolated molecule is 0.18, $k_j \simeq 2 \times 10^6\ s^{-1}$; with $k_i = 3.5 \times 10^6\ s^{-1}$ eq. (1) allows an estimation of $k_s = 1 \times 10^6\ s^{-1}$ ($\lambda_2^{-1} = 470$ ns).

[35] SCHRÖDER et al. [5] have found that the T_1^v absorption, in the observation region $\lambda \geqslant 380$ nm, is red shifted with respect to the relaxed state T_1. The spectral T - T absorption area of T_1^v between 380 nm and 420 nm decreased with time by 1.8 times. However this spectrum includes two band progressions (408 nm and 390 nm) whereas for the equilibrated spectrum only one band (397 nm) was considered. The 390 nm band at low pressures corresponds to the second band (377 nm) at high pressures (see the high pressure spectrum reported in ref. [1]; there is a misprint in the second band, $\nu\ (cm^{-1}) = 26{,}546\ cm^{-1}$). Since to estimate relative concentrations we have to compare the same bands in spectra, the relevant ratios of areas, A, are $A_{408}/A_{397} \simeq 1.18$ or $(A_{408} + A_{390})/(A_{397} + A_{377}) \simeq 1.13$: These factors are too low to explain the increase in ϕ_T by a factor of 2.0 upon addition of 2.5 Torr of argon. So the net increase in triplet concentration is 1.7.

[36] Benzene, anthracene and naphthalene have the same pressure dependence up to 2.5 Torr of pressure [4, 5, 16] when excited at the lowest levels in S_1. From the triplet yield in the vapour phase [2] a value of $\phi_T^o = 0.16$ can be estimated for naphthalene.

[37] G. S. BEDDARD, S. J. FORMOSINHO and G. PORTER, *Chem. Phys. Letters*, 1973, **22**, 235.

ENVELOPE SOLITONS IN A PLASMA STRIP-LINE

A. B. SÁ and J. T. MENDONÇA

Centro de Electrodinâmica
Instituto Superior Técnico, 1096 Lisboa Codex, Portugal

(Received 27 July 1983; revised version 7 March 1984; final form in 1 October 1984)

ABSTRACT — We present some results of a study of the propagation of nonlinear wavepackets in a plasma strip-line system, which can be described as a nonlinear dispersive transmission line.

I – INTRODUCTION

In the last few years much attention has been given to the propagation of solitons in physical systems. In particular, it is now well-known that a plasma can propagate envelope solitons with central frequency nearly equal to the electron plasma frequency. This effect has been studied in uniform [1] and slightly nonuniform [2] semi-infinite plasmas. However, from the experimental point of view it is perhaps more suitable to study a configuration in which the transverse dimension of the plasma is finite. This is the reason why in this paper we discuss the propagation of envelope solitons in a plasma strip-line system. Such a system can be understood as a nonlinear transmission line, where the nonlinearity is associated to the plasma motion.

In Section II we study the plasma strip-line element with which we can construct a transmission line. We will study its properties in the linear approximation, assuming that the plasma electrons are at rest in the absence of an external perturbation. In Section III we take into account the existence of a finite electron temperature. In Section IV we show how a nonlinear transmission line equivalent to a long plasma strip-line can be constructed. In Section V we discuss the equation of propagation along this line. In the linear approximation we obtain the dispersion

relation equivalent to that of the line. In the nonlinear regime we show that the equation of propagation for the envelope of a wavetrain can be reduced to the nonlinear Schrodinger equation, if the carrier frequency of the wavetrain is nearly equal to the electron plasma frequency. The soliton solution of the nonlinear Schrodinger equation is then of the Langmuir type. However, the associated electric field in the plasma is perpendicular and not paralell to the direction of propagation, as it is the case in the usual Langmuir solitons. The conclusions are stated in Section VI.

II — COLD PLASMA CONDENSER

We consider a plasma slab of uniform density and thickness a placed between two infinite plane plates P_1 and P_2 (see Figure 1). The distance between plates is l and we apply a potential

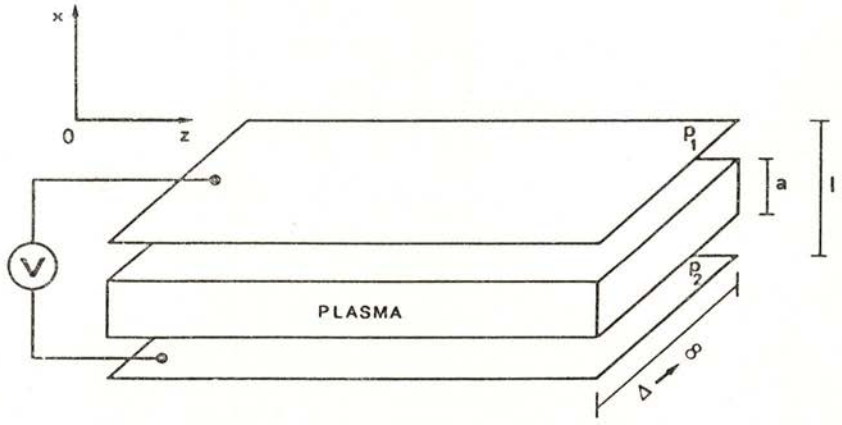

Fig. 1 — Model of the plasma strip-line system.

$V(t) = V_0 \exp(-i\omega t)$ to the plates. The electron motion is described with the aid of hydrodynamic equations which include a kinetic pressure term. The ions are assumed fixed. The electron density n and velocity v are then described by:

$$\begin{aligned} &\partial n / \partial t + \partial (nv) / \partial x = 0 \\ &(\partial / \partial t + \partial v / \partial x)\, v = -(e/m)\, E - \nu_c v - (S_e^2 / n)\, \partial n / \partial x \end{aligned} \tag{1}$$

where E is the electric field inside the plasma, ν_c is the electron collision frequency and $S_e^2 = 3\,K\,T_e / m$, where T_e is the electron temperature. The electric field E also obeys the Poisson equation, if electromagnetic corrections are neglected:

$$\partial E / \partial x = (e / \varepsilon_0)\ (n_0 - n) \tag{2}$$

where n_0 is the mean electron density. On the other hand, the parameters describing the exterior properties of the plasma strip-line system are the current density J and the potential V between plates, which are determined by:

$$\begin{aligned} J &= \varepsilon_0\, \partial E / \partial t - e\, n\, v = \varepsilon_0 \partial E_e / \partial t \\ V &= E_e\ (l - a) + \int_{-a/2}^{+a/2} E\ dx \end{aligned} \tag{3}$$

where E_e is the electric field outside the plasma, in the vacuum region laying between the plasma and each plate.

Let us now take the cold plasma approximation ($T_e = S_e = 0$). In that case we assume homogeneity along x and, after time Fourier analysis of equations (1) - (3) we find, for each component ω of the Fourier spectrum,

$$\begin{aligned} J &= -i\,\omega\,\varepsilon_0\ E_e = -i\,\omega\,\varepsilon_0\,\varepsilon(\omega)\ E \\ V &= [(l - a)\ \varepsilon(\omega) + a]\ E \end{aligned} \tag{4}$$

where $\varepsilon(\omega)$ is the cold plasma dielectric constant:

$$\varepsilon(\omega) = 1 - (\omega_p / \omega)^2\ (1 + i\,\nu_c / \omega)^{-1} \tag{5}$$

where $\omega_p = (e^2\, n_0 / \varepsilon_0\, m)^{1/2}$ is the electron plasma frequency. From equation (4) we get then the impedance of the plasma strip-line, per unit area,

$$Z = V / J = [(l - a) + a\,\varepsilon(\omega)^{-1}] / (-i\,\omega\,\varepsilon_0) \tag{6}$$

It is easy to see that this impedance is composed by a series of two capacities C_v and C_ω, such that:

$$C_v = \varepsilon_0 / (l - a) \quad , \quad C_\omega = {}_0\,\varepsilon(\omega) / a \tag{7}$$

Replacing (5) in the equation for C_ω we obtain circuit elements which do not depend on the frequency ω. In fact, the impedance Z_ω associated to C_ω can be writen as:

$$Z_\omega = i / (\omega C_\omega) = (R_p - i\omega L_p) / (1 - \omega^2 L_p C_p - i\omega R_p C_p) \tag{8}$$

where the resistance R_p, the inductance L_p and the capacity C_p are defined by:

$$R_p = a\nu_c / (\varepsilon_o \omega_p^2) \quad , \quad L_p = a / (\varepsilon_o \omega_p^2) \quad , \quad C_p = \varepsilon_o / a \tag{9}$$

Thus Z_ω is a parallel R L C circuit and the plasma condenser is equivalent to such circuit in series with C_v.

A resonance ($Z = 0$) occurs for

$$\omega = \omega_p \sqrt{1 - (a / l)} \tag{10}$$

as can be seen from equation (6) if the damping terms are neglected; and an anti-resonance ($Z \to \infty$) for $\varepsilon \to 0$, which, in the collisionless limit, leads to $\omega = \omega_p$.

III — HOT PLASMA CONDENSER

We consider now the situation where $T_e \neq 0$. In this case we can no longer neglect the spatial perturbation in the x direction. Making a Fourier transform in time, we get from equation (1) the following expressions for the electron density and velocity perturbations:

$$\begin{aligned} \tilde{n} &= n_o / (i\omega) \cdot \partial v / \partial x \\ v &= (1 / i\omega) (1 + i\nu_c / \omega)^{-1} (e E / m + S_e^2 / n_o \cdot \partial \tilde{n} / \partial x) \end{aligned} \tag{11}$$

where $\tilde{n} = n - n_o$.

Using equation (2) and after eliminating v and n, we obtain the following equation for the electric field:

$$[\partial^2 / \partial x^2 + k^2] \partial E / \partial x = 0 \tag{12}$$

where

$$k^2 = [\omega^2 (1 + i \nu_c / \omega) - \omega_p^2] / S_e^2 \tag{13}$$

The general solution of this equation is of the form:

$$E = E_o + A \cos kx + B \sin kx \tag{14}$$

Assuming now that the velocity at the plasma boundary ($x = \pm a / 2$) is equal to zero, we get from the Fourier transform of equation (3a) the following result:

$$B = 0 \quad , \quad E_o + A \cos (k a / 2) = E_e \tag{15}$$

This means that the field (14) reduces to a purely time varying field E_o plus a space dependent field of cosinus form. Returning to equation (11) we get:

$$\begin{aligned} \tilde{n} &= (\varepsilon_o \, k / e) \; A \sin kx \\ v &= (e / m) \; (1 / i\omega) \; (1 + i \nu_c / \omega)^{-1} \; . \\ &\quad \cdot \; [E_o + (1 + k^2 S_e^2 / \omega_p^2) \; A \cos kx] \end{aligned} \tag{16}$$

Using once more the assumption that the velocity is zero at $x = \pm a / 2$ we get from equations (15b) and (16b):

$$\begin{aligned} A &= -(\omega_p / k S_e)^2 \; E_e \sec (ka / 2) \\ E_o &= E_e \; (1 + \omega_p^2 / k^2 S_e^2) \end{aligned} \tag{17}$$

We can now express the external potential drift V as a function of E_e . Using (17) in the Fourier transform of equation (3) we get:

$$V = E_e \; [l + a \, \omega_p^2 / (k^2 S_e^2) - 2 \, \omega_p^2 / (k^3 S_e^2) \tan (ka / 2)] \tag{18}$$

The plasma condenser impedance can be easily obtained, if we use $J = -i \omega \varepsilon_o E_e$:

$$Z = -i/(\omega \varepsilon_o) \; . \; \omega_p^2/(k^3 S_e^2) \; [-l k^3 S_e^2/\omega_p^2 - ka + 2 \tan (ka/2)] \tag{19}$$

This equation as well as equation (6), are well known in the literature [3], but here we have used a more straightforward calculation. The anti-resonances of the system ($Z \to \infty$) are now given by the condition $\cos (ka / 2) = 0$, which leads to:

$$\omega_N = \omega_p \; [1 + (2N + 1)^2 \; \pi^2 \; \lambda_D^2 / a^2]^{1/2} \tag{20}$$

where $N = 0, 1, 2, \ldots$ and $\lambda_D^2 = S_e^2 / \omega_p^2$. The resonances ($Z \to 0$) are obtained by solving the equation (cf. [3]):

$$\tan (ka/2) = (ka/2) + 1/2\ l\ k^3\ \lambda_D^2 \qquad (21)$$

When $\omega < \omega_p$ the wavenumber becomes imaginary (cf. eq. (13)); putting $z = -i\,ka/2$ we can rewrite eq. (21) in the form:

$$\tanh z - z + z^3\ 4\,l\ \lambda_D^2 / a^3 = 0 \qquad (22)$$

When $|ka| << 1$ an expansion of eq. (21) or (22) leads to:

$$\omega = \omega_p\ [1 - 10\ \lambda_D^2 / a^2 + 120\ l\,\lambda_D^4 / a^5]^{1/2} \qquad (23)$$

In the general case (21) has solutions k_N ($N = 1, 2, \ldots$) such that

$$k_N\ a/2 = x_N + \delta_N \qquad (24)$$

where x_N is the Nth non-zero root of $\tan x = x$ and $\delta_N \to 0$ when $\lambda_D << a$ ($x_N + \delta_N \to (2N+1)\,\pi/2$ when $\lambda_D >> a$). An additional solution exists, given by (21) or (22) as $4\,l\,\lambda_D^2 / a^3$ is larger or smaller than 1/3, respectively; when $\lambda_D << a$ then $z^2 \to a^3 / (4\,l\,\lambda_D^2)$.

Comparing the results with those obtained in the previous section we see that the influence of the temperature is to replace the anti-resonance $\omega = \omega_p$ by an infinite number of anti-resonances $\omega = \omega_N$ (eq. (20)), which when $\lambda_D << a$ (corresponding to the usual situation in laboratory experiments) lie close to ω_p. On the other hand the resonance $\omega_p [1 - (a/l)]^{1/2}$ is also replaced by an infinite number of resonances. Since, from (13),

$$\omega = \omega_p [1 + (2\lambda_D / a)^2\ (k\ a/2)^2]^{1/2} \qquad (25)$$

it is easy to see that, for $\lambda_D << a$, such resonances (eq. (24)) lie close to ω_p, but the "additional solution" lies close to $\omega_p [1 - (a/l)]^{1/2}$.

If the nonlinear terms of equations (1) - (3) are now taken into account we get an expression for the impedance Z which is formally analogous to equation (19) but where ω_p is replaced by an effective plasma frequency which depends on the square amplitude of the potential:

$$\omega_{eff}^2 = \omega_p^2\ (1 - \alpha |V|^2) \qquad (26)$$

The perturbative nonlinear analysis is quite lengthy and will not be presented here. We just quote the approximate value for the parameter α [4]:

$$\alpha = \alpha' \{ 1 - 1/3 \ (\omega_p / kS_e)^4 \ [1 + (kS_e / \omega_p)^2]^2 \\ [1/2 + 2 \ (\omega_p / \omega)^2 \ (1 + (kS_e / \omega_p)^2)] \} \qquad (27)$$

with $\alpha' = \varepsilon_o / (2 n_o T_e a^2)$

This nonlinear parameters can be justified in a rather simple way. If we take the equation of motion in the x direction and average over a time scale of the order of $1 / \omega_p$, we get for the mean velocity the following equation

$$\partial < v > / \partial t = - (e / m) \cdot \partial / \partial x \ (\varepsilon_o | E |^2 / e n_o) \qquad (28)$$

This equation shows that there exists an effective potential V_{eff} acting on the electrons and making them move (in a time scale much larger than $1 / \omega_p$):

$$V_{eff} = \varepsilon_o | E |^2 / (e n_o) \qquad (29)$$

Assuming that the electrons reach thermodynamic equilibrium in this potential [1], we get for the mean density:

$$< n > = n_o \ \exp \ (- eV_{eff} / K T_e) \qquad (30)$$

Assuming now that $eV_{eff} << KT_e$, the mean electron density will be given by:

$$< n > = n_o \ (1 - eV_{eff} / K T_e) \qquad (31)$$

Using (29) and considering that $| E |^2$ is proportional to $| \tilde{V} |^2$ we can see that this nonlinear correction to the mean electron density is of the form $- \alpha | \tilde{V} |^2$, as stated above.

IV — EQUIVALENT TRANSMISSION LINE

We are now able to define the nonlinear transmission line, which is an electric analog of the strip-line plasma system. This line can be viewed as an infinite series of condenser elements,

each of which is described by the equations deduced in the previous section. In order to have a complete description of the line we must add an inductance L_l, and a resistance R_l has to be retained when we consider the propagation along z. We can easily obtain the equivalent circuit of fig. 2, where the cold plasma limit was considered. The plasma inductance $L_p(V^2)$ is given by equation (9) where ω_p^2 was replaced by ω_{eff}^2. In the expression of R_p we neglect the nonlinear corrections to the plasma frequency, because R_p is already a small quantity. In this work we will be interested only on the complete case of a transmission line without losses ($R_l = R_p = 0$). We will also take $l = a$ in the configuration of figure 1, which means $C_v = \infty$. It can be shown [4] that in the most general case the nonlinear solutions are quite similar to those obtained here. In the assumed

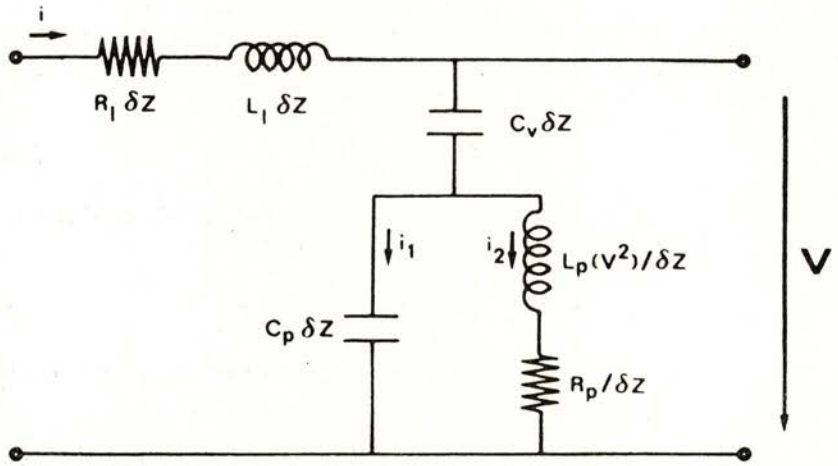

Fig. 2 — Equivalent electric circuit to the transmission line.

approximation we can see from figure 2 that the current flowing in the circuit elements is given by:

$$\partial i / \partial t = (1 / L_l)\, \partial V / \partial z \tag{32}$$

On the other hand we also have:

$$\delta i = (\partial i / \partial z)\ \delta z = i_1 + i_2 \tag{33}$$

where the currents i_1 and i_2 are given by:

$$i_1 = C_p \, \delta z \cdot \partial V / \partial t \quad , \quad i_2 = (\delta z / L_p) \int V dt \tag{34}$$

From these equations we can easily get the equation of the potential perturbation along the line:

$$\partial^2 V / \partial t^2 - (1 / C_p L_l) \partial^2 V / \partial z^2 + V / (C_p L_p) = 0 \tag{35}$$

V – ENVELOPE SOLITONS

Let us consider now a potential of the form:

$$V (z , t) = \tilde{V} (z , t) \, e^{-i \omega t} \tag{36}$$

where $\tilde{V} (z , t)$ is a slowly varying amplitude, in the sense that:

$$| \partial \tilde{V} / \partial t | \ll \omega \, | \tilde{V} | \tag{37}$$

Replacing (36) in (35) and taking (37) into account we get an equation of propagation for the envelope in the form:

$$- 2 i \omega \partial \tilde{V} / \partial t - \omega^2 \tilde{V} - (1 / C_p L_l) \partial^2 \tilde{V} / \partial z^2 + \tilde{V} / (C_p L_p) = 0 \tag{38}$$

If we use now the nonlinear expression for the plasma inductance L_p we get:

$$1 / (C_p L_p) = \omega_p^2 (1 - \alpha | \tilde{V} |^2) \tag{39}$$

Assuming that the wave frequency ω is nearly equal to the electron plasma frequency, equation (38) reduces to:

$$2 i \omega \, \partial \tilde{V} / \partial t + \omega^2 \alpha | \tilde{V} |^2 \, \tilde{V} + (1 / C_p L_l) \partial^2 \tilde{V} / \partial z^2 = 0 \tag{40}$$

Using now space and time adimensional variables:

$$\tau = (\omega / 2) t \quad , \quad \mu = z \omega \, (C_p L_l)^{1/2} = z \, (L_l / L_p^*)^{1/2} \tag{41}$$

where L_p^* is the linearised plasma inductance we finally obtain:

$$i\,\partial\,\tilde{V}/\partial\,\tau + \partial^2\tilde{V}/\partial\,\mu^2 + \alpha\,|\tilde{V}|^2\,\tilde{V} = 0 \qquad (42)$$

This is the well known nonlinear Schrodinger equation which, for $\tilde{V}$ tending to zero at infinity ($\tilde{V} \to 0$ for $z \to \infty$) has the following soliton solution [5]:

$$\tilde{V} = A\,(2/\alpha)^{1/2}\,\exp\{\,i\,[\,(B/2)\,\mu - (B^2/4 - A^2)\,\tau\,]\,\}\,\operatorname{sech}\,[\,A\,(\mu - B\,\tau)\,] \qquad (43)$$

where A and B are two constants of integration. The first constant A defines the amplitude of the soliton perturbation and the second one B defines the velocity at which this perturbation moves along the line. We can then specify B , because it has to be equal to the usual group velocity v_g in the coordinates μ and τ . In order to determine v_g we return to equation of propagation (35). After linearization and using $V = V_0 \exp i\,(kz - \omega\,t)$ we get the linear dispersion relation of the line which describes the evolution of each Fourier component of the soliton spectrum.

$$\omega^2 = \omega_p^2 + k^2/(C_p L_l) \qquad (44)$$

The phase and group velocities along the line (in the coordinates z and t) are given by:

$$v_\varphi = \omega/k = \omega_p\,[\,1/k^2 + 1/(C_p\,L_l\,\omega_p^2)\,]^{1/2}$$
$$v_g = 1/(C_p\,L_l\,v_\varphi) \qquad (45)$$

We can then state the explicit form of the constant B:

$$B = 2\,[\,1 + \omega_p^2\,C_p\,L_l/k^2\,]^{-1/2} \qquad (46)$$

This equation completely specifies the soliton solution of (43).

VI — CONCLUSIONS

We have shown in this work that a long plasma strip-line system can be described by an equivalent transmission line. This line has nonlinear properties, which are associated with the

nonlinear motion of the plasma particles induced by the potential applied to the transmission line. We have determined the linear dispersion relation of the line and as our main result, we have shown that such a line can propagate envelope solitons, which are similar to the well known Langmuir solitons. However the nonlinear equation of propagation along the line differs slightly from the Zakharov equation which describes the Langmuir solitons in an unbounded plasma. The main difference is that our solitons are solitons in the strict sense, as defined by Scott et al. [6], and the usually called one dimensional Langmuir solitons are solitary waves which are not solitons in this sense [7]. In the case of a line with a finite resistance R_p we can also get soliton solutions propagating along the line with a slight damping [8].

This work remains valid only in the limit of low electronic temperatures. In the case of finite temperatures we have to compare the spectral width of the soliton solution with the distance between two neighbouring resonances in order to conclude about the validity of the previous results. However it is quite obvious that in the general case the nonlinear equation of propagation cannot be written in the simple form used here. The general features of soliton propagation using a consistent theory for a finite temperature plasma will be discussed elsewhere.

REFERENCES

[1] L. I. RUDAKOV, *Dokl. Akad. Nauk SSSR.* **207**, (1972), 821.

[2] A. H. CHEN and C. S. LIN, *Phys. Rev. Letters*, **37**, (1976), 693.

[3] P. E. VANDENPLAS, *Electron Waves and Resonances in Bounded Plasmas* (Wiley-Interscience, 1968).

[4] J. T. MENDONÇA and A. B. SÁ, to be published.

[5] R. K. DODD, J. C. EIBBECK, J. D. GIBBON, and H. C. MORRIS, *Solitons and Nonlinear Wave Equations* (Academic Press, 1982).

[6] A. C. SCOTT, F. Y. F. CHU, and D. W. MCLAUGHLIN, *Proc. IEEE* **61**, (1973), 1443.

[7] J. GIBBONS, S. G. THORNHILL, M. J. WARDROP and D. TER HAAR, *J. Plasma Phys.* **17**, (1977), 153.

[8] A. B. SÁ, J. HORMIGO and J. T. MENDONÇA, Communication to the 1982 Conference on Plasma Physics, Goteborg, Sweden (1982).

FIELD — EFFECT MEASUREMENTS IN DOPED HYDROGENATED AMORPHOUS SILICON FILMS

C. S. FURTADO

Centro de Física da Radiação e dos Materiais da Universidade de Coimbra
(INIC) — Universidade. 3000 Coimbra, Portugal

(Received 6 June 1984)

ABSTRACT — Field-effect measurements were performed at several temperatures in hydrogenated amorphous silicon (a - Si : H) films with different doping concentrations. These films were prepared by sputtering of ions in the liquid phase followed by activated reaction in a plasma of argon and hydrogen [1]. The process of preparation of the samples and the method of measurement are described. It is attempted to correlate the properties of the films with parameters of their preparation. The screening responsible for the field-effect is, at lower temperatures, ascribed to the localized states situated near the Fermi level, whereas at higher temperatures the dominant role is played by the mobile carriers in the extended states. The process of calculation of the field-effect electronic density, N_{FE} [2], is presented; in our samples it falls within the range 10^{16} - 10^{19} cm^{-3} eV^{-1}. The interpretation of the results is assisted by knowledge of the values of the electrical conductivity, which help to understand the mechanisms involved.

1 — INTRODUCTION

Amorphous semiconductors with tetrahedral bonds, as it is the case of the amorphous silicon (a-Si), exhibit a continuous distribution of the electronic states in the forbidden gap, defined between the mobility edges, E_v and E_c, of the valence and conduction bands. Hydrogenated amorphous silicon (a - Si : H) deposited on substrates at a temperature around 250°C, shows, because of a reduction in dangling bonds through liaisons with hydrogen atoms, a low value of the state density in the central region of the forbidden gap. As a consequence [3], it is possible

to dope a - Si : H films, leading that way to type - n or type - p semiconductors.

When a transverse electric field is applied across a dielectric material, the resistance of the sample is changed. The measurement of this change in the resistance of a film, due to the field-effect, has been a method largely used to evaluate the density of states N (E) [4]. In this paper the approach proposed by Mahan and Bube [2] has been admited, by considering a field-effect electronic density, N_{FE}, in order to characterize the distribution of states. Parameters related to the resistivity of the samples are also presented.

It must be said that the measurements have been performed on samples which have been produced using a new method already described [1].

2 — EXPERIMENTAL CONSIDERATIONS

The samples were obtained by sputtering of ions from the liquid phase, followed by an activated reaction taking place in a plasma of argon and hydrogen. The liquid phase was obtained on the top of n - and p - type cylinders of silicon, with different

TABLE

Sample	Ingot ohm-cm /Type	Substrate	Flow rate (cm^3/min) H_2	Ar	Deposition Time (min)	Film Thickness (μm)
RE 12	2 p	Mica	37	30	1.5	0.9
RE 20	.02 p	Glass 7059 + Al + SiO_2 (0.2 μm)	37	30	2.5	1.2
RE 23	10 n	Glass 7059 + Al + SiO_2 (0.1 μm)	36	28	2.5	0.5
RE 35	.02 p	Mica	33	11.5	2.5	0.8
RE 36	.02 p	Mica	30	15.5	2.5	0.7
RE 37	.02 p	Mica	10	35	2.5	0.8
RE 38	.02 p	Mica	6	39	2.5	0.9

concentrations of doping, by means of the bombardment of a focused beam of 8.2 keV electrons, the beam power being 1.6 kW. The substrate, connected to earth, was maintained during growing at a temperature of 250°C. The pressure in the reaction chamber was initially less than 10^{-5} Torr, taking during deposition a value of 3 mbar (except for sample RE37 in which the value was 1 mbar). In the Table, further characteristics of the measured samples are given.

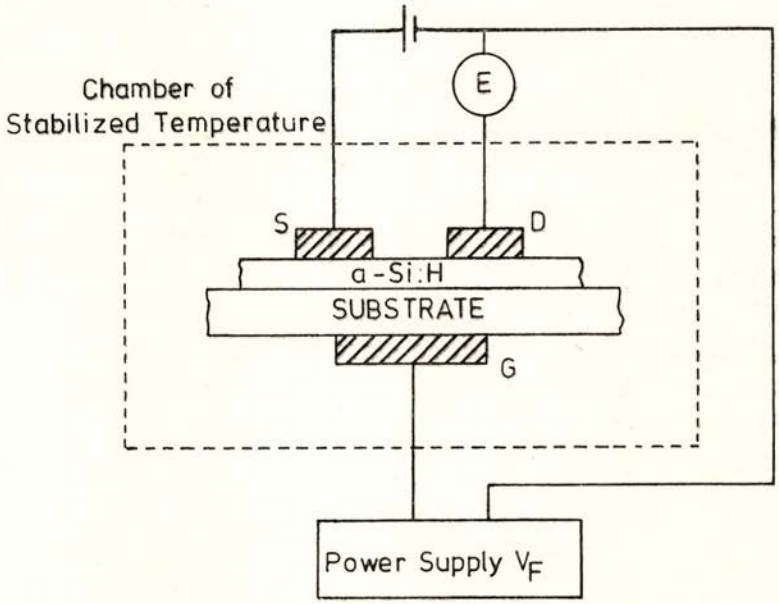

Fig. 1 — Experimental set-up for measurement of the field-effect (schematic).

The dielectric layer of SiO_2 was processed by the same method as described for the a - Si : H film; in the chamber a mixture of argon and oxygen gases was used, the time of deposition being 2.5 minutes. Aluminium contacts were used with the type - p specimens but with the RE23 sample, of type - n, the contacts were made of superposed layers of antimonium and gold.

Figure 1 represents the set-up used to perform the field-effect measurements. The substrate plays the role of insulating dielectric

in the conventional IGFET geometry, the distance between the source S and the drain D being of the order of 100 μm. A field voltage V_F, varying between -100 and $+100$ V, is applied to the field electrode, the gate G. A variable channel voltage, V_c, is used between the source and the drain, and the corresponding current is measured by an electrometer (Keithley 614 Electrometer).

The thickness of the films was measured with a Talysurf.

3 — RESULTS AND COMMENTS

The transverse electric field imposed across the film and the dielectric substrate creates a space charge layer near the film – substrate interface which commands the resistance of the film. Since this space charge resides predominantly in localized gap states, the field-effect provides information about the corresponding density of states.

For different temperatures, with a constant channel voltage V_c, values of the source-drain current, I_{SD}, were obtained as a function of the gate voltage, V_F (field voltage). Being I_o the value of the current I_{SD} for $V_F = 0$, we can write

$$V_c = R_o \, I_o$$

When $V_F \neq 0$ we have

$$V_c = (R_o + \Delta R) \, I_{SD}$$

and therefore

$$\Delta R / R = (I_o / I_{SD}) - 1$$

Plotting $\Delta R / R$ in terms of V_F (as an example, see Figure 2), we can easily evaluate $R / (dR / dV_F)$ for $V_F = 0$, which is simply the inverse of the slope at the origin for each one of the curves. This parameter is fundamental for the kind of presentation and analysis of the results here exposed. The resistance change is due to band bending created by the spatial charge which screens the external electrical field.

It is appropriate to consider a quantity N_{FE}, called the field-effect state density and given, for the case of small changes in resistance, by

$$N_{FE} = (R / (dR / dV_F))_0 \cdot \varepsilon_d / (e\,d\,D\,k\,T)$$

where ε_d is the dielectric constant of the dielectric material used, e is the electronic charge, d is the thickness of the dielectric

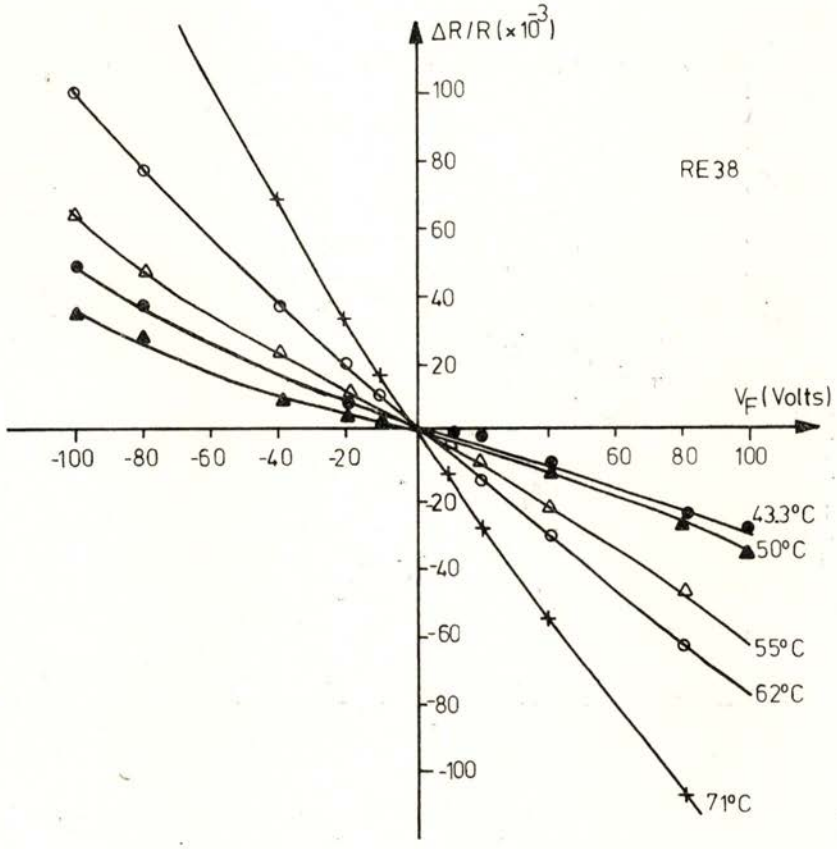

Fig. 2 — $\Delta R/R$ as a function of V_F for the sample RE 38.

material, D is the thickness of the amorphous film, k is the Boltzmann constant, T is the absolute temperature and

$(R / (dR / dV_F))_0$ has the meaning referred above. In principle, a temperature independent N_{FE} means that the screening is provided by localized states situated near the Fermi level. In case of N_{FE} being thermally activated, the corresponding thermal activation energy corresponds to the energy difference between the level of screening and the Fermi level.

The results obtained with the samples RE12, RE20, RE23, RE35, RE36, RE37 and RE38 are shown in Figure 3. The observed

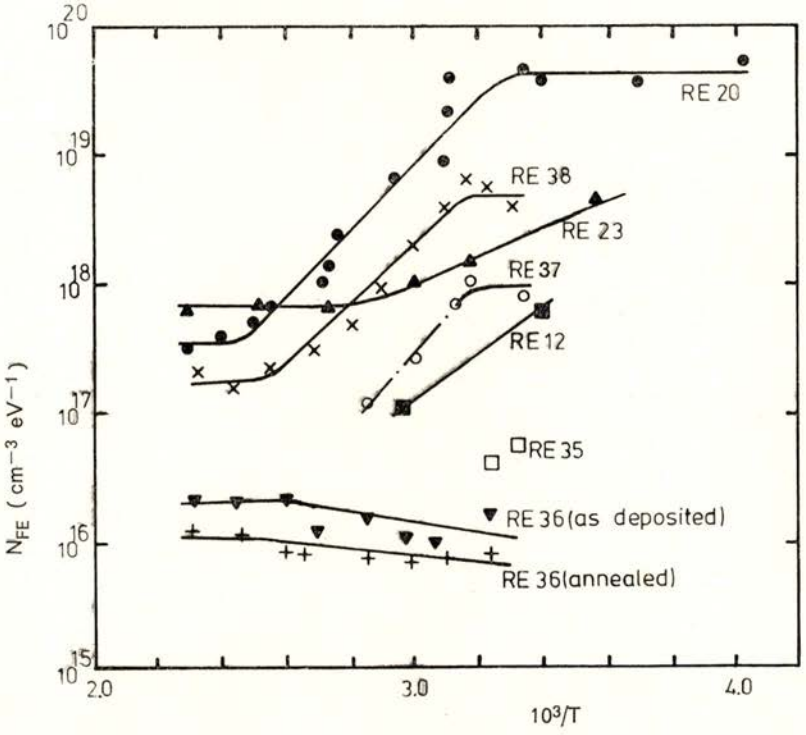

Fig. 3 — Field-effect state density as a function of the inverse temperature for samples RE 12, RE 20, RE 23, RE 35, RE 36, RE 37 and RE 38.

density of states varies within the range $16^{16} - 10^{19}$ cm^{-3} eV^{-1}, which shows agreement with figures obtained by other authors [5, 6] in samples produced by glow discharge. However, the general features of these curves do not show similarity with

those referred in the literature. As a matter of fact, in our samples the density of carriers N_{FE}, responsible for the screening, not only decreases with temperature but also shows a tendency to level-off at high values of temperature. This behaviour is rather odd and appears to be in disagreement with the thermal variation of the electrical conductivity measured in the same specimens, as can be seen in Figure 4.

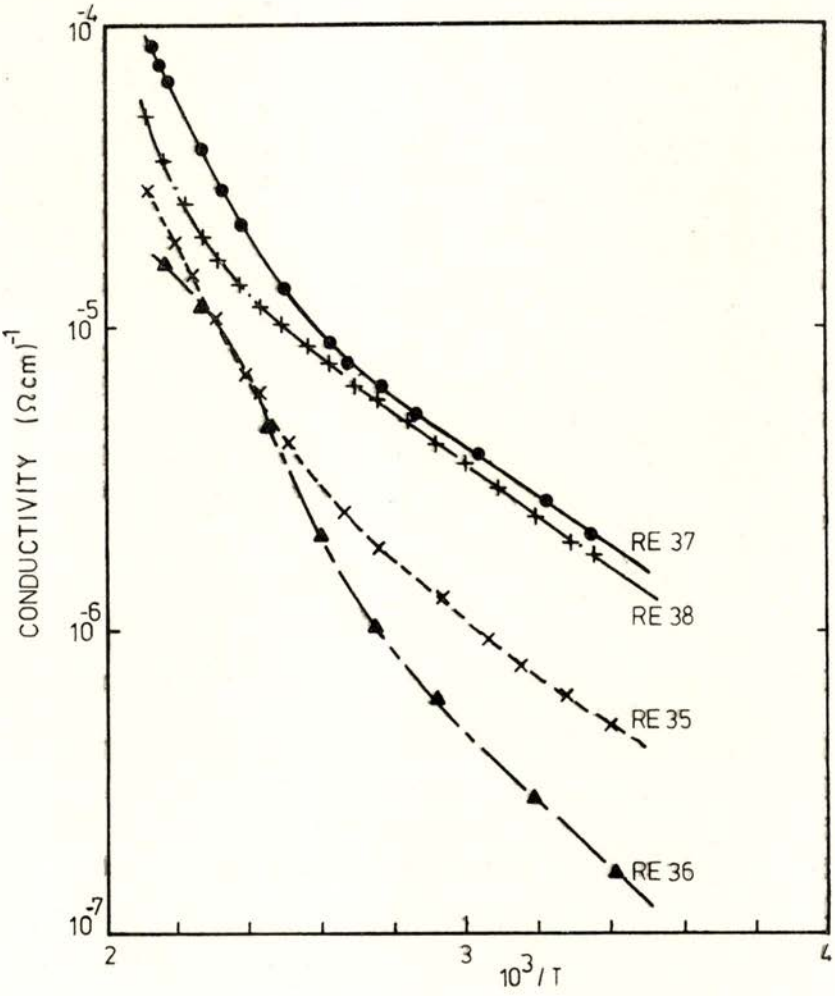

Fig. 4 — Electrical conductivity as a function of temperature for samples RE 35, RE 36, RE 37 and RE 38.

It could be thought that incorrections or deficiencies in the experimental set-up were the cause of these discrepancies. However, it is difficult to accept this sort of explanation, since the results obtained with several samples in different conditions exhibit, besides reproducibility, a pattern of reasonable global coherence. Can it be the case that phenomena of recombination take place in these doped samples under stationary conditions of the field voltage, the rate of which increases with temperature? Another possible interpretation for the source of the observed behaviour can be found in the fact that the field-effect current is usually confined inside a narrow channel, 20-100 Å thick, under a strong accumulation of charge carriers [7]. The surface, both in the immediate vicinity of the substrate and in the first deposited layers, will present electronic states which are mainly responsible for the screening of the electrostatic field. That would explain the different observed thermal behaviour of the electrical conductivity which is essentially dependent on the bulk electronic states.

I wish to thank Prof. J. C. Anderson for the kind hospitality extended to me at the Materials Section, Department of Electrical Engineering of the Imperial College of Science and Technology (London) and the Calouste Gulbenkian Foundation, Academia de Ciências de Lisboa and Royal Society (London) for their benevolent support.

REFERENCES

[1] J. C. ANDERSON, S. BISWAS and C. S. FURTADO, Preparation of Amorphous, Si : H, IX International Vacuum Congress, Madrid (1983).

[2] J. E. MAHAN and R. H. BUBE, *J. Non-Cryst. Solids*, **24**, 29 (1977).

[3] W. E. SPEAR and P. G. LE COMBER, *Phil. Mag.*, **33**, 935 (1976).

[4] M. J. POWELL, *Phil. Mag.* **B43**, 93 (1981).

[5] ZIMMER S. JAN and RICHARD H. BUBE, *J. Electron. Mat.*, **8**, 47 (1979).

[6] NANCY B. GOODMAN, *Phil. Mag.*, **B45**, 407 (1982).

[7] N. B. GOODMAN and H. FRITZSCHE, *Phil. Mag.*, **B42**, 149 (1980).

CONTENTS

FASCÍCULO 1-2

GENERAL AND MATHEMATICAL PHYSICS

Les Transitions de Connectivité
P. G. DE GENNES 1

Frustrated Spin Systems (a review)
A. ERZAN 9

ATOMIC AND NUCLEAR PHYSICS

The LX-Ray Spectrum of Argon, Krypton and Xenon
M. T. RAMOS, J. G. FERREIRA, M. L. CARVALHO and L. SALGUEIRO 55

$\beta+$/EC Decay of ^{181}Au : γ-Ray Identification
F. BRAGANÇA GIL, C. BOURGEOIS, P. KILCHER, G. PAROT, M. G. PORQUET, B. ROUSSIÈRE, J. SAUVAGE-LETESSIER and the ISOCELE Collaboration 59

D-State and Nuclear Structure Effects in (d, α) Reactions
F. D. SANTOS and A. M. EIRÓ 65

Nuclear Hydrodynamics
J. P. DA PROVIDÊNCIA 89

Effects of the Magnetic Field Shape in the Characteristics of a Double Focusing Electron Spin Polarimeter
P. AMORIM and J. P. RIBEIRO 99

CONDENSED MATTER PHYSICS

Approximate Solution for the Concentrations of Imperfections in a Pure Metal Oxide MO_y with Schöttky Disorder
C. A. C. SEQUEIRA 111

CONTENTS

FASCÍCULO 3-4

GENERAL AND MATHEMATICAL PHYSICS

A Compendium on Directed and 3-D Undirected Lattice Data

J. A. M. S. DUARTE 119

Errata and Addenda: Frustated Spin Systems

A. ERZAN 139

MOLECULAR AND CONDENSED MATTER PHYSICS

Misfit Dislocations in Crystalline Interfaces

M. A. FORTES 143

Coupling in One-Electron Transfer Processes

A. C. MOUTINHO 157

Transport Properties of n-Type Ferromagnetic Semiconductor $HgCr_2Se_4$

J. L. RIBEIRO, M. R. CHAVES, J. M. MOREIRA, J. B. SOUSA, A. SELMI and P. GIBART 169

Polarization Reversal of SbSI

A. GONÇALVES DA SILVA, M. R. CHAVES, A. ALMEIDA, and M. H. AMARAL 185

Intersystem Crossing in Hexafluorobenzene and Benzene Vapours. The Role of Local Modes on the Nonstatistical Behaviour of Benzene

S. J. FORMOSINHO and A. M. DA SILVA 205

PLASMA PHYSICS

Envelope Solitons in a Plasma Strip-Line

A. B. SÁ and J. T. MENDONÇA 217

APPLIED PHYSICS

Field Effect Measurements in Doped Hydrogenated Amorphous Silicon Films

C. S. FURTADO 229

AUTHOR INDEX

ALMEIDA, A. — See A. GONÇALVES DA SILVA

AMARAL, M. H. — See A. GONÇALVES DA SILVA

AMORIM, P., RIBEIRO, J. P. — Effects of the Magnetic Field Shape in the Characteristics of a Double Focusing Electron Spin Polarimeter 99

BOURGEOIS, C. — See F. B. GIL

CARVALHO, M. L. — See M. T. RAMOS

CHAVES, M. R. — See A. GONÇALVES DA SILVA and J. L. RIBEIRO

DE GENNES, P. — Les Transitions de Connectivité 1

DUARTE, J. A. M. S. — A Compendium on Directed and 3-D Undirected Lattice Data 119

EIRÓ, A. M. — See F. D. SANTOS

ERZAN, A. — Frustrated Spin Systems (a review) 9

Errata and Addenda 139

FERREIRA, J. G. — See M. T. RAMOS

FORMOSINHO, S. J., SILVA, A. M. DA — Intersystem Crossing in Hexafluorobenzene and Benzene Vapours. The Role of Local Modes on the Nonstatistical Behaviour of Benzene 205

FORTES, M. A. — Misfit Dislocations in Crystalline Interfaces 143

FURTADO, C. S. — Field Effect Measurements in Doped Hydrogenated Amorphous Silicon Films 229

GIBART, P. — See A. GONÇALVES DA SILVA

GIL, F. B., BOURGEOIS, C., KILCHER, P., PAROT, G., PORQUET, M. G., ROUSSIÈRE, B., SAUVAGE-LETESSIER, J. and the ISOCELE Collaboration - β^+ / EC Decay of ^{181}Au: γ-Ray Identification 59

KILCHER, P. — See F. B. GIL

MENDONÇA, J. T. — See A. B. SÁ

MOREIRA, J. M. — See J. L. RIBEIRO

MOUTINHO, A. C. — Coupling in One-Electron Transfer Processes . . . 157

PAROT, G. — See F. B. GIL

PORQUET, M. G. — See F. B. GIL

PROVIDÊNCIA, J. P. DA — Nuclear Hydrodynamics 89

RAMOS, M. T., FERREIRA, J. G., CARVALHO, M. L., SALGUEIRO, L. — The LX - Ray Spectrum of Argon, Krypton and Xenon 55

RIBEIRO, J. L., CHAVES, M. R., MOREIRA, J. M., SOUSA, J. B., SELMI, A., GIBART, P. — Transport Properties of n - Type Ferromagnetic Semiconductor $HgCr_2Se_4$ 169

RIBEIRO, J. P. — See P. AMORIM

ROUSSIÈRE, B. — See F. B. GIL

SÁ, A. B., MENDONÇA, J. T. — Envelope Solitons in a Plasma Strip-Line 217

SALGUERO, L. — See M. T. RAMOS

SANTOS, F. D., EIRÓ, A. M. — D - State and Nuclear Structure Effects in (d , α) Reactions 65

SAUVAGE-LETESSIER, J. — See F. B. GIL

SELMI, A. — See J. L. RIBEIRO

SEQUEIRA, C. A. C. — Approximate Solution for the Concentrations of Imperfections in a Pure Metal Oxide MO_y with Schöttky Disorder 111

SILVA, A. M. DA — See S. J. FORMOSINHO

SILVA, A. G. DA, CHAVES, M. R., ALMEIDA, A., AMARAL, M. H. — Polarization Reversal of SbSI 185

SOUSA, J. B. — See J. L. RIBEIRO

Composto e impresso na *Imprensa Portuguesa* • Rua Formosa, 108-116 • 4000 PORTO

SOCIEDADE PORTUGUESA DE FÍSICA
AV. REPÚBLICA 37-4.°, 1000 LISBOA, PORTUGAL

PORTUGALIAE PHYSICA publishes articles or research notes with original results in theoretical, experimental or applied physics; invited review articles may also be included.

Manuscripts, with an abstract, may be written in English or French; they should be typewritten with two spaces and in duplicate. Figures or photographs must be presented in separate sheets and be suitable for reproduction with eventual reduction in size; captions should make the figures intelligible without reference to the text. Authors are requested to comply with the accepted codes concerning references.

There is no page charge. Author(s) will get 50 free reprints (without covers); these are to be shared among all the authors of the article. Authors interested in more reprints should say so when sending their manuscripts; quotations shall be sent with the proofs.

Subscription rates for volume 15:

3,600 Escudos (US$24) — individuals
9,000 Escudos (US$60) — libraries

PORTUGALIAE PHYSICA may also be sent on an exchange basis; we wellcome all suggestions to such effect.

All mail to be addressed to

PORTUGALIAE PHYSICA

C/O LABORATÓRIO DE FÍSICA, FACULDADE DE CIÊNCIAS
PRAÇA GOMES TEIXEIRA
4000 PORTO PORTUGAL

PORTUGALIAE PHYSICA

VOL. 15 · NUMB 3/4 · 1984

CONTENTS

GENERAL AND MATHEMATICAL PHYSICS

A Compendium on Directed and 3-D Undirected Lattice Data
J. A. M. S. DUARTE 119

Errata and Addenda: Frustated Spin Systems
A. ERZAN 139

MOLECULAR AND CONDENSED MATTER PHYSICS

Misfit Dislocations in Crystalline Interfaces
M. A. FORTES 143

Coupling in One-Electron Transfer Processes
A. C. MOUTINHO 157

Transport Properties of n-Type Ferromagnetic Semiconductor $HgCr_2Se_4$
J. L. RIBEIRO, M. R. CHAVES, J. M. MOREIRA, J. B. SOUSA, A. SELMI and P. GIBART 169

Polarization Reversal of SbSI
A. GONÇALVES DA SILVA, M. R. CHAVES, A. ALMEIDA, and M. H. AMARAL 185

Intersystem Crossing in Hexafluorobenzene and Benzene Vapours. The Role of Local Modes on the Nonstatistical Behaviour of Benzene
S. J. FORMOSINHO and A. M. DA SILVA 205

PLASMA PHYSICS

Envelope Solitons in a Plasma Strip-Line
A. B. SÁ and J. T. MENDONÇA 217

APPLIED PHYSICS

Field Effect Measurements in Doped Hydrogenated Amorphous Silicon Films
C. S. FURTADO 229

CONTENTS AND AUTHOR INDEX (VOL. 15) 237

ISSN 0048-4903 POPYA4 15 (3/4) 119-240 (1984)